Theoretical and Computational Methods for Fractional Viscoelastic Models

Ahlam Saqer Alghamdi

A thesis submitted for the degree of
Doctor of Philosophy

Cardiff University
March 2025

Abstract

This thesis investigates the behaviour of viscoelastic fluids, such as stress relaxation under constant deformation and time-dependent deformation recovery following load removal, and explores how to characterize this behaviour using mechanical models. These models demonstrate how fractional viscoelastic models can be derived using spring-pot elements arranged in series and/or parallel. To accurately capture the complex behaviour of viscoelastic fluids, numerical techniques for solving fractional viscoelastic models are developed, as these models frequently employ fractional differential equations to account for the material's characteristics and memory effects.

New fractional viscoelastic models have been derived by extending the single-mode fractional Maxwell model to a multi-mode framework by considering springpots arranged in series and/or parallel to study more complex behaviour. Our theoretical analysis has derived new expressions for the exact solution of these models equations—using the Laplace transform of the Green's function and expanding in terms of the Mittag-Leffler function (MLF)—as well as for the relaxation time and the dynamic moduli in both single-mode and multi-mode settings. This method highlights its effectiveness as a powerful tool for solving various fractional differential equations and boundary value problems in real-world applications, while also providing a strong foundation for future studies.

Furthermore, an accurate numerical method has been developed to solve two coupled fractional differential equations for Taylor-Couette flow by employing a spectral approximation for spatial discretization and a finite difference scheme for temporal discretization. High-order schemes ensure accurate modelling of complex fluid behaviour, and the convergence properties of the numerical scheme are investigated. Numerical results are presented which highlight the influence of the parameters in the fractional viscoelastic models on the numerical predictions.

Table of Contents

List of Figures and Tables

Acknowledgements

I start by expressing my heartfelt thanks to Allah, the Most Merciful and Compassionate. It is through his endless grace and blessings that I have received the strength, guidance, and inspiration needed to navigate the difficulties of this academic path.

I would like to extend my sincere gratitude to my supervisors, Prof. Tim Phillips and Prof. Nikolai Leonenko, for their continuous support of my PhD study and related research, for their patience, motivation, and immense knowledge. Their guidance helped me throughout my research and writing of this thesis. I could not have imagined having better advisors and mentors for my PhD study. I genuinely cannot thank both of you enough for everything you have done over the last few years. It has been a pleasure to work with you, and I hope to be able to do so again in the future.

I am also grateful to the Saudi government, the Ministry of Education, Albaha University, and the Saudi Cultural Bureau in London for providing the financial support that enabled me to pursue this research.

I would like to express my sincere gratitude to the academic and professional staff at Abacws for their kindness, support, and guidance. I am especially thankful to Prof. Jonathan Gillard, Review Panel Convenor, for his invaluable feedback and encouragement. I would also like to express my appreciation to my colleagues in the Applied and Computational Mathematics group for their insightful discussions and continued encouragement during challenging times.

I am deeply thankful to Layla, Mohammed, and Saeideh for their continuous support from the very start of this journey. They have always provided guidance, encouragement, and unwavering support. Their kindness and companionship have made this experience truly special.

My appreciation goes to my friends in Saudi Arabia, Emtinan, Samaher, Atheer, Dr.Jameel, Dalal, Rana, Modhi, Amal, Manal, Alia, Rehab, Shahd, Faizah, for their camaraderie, stimulating discussions, and unwavering support during challenging times.

Last but not least, I owe my deepest gratitude to my family for their unconditional love, patience, and belief in me. Their support has been my anchor throughout this journey and my life in general.

Chapter 1

Introduction

In our daily lives, we come into contact with many different kinds of fluid, each with unique properties. These include complex fluids, which are characterized by their complex internal interactions and structures which produce unusual and frequently unexpected behaviours. Unlike simple fluids such as water or oil, complex fluids can transition between solid-like and fluid-like states depending on external conditions, making them a fascinating subject of study across diverse fields including industry, engineering, biology, and other scientific disciplines. Complex fluids are typically classified as non-Newtonian and often viscoelastic since their mechanical behaviour deviates from that of classical Newtonian fluids, such as water under standard conditions (Shah Driscoll, 2024; Toschi Sega, 2019; Deville Gatski, 2012).

Many industrial processes, such as those in the food, cosmetics, and pharmaceutical industries, are dependent on complex fluids. For example, the smoothness and stability of products such as lotions, toothpaste, and mayonnaise are determined by their complex fluid characteristics. Understanding these features aids to raise the quality of products and streamline production processes (Galindo-Rosales, 2018).

The study of complex fluids in engineering can result in innovative products and procedures. This involves developing cutting-edge materials with special qualities, improving drilling fluids, and processes lubricants that work better (Saramito, 2016). An understanding of the behaviour and properties of complex fluids like blood and mucus is important for many physiological processes in medicine. The design of medical equipment and therapies can be enhanced by characterising the flow characteristics of biological fluids, such as blood. For instance, improving medicine delivery systems or creating better blood substitutes (Barbati ., 2016; Saramito, 2016).

The optimization of these processes significantly depends on the ability to understand and model viscoelasticity.

1.1 Challenges in Modeling

Viscoelastic fluids exhibit both fluid-like (viscous) and solid-like (elastic) behaviour, in contrast to Newtonian fluids, which have a linear relationship between stress and strain. These fluids exhibit dual behaviour, meaning that depending on variables such as the rate and duration of applied stresses, they could resist flow (elastic behaviour), flow in response to applied stress (viscous behaviour), or do both. Predicting these interactions in real world situations requires accurate modelling, particularly for complex flows observed in biological, engineering, and industrial settings (Giga ., 2017; Bird ., 1987). To study challenges in modelling viscoelastic fluids, it is necessary to account for history-dependent effects when analysing time-dependent characteristics, like rheopexy or thixotropy (Hohenegger McKinley, 2018). In industrial applications, these fluids frequently flow through complex geometries, creating complex flow patterns driven by normal stress variations, shear thickening, and shear thinning. Furthermore, sophisticated methods and computational resources are required to model their multiscale interactions at the molecular and macroscopic levels (Afonso, 2018). A further level of complexity is added by boundary conditions, such as slip, wall effects, and surface tension variations, which makes precise simulation and prediction particularly challenging (for an overview, see Bird . (1987), for example).

1.2 Material characterization.

Shear and Extensional Viscosity

Basic characteristics that are utilised to describe fluid behaviour include shear viscosity and extensional viscosity. Shear viscosity is the ratio of shear stress to shear rate and is used to measure a fluid's resistance to shear flow, in which fluid layers move parallel to

one another at varying speeds:

$$\eta = \frac{\tau}{\dot{\gamma}} \tag{1.1}$$

where η is the shear viscosity, τ is the shear stress, and $\dot{\gamma}$ is the shear rate (Yahia ., 2016). As an illustration, consider honey flowing down a slope, where its layers are resistant to slipping past one another.

However, extensional viscosity, which is the ratio of extensional stress to the rate of extension, measures a fluid's resistance to elongational flow, such as pulling or stretching:

$$\eta_e = \frac{\tau_e}{\dot{\epsilon}} \tag{1.2}$$

where η_e is the extensional viscosity, τ_e is the extensional stress, and $\dot{\epsilon}$ is the rate of extension.

Chewing gum's resistance to the applied pulling force during stretching serves as an example of extensional viscosity.

Stress and Strain

In fluid deformation, stress and strain are key concepts. Stress is the internal force per unit area resulting from external forces,

$$\tau = \frac{F}{A} \tag{1.3}$$

where τ is the stress, F is the applied force, and A is the area over which the force is applied.

The unit of stress is a Pascal (Pa), which is equivalent to Newtons per square meter $\mathrm{N/m^2}$. Furthermore, strain is a measurement of deformation that indicates how far apart particles are in a material body when compared to a reference length.

$$\epsilon = \frac{\Delta L}{L_0} \tag{1.4}$$

where $\Delta L = L - L_0$ represents the change in length of the material due to the applied force or deformation, where L is the final length of the material after deformation, and L_0

is the original length of the material before any force or deformation is applied. It serves as the reference length for measuring strain.

Since strain has no units, it is a dimensionless quantity. A percentage is frequently used to express it. These formulas and units are essential for understanding how various stresses and deformations affect materials.

Stress comes in many different forms, shear stress results from forces that are parallel to and lay in the plane of the cross-sectional area, whereas normal stress results from forces that are perpendicular to a cross-sectional area of the material.

Two different forms of stress can be applied to a material: Tensile stress is the external force applied to a material's surface area that causes it to stretch. The force that causes a material to deform, resulting in a decrease in volume, is known as compression stress.

According to how the stress is applied, there are two different forms of strain that a body can experience: Tensile strain is the term for a solid body's deformation or lengthening brought on by the application of a tensile force or stress. In contrast, when equal and opposing pressures are used to compress a body, compressive strain is created.

The definitions of stress and strain given above can be applied to forces that cause compression or tension. Tensile stress and strain result from the application of a tensile force. Compressive stress and strain result from the application of a compressive force.

(see e.g (Halliday ., 2010; Tattersall Banfill, 1983; Barnes, 2000; Owens Phillips, 2002).

The simplest model for describing the constitutive response of viscoelastic fluids was introduced by Maxwell. Through the use of a differential equation, the Maxwell model describes linear viscoelastic materials by combining their viscous and elastic properties.

$$\tau(t) + \lambda \frac{d\tau}{dt} = \eta_0 \frac{d\gamma}{dt} \tag{1.5}$$

where τ is the shear stress, $\lambda = \frac{\eta_0}{G_0}$ is the characteristic relaxation time of the fluid,η_0 is the viscosity (rate-independent) and G_0 is the elastic modulus of the material, and $\frac{d\gamma}{dt}$ is the rate of strain.

As an alternative, the stress response can be represented by an equivalent integral form

as

$$\tau(t) = \int_{-\infty}^{t} \dot{\gamma}(t') G_0 e^{-t/\lambda}\, dt', \tag{1.6}$$

where the time-dependent relaxation modulus of the linear Maxwell model (the response of the stress to a jump in deformation at $t' = 0$) is $G(t) = G_0 e^{-t/\lambda}$, and it is assumed that the fluid is at rest for $t < 0$. We can write Eq. (1.6) in terms of G as follow,

$$\tau(t) = \int_{-\infty}^{t} G(t - t')\dot{\gamma}(t')\, dt', \tag{1.7}$$

For linear viscoelastic deformations of complicated materials, this is one particular form of the Boltzman integral (Bird ., 1987). Several complex viscoelastic fluids exhibit this kind of Maxwell–Debye relaxation (exponential decay), but other materials exhibit other kinds of fading memory, such as algebraic decay (see, for instance, the work by Keshavarz et al. (Keshavarz ., 2017) on biopolymer gels and Ng et al. (Ng ., 2006) on bread dough), where the relaxation modulus with $0 < \beta < 1$ is expressed as,

$$G(t) = \mathbb{S} t^{-\beta} \tag{1.8}$$

where $\mathbb{S}$ a scalar measure of the gel strength.

Additionally, under oscillatory stress or strain, the viscoelastic response can be described in terms of the storage modulus G' and loss modulus G'', which characterise the material's elastic energy and dissipative energy, respectively. These moduli depend on frequency (ω), and are given by

$$G'(\omega) = \frac{G_0 \omega^2 \lambda^2}{1 + \omega^2 \lambda^2}, \tag{1.9}$$

and

$$G''(\omega) = \frac{G_0 \omega \lambda}{1 + \omega^2 \lambda^2}. \tag{1.10}$$

The dimensionless product $\omega\lambda$ is known as the Deborah number. It has been demonstrated that, at least in the limit of small deformations, several types of complex materials exhibit Maxwell behaviour with a single relaxation time scale. Specifically, complex fluids com-

posed of self-assembling worm-like surfactants or perfectly reversible networks frequently display Maxwell-like behaviour for small deformation amplitudes and a single dominant relaxation time scale (Parada Zhao, 2018; Rehage Hoffmann, 1991; Pipe ., 2010).

The relationships in Eq. (1.9) and Eq. (1.10) illustrate how the balance between elastic and viscous responses changes with frequency, providing critical insights into material behaviour (see Maxwell (1867); Bird . (1987); Tschoegl (2012); Ferras . (2018); Rathinaraj . (2021), for example).

1.3 Fractional Constitutive Modelling

While fundamental 'Classical Constitutive Modelling' was covered briefly in the previous section, fractional models are a natural generalisation and enhance their predictive capability. Currently, fractional calculus is crucial for studying relaxation processes, which include the connections between stress and strain in polymeric materials. This is the process in which first-order derivatives in the rheological constitutive equations are replaced by fractional derivatives, as described by Ferras . (2018) after Schiessel Blumen (1993). Ferras . (2018) redefined the relaxation modulus for such materials as

$$G(t) = \frac{\mathbb{V}}{\Gamma(1-\beta)} t^{-\beta} \tag{1.11}$$

then, Eq. (1.6) can be expressed as follows:

$$\tau(t) = \frac{1}{\Gamma(1-\beta)} \int_0^t \mathbb{V}(t-t')^{-\beta} \dot{\gamma}(t') dt' \tag{1.12}$$

Here, $\mathbb{V}$ is a constant for a given β, with physical dimensions of $\mathrm{Pa} \cdot \mathrm{s}^{\beta}$. It represents a generalized modulus or a quasi-property.

The Caputo fractional derivative is defined as a generalized derivative. For $0 < \beta < 1$, the Caputo derivative of a function F is given by:

$${}_0^c D_t^{\beta} F(t) = \frac{1}{\Gamma(1-\beta)} \int_0^t (t-t')^{-\beta} \frac{dF}{dt'} dt' \tag{1.13}$$

(see e.g Caputo (1969); Diethelm (2010); Ferras . (2018); Mainardi (2010)).

The constitutive relationship Eq.(1.12) for a material showing power law relaxation of the form in Eq. (1.8) can be modified to

$$\tau(t) = \mathbb{V}\, {}_0^c D_t^\beta \gamma(t) \tag{1.14}$$

because of the clear similarity between Eq. (1.12) and the Caputo derivative Eq. (1.13). ${}_0^c D_t^\beta \gamma(t) = \dfrac{d^\beta \gamma}{dt^\beta}$ is the concise notation that yields the fractional constitutive law

$$\tau(t) = \mathbb{V} \frac{d^\beta \gamma(t)}{dt^\beta} \tag{1.15}$$

The Riemann–Liouville fractional derivative is an alternative fractional derivative that could have been utilized. However, we have decided to use the Caputo derivative in this thesis since the initial conditions are much simpler to interpret in this setting, and also the Caputo derivative of a constant is zero (${}_0^c D_t^\beta a \equiv 0$, when a is a constant).

Therefore, the following differential equation describes the fractional Maxwell model (FMM) that relates the stress and strain rate:

$$\tau(t) + \frac{\mathbb{V}}{\mathbb{G}} \frac{d^\alpha \tau(t)}{dt^\alpha} = \mathbb{V} \frac{d^\beta \gamma(t)}{dt^\beta}, \tag{1.16}$$

where we assume that $0 < \alpha \leq \beta \leq 1$ without loss of generality.

Regression to experimental data is required to find the four parameters for this model, which include two quasi-properties $\mathbb{V}, \mathbb{G}$ and two fractional exponents α, β. Compared to the classical Maxwell model, this four-parameter linear viscoelastic model is capable of describing a much larger class of complex fluid dynamics. The FMM takes into account a wide variety of distinct relaxation processes.

1.4 Numerical Methods for Fractional Models

A fascinating area of study in fractional differential equations (FDE) research is determining how to approximate various types of FDEs analytically and/or numerically (Daftardar-Gejji Babakhani, 2004; Podlubny, 1999). Solving fractional differential equations (FDEs) presents several challenges due to the complexity of fractional derivatives, which contain integral operators with memory effects, making them computationally intensive and difficult to interpret (Troparevsky ., 2019). Since many problems have no precise or exact solutions, various series analytical and numerical techniques have been proposed and investigated in recent decades to solve FDEs, particularly nonlinear FDEs. Furthermore, providing appropriate initial or boundary conditions is challenging, as fractional derivatives depend on the entire history of the function rather than local values (Garrappa, 2018). A lack of standardised tools equivalent to those for classical differential equations and high computing costs are other challenges faced by numerical approaches, particularly when dealing with high-dimensional problems or long time intervals (Garrappa, 2018). Numerous techniques have been developed to overcome these problems. The use of Laplace and Fourier transforms for linear FDEs and special functions such as the Mittag-Leffler function (Podlubny, 1997; Yang ., 2010) are examples of analytical methods that have been employed. Numerical techniques that have been developed include: the spectral collocation scheme (Doha ., 2011), finite difference methods (Ferras ., 2018), finite element methods (Troparevsky ., 2019), fractional differential transform scheme (Kumar, Kumar ., 2020), fractional Adams scheme (Diethelm ., 2004), variational iteration method (He, 2007), homotopy analysis scheme (Kumar, Ghosh ., 2020) and adomain decomposition scheme (Momani Al-Khaled, 2005).

Recent developments have enhanced standard numerical techniques by introducing two effective methods for solving initial value problems (IVPs) in both linear and nonlinear fractional differential equations (FDEs) of order $\beta \in (0, 1)$. Examples of these methods are the midpoint and Heun methods (Kumar ., 2024). These techniques aim to enhance convergence and accuracy of the numerical techniques for solving FDEs, for example when

simulating the dynamics of population expansion.

Efficiency is further increased by methods that combine analytical and numerical techniques. Despite these developments, research into solving FDEs is ongoing, with attempts being made to develop techniques that improve accuracy and efficiency and resolve outstanding issues.

1.5 Generalised Fractional Constitutive Models and their Numerical Solution

The original contributions to the modelling and computational aspects of fractional models that form the substance of this thesis are highlighted in this section. Modelling has led to the development of various formulations of fractional viscoelastic models, including extensions to the traditional fractional Maxwell model by incorporating extra fractional derivatives. These enhancements provide a more comprehensive framework for describing the complex viscoelastic behaviour of materials, such as those displaying fading memory with non-exponential relaxation. In order to provide an analytical understanding of the behaviour of these extended models, Green's function solutions are derived and presented. In terms of computation, sophisticated numerical methods were used to successfully solve fractional differential equations. This involves developing and validating enhanced techniques for computing important viscoelastic characteristics, including complex moduli, loss, and storage, as well as relaxation times. In order to study the asymptotic behaviour of fractional models and provide accurate predictions of material responses under different circumstances, new algorithms were also developed. Additionally, a new numerical technique is employed to solve a specific set of fractional differential equations, enabling the investigation of the stationary and unstable unidirectional flow of fractional viscoelastic fluids within a real concentric cylinder rheometer. In this study, we utilize spectral methods, which offer enhanced accuracy in both time and space, further improving the precision of our numerical approach. These contributions significantly improve our understanding of and ability to use fractional models in viscoelasticity.

1.6 Objectives and Outline of Thesis

The outline of this thesis is as follows.

In Chapter 2, an introduction to the spectral method is presented highlighting the advantages of the method. An example showing how the spectral method is used to approximate the solution of the weak formulation of the partial differential equations in one and two dimensions is described. Also, we present software that has been developed using Matlab and provide examples to demonstrate the behaviour and convergence of the spectral approximation.

The principal concepts of fractional calculus are introduced in Chapter 3. This chapter includes an introduction to the Laplace transform for fractional derivatives. Additionally, it introduces Mittag-Leffler (ML) functions and their related Laplace transforms for different sets of parameters. Furthermore, the features and uses of the Green's function approach for solving fractional differential equations are highlighted.

In Chapter 4, an overview of mechanical models for representing viscoelastic behaviour is given. The derivation of the Green's function solution for the single-mode Fractional Maxwell Model, utilizing the Laplace transform of the two-parameter Mittag-Leffler function is presented. This is an original contribution. Furthermore, we consider an extension of the general fractional Maxwell model by including additional fractional time derivatives. A Green's function solution for this model is also obtained using the Laplace transform method. We derive formulas for the complex modulus, storage modulus, and loss modulus in order to analyse these models in terms of their rheological behaviour. Additionally, we show how to determine a material's relaxation time. We present numerical results for the Fractional Maxwell Model (FMM), Fractional Maxwell Liquid (FML), and Fractional Maxwell Gel (FMG) that analyse the asymptotic behaviour of the storage modulus G' and loss modulus G''.

The chapter concludes by performing numerical simulations using the new models and comparing their predictive properties for different model and material parameters. Comparisons are also made with relevant experimental data.

In Chapter 5, we outline some fundamental notions that are essential to studying the behaviour of numerical techniques for dealing with fractional derivatives. For two ranges of fractional order $0 < \alpha < 1$ and $1 < \alpha < 2$, a first-order difference scheme is derived using the Caputo fractional derivative. These concepts are then extended to a second-order difference schemes for the two ranges of fractional order α. Additionally, we use difference approach to derive the first-order and the second-order temporal discretisation for the Fractional Viscoelastic Fluid model for the special case of fractional order $\alpha = 1$. In Chapter 6, we present a novel solution to the steady and unsteady unidirectional flow of fractional viscoelastic fluids inside a real concentric cylinder rheometer (the Taylor–Couette geometry) by extending the computational model in the paper of Ferras . (2018) using spectral methods. A Matlab code was developed. We present a numerical discretisation of the problem based on spectral approximations in space and finite differences in time. The linear system for the unknowns at each time step is formed by applying these techniques to the governing equations for shear stress and velocity. Moreover, we investigate the convergence behaviour of the spectral approximation. We describe the advantages and disadvantages of both approaches while comparing some numerical findings with the finite difference approach of Ferras . (2018) to demonstrate the validity of this contribution. By the end of this chapter, we formulate and study the fully coupled problem in Section 4 of Ferras . (2018). We then examine how fractional orders affect the velocity and shear stress estimates and briefly explain the stress relaxation that was obtained for the FMM.

In Chapter 7, we present enhanced fractional viscoelastic models and higher-order temporal numerical scheme in the context of the Single-Mode and Multi-Mode Fractional Maxwell Models for the Taylor-Couette problem. The derivation begins with the weak form of the system of equations, followed by the temporal discretization using first-order and second-order difference schemes for the time-fractional derivative to improve numerical accuracy. Additionally, spectral approximations are employed for the spatial discretization. These techniques are applied to the governing equations for velocity and shear stress, resulting in a linear system for the unknowns at each time step. Numeri-

cal results are provided to validate the proposed approach and examine the evolution of velocity and shear stress within the Taylor-Couette geometry.

Chapter 8 summarises original contributions of this thesis and discusses possible directions for future study.

All of the simulations performed in this thesis were carried out using MATLAB.

Chapter 2

Spectral Methods

2.1 Introduction

Spectral methods are one of the most powerful techniques used in scientific computing and applied mathematics to solve differential equations using global approximations, and were first presented by Gottlieb Orszag (1977). The main idea of the spectral method is as follows. First, write the approximate solution as a linear combination of particular basis functions with unknown coefficients, where, the basis functions are infinitely differentiable global functions defined over the whole domain, for example, Legendre polynomials, trigonometric functions, Jacobi polynomials, Chebyshev polynomials. This is a distinctive feature of spectral methods which distinguishes them from finite-element and finite-difference methods. Second, construct a system of linear equations for the unknown coefficients in this expansion. Lastly, solve the linear system to find these coefficients. Spectral methods converge exponentially when the solution of the differential equation is smooth, which makes them more accurate than local methods. Spectral methods are superior in terms of spatial accuracy for well-behaved problems (Canuto ., 2012; Childs Liu, 2020; Kang Suh, 2008).

This chapter is structured as follows: in Sections 2.2 and 2.3 the numerical discretization of Boundary Value Problems (BVP) in 1D and 2D, is derived, and the accuracy of the spatial method is verified by considering some benchmark problems that have been studied by many researchers (see Owens Phillips (2002), for example). Some concluding remarks are made in Section 2.4.

2.2 Boundary Value Problems in 1D

Consider the model convection-diffusion problem :

$$-\epsilon u'' + bu' = f, \quad x \in (-1, 1) \tag{2.1}$$

with boundary conditions

$$u(-1) = u_L, \qquad u(1) = u_R \tag{2.2}$$

Equations (2.1)-(2.2), represent the strong form of the problem. One goal of the spectral method is to solve these equations in their equivalent weak form. The weak formulation is obtained by multiplying the strong form of the equation by an appropriate test function chosen from a suitable function space, and then integrating the equation over the entire domain. The benefit of this method is that it reduces the order of the differential equation by using integration by parts to find a solution in a larger space.

Before we write out the weak formulation, we must define a suitable function space for the solution $V = H^1(I)$ where $I = (-1, 1)$. The weak formulation of the continuous equation is then: Find $u \in V$ such that

$$\int_{-1}^{1} \epsilon u'v'dx + \int_{-1}^{1} bu'vdx = \int_{-1}^{1} fvdx \tag{2.3}$$

The weak formulation is then: find $u \in V$ such that

$$a(u, v) = (f, v), \qquad \forall v \in W \tag{2.4}$$

where $(.,.)$ denotes the inner product on L^2. Here V and W represent the trial and test spaces, respectively, and the bilinear form $a(.,.)$ is defined as:

$$a(u, v) = \int_{-1}^{1} (\epsilon u'v' + bu'v)dx \tag{2.5}$$

The spectral method is now applied to the solution of the equation (2.4) utilising expansions based on Legendre polynomials $L_k(x) \equiv P_k^{(0,0)}(x)$ in which the weight function is $\omega(x) = 1$. Two methods exist for approximating the solution with Legendre polynomials: expansions based on orthogonal polynomials modal or Lagrange interpolant nodel. The solution is expanded in terms of Lagrange interpolants using the Gauss-Lobatto-Legendre (GLL) points:

$$u_N(x) = \sum_{i=0}^{N} u_i h_i(x) \tag{2.6}$$

where

$$h_i(x) = -\frac{(1-x^2)L'_N(x)}{N(N+1)L_N(x_i)(x-x_i)} \tag{2.7}$$

are Lagrange basis functions. The zeros of $(1-x^2)L'_N(x)$ are the points $x_i, i = 0, \ldots, N$, also referred to as the Gauss-Lobatto-Legendre points. The approximation to $u(x_i)$ is u_i. In the case of the weak formulation, the unknown nodal values $u_i, i = 0, ..., N$, is collocation or Galerkin method.

The basis functions for the test space in the Galerkin method are selected from the trial space, i.e. $W^N \subset V^N$.

Next, we select conforming approximation spaces V^N, i.e., $V^N \subset V$, where the test space is

$$V_0^N = \{v \in P_N(-1,1) : v(-1) = 0 = v(1)\} \tag{2.8}$$

and the trial space is specified as,

$$V_E^N = \{v \in P_N(-1,1) : v(-1) = u_L,\ v(1) = u_R\} \tag{2.9}$$

and $P_N(-1,1)$ is the space of polynomials of degree no greater than N on the interval I. This allows us to create the Galerkin approximation. Consequently, the discrete weak problem must be solved in order to obtain the Galerkin approximation (2.4): Find $u^N \in V_E^N$

$$\epsilon(u'_N, v'_N)_N + b(u'_N, v_N)_N = (f, v'_N)_N, \qquad \forall v_N \in P_N(I) \cap H_0^1(I) \tag{2.10}$$

The discrete inner product $(.,.)_N$ is defined as ,

$$(\phi, \psi)_N = \sum_{j=0}^{N} \omega_j \phi(x_j)\psi(x_j) \tag{2.11}$$

where

$$\omega_j = \frac{2}{N(N+1)} \frac{1}{L_N^2(x_j)}, \qquad j = 0, 1, \ldots, N \tag{2.12}$$

provides the weights in such a way that, whenever ϕ is a polynomial of degree $2N-1$ or less, the quadrature rule

$$\int_{-1}^{1} \phi(x)dx = \sum_{i=0}^{N} \omega_i \phi(x_i) \tag{2.13}$$

is exact.

We employ the interpolants $h_k(x)$, $k = 1, \ldots, N-1$, as test functions in (2.10) to derive

$$\epsilon(u_N', h_k')_N + b(u_N', h_k)_N = (f, h_k)_N, \quad k = 1, \ldots, N-1, \tag{2.14}$$

or,

$$\sum_{j=0}^{N} \omega_j [\epsilon u_N'(x_j)h_k'(x_j) + b u_N'(x_j)h_k(x_j)] = \sum_{j=0}^{N} \omega_j f(x_j)h_k(x_j), \quad k = 1, \ldots, N-1 \tag{2.15}$$

where

$$u_N'(x) = \sum_{i=0}^{N} u_i h_i'(x) \tag{2.16}$$

Therefore equation (2.15) becomes,

$$\sum_{j=0}^{N} \omega_j \epsilon \left(\sum_{i=0}^{N} u_i h_i'(x_j) \right) h_k'(x_j) + b \left(\sum_{i=0}^{N} u_i h_i'(x_j) \right) h_k(x_j) = \sum_{j=0}^{N} \omega_j f(x_j)h_k(x_j), \quad k = 1, \ldots, N-1 \tag{2.17}$$

Recall that,

$$h_k(x_j) = \delta_{k,j} = \begin{cases} 1 & , \ k = j \\ 0 & , \ k \neq j \end{cases} \tag{2.18}$$

and define

$$D_{j,i} = h_i'(x_j) \tag{2.19}$$

where D is the Legendre pseudospectral differentiation matrix. The entries of D for the Legendre polynomials have the explicit expression:

$$D_{j,i} = \begin{cases} \dfrac{1}{(x_j - x_i)} \dfrac{L_N(x_j)}{L_N(x_i)} & , \ j \neq i \\ 0 & , \ 1 \leq j = i \leq N-1 \\ \dfrac{-N(N+1)}{4} & , \ j = i = 0 \\ \dfrac{N(N+1)}{4} & , \ j = i = N \end{cases} \tag{2.20}$$

As a result, equation (2.17) becomes,

$$\sum_{i=0}^{N} \left[\epsilon \sum_{j=0}^{N} \omega_j h_i'(x_j) h_k'(x_j) + b\omega_k h_i'(x_k) \right] u_i = \omega_k f(x_k) \tag{2.21}$$

$$\sum_{i=0}^{N} \left[\epsilon \sum_{j=0}^{N} \omega_j D_{j,i} D_{j,k} + b\omega_k D_{k,i} \right] u_i = \omega_k f(x_k) \tag{2.22}$$

This is the system of $N-1$ equations for the $N-1$ unknowns $u_i, i = 1, \ldots, N-1$, and $u_0 = \alpha, u_N = \beta$ are known values.

Define

$$A_{k,i} = \epsilon \sum_{j=0}^{N} \omega_j D_{j,i} D_{j,k} + b\omega_k D_{k,i} \tag{2.23}$$

then

$$\sum_{i=0}^{N} A_{k,i} u_i = b_k$$

where

$$b_k = \omega_k f(x_k)$$

Since $u_0 = \alpha$ and $u_N = \beta$ are known values,

$$\sum_{i=1}^{N-1} A_{k,i} u_i = b_k - A_{k,0}\,\alpha - A_{k,N}\,\beta, \qquad k = 1, \ldots, N-1 \tag{2.24}$$

see (Owens Phillips, 2002; Burden Faires, 1997). Thus we have derived the linear system $Au = b$ where $u = (u_1, \ldots, u_{N-1})^T$.

2.2.1 Numerical Examples and Comparisons

Example 1. Consider the boundary value problem

$$-\epsilon u'' + bu' = f, \qquad x \in (-1, 1) \tag{2.25}$$

with boundary conditions

$$u(-1) = 0 \quad u(1) = 0 \tag{2.26}$$

and exact solution is $u(x) = \sin(\pi x)$. The function f is given by:

$$f = \epsilon\pi^2 \sin(\pi x) + b\pi \cos(\pi x) \tag{2.27}$$

In Table 2.1, we calculate the L^2 norm error for different values of N at each pair values of ϵ and b. We note that the L^2 norm error decreased when the number of nodes N is increasing. Fig. 2.1 shows the norm of the error decreases with N.

ϵ	b	$N = 4$	$N = 8$	$N = 12$	$N = 16$	$N = 20$
1	0	0.07508	2.3776×10^{-05}	3.1193×10^{-09}	1.6709×10^{-13}	1.4499×10^{-14}
1	1	0.11998	0.0001102	3.062×10^{-08}	2.7967×10^{-12}	1.6704×10^{-14}
0.1	1	0.86647	0.00089145	2.6888×10^{-07}	2.59×10^{-11}	5.12×10^{-15}
0.1	10	9.3577	0.011417	2.7545×10^{-06}	2.0402×10^{-10}	7.8208×10^{-15}

Table 2.1: Dependence of the L^2 norm of the error on N for different values of ϵ and b.

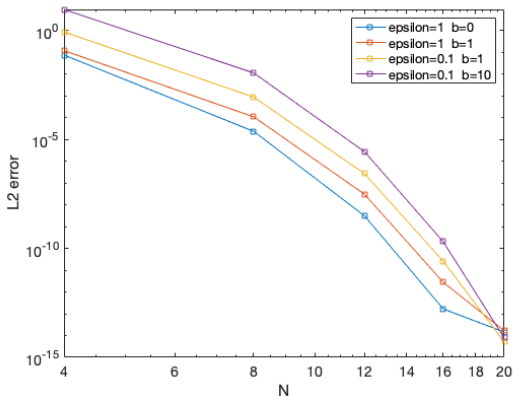

Figure 2.1: Dependence of the L^2 norm of the error on N.

Example 2. Consider the boundary value problem

$$-\epsilon u'' + bu' = f, \qquad x \in (-1, 1) \tag{2.28}$$

with boundary conditions

$$u(-1) = -e^{-1} \quad u(1) = -e^{1} \tag{2.29}$$

The exact solution is defined by

$$u(x) = e^{x}\ \cos(\pi x) \tag{2.30}$$

and the source term $f(x)$ is:

$$f(x) = \epsilon\, e^{x}[2\pi \sin(\pi x) + (\pi^2 - 1)\cos(\pi x)] + b\, e^{x}[\cos(\pi x) - \pi \sin(\pi x)] \tag{2.31}$$

Table 2.2 gives the L^2 norm of the error for various values of N for each pair of ϵ and b values. We found that if the number of nodes N increased, the values of L^2 norm error decreased, and Fig.2.2 displays that.

ϵ	b	$N=4$	$N=8$	$N=12$	$N=16$	$N=20$
1	0	0.12451	0.00011221	1.4702×10^{-08}	1.6243×10^{-12}	1.1689×10^{-14}
1	1	0.13855	4.0484×10^{-05}	5.3125×10^{-08}	4.2505×10^{-12}	2.1483×10^{-14}
0.1	1	1.1107	0.00065999	3.6054×10^{-07}	5.2954×10^{-11}	8.6055×10^{-15}
0.1	10	11.9258	0.0088735	3.63422×10^{-06}	4.202×10^{-10}	8.2754×10^{-15}

Table 2.2: Dependence of the L^2 norm of the error on N for different values of ϵ and b.

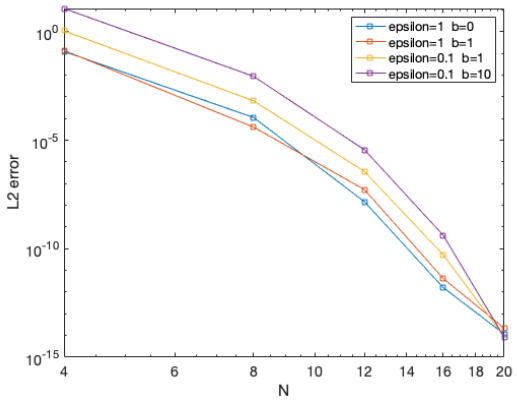

Figure 2.2: Dependence of the L^2 norm of the error on N.

2.3 Boundary Value Problems in 2D

Consider the Poisson's equation.

$$-\nabla^2 u = f, \qquad (x, y) \in [-1, 1] \times [-1, 1] \tag{2.32}$$

with boundary conditions

$$u = 0, \quad \text{on } \partial\Omega \tag{2.33}$$

Equations (2.32)-(2.33) are the strong formulation of the problem. The spectral approach aims to solve these equations in their weak form equivalent.

The weak formulation is generated by multiplying the strong form of the equations by a suitable test function selected from a suitable function space. Therefore we define a test space: (Owens Phillips, 2002; Burden Faires, 1997)

$$W = \{v \in H^1(\Omega) : v = 0 \; on \, \partial\Omega\} \tag{2.34}$$

Then

$$-\nabla^2 u.v = f.v \tag{2.35}$$

Integrating the equation over the entire domain

$$\iint_\Omega -\nabla^2 u.v \, dx \, dy = \iint_\Omega f.v \, dx \, dy \tag{2.36}$$

and applying integration by parts on the left-hand side we obtain,

$$\iint_\Omega \nabla u \cdot \nabla v \, dx \, dy - \int_{\partial\Omega} (\nabla u \cdot \overrightarrow{n}) v \, ds = \iint_\Omega f v \, dx \, dy \tag{2.37}$$

where $\nabla u \cdot \overrightarrow{n} = \dfrac{\partial u}{\partial x} n_x + \dfrac{\partial u}{\partial y} n_y$, and ds is the differential arc length along the boundary $\partial\Omega$.

Since $v = 0$ on $\partial\Omega$, we have

$$\iint_\Omega \nabla u \cdot \nabla v \, dx \, dy = \iint_\Omega f v \, dx \, dy \tag{2.38}$$

This is the weak formulation of equation (2.32), and can be written in the bilinear form: Find $u \in W$ s.t

$$a(u, v) = L(v) \quad , \forall v \in W \tag{2.39}$$

where the bilinear form $a(.,.)$ is defined by

$$a(u, v) = \iint_\Omega \nabla u \cdot \nabla v \, dx \, dy \tag{2.40}$$

and the linear formulation $L(.)$ is define by

$$L(v) = \iint_\Omega f v \, dx \, dy \tag{2.41}$$

The Galerkin approximation for (2.39) is: Find $u^N \in W^N$ such that

$$a(u_N, v_N) = L(v_N) \quad , \forall v_N \in W^N \tag{2.42}$$

Thus,

$$\iint_{\Omega} \nabla u_N \cdot \nabla v_N \, dx \, dy = \iint_{\Omega} f v_N \, dx \, dy \tag{2.43}$$

Since the approximation is conforming, i.e. $W^N \subset W$ we can substitute v^N in (2.39),

$$a(u, v_N) = L(v_N) \tag{2.44}$$

Then,

$$\iint_{\Omega} \nabla u \cdot \nabla v_N \, dx \, dy = \iint_{\Omega} f \cdot v_N \, dx \, dy \tag{2.45}$$

subtracting (2.45)-(2.43), we have

$$\iint_{\Omega} (\nabla u - \nabla u_N) \cdot \nabla v_N \, dx \, dy = 0 \tag{2.46}$$

Hence,

$$a(\nabla u - \nabla u_N, v_N) = 0, \quad \forall v_N \in W^N \tag{2.47}$$

To determine the Galerkin approximation we need to generate a linear system of equations of the form $Au = b$. To formulate the discrete weak problem(2.42), we consider

$$u_N(x, y) = \sum_{i=0}^{N} \sum_{j=0}^{N} u_{i,j} h_i(x) h_j(y) \tag{2.48}$$

$$v_N(x, y) = h_k(x) h_l(y), \qquad 1 \leq k, l \leq N - 1 \tag{2.49}$$

The L.H.S of (2.42) becomes

$$\begin{aligned}
a(u_N, v_N)_N &= \iint_\Omega \nabla u_N \cdot \nabla v_N \, dx \, dy \\
&= \iint_\Omega \left[\frac{\partial u_N}{\partial x} \frac{\partial v_N}{\partial x} + \frac{\partial u_N}{\partial y} \frac{\partial v_N}{\partial y} \right] dx \, dy \\
&= \iint_\Omega \left[\left(\sum_{i=0}^{N} \sum_{j=0}^{N} u_{i,j} h_i'(x) h_j(y) \right) h_k'(x) h_l(y) \right. \\
&\quad \left. + \left(\sum_{i=0}^{N} \sum_{j=0}^{N} u_{i,j} h_i(x) h_j'(y) \right) h_k(x) h_l'(y) \right] dxdy \\
&\simeq \sum_{m=0}^{N} \sum_{n=0}^{N} w_m w_n \left[\frac{\partial u_N}{\partial x}(x_m, y_n) \frac{\partial v_N}{\partial x}(x_m, y_n) + \frac{\partial u_N}{\partial y}(x_m, y_n) \frac{\partial v_N}{\partial y}(x_m, y_n) \right] \\
&= \sum_{m=0}^{N} \sum_{n=0}^{N} w_m w_n \left[\left(\sum_{i=0}^{N} \sum_{j=0}^{N} u_{i,j} h_i'(x_m) h_j(y_n) \right) h_k'(x_m) h_l(y_n) \right. \\
&\quad \left. + \left(\sum_{i=0}^{N} \sum_{j=0}^{N} u_{i,j} \; h_i(x_m) h_j'(y_n) \right) \; h_k(x_m) h_l'(y_n) \right]
\end{aligned} \tag{2.50}$$

The right hand side of (2.42) is

$$\iint_\Omega f v_N \, dx \, dy \quad \simeq \quad \sum_{m=0}^{N} \sum_{n=0}^{N} w_m w_n f(x_m, y_n) h_k(x_m) h_l(y_n) \tag{2.51}$$

Using the Kronecker delta property,

$$h_k(x_m) = \delta_{m,k} = \begin{cases} 1 & , \; k = m \\ 0 & , \; k \neq m \end{cases} \tag{2.52}$$

and define

$$D_{m,i} = h_i'(x_m) \tag{2.53}$$

Equations (2.50) and (2.51) become

$$\sum_{m=0}^{N}\sum_{n=0}^{N} w_m w_n \left[\left(\sum_{i=0}^{N} u_{i,n} D_{m,i}\right)\left(D_{m,k}\delta_{l,n}\right)\right] + \sum_{m=0}^{N}\sum_{n=0}^{N} w_m w_n \left[\left(\sum_{j=0}^{N} u_{m,j} D_{n,j}\right)\left(\delta_{k,m} D_{n,l}\right)\right] = \sum_{m=0}^{N}\sum_{n=0}^{N} w_m w_n f_{m,n}\delta_{m,k}\delta_{n,l}$$

$$w_l \sum_{i=0}^{N}\left[\sum_{m=0}^{N} w_m D_{m,i} D_{m,k}\right] u_{i,l} + w_k \sum_{j=0}^{N}\left[\sum_{n=0}^{N} w_n D_{n,j} D_{n,l}\right] u_{k,j} = w_k w_l f_{k,l} \tag{2.54}$$

then

$$w_l \sum_{i=0}^{N} B_{i,k} u_{i,l} + w_k \sum_{j=0}^{N} C_{j,l} u_{k,j} = w_k w_l f_{k,l} \tag{2.55}$$

where

$$B_{i,k} = \sum_{m=0}^{N} w_m D_{m,i} D_{m,k} \tag{2.56}$$

$$C_{j,l} = \sum_{n=0}^{N} w_n D_{n,j} D_{n,l} \equiv B_{j,l} \tag{2.57}$$

Equation (2.54) for $1 \le k, l \le N-1$ represents a linear system $Au = b$ of $(N-1)^2$ equations for the $(N-1)^2$ unknowns $u_{i,j},\ i, j = 1, \ldots, N-1$, with $u = 0$ on the boundary.

Let $I = (l-2)(N-1) + (k-1)$ and $J = (j-2)(N-1) + (i-1)$.

Then, the system reduces to

$$\sum_{J=1}^{(N-1)^2} A_{IJ} u_J = F_I, \qquad I = 1, \ldots, (N-1)^2 \tag{2.58}$$

where

$$A_{IJ} = w_l \sum_{m=0}^{N} w_m D_{m,i} D_{m,k} + w_k \sum_{n=0}^{N} w_n D_{n,j} D_{n,l} \tag{2.59}$$

and

$$F_L = w_k w_l f(x_k, y_l) \tag{2.60}$$

2.3.1 Numerical Examples and Comparisons

Example 1. Consider the boundary value problem

$$-\nabla^2 u = 2\pi^2 \sin(\pi x)\sin(\pi y), \qquad (x, y) \in [-1, 1] \times [-1, 1] \tag{2.61}$$

with boundary conditions

$$u(\pm 1, y) = u(x, \pm 1) = 0 \tag{2.62}$$

and exact solution $u(x, y) = \sin(\pi x)\sin(\pi y)$.

Table 2.3 illustrates the exponential convergence behaviour of the L^2 norm of the error for various values of N, and Fig. 2.3 displays that. The exact and approximate solutions are plotted in Fig. 2.4 when $N = 24$.

N	$L^2 error$
4	0.093892
8	5.2969×10^{-05}
12	9.2122×10^{-09}
16	5.8203×10^{-13}
20	3.3692×10^{-14}
24	1.5232×10^{-14}
32	8.4388×10^{-14}

Table 2.3: Dependence of the L^2 norm of the error fon N.

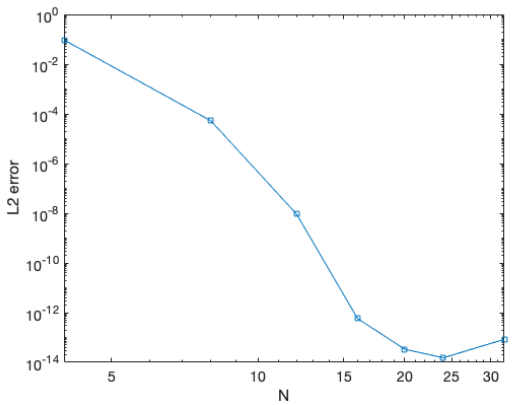

Figure 2.3: Plot showing the dependence of the L^2 norm of the error on N.

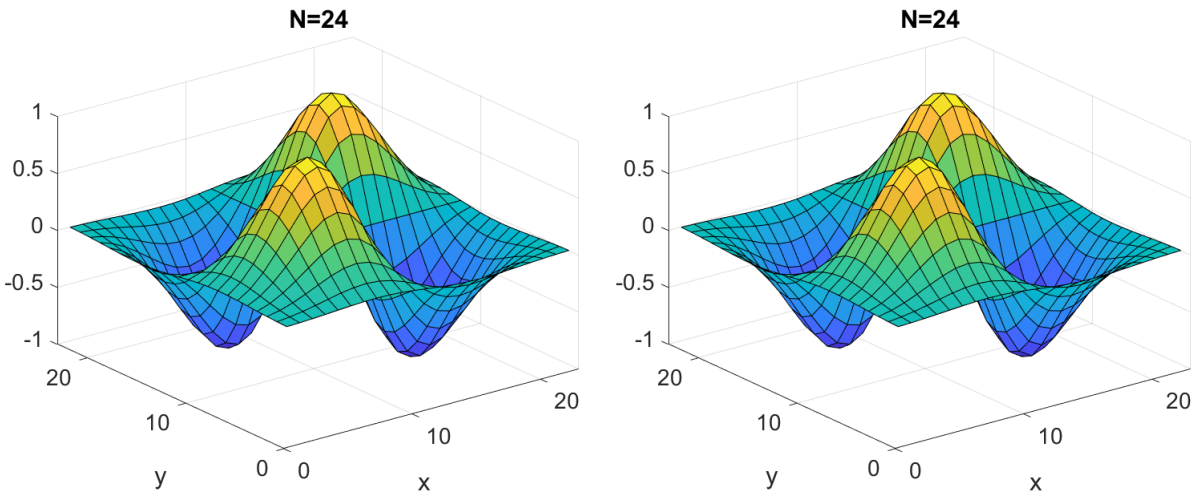

(a) (b)

Figure 2.4: (a) Exact and (b) approximate solutions of Poisson equation for $N = 24$. The exact solution is plotted using the GLL nodes.

Example 2. Consider the boundary value problem

$$-\nabla^2 u = 2\pi^2 \cos(\pi x)\cos(\pi y), \qquad (x, y) \in [-1, 1] \times [-1, 1] \tag{2.63}$$

with non-zero Dirichlet boundary conditions

$$u(\pm 1, y) = -\cos(\pi y) \tag{2.64}$$

$$u(x, \pm 1) = -\cos(\pi x) \tag{2.65}$$

and exact solution $u(x, y) = \cos(\pi x)\cos(\pi y)$.

Table 2.4 illustrates the exponential convergence behaviour of the L^2 norm of the error on N, and Fig. 2.5 plots this error which demonstrates exponential convergence to the true solution of the problem. The exact and approximate solutions are plotted in Fig. 2.6 when $N = 24$.

N	L^2 error
4	0.11923
8	1.2967×10^{-04}
12	3.7173×10^{-08}
16	3.2728×10^{-12}
20	1.8261×10^{-14}
24	4.1907×10^{-14}
32	8.911×10^{-14}

Table 2.4: Dependence of the L^2 norm of the error on N.

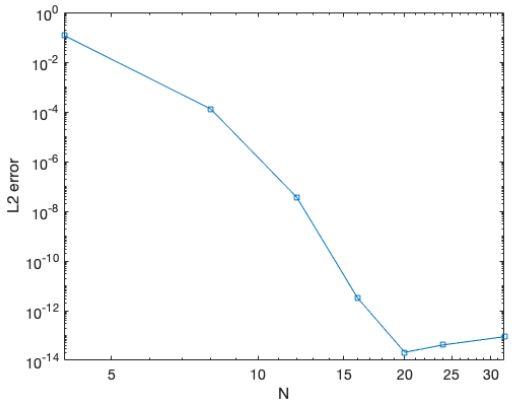

Figure 2.5: Plot showing the dependence of the L^2 norm of the error on N.

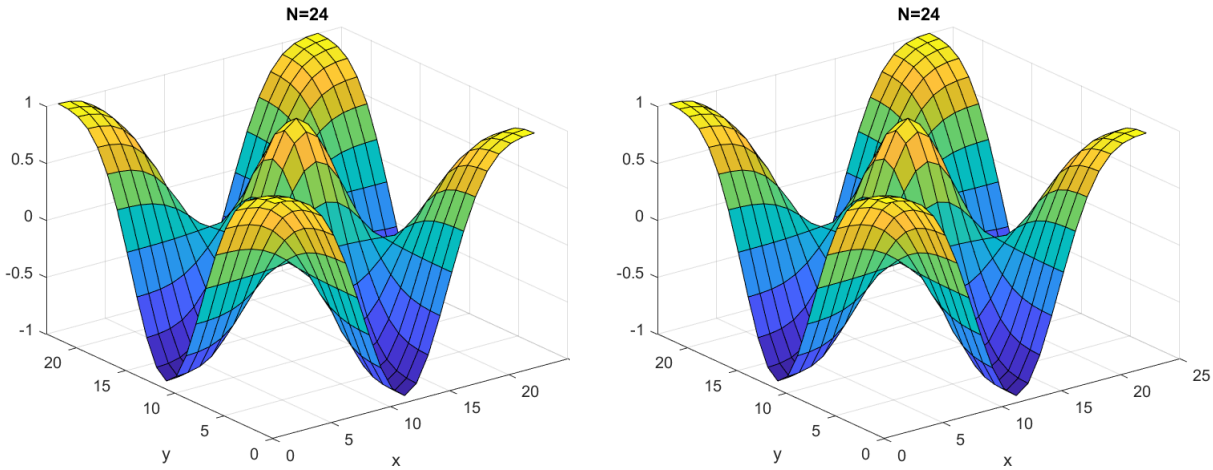

(a) (b)

Figure 2.6: (a) Exact and (b) approximate solutions of Poisson equation for $N = 24$. The exact solution is plotted using the GLL nodes.

2.4 Conclusions

We can come to the following conclusion based on the findings of this chapter: The weak versions of the convection-diffusion problem and Poisson's equation are discretized using the spectral technique. The so-called "exponential convergence" has been demonstrated in the results and figures showing the behaviour of the L_2 norm of the error on N, further demonstrating the outstanding error features of spectral approaches.

Chapter 3

Fundamentals of Fractional Calculus

3.1 Introduction

Mathematical models are often governed by integral and/or differential equations of integer order. With applications in a wide range of fields, such as computer science, biology, engineering, geophysics, physics, economics, and finance, the so-called fractional calculus has attracted a lot of attention recently (Consiglio Mainardi, 2021; Machado ., 2011).

A fractional derivative is an operator that generalizes the notion and definition of the standard ordinary derivative. In other words, if the fractional derivative of order α is denoted by the operator D^{α}, then it reduces to the ordinary differential operator D when $\alpha = 1$. It was not until the late 1900s that fractional differential equations—especially those with real or complex order derivatives—started to be used more frequently to model the irregular dynamics of many processes connected to complex systems (Samko ., 1993; Gorenflo Mainardi, 1997; Baleanu ., 2012).

Differentiation is made relatively easy by ordinary derivatives, which make it possible to apply rules like the chain rule in a straightforward way. The differentiation of composite functions is made more difficult by fractional derivatives, which rely on memory-based integral formulations. Because of this additional complexity, fractional derivatives are especially useful when modelling memory-dependent systems where past states affect current behaviour, including viscoelastic materials and anomalous diffusion (Baleanu ., 2012).

To solve fractional differential equations, a practical and simple-to-use approach is necessary. Many established techniques have distinct limitations. The techniques discussed by Oldham Spanier (1974) and Miller Ross (1993) for fractional differential equations of rational order are inapplicable when dealing with differential equations of more arbitrary

real orders. Conversely, the series method (Oldham Spanier, 1974; Friedrich, 1991) and the iteration method (Samko ., 1987) enable the solution of fractional differential equations of arbitrary real order, but are only effective for relatively simple equations. The one-parameter Mittag-Leffler function $E_\alpha(z) = \sum_{j=0}^{\infty} \frac{z^j}{\Gamma(\alpha j+1)}, z \in \mathbb{C}$, was employed by several researchers in their studies (see Bagley Calico (1991); Caputo Mainardi (1971), for example). The Fox H-function (Fox, 1961), which appears to be too generic to be employed regularly in applications, is preferred by some other authors (Schneider Wyss, 1989; Baumann, 1991).

A method that is free of the issues mentioned above and appropriate for a wide variety of initial value problems for fractional differential equations was developed by Podlubny (1997) in place of the diversity of approaches described above. The formula for the Laplace transform of the Mittag-Leffler function in two parameters, $E_{\alpha,\gamma}(x)$, serves as the foundation for this method, which applies Laplace transform methodology.

This chapter, which is divided into the following five sections, covers some of the fundamental concepts associated with fractional calculus. Section 3.2 introduces the Laplace transform for fractional derivatives. In Section 3.3, Mittag-Leffler (ML) functions and their Laplace transforms for different numbers of parameters are presented. Conclusions are presented in Section 3.4.

3.1.1 Fractional operators

1. **Riemann–Liouville fractional derivatives**

   The Riemann-Liouville fractional derivative of order $\alpha > 0$ is defined by:

$$ {}_aR_t^\alpha g(t) = \frac{1}{\Gamma(n-\alpha)} \frac{d^n}{dt^n} \int_a^t (t-t')^{n-\alpha-1} g(t')dt', \;\; n-1 < \alpha < n, \;\; n = 1, 2, \ldots, \;\; 0 \le t \le T \tag{3.1} $$

   where g is a function for which the integral (3.1) exists, for example, $g \in C^n[0, T]$.

   When $a \to -\infty$ this is known as Weyl's fractional derivative.

Weyl's composition rule

$$\frac{\partial^\alpha}{\partial t^\alpha}\left(\frac{\partial^\beta}{\partial t^\beta}\right)g(t) = \frac{\partial^{\alpha+\beta}}{\partial t^{\alpha+\beta}}\,g(t),\ 0 \le t \le T,\ 0 < \alpha,\ \beta < 1,\ 0 < \alpha+\beta < 1, \tag{3.2}$$

where $\dfrac{\partial^\alpha}{\partial t^\alpha} =_a R_t^\alpha$, and ${}_aR_t^\alpha$ is the Riemann-Liouville fractional derivative of order α.

For $g \in C^1[0,T]$, Eq. (3.2) is satisfying $g(0) = \dfrac{\partial^\alpha}{\partial t^\alpha}g(0) = 0$

Properties of the Riemann-Liouville fractional derivative:

- the Riemann–Liouville fractional integral is

$$I_t^\alpha g(t) =_a R_t^{-\alpha} g(t) = \frac{1}{\Gamma(\alpha)}\int_a^t (t-t')^{\alpha-1} g(t')dt',\ \ \alpha > 0, \tag{3.3}$$

  for function g for which this integral exists.

- ${}_aR_t^{-\alpha_2}({}_aR_t^{-\alpha_1}g(t)) =_a R_t^{-(\alpha_1+\alpha_2)}g(t),\ \ 0 < \alpha_1, \alpha_2 < 1,\ 0 < \alpha_1 + \alpha_2 < 1$

- the Riemann–Liouville fractional derivative satisfies

$${}_aR_t^\alpha g(t) = \frac{d^p}{dt^p}({}_aR_t^{-(p-\alpha)}g(t)),\ \ p-1 < \alpha \le p,\ p = 1, 2, \ldots$$

- In particular if $p = 1$, then for $0 < \alpha \le 1$:

$${}_aR_t^\alpha g(t) = \frac{d}{dt}({}_aR_t^{-(1-\alpha)}g(t))$$

- ${}_aR_t^{\alpha_1}({}_aR_t^{-\alpha_2}g(t)) =_a R_t^{\alpha_1-\alpha_2}g(t),\quad \alpha_1 > \alpha_2 \ge 0.$

2. **Caputo fractional derivative**

The Caputo fractional derivative of order $\alpha > 0$ with $a = 0$, denoted by ${}_0D_t^\alpha$, is obtained by interchanging the order of differentiation and integration in equation (3.1). It is defined as follows:

$$D_t^\alpha g(t) = \frac{1}{\Gamma(1-\alpha)}\int_0^t (t-t')^{-\alpha} g^{(1)}(t')dt',\ 0 \le t \le T,\ 0 < \alpha \le 1 \tag{3.4}$$

where $g^{(1)}(t) = \dfrac{dg(t)}{dt}$, $g \in C^1[0,T]$.

More generally,

$$D_t^\alpha g(t) = \begin{cases} \dfrac{1}{\Gamma(m-\alpha)} \displaystyle\int_0^t (t-t')^{m-\alpha-1} g^{(m)}(t')dt' & , \ m-1 < \alpha < m \\ \\ \dfrac{d^m}{dt^m} g(t) & , \ \alpha = m, \end{cases} \tag{3.5}$$

where m is a positive integer, $m \in \mathcal{N}$.

The Caputo fractional derivative is equivalent to the regularised Riemann-Liouville fractional derivative since

$$\begin{aligned} D_t^\alpha g(t) &= R_t^{-(1-\alpha)} \frac{d}{dt} g(t) \\ &= \frac{1}{\Gamma(1-\alpha)} \left[\frac{d}{dt} \int_0^t (t-t')^{-\alpha} g(t')dt' - \frac{g(0)}{t^\alpha} \right] \\ &= R_t^\alpha g(t) - \frac{g(0)}{t^\alpha \Gamma(1-\alpha)}, \ \ 0 < \alpha \leq 1, \end{aligned} \tag{3.6}$$

since $R_t^\alpha 1 = \frac{1}{t^\alpha \Gamma(1-\alpha)}$.

The material described in Sections 3.2 and 3.3 is based on the contribution of Podlubny (1997).

3.2 Laplace Transforms

In physical and mathematical applications where initial conditions are typically represented in terms of integer-order derivatives, we highlight the substantial importance of the Caputo fractional derivative in solving initial-value problems. The Laplace transform makes it simple to see this. The Laplace transform of a function $f(t)$ is defined by

$$\tilde{f}(s) = \mathcal{L}\{f(t); s\} = \int_0^\infty e^{-st} f(t)\, dt, \ \ s > 0 \tag{3.7}$$

The Laplace transform of the Caputo derivative of order α of a function $f(t)$ with $m-1 < \alpha \leq m$ is

$$\mathcal{L}\{D_t^\alpha f(t); s\} = s^\alpha \tilde{f}(s) - \sum_{k=0}^{m-1} s^{\alpha-1-k} f^{(k)}(0^+) \tag{3.8}$$

where $f^{(k)}(0^+) := \lim_{t\to 0^+} D_t^k f(t)$.

The Laplace transform of the Riemann-Liouville derivative of order α has the following equivalent rule:

$$\mathcal{L}\{R_t^\alpha f(t); s\} = s^\alpha \tilde{f}(s) - \sum_{k=0}^{m-1} s^{m-1-k} g^{(k)}(0^+) \tag{3.9}$$

where $g^{(k)}(0^+) := \lim_{t\to 0^+} D_t^k g(t)$, $g(t) := I_t^{m-\alpha} f(t)$ where $I_t^{m-\alpha}$ is defined in Eq. (3.3)

(Consiglio Mainardi, 2021; Kexue Jigen, 2011; Mainardi, 2010; Bagley Torvik, 1983).

3.3 Mittag-Leffler functions (MLF)

Magnus Gustaf Mittag-Leffler, a Swedish mathematician, developed methods for the summation of divergent series at the beginning of the 19th century, which led to the development of the Mittag-Leffer (ML) function. Studying ML functions is primarily motivated by their significance in fractional calculus, where they play the same essential role as the exponential function in integer order calculus (Podlubny, 1997; Garra Garrappa, 2018; Nigmatullin, 1984).

3.3.1 Mittag-Leffler function in one parameter

Definition

A one-parameter Mittag-Leffler type function is defined by the series expansion

$$E_\alpha(z) = \sum_{k=0}^{\infty} \frac{z^k}{\Gamma(\alpha k + 1)}, \quad z \in \mathbb{C}, \quad 0 < \alpha < 1 \tag{3.10}$$

Fact 1:

If $-t = z$, $t \geq 0$ and real, then

- Generalization of the Exponential Function:

When $\alpha = 1$, the Mittag-Leffler function reduces to the exponential function $E_1(-t) = e^{-t}$.

- Asymptotic Behaviour:

  Fig. 3.1 exhibits some plots of $E_\alpha(-t^\alpha)$ for some values of the parameter α where $0 < \alpha < 1$ where $E_\alpha(-t^\alpha) \simeq \frac{c_\alpha}{t^\alpha}$, as $t \to \infty$, where $c_\alpha = \frac{1}{\Gamma(1-\alpha)}$. The constant c_α is known as the Poincaré asymptotic (Mainardi, 2013; Apelblat, 2020). Also

$$\frac{1}{1 + x\,\Gamma(1-\alpha)} \leq E_\alpha(-x) \leq \frac{1}{1 + \frac{x}{\Gamma(1+\alpha)}}, \quad x \geq 0 \tag{3.11}$$

  (see Simon (2014))

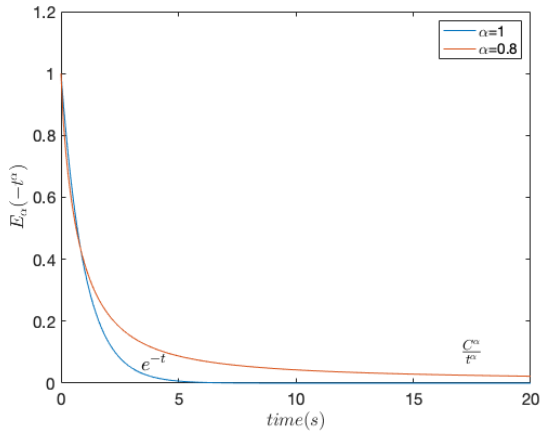

Figure 3.1: The Mittag-Leffler function $E_\alpha(-t^\alpha)$ for $\alpha = 0.8, 1$ and $0 \leq t \leq 20$.

Fact 2:

The function $f(t) = E_\alpha(\lambda t), \;\; t, \lambda \in$, is the eigenfunction of the fractional equation:

$$\partial_t^\alpha f(t) = \lambda f(t) \tag{3.12}$$

where ∂_t^α is the Caputo fractional derivative (Meerschaert Sikorskii, 2019).

3.3.2 Mittag-Leffler function in two parameters

Definition

The following series expansion defines a two-parameter function of Mittag-Leffler type

(Szegö, 1955) as

$$E_{\alpha,\beta}(z) = \sum_{k=0}^{\infty} \frac{z^k}{\Gamma(\alpha k + \beta)}, \quad z \in \mathbb{C}, \quad \alpha > 0, \beta > 0 \tag{3.13}$$

Fact:

If $0 < \alpha < 1$, then the Poincaré asymptotic expansion is

$$E_{\alpha,\beta}(z) \cong -\sum_{k=1}^{N^*} \frac{1}{\Gamma(\beta - \alpha k)} \frac{1}{z^k}, \quad z \to -\infty \tag{3.14}$$

where $N^* \in N$ and $N^* \neq 1$ (Haubold ., 2011).

When $z = -x$, $x \in$, the Poincaré asymptotic expansion is

$$E_{\alpha,\beta}(-x) \cong -\sum_{k=1}^{\infty} \frac{(-1)^k}{x^k \ \Gamma(\beta - \alpha k)}, \quad x \to +\infty \tag{3.15}$$

where $x \geq 0$, x is real.

Relationship to other functions

Some special cases of the ML function are as follows:

1.
$$\begin{aligned} E_{1,1}(z) &= e^z, & E_{1,2}(z) &= \frac{e^z - 1}{z} \\ E_{2,1}(z) &= \cosh\left(\sqrt{z}\right), & E_{2,2}(z) &= \frac{\sinh\left(\sqrt{z}\right)}{\sqrt{z}} \end{aligned} \tag{3.16}$$

2. The Mittag-Leffler function in one parameter is obtained for $\beta = 1$ as $E_{\alpha,1}(z) = \sum_{k=0}^{\infty} \frac{z^k}{\Gamma(\alpha k+1)} \equiv E_{\alpha}(z)$ (Podlubny, 1997).

The Laplace transform of the Mittag-Leffler function in two parameters

The Laplace transform of the following function

$$E_{\alpha,\beta}^{(k)}(t) = \frac{d^k}{dt^k} E_{\alpha,\beta}(t), \quad t \in, \quad k = 1, 2, \ldots \tag{3.17}$$

follows from relationship (3.16). The Mittag-Leffler function $E_{\alpha,\beta}$ is a generalization of the exponential function e^z, and the exponential function is a particular case of the Mittag-Leffler function $\alpha = \beta = 1$. Therefore, the Laplace transform of the Mittag-Leffler function is

$$\mathcal{L}\{E^{(k)}_{\alpha,\beta}(t);\mathfrak{p}\} = \int_0^\infty e^{-\mathfrak{p}t}\ t^{\alpha k+\beta-1}\ E^{(k)}_{\alpha,\beta}(\pm at^\alpha)\ dt = \frac{k!\ \mathfrak{p}^{\alpha-\beta}}{(\mathfrak{p}^\alpha \mp a)^{k+1}}, \mathfrak{p} > 0 \tag{3.18}$$

where $Re(\mathfrak{p}) > |a|^{\frac{1}{\alpha}}$.

3.3.3 Mittag-Leffler function in three parameters

Definition

A three-parameter Mittag-Leffler function called the Prabhakar function is examined. In models of Havriliak-Negami type, this function is essential in explaining the anomalous dielectric characteristics in disordered materials and heterogeneous systems that exhibit simultaneous nonlocality and nonlinearity (Garra Garrappa, 2018).

$$E^{(\gamma)}_{\alpha,\beta}(z) = \frac{1}{\Gamma(\gamma)}\sum_{k=0}^{\infty}\frac{\Gamma(\gamma+k)\ z^k}{k!\ \Gamma(\alpha k+\beta)}, \quad z \in \mathbb{C}, \quad \alpha,\beta,\gamma > 0 \tag{3.19}$$

Note that,

$$E^{(n)}_{\alpha,\beta}(x) = n!\ E^{\ (n+1)}_{\alpha,\ n\ \alpha+\beta}(x). \tag{3.20}$$

The Laplace transform of the Mittag-Leffler function in three parameters

$$\mathcal{L}\{E^{(\gamma)}_{\alpha,\beta}(t);\mathfrak{p}\} = \int_0^\infty e^{-\mathfrak{p}t}\ t^{\beta-1}\ E^{(\gamma)}_{\alpha,\beta}(at^\alpha)\ dt = \frac{1}{\mathfrak{p}^\beta}\sum_{k=0}^{\infty}\frac{\Gamma(\gamma+k)}{\Gamma(\gamma)}\left(\frac{a}{\mathfrak{p}}\right)^k \tag{3.21}$$

and

$$\mathcal{L}\left(t^{\beta-1}E^{(\gamma)}_{\alpha,\beta}(xt^\alpha);\mathfrak{p}\right) = \frac{\mathfrak{p}^{\alpha\gamma-\beta}}{(\mathfrak{p}^\alpha - x)^\gamma}, \quad \mathfrak{p} > |x|^{\frac{1}{\alpha}} \tag{3.22}$$

The Riemann-Liouville fractional derivative of the Mittag-Leffler function in three parameters is

$$R_t^{\gamma}\left[t^{\alpha k+\beta-1}E_{\alpha,\beta}^{(k)}(\lambda t^{\alpha})\right] = t^{\alpha k+\beta-\gamma-1}E_{\alpha,\beta-\gamma}^{(k)}(\lambda t^{\alpha}), \alpha,\beta>0, 0<\gamma<1, \lambda>0 \tag{3.23}$$

3.3.4 Tools for testing candidate solutions

A rule for fractional differentiation of an integral depending on a parameter

When the upper limit also depends on the parameter we have:

$${}_a\mathcal{D}_t{}^{\alpha}\int_a^t F(t,t')\,dt' = \int_a^t {}_{t'}\mathcal{D}_t{}^{\alpha}F(t,t')\,dt' + \lim_{t'\to t-0}\ {}_{t'}\mathcal{D}_t{}^{\alpha-1}F(t,t'), \quad 0<\alpha<1. \tag{3.24}$$

3.4 Conclusions

In this chapter we have introduced the basic ideas and notations associated with fractional calculus. In particular, we have defined various fractional derivatives and stated their key properties. These concepts underpin the theoretical work in this thesis. More specifically, we have introduced the fractional operators. In the upcoming chapters, these will be used to define the time fractional derivative of Fractional Maxwell Models (FMM). As well as, we have presented the Mittag-Leffler function (MLF) and Laplace transform, which are used to define the Green's function approach. The next chapter will employ this technique to derive exact solutions to the fractional differential equations. This technique is one of the most effective methods for dealing with the Caputo fractional derivative due to several key advantages. First, it simplifies complex problems by transforming complex fractional differential equations into simpler algebraic equations through the application of the Laplace transform. Additionally, it effectively represents fractional behaviour, much like the exponential function in classical equations, with the Mittag-Leffler function naturally capturing the dynamics of systems with fractional characteristics. Moreover, this approach is highly applicable to real-world problems, as the Caputo derivative allows for the straightforward incorporation of initial conditions, making it particularly useful in

practical applications. Therefore, this approach which is the combination of the Laplace transform and Mittag-Leffler function (MLF) is an effective tool for solving fractional differential equations since it can be applied to a wide range of equations and boundary value problems.

Chapter 4

Fractional Maxwell Models

4.1 Introduction

This chapter demonstrates how the behaviour of viscoelastic fluids can be characterized using mechanical models and how general fractional models can be derived by arranging spring-pot elements in series and/or parallel. Subsequently, these models are used to fit experimental data and the quality of the fractional modes is assessed by considering oscillatory shear data across the frequency range using curve fitting techniques.

This chapter begins with a brief summary of the viscoelastic behaviour that can be described using mechanical models, as detailed in Section 4.2.

In Section 4.3, the Green's function solution of the Single-Mode fractional Maxwell model is derived using the formula for the Laplace transform of the Mittag-Leffler function in two parameters. This is an original contribution. We also derive expressions of the complex, storage, and loss modulus, and show how the relaxation time of a material may be determined. At the end of this section, the asymptotic behaviour of the storage, G', and loss, G'', moduli for the Fractional Maxwell Model (FMM), the Fractional Maxwell Liquid (FML), and the Fractional Maxwell Gel (FMG) is investigated. Also, we employ curve fitting techniques to evaluate the model's validation and accuracy across its frequency range.

In Section 4.4, an extension of the general fractional Maxwell model is proposed by introducing an additional fractional time derivative, effectively adding a spring-pot element in series. The corresponding fractional Green's function solution is obtained using the Laplace transform of the Mittag-Leffler function in two parameters. Additionally, we derive expressions for the loss, storage, and complex moduli before determining the relax-

ation time. The asymptotic behaviour of the storage and loss moduli for the Fractional Maxwell Model (FMM), Fractional Maxwell Liquid (FML), and Fractional Maxwell Gel (FMG) is studied. Finally, we employ curve fitting techniques to evaluate the model's validation and accuracy across its frequency range. In Section 4.5, an extension of the general fractional Maxwell model is proposed by introducing two additional fractional time derivatives, effectively adding fractional elements in parallel. The corresponding fractional Green's function solution is obtained using the Laplace transform of the two-parameter Mittag-Leffler function. Additionally, expressions for the dynamic modulus are derived. Conclusions are presented in Section 4.6.

4.2 Description of Viscoelastic Behaviour using Mechanical Models

A variety of complex fluids and soft solids, from everyday products to fracking fluids, possess viscoelastic characteristics that are described by various kinds of relaxation time scales. This can provide significant challenges to the quantitative constitutive modelling of the material's behaviour. In its most basic form, a linear elastic spring (Hooke's law) and a constant viscosity dashpot (Newton's law) can be mechanically combined to model both solid-like and liquid-like behaviour for a viscoelastic material. The stress-strain relations for elastic solids and viscous fluids are given by

$$\tau_e(t) = \mathbb{G}\ \gamma_e(t), \tag{4.1}$$

$$\tau_v(t) = \eta\, \dot{\gamma}_v(t), \tag{4.2}$$

respectively, where the strain is denoted by $\gamma_e(t)$, the stress is $\tau(t)$, the strain rate is $\dot{\gamma}_v$, the elastic shear modules is $\mathbb{G}$, the viscosity coefficient is η, and the subscripts e and v denote the elastic and viscous behaviour, respectively (Schiessel Blumen, 1993; Bird ., 1987). These two models can be represented in terms of mechanical models as shown in Fig. 4.1 where the spring describes elastic behaviour and the dash-pot represents viscous

behaviour.

Figure 4.1: Basic elements of a mechanical model: (a) spring; (b) dashpot.

4.2.1 The Maxwell model

In the framework of mechanical models, the Maxwell model, which was developed by Maxwell (1867), can be represented by coupling a dashpot and a linear spring in series. This configuration is shown in Fig. 4.2. The total stress of the system can be calculated as follows:

Let $\dot{\gamma}_e$ and $\dot{\gamma}_v$ be the rate of strain due to the spring and dashpot, respectively, then

$$\tau(t) = \tau_e(t) = \tau_v(t) \tag{4.3}$$

$$\dot{\gamma} = \dot{\gamma}_e + \dot{\gamma}_v \tag{4.4}$$

Substituting Eq.(4.1) and Eq.(4.2) into Eq.(4.4) gives the following equation relating the total stress and strain for the Maxwell model

$$\tau(t) + \lambda\,\dot{\tau}(t) = \eta\,\dot{\gamma} \tag{4.5}$$

where $\dot{\tau}$, $\dot{\gamma}$ denote the rates of stress and strain, respectively, and the relaxation time is defined as the ratio of the dashpot's viscosity coefficient to the linear spring's stiffness, i.e. $\lambda = \frac{\eta}{\mathbb{G}}$ (Bird ., 1987; Larson, 1999; Hajikarimi Nejad, 2021).

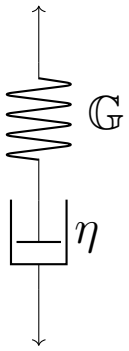

Figure 4.2: Maxwell model

4.2.2 The generalized Maxwell model

Combining Maxwell models in parallel allows us to model viscoelstic materials that possess a spectrum of relaxation times rather than a single relaxation time. The mechanical model for a two-mode Maxwell model is shown in Fig. 4.3.

Expressions for the stress and strain of the system can be derived as follows. Since the generalised Maxwell model is connected in parallel:

$$\tau(t) = \tau_{m_1}(t) + \tau_{m_2}(t) \tag{4.6}$$

$$\gamma(t) = \gamma_1(t) = \gamma_2(t) \tag{4.7}$$

where subscript m_1 refers to Maxwell element 1 that can be simply described as Eq.(4.8), and m_2 refers to Maxwell element 2 described as Eq.(4.9), respectively. For each of the elements we have

$$\tau_1(t) + \lambda_1 \dot{\tau}_1(t) = \eta_1 \dot{\gamma}(t) \tag{4.8}$$

$$\tau_2(t) + \lambda_2 \dot{\tau}_2(t) = \eta_2 \dot{\gamma}(t) \tag{4.9}$$

Since the total stress of the system is

$$\tau(t) = \tau_1(t) + \tau_2(t)$$

then,

$$\tau_2(t) = \tau(t) - \tau_1(t)$$

Substituting for $\tau_2(t)$ in Eq.(4.9) yields

$$(\tau(t) - \tau_1(t)) + \lambda_2 \left(\dot{\tau}(t) - \dot{\tau}_1(t)\right) = \eta_2 \, \dot{\gamma}(t) \tag{4.10}$$

then,

$$\dot{\tau}_1(t) = \frac{1}{\lambda_2} \left[-\eta_2 \, \dot{\gamma}(t) + \tau(t) - \tau_1(t) + \lambda_2 \dot{\tau}(t)\right] \tag{4.11}$$

substituting for $\dot{\tau}_1(t)$ in Eq.(4.8) gives

$$\tau_1(t) + \frac{\lambda_1}{\lambda_2} \left[-\eta_2 \, \dot{\gamma}(t) + \tau(t) - \tau_1(t) + \lambda_2 \dot{\tau}(t)\right] = \eta_1 \, \dot{\gamma}(t) \tag{4.12}$$

which, on rearrangement gives

$$\left(1 - \frac{\lambda_1}{\lambda_2}\right) \tau_1(t) = \left(\eta_1 + \frac{\lambda_1}{\lambda_2} \, \eta_2\right) \dot{\gamma}(t) - \frac{\lambda_1}{\lambda_2} \, \tau(t) - \lambda_1 \, \dot{\tau}(t) \tag{4.13}$$

or

$$\tau_1(t) = \frac{1}{(\lambda_2 - \lambda_1)} \left[(\lambda_2 \, \eta_1 + \lambda_1 \, \eta_2)\dot{\gamma}(t) - \lambda_1 \, \tau(t) - \lambda_1 \, \lambda_2 \, \dot{\tau}(t)\right] \tag{4.14}$$

Taking the 1^{st} derivative of Eq.(4.14) gives

$$\dot{\tau}_1(t) = \frac{1}{(\lambda_2 - \lambda_1)} \left[(\lambda_2 \, \eta_1 + \lambda_1 \, \eta_2) \, \ddot{\gamma}(t) - \lambda_1 \, \dot{\tau}(t) - \lambda_1 \, \lambda_2 \, \ddot{\tau}(t)\right] \tag{4.15}$$

In order to derive the equation for the total stress $\tau(t)$, which is the constitutive equation for the generalised Maxwell model, substitute for $\tau_1(t)$ and $\dot{\tau}_1(t)$ in Eq. (4.8) using Eq.(4.14) and Eq.(4.15) which gives

$$\tau(t) + (\lambda_1 + \lambda_2) \, \dot{\tau}(t) + (\lambda_1 \, \lambda_2) \, \ddot{\tau}(t) = (\eta_1 + \eta_2)\dot{\gamma}(t) + (\lambda_2 \, \eta_1 + \lambda_1 \, \eta_2) \, \ddot{\gamma}(t) \tag{4.16}$$

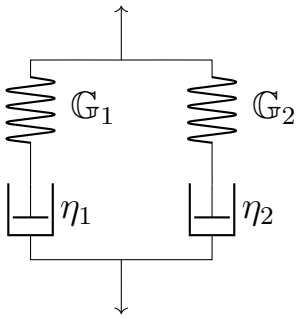

Figure 4.3: Generalized Maxwell model

4.2.3 Fractional Models

The integer-order viscoelastic models have the advantage of using spring-dashpot components to describe linear behaviour viscoelastic materials. The accurate description of the viscoelastic response with such models normally needs a series of model components. For example, the generalized Maxwell model requires 8–25 elements to describe the mechanical behaviour of a bituminous material accurately. Therefore using integer-order models means that many parameters may be needed to describe the desired model. Having a large number of parameters increases calculation time, and so models with a large number of parameters are not practical to use in real-world applications. Therefore, alternative models that have a fewer parameters are performed. Several fractional-order models have been developed to solve the aforementioned problem and decrease the required number of parameters without reducing the precision of the model (Hajikarimi Nejad, 2021).

Simple Fractional Element

Since most viscous materials consist of solid and liquid components, there is a mechanical element that interpolates between a spring ($\alpha = 0$) and dashpot ($\alpha = 1$) (see Fig 4.4), and this mechanical element can be used to describe the behaviour of viscous materials. Schiessel . (1995) derive an expression in terms of three parameters; an elastic modulus $\mathbb{E}$, a time scale λ, and a fractional exponent $0 \leq \alpha \leq 1$. The stress is, thus, written as

$$\tau(t) = \mathbb{E}\lambda^{\alpha} \frac{\partial^{\alpha}\gamma}{\partial t^{\alpha}}$$

However, only the quantities of $\mathbb{E}\lambda^{\alpha}$ and α can actually be measured experimentally.

This response can be written in terms of a fractional derivative as follows:

$$\tau(t) = \mathbb{V}\frac{\partial^{\alpha}\gamma}{\partial t^{\alpha}}, \tag{4.17}$$

where $\mathbb{V} = \mathbb{E}\lambda^{\alpha}$ is a quasi-property with units of Pa.s$^{\alpha}$ (Koeller, 1984; Torvik Bagley, 1984).

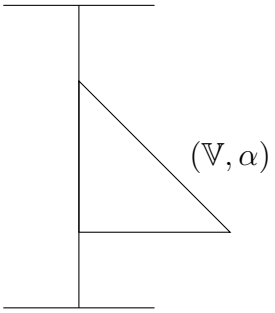

Figure 4.4: Spring-Pot Element

4.3 Single-Mode Fractional Maxwell Model

In order to create fractional constitutive models that can represent more complex rheological responses, researchers have constructed spring-pot elements in series and parallel (Koeller, 1984; Palade ., 1996). The Fractional Maxwell Model (FMM) is a commonly used combination in the literature. It is depicted in Figure 4.5 and includes the elements of a linear combination of two spring-pots in series (Friedrich, 1991). Since most complex materials display different power-law behaviour at short and long time scales, which may be well characterised by the FMM, this fractional framework is extensively applicable (Friedrich, 1991; Mainardi, 2010; Yang ., 2010; Jaishankar McKinley, 2014; Faber ., 2017; Schiessel ., 1995).

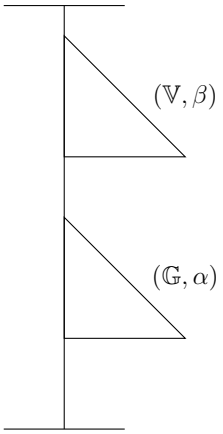

Figure 4.5: Single-Mode Fractional Maxwell Model

4.3.1 Derivation of the Single-Mode Fractional Maxwell Model

The series combination indicates that the total stress and strain of the system satisfy the following relationships in terms of the stress and strain of the individual components:

$$\tau(t) = \tau_1(t) = \tau_2(t) \tag{4.18}$$

$$\dot{\gamma}(t) = \dot{\gamma}_1(t) + \dot{\gamma}_2(t) \tag{4.19}$$

where $\tau(t)$ is the stress and $\dot{\gamma}(t)$ is the strain rate for the FMM.

For each spring-pot we have

$$\tau_1(t) = \mathbb{V}\,\frac{d^{\beta}\gamma_1(t)}{dt^{\beta}} \tag{4.20}$$

$$\tau_2(t) = \mathbb{G}\,\frac{d^{\beta-\alpha}\gamma_2(t)}{dt^{\beta-\alpha}} \tag{4.21}$$

where $0 < \alpha \leq \beta \leq 1$.

For a fixed β and $\beta - \alpha$, the constants $\mathbb{V}$ and $\mathbb{G}$ have physical dimensions Pa.s$^{\beta}$ and Pa.s$^{\beta-\alpha}$, respectively. The constants $\mathbb{V}$ and $\mathbb{G}$ represent a quasi-property and a generalised modulus, respectively. These quasi-properties are more clearly recognized as the numerical measurements of a dynamical process, as they are not actual material properties like a modulus or viscosity.

Now

$$\gamma(t) = \gamma_1(t) + \gamma_2(t) \tag{4.22}$$

so that

$$\frac{d^\beta \gamma(t)}{dt^\beta} = \frac{d^\beta \gamma_1(t)}{dt^\beta} + \frac{d^\beta \gamma_2(t)}{dt^\beta} \tag{4.23}$$

Now, from Eq.(4.18) and Eq.(4.20) we obtain

$$\frac{d^\beta \gamma_1(t)}{dt^\beta} = \frac{1}{\mathbb{V}}\tau_1(t) = \frac{1}{\mathbb{V}}\tau(t) \tag{4.24}$$

and from Eq.(4.18) and Eq.(4.21) we obtain

$$\frac{d^\alpha \tau_2(t)}{dt^\alpha} = \frac{d^\alpha \tau(t)}{dt^\alpha} = \mathbb{G}\frac{d^\alpha}{dt^\alpha}\left(\frac{d^{\beta-\alpha}\gamma_2(t)}{dt^{\beta-\alpha}}\right) = \mathbb{G}\frac{d^\beta \gamma_2(t)}{dt^\beta} \tag{4.25}$$

Therefore, the constitutive equation for a single fractional Maxwell element is

$$\tau(t) + \frac{\mathbb{V}}{\mathbb{G}}\frac{d^\alpha \tau(t)}{dt^\alpha} = \mathbb{V}\frac{d^\beta \gamma(t)}{dt^\beta}, \quad 0 < \alpha \leq \beta \leq 1 \tag{4.26}$$

where $\frac{\mathbb{V}}{\mathbb{G}}$ is the relaxation time of the fluid and $\mathbb{V}$ is the viscosity (rate-independent). Eq.(4.26) is a constitutive equation with the ability to describe three different states: a linear elastic solid when $(0 < \alpha = \beta < 1)$, a viscous Newtonian fluid when $(0 < \alpha < 1, \beta = 1)$, and a combination of both states when $(0 < \alpha < \beta < 1)$ (Rathinaraj ., 2021; Yang ., 2010; Ferras ., 2018).

The relationship between $(\mathbb{E}_1, \lambda_1, \mathbb{E}_2, \lambda_2)$, $(\mathbb{E}, \lambda^\alpha)$ and $\mathbb{V}, \mathbb{G}$ is the following:

For each spring-pot we have

$$\tau_1(t) = \mathbb{E}_1 \lambda_1^\beta \frac{d^\beta \gamma_1}{dt^\beta} \tag{4.27}$$

$$\tau_2(t) = \mathbb{E}_2 \lambda_2^{\beta-\alpha} \frac{d^{\beta-\alpha}\gamma_2}{dt^\beta} \tag{4.28}$$

where $0 < \alpha \leq \beta \leq 1$.

Then, we have

$$\gamma_1(t) = \frac{1}{\mathbb{E}_1 \lambda_1^{\beta}} \frac{d^{-\beta}\tau_1(t)}{dt^{-\beta}} = \frac{1}{\mathbb{E}_1 \lambda_1^{\beta}} \frac{d^{-\beta}\tau(t)}{dt^{-\beta}} \tag{4.29}$$

$$\gamma_2(t) = \frac{1}{\mathbb{E}_2 \lambda_2^{\beta-\alpha}} \frac{d^{-(\beta-\alpha)}\tau_2(t)}{dt^{-(\beta-\alpha)}} = \frac{1}{\mathbb{E}_2 \lambda_2^{\beta-\alpha}} \frac{d^{-(\beta-\alpha)}\tau(t)}{dt^{-(\beta-\alpha)}} \tag{4.30}$$

Substituting Eq.(4.29) and Eq.(4.30) into the following equation

$$\gamma = \gamma_1 + \gamma_2 \tag{4.31}$$

yields

$$\frac{1}{\mathbb{E}_1\ \lambda_1^{\beta}} \frac{d^{-\beta}\tau(t)}{d\,t^{-\beta}} + \frac{1}{\mathbb{E}_2\ \lambda_2^{\beta-\alpha}} \frac{d^{-(\beta-\alpha)}\tau(t)}{dt^{-(\beta-\alpha)}} = \gamma(t) \tag{4.32}$$

Rearranging Eq.(4.32) and applying the operator $\frac{d^{\beta}}{dt^{\beta}}$ we obtain the following equation

$$\tau(t) + \frac{\mathbb{E}_1\ \lambda_1^{\beta}}{\mathbb{E}_2\ \lambda_2^{\beta-\alpha}} \frac{d^{\alpha}\tau(t)}{d\,t^{\alpha}} = \mathbb{E}_1\ \lambda_1^{\beta}\ \frac{d^{\beta}\gamma(t)}{dt^{\beta}} \tag{4.33}$$

We assume $\beta \geq \alpha$ without loss of generality. When $\beta = \alpha$, we recover the single fractional element.

Now, consider $\beta > \alpha$, then Eq.(4.33) can be simplified by setting

$$\lambda = \left(\frac{\mathbb{E}_1\ \lambda_1^{\beta}}{\mathbb{E}_2 \lambda_2^{\beta-\alpha}} \right)^{\frac{1}{\alpha}}, \quad \mathbb{E} = \mathbb{E}_1 \left(\frac{\lambda_1}{\lambda} \right)^{\beta} \tag{4.34}$$

This leads to the equation

$$\tau(t) + \lambda^{\alpha} \frac{d^{\alpha}\tau(t)}{d\,t^{\alpha}} = \mathbb{E}\lambda^{\beta}\ \frac{d^{\beta}\gamma(t)}{dt^{\beta}} \tag{4.35}$$

where

$$\lambda^{\alpha} = \left[\left(\frac{\mathbb{E}_1 \lambda_1^{\beta}}{\mathbb{E}_2 \lambda_2^{\beta-\alpha}} \right)^{\frac{1}{\alpha}} \right]^{\alpha} = \frac{\mathbb{E}_1 \lambda_1^{\beta}}{\mathbb{E}_2 \lambda_2^{\beta-\alpha}} \equiv \frac{\mathbb{V}}{\mathbb{G}} \tag{4.36}$$

and

$$\mathbb{E}\lambda^{\beta} = \mathbb{E}_1 \left(\frac{\lambda_1}{\lambda} \right)^{\beta} \lambda^{\beta} = \mathbb{E}_1 \lambda_1^{\beta} \equiv \mathbb{V} \tag{4.37}$$

then, Eq.(4.35) becomes

$$\tau(t) + \frac{\mathbb{V}}{\mathbb{G}} \frac{d^{\alpha}\tau(t)}{d\, t^{\alpha}} = \mathbb{V} \frac{d^{\beta}\gamma(t)}{dt^{\beta}} \tag{4.38}$$

(see Yang . (2010); Stankiewicz (2018))

4.3.2 Derivation of the Exact Solution

In a novel approach, we will solve Eq. (4.26) exactly by defining the relaxation modulus to be the Laplace transform of the Green's function which will be expressed in terms of the Mittag–Leffler function (MLF). This is different to the standard approach which utilizes the Fourier transform.

Theorem 1

Consider the generalized fractional Maxwell model

$$\tau(t) + \lambda^{\alpha} \frac{\partial^{\alpha}\tau(t)}{\partial t^{\alpha}} = \mathbb{E}\ \lambda^{\beta}\ \frac{\partial^{\beta}\gamma(t)}{\partial t^{\beta}} \tag{4.39}$$

where $0 < \alpha \leq \beta \leq 1$.

The formal solution of Eq.(4.39) is given by Schiessel . (1995) as

$$\tau(t) = \int_{-\infty}^{t} G(t - t')\dot{\gamma}(t')dt' \tag{4.40}$$

where $G(t)$ is the relaxation modulus that is defined by the fractional Green's function as follows:

$$G(t) = \mathbb{E}\left(\frac{t}{\lambda}\right)^{\alpha-\beta} E_{\alpha,\alpha-\beta+1}\left[-\left(\frac{t}{\lambda}\right)^{\alpha}\right] \tag{4.41}$$

where $E_{\alpha,\beta}$ is the Mittag–Leffler function (Podlubny, 1999):

$$E_{\alpha,\beta}(x) = \sum_{k=0}^{\infty} \frac{x^{k}}{\Gamma(\alpha k + \beta)}, \quad \alpha > 0, \beta > 0 \tag{4.42}$$

Then Eq. (4.40) written in terms of the Green's function solution is

$$\tau(t) = \frac{\mathbb{E}\ \lambda^{\beta}}{\lambda^{\alpha}} \int_{-\infty}^{t} (t-t')^{\alpha-\beta} E_{\alpha,\alpha-\beta+1}\left[-\frac{1}{\lambda^{\alpha}}(t-t')^{\alpha} \right] \dot{\gamma}(t')dt' \tag{4.43}$$

Proof

We interpret Eq. (4.39) as

$$\tau(t) + \lambda^{\alpha}\ \partial^{\alpha}\tau(t) = \mathbb{E}\ \lambda^{\beta}\ \partial^{\beta-1}\ (\partial\gamma(t)),\ \ \alpha < \beta \tag{4.44}$$

Applying the operator $\partial^{1-\beta}$ to Eq. (4.44), and using Weyl's rule (see Eq. (3.2)), gives

$$B\ \partial^{1-\beta}\tau(t) + A\ \partial^{1+\alpha-\beta}\tau(t) = C\ \dot{\gamma}(t) \tag{4.45}$$

where

$$A = \frac{\lambda^{\alpha}}{\mathbb{E}\ \lambda^{\beta}},\quad B = \frac{1}{\mathbb{E}\ \lambda^{\beta}},\quad C = 1$$

For simplicity let

$$\bar{\beta} = 1 + \alpha - \beta > \bar{\alpha} = 1 - \beta,\quad (0 < \bar{\alpha} \leq \bar{\beta} \leq 1) \tag{4.46}$$

then Eq.(4.45) becomes

$$A\ \partial^{\bar{\beta}}\tau(t) + B\ \partial^{\bar{\alpha}}\tau(t) = \dot{\gamma}(t) \tag{4.47}$$

If $G(t)$ is the fractional Green's function of the following equation

$$\mathcal{L}\{\tau(t)\} = f(t), \tag{4.48}$$

with special initial conditions with $f(t) = \dot{\gamma}(t)$ and $\mathcal{L}$ is the operator

$$\mathcal{L} = A\partial^{\bar{\beta}} + B\partial^{\bar{\alpha}},\quad \bar{\beta} > \bar{\alpha} \tag{4.49}$$

then the Green's function solution of equation (4.47) is

$$\tau(t) = \int_{-\infty}^{t} G(t,t')f(t')dt' \tag{4.50}$$

where $G(t,t') \equiv G(t-t')$.

To derive Eq. (4.43) we apply Eq.(3.2) from (Podlubny, 1997) in the limit as $a \to -\infty$ and evaluate the operators ${}_{-\infty}\mathcal{D}_t^{\sigma_1}$, ${}_{-\infty}\mathcal{D}_t^{\sigma_2}$,..., ${}_{-\infty}\mathcal{D}_t^{\sigma_n}$ using the rule in Eq. (3.21) and condition (2) from the definition of Green's function in Podlubny (1997), page. (19). This gives

$${}_{-\infty}\mathcal{L}_t\tau(t) \equiv {}_{-\infty}\mathcal{D}_t^{\sigma_n}\tau(t) + \sum_{k=1}^{n-1} p_k(t)\,{}_{-\infty}\mathcal{D}_t^{\sigma_{n-k}}\tau(t) + p_n(t)\tau(t), \tag{4.51}$$

where

$$\begin{aligned}
{}_{-\infty}\mathcal{D}_t{}^{\sigma_1}\tau(t) &= {}_{-\infty}\mathcal{D}_t{}^{\alpha_1}\int_{-\infty}^{t} G(t,t')f(t')dt' \\
&= \int_{-\infty}^{t} {}_{t'}\mathcal{D}_t{}^{\alpha_1}G(t,t')f(t')dt' + \lim_{t'\to t-0} {}_{t'}\mathcal{D}_t{}^{\alpha_1-1}G(t,t')f(t') \\
&= \int_{-\infty}^{t} {}_{t'}\mathcal{D}_t{}^{\sigma_1}G(t,t')f(t')dt'
\end{aligned} \tag{4.52}$$

... ...

$$\begin{aligned}
{}_{-\infty}\mathcal{D}_t{}^{\sigma_{n-1}}\tau(t) &= {}_{-\infty}\mathcal{D}_t{}^{\alpha_{n-1}}({}_{-\infty}\mathcal{D}_t{}^{\sigma_{n-2}}) \\
&= {}_{-\infty}\mathcal{D}_t{}^{\alpha_{n-1}}\int_{-\infty}^{t} {}_{t'}\mathcal{D}_t{}^{\sigma_{n-2}}G(t,t')f(t')dt' \\
&= \int_{-\infty}^{t} {}_{t'}\mathcal{D}_t{}^{\alpha_{n-1}}({}_{t'}\mathcal{D}_t{}^{\sigma_{n-2}}G(t,t'))f(t')dt' + \lim_{t'\to t-0} {}_{t'}\mathcal{D}_t{}^{\alpha_{n-1}\,-1}({}_{t'}\mathcal{D}_t{}^{\sigma_{n-2}}G(t,t'))f(t') \\
&= \int_{-\infty}^{t} {}_{t'}\mathcal{D}_t{}^{\sigma_{n-1}}G(t,t')f(t')dt'
\end{aligned} \tag{4.53}$$

$$
\begin{aligned}
{}_{-\infty}\mathcal{D}_t^{\sigma_n}\tau(t) &= {}_{-\infty}\mathcal{D}_t^{\alpha_n}({}_{-\infty}\mathcal{D}_t^{\sigma_{n-1}}) \\
&= {}_{-\infty}\mathcal{D}_t^{\alpha_n}\int_{-\infty}^{t} {}_{t'}\mathcal{D}_t^{\sigma_{n-1}}G(t,t')f(t')dt' \\
&= \int_{-\infty}^{t} {}_{t'}\mathcal{D}_t^{\alpha_n}({}_{t'}\mathcal{D}_t^{\sigma_{n-1}}G(t,t'))f(t')dt' + \lim_{t'\to t-0} {}_{t'}\mathcal{D}_t^{\alpha_n-1}({}_{t'}\mathcal{D}_t^{\sigma_{n-1}}G(t,t'))f(t') \\
&= \int_{-\infty}^{t} {}_{t'}\mathcal{D}_t^{\sigma_n}G(t,t')f(t')dt' + f(t)
\end{aligned}
\tag{4.54}
$$

Multiplying these equations by the corresponding coefficients, summing and using condition (1) from the definition of Green's function when $(-\infty < t' < t)$, and substituting into Eq. (4.51) we obtain

$$
{}_{-\infty}\mathcal{L}_t\tau(t) = \int_{-\infty}^{t} {}_{t'}\mathcal{L}_t G(t,t')f(t')dt' + f(t) = f(t) \tag{4.55}
$$

So we have proved that Eq.(4.50) is the Green's function solution of Eq.(4.48). Now, we need to find $G(t,t')$. Since Eq. (4.47) is a three-term differential equation, then the fractional Green's function $G(t)$ can be obtained by the inverse Laplace transform of the following function

$$
g(p) = \frac{1}{Ap^{\bar{\beta}} + Bp^{\bar{\alpha}} + C} \tag{4.56}
$$

Since $C = 0$, then the Laplace inverse can be performed in the same way as in the case of the two-term equation in (Podlubny, 1997), Eq. (4.2)

$$
g(p) = \frac{1}{Ap^{\bar{\beta}} + Bp^{\bar{\alpha}}} = \frac{1}{A}\,\frac{p^{-\bar{\alpha}}}{p^{\bar{\beta}-\bar{\alpha}} + \frac{B}{A}} \tag{4.57}
$$

using the formula for the Laplace transform of the Mittag-Leffler function in two parameters

$$
\mathcal{L}\{E_{\tilde{\alpha},\tilde{\beta}}\ (t); p\} = \int_0^{\infty} e^{-pt}\ t^{\tilde{\beta}-1}\ E_{\tilde{\alpha},\tilde{\beta}}\ (\pm a\ t^{\tilde{\alpha}})\ dt = \frac{p^{\tilde{\alpha}-\tilde{\beta}}}{(p^{\tilde{\alpha}} \mp a)} \tag{4.58}
$$

To obtain the Laplace inverse of equation (4.57), let $\tilde{\alpha} - \tilde{\beta} = -\bar{\alpha}$; $\tilde{\alpha} = \bar{\beta} - \bar{\alpha}$; $a = -\frac{B}{A}$ then, $\tilde{\beta} = \tilde{\alpha} + \bar{\alpha} = 1 + \alpha - \beta$; $\tilde{\alpha} = \bar{\beta} - \bar{\alpha} = \alpha$.

Thus, the Green's function is of the form

$$\begin{aligned} G(t) &= \frac{1}{A} t^{\tilde{\beta}-1} E_{\tilde{\alpha},\tilde{\beta}}(-at^{\tilde{\alpha}}) \\ &= \frac{1}{A} t^{\alpha-\beta} E_{\alpha,1+\alpha-\beta}\left(-\frac{B}{A}t^{\alpha}\right) \end{aligned} \tag{4.59}$$

and we are consistent with Eq. (4.43) i.e.

$$\tau(t) = \frac{1}{A}\int_{-\infty}^{t} (t-t')^{\alpha-\beta} E_{\alpha,\alpha-\beta+1}\left[-\frac{B}{A}(t-t')^{\alpha}\right]\dot{\gamma}(t')dt' \tag{4.60}$$

4.3.3 Determination of the Dynamic Moduli

Now, we will introduce the three fundamental equations of the GFMM (Eq. (4.39)) that describe viscoelastic characteristics: the complex, storage, and loss moduli.

The relaxation modulus, $G(t)$, for the FMM is obtained by determining the stress response of Eq. (4.39) to an applied step strain function $\gamma = \gamma_0 H(t)$ (Friedrich, 1991).

The FMM's characteristic relaxation time is described by Jaishankar McKinley (2014) as follows

$$\lambda_c = \left(\frac{\mathbb{V}}{\mathbb{G}}\right)^{\frac{1}{\alpha}} \tag{4.61}$$

The intersection of the relaxation modulus's two asymptotic responses for long and short times, as shown in Eq. (4.41), corresponds to this characteristic time. To non-dimensionalize the relaxation modulus in Eq. (4.41), define a characteristic modulus G_c in terms of the characteristic relaxation time λ_c and the quasi-property $\mathbb{V}$. This can be expressed as

$$G_c = \mathbb{V}\lambda_c^{-\beta} \equiv \left(\frac{\mathbb{G}^{\beta}}{\mathbb{V}^{\beta-\alpha}}\right)^{\frac{1}{\alpha}} \tag{4.62}$$

As a result, the relaxation modulus has the following dimensionless representation:

$$\frac{G(t)}{G_c} = \left(\frac{t}{\lambda_c}\right)^{\alpha-\beta} E_{\alpha,\alpha-\beta+1}\left(-\left(\frac{t}{\lambda_c}\right)^{\alpha}\right) \tag{4.63}$$

where $0 < \alpha \leq \beta \leq 1$.

Equation (4.26) can be transformed from the time domain into the frequency domain

(ω is the frequency of strain oscillation (rad/s)) using the Fourier integral transform to obtain the complex modulus

$$G^*(\omega) = G'(\omega) + i\,G''(\omega) \tag{4.64}$$

where G' and G'' are known, respectively, as the storage and loss moduli. Collectively, they are referred to the dynamic moduli.

The Fourier transform of a function f is given by

$$\mathcal{F}\left[f(t);\omega\right] = \tilde{f}(\omega) = \int_{-\infty}^{\infty} dt\ f(t)\ e^{-i\omega t} \tag{4.65}$$

where ω is the angular velocity.

The Fourier transform of the fractional derivative of a function f is obtained by simple multiplication with $\tilde{f}$ (Hristov, 2018; Adolfsson Enelund, 2003)

$$\mathcal{F}\left[\frac{d^\alpha f(t)}{dt^\alpha};\omega\right] = (i\omega)^\alpha \tilde{f}(\omega), \quad 0 < \alpha < 1 \tag{4.66}$$

Hence, the Fourier transform of Eq.(4.26) is

$$\tilde{\tau}(\omega) + \frac{\mathbb{V}}{\mathbb{G}}(i\omega)^\alpha\ \tilde{\tau}(\omega) = \mathbb{V}\ (i\omega)^\beta\ \tilde{\gamma}(\omega) \tag{4.67}$$

where $\tilde{\tau}(\omega)$ and $\tilde{\gamma}(\omega)$ are the Fourier transforms of τ and γ, respectively.

Subsequently, the complex modulus of the fractional Maxwell model which describes its response to a small amplitude oscillatory shear (SAOS) deformation, is as follows:

$$G^*(\omega) \equiv \frac{\tilde{\tau}(\omega)}{\tilde{\gamma}(\omega)} = \frac{\mathbb{V}(i\omega)^\beta}{1 + \frac{\mathbb{V}}{\mathbb{G}}(i\omega)^\alpha} \tag{4.68}$$

The complex modulus can be non-dimensionalized using $\lambda_c = \left(\frac{\mathbb{V}}{\mathbb{G}}\right)^{\frac{1}{\alpha}}$ and $G_c = \mathbb{V}\lambda_c^{-\beta} \equiv \left(\frac{\mathbb{G}^\beta}{\mathbb{V}^{\beta-\alpha}}\right)^{\frac{1}{\alpha}}$, to obtain:

$$\begin{aligned}\frac{G^*(\omega)}{G_c} &= \frac{(i\omega\lambda_c)^\beta}{1+(i\omega\lambda_c)^\alpha} \\ &= \frac{(\omega\lambda_c)^\beta\,(e^{i\pi/2})^\beta}{1+(\omega\lambda_c)^\alpha\,(e^{i\pi/2})^\alpha} \\ &= \frac{(\omega\lambda_c)^\beta\,[\cos(\pi\beta/2)+i\,\sin(\pi\beta/2)]}{1+(\omega\lambda_c)^\alpha\,[\cos(\pi\alpha/2)+i\,\sin(\pi\alpha/2)]}\end{aligned} \tag{4.69}$$

Multiplying Eq. (4.69) by the complex conjugate of the denominator which is

$$\bar{D} = [1+(\omega\,\lambda_c)^\alpha\cos(\pi\alpha/2)] - i\,(\omega\,\lambda_c)^\alpha\,\sin(\pi\alpha/2),$$

we obtain

$$\begin{aligned}\frac{G^*(\omega)}{G_c} = &\left[\frac{(\omega\,\lambda_c)^\beta\,\cos(\pi\beta/2)+(\omega\,\lambda_c)^{\alpha+\beta}\cos(\pi(\beta-\alpha)/2)}{1+2(\omega\,\lambda_c)^\alpha\cos(\pi\alpha/2)+(\omega\,\lambda_c)^{2\alpha}}\right] \\ &+ i\left[\frac{(\omega\,\lambda_c)^\beta\,\sin(\pi\beta/2)+(\omega\,\lambda_c)^{\alpha+\beta}\sin(\pi(\beta-\alpha)/2)}{1+2(\omega\,\lambda_c)^\alpha\cos(\pi\alpha/2)+(\omega\,\lambda_c)^{2\alpha}}\right]\end{aligned} \tag{4.70}$$

The real and imaginary parts of the complex modulus provide us with the storage and loss moduli of the complex fluid, respectively. The viscous component of energy is represented by the loss modulus G'', which measures the energy dissipated as heat, while the elastic component that characterises the capacity to store energy is measured by the storage modulus G'.

Therefore, from Eq. (4.70) the storage modulus of the complex fluid is

$$\frac{G'(\omega)}{G_c} = \frac{(\omega\,\lambda_c)^\beta\,\cos(\pi\beta/2)+(\omega\,\lambda_c)^{\alpha+\beta}\cos(\pi(\beta-\alpha)/2)}{1+2(\omega\,\lambda_c)^\alpha\cos(\pi\alpha/2)+(\omega\,\lambda_c)^{2\alpha}} \tag{4.71}$$

and the loss modulus is

$$\frac{G''(\omega)}{G_c} = \frac{(\omega\,\lambda_c)^{\beta}\,\sin(\pi\beta/2) + (\omega\,\lambda_c)^{\alpha+\beta}\sin(\pi(\beta-\alpha)/2)}{1 + 2(\omega\,\lambda_c)^{\alpha}\cos(\pi\alpha/2) + (\omega\,\lambda_c)^{2\alpha}} \tag{4.72}$$

The phase angle, $\tan\delta$, that characterizes the ratio between energy dissipation and energy storage, is defined by

$$\tan\delta(\omega) = G''(\omega)/G'(\omega) \tag{4.73}$$

4.3.4 Numerical Results

Figure 4.6 provides insight into how different models for a material might respond to different stresses or deformations, highlighting different aspects of viscoelastic behaviour. The Fractional Maxwell Gel (FMG) and the Fractional Maxwell Liquid (FML) are two significant limiting instances of the Fractional Maxwell model (FMM).
The Fractional Maxwell Liquid (FML) model corresponds to $\beta = 1$, resulting in a constant and bounded shear viscosity. This makes it well-suited for describing fluid-like materials in a pre-gel state, such as biopolymer solutions or polymer melts. These materials exhibit continuous flow under constant stress, with a viscous response that dominates over time. This behaviour is characterized by a significantly larger loss modulus G'' compared to the storage modulus G' at low frequencies, indicating substantial energy dissipation during deformation. Consequently, complex fluids in the pre-gel state have been effectively described using the three-parameter FML model $(\mathbb{G}, \alpha, \mathbb{V})$. Mechanically, the FML model can be represented by a dashpot and a spring-pot in series.

Furthermore, the Fractional Maxwell Gel (FMG) is used to describe gel-like materials that show both solid-like (elastic) and liquid-like (viscous) properties. These materials can support some level of deformation without flowing completely, and they exhibit a balance between elasticity and viscosity, where $0 \leq \alpha = \beta \leq 1$. This model is suitable for materials like gels, which can stretch or deform but will still flow if subjected to sustained stress. The plateau modulus of the gel $(G'(\omega \to \infty) = \mathbb{G}(Pa))$ is characterised by the quasi-property $\mathbb{G}$, and thus the FMG model effectively represents the mostly elastic be-

haviour of viscoelastic materials beyond the gel point. The mechanical interpretation of the three-parameter FMG model ($\mathbb{G}$, α, and $\mathbb{V}$) is represented as a series combination of a spring and a spring-pot. In terms of viscoelastic properties, the storage modulus G' and the loss modulus G'' are comparable in magnitude, especially at intermediate frequencies. This indicates a balance between energy storage and dissipation.

The Fractional Maxwell Model (FMM) is a more general model that can describe a wide range of viscoelastic behaviours, depending on the parameters chosen. It can interpolate between solid-like, gel-like, and liquid-like behaviour by adjusting the order of the fractional derivatives in the model, i.e. $0 \leq \alpha \leq \beta \leq 1$. It is used for a wide range of materials, from purely elastic solids to highly viscous liquids, depending on the specific parametrization. For viscoelastic properties, the model allows for a broad spectrum of responses by varying the fractional order α, β, so G' and G'' can exhibit either a dominance of elasticity, viscosity, or a mix of both. When one of the quasi-properties diverges to infinity ($\mathbb{V} \to \infty$ or $\mathbb{G} \to \infty$), the FMM also reduces to a simple single spring-pot element or Scott Blair element, as shown graphically in Fig. 4.4. As a last note, just to be thorough, we see that the simple Maxwell model given in Eq.(4.5) arises from the particular situation $\alpha = \beta = 1$, and the quasi-properties $\mathbb{V}$ and $\mathbb{G}$ reduce to the viscosity η_0 and shear modules G_0, respectively (see, Rathinaraj . (2021); Keshavarz . (2021); Schmidt . (2024); Sadman . (2017).

Table 4.1 tabulates the asymptotic behaviour of the complex moduli in the limits $\omega\,\lambda_c \ll 1$ and $\omega\,\lambda_c \gg 1$ for these three standard models, which may be obtained from Eqs. (4.71) and (4.72).

The magnitude of the complex viscosity is defined as follows using the formulas given in Equations (4.71) and (4.72)

$$|\eta^*(\omega)| = \frac{\sqrt{G'(\omega)^2 + G''(\omega)^2}}{\omega} \tag{4.74}$$

		$\omega\,\lambda_c \ll 1$	$\omega\,\lambda_c \gg 1$
FMM	G'/G_c	$(\omega\lambda_c)^{\beta}\cos(\pi\beta/2)$	$(\omega\,\lambda_c)^{\beta-\alpha}\ \cos(\pi(\beta-\alpha)/2)$
	G''/G_c	$(\omega\,\lambda_c)^{\beta}\sin(\pi\beta/2)$	$(\omega\,\lambda_c)^{\beta-\alpha}\ \sin(\pi(\beta-\alpha)/2)$
FML	G'/G_c	$(\omega\,\lambda_c)^{1+\alpha}\ \cos(\pi(1-\alpha)/2)$	$(\omega\,\lambda_c)^{1-\alpha}\cos(\pi(1-\alpha)/2)$
	G''/G_c	$\omega\,\lambda_c$	$(\omega\,\lambda_c)^{1-\alpha}\sin(\pi(1-\alpha)/2)$
FMG	G'/G_c	$(\omega\,\lambda_c)^{\beta}\cos(\pi\beta/2)$	1
	G''/G_c	$(\omega\,\lambda_c)^{\beta}\sin(\pi\beta/2)$	$(\omega\,\lambda_c)^{-\beta}\sin(\pi\beta/2)$

Table 4.1: The asymptotic behaviour of the storage G' ($\lim_{\omega\,\lambda_c\to\,0} G'(t)$, $\lim_{\omega\,\lambda_c\to\,\infty} G'(t)$) and loss modulus G'' ($\lim_{\omega\,\lambda_c\to\,0} G''(t)$, $\lim_{\omega\,\lambda_c\to\,\infty} G''(t)$) for the Fractional Maxwell Model (FMM) $0 < \alpha < \beta < 1$, the Fractional Maxwell Liquid (FML) $\beta = 1$, and the Fractional Maxwell Gel (FMG) $\alpha = \beta$

which may be expressed as follows using the four FMM parameters:

$$\frac{|\eta^*(\omega)|}{\mathbb{V}\lambda_c^{1-\beta}} = \frac{1}{\sqrt{(\omega\,\lambda_c)^{2-2\beta} + 2(\omega\,\lambda_c)^{2-2\beta+\alpha}\,\cos(\pi\alpha/2) + (\omega\,\lambda_c)^{2(1+\alpha-\beta)}}} \tag{4.75}$$

These concepts are illustrated in Fig. 4.6 for the FMM, FML, and FMG models. While the results are similar to those reported by (Rathinaraj ., 2021) (see Fig.2 in their paper), they were obtained here using a different method. The plots were generated using data from the same source. Fig. 4.6 (a) shows the dependence of the relaxation modulus on dimensionless time for these models. At short times ($t \to 0$), the relaxation modulus $G(t)$ typically reflects the immediate elastic response of the material. For the Fractional Maxwell Model (FMM) and Fractional Maxwell Gel (FMG), $G(t)$ is expected to follow a power-law decay. In this regime, the material exhibits more solid-like behaviour, with the relaxation modulus decreasing gradually as time progresses. At long times ($t \to \infty$), the relaxation modulus reflects the transition from elastic to more viscous behaviour. For the Fractional Maxwell Liquid (FML), $G(t)$ decays more rapidly, indicating that the material behaves more like a liquid over longer time scales. The FMM and FMG models show a continued power-law decay but with different exponents, indicating different balances between elastic and viscous responses. Fig. 4.6 (b) shows the variation of the complex viscosity across different Deborah numbers ($\omega\,\lambda_c$) for the FMM, FML, and FMG models. At low frequencies, the complex viscosity $\eta^*(\omega)$ is dominated by the material's viscous behaviour. The FML model, which behaves more like a liquid, shows a high viscosity at

low frequencies. The viscosity decreases as frequency increases, indicating shear-thinning behaviour typical of complex fluids. The FMM and FMG also exhibit a similar trend but may start at lower viscosity levels depending on the parameters. At high frequencies, the material exhibits more elastic behaviour, and the viscosity stabilizes or decreases more slowly. The complex viscosity $\eta^*(\omega)$ continues to decrease slowly, reflecting the material's transition to a more elastic response. The rate of this change depends on the specific model (FMM, FML, or FMG), with each showing a distinct response curve.

Moreover, Fig. 4.6 (c,d) shows the variation of dynamic moduli across different Deborah numbers ($\omega\,\lambda_c$) for the FMM, FML, and FMG models. Fig. 4.6 (c) illustrates the storage modulus G', which indicates the material's elasticity or solidity. As the material stores more elastic energy, G' gradually increases with increasing frequency. At high frequencies, the material transitions from a more elastic to a stiffer state. As the frequency continues to rise, G' typically increases until it reaches a plateau or steady state, where the material mostly exhibits elastic behaviour. Fig.4.6 (d) shows the loss modulus G'' represents the material's viscous or liquid-like characteristics, which showing how much energy is dissipated as heat. Initially, G'' increases as the frequency increases, indicating that the material behaves more viscous with increased frequency of oscillations. As the frequency continues to increase, G'' may decrease after reaching a peak, as the material shifts towards more elastic behaviour, leading to less energy loss. Finally, Fig.4.6 (e) shows that the difference between the phase angle for the FMM and the FML is larger at low frequencies, indicating that these materials exhibit more viscous behaviour over longer times. On the other hand, the phase angle of the FMG , which describes gel-like behaviour, is smaller, indicating that it is mostly elastic at low frequencies. The phase angle for FML and FMG decreases with increasing frequency, indicating a shift toward more elastic behaviour. The FMG is consistent with its essentially elastic response throughout a wide variety of timescales by approaching a very low or constant phase angle at high frequencies.

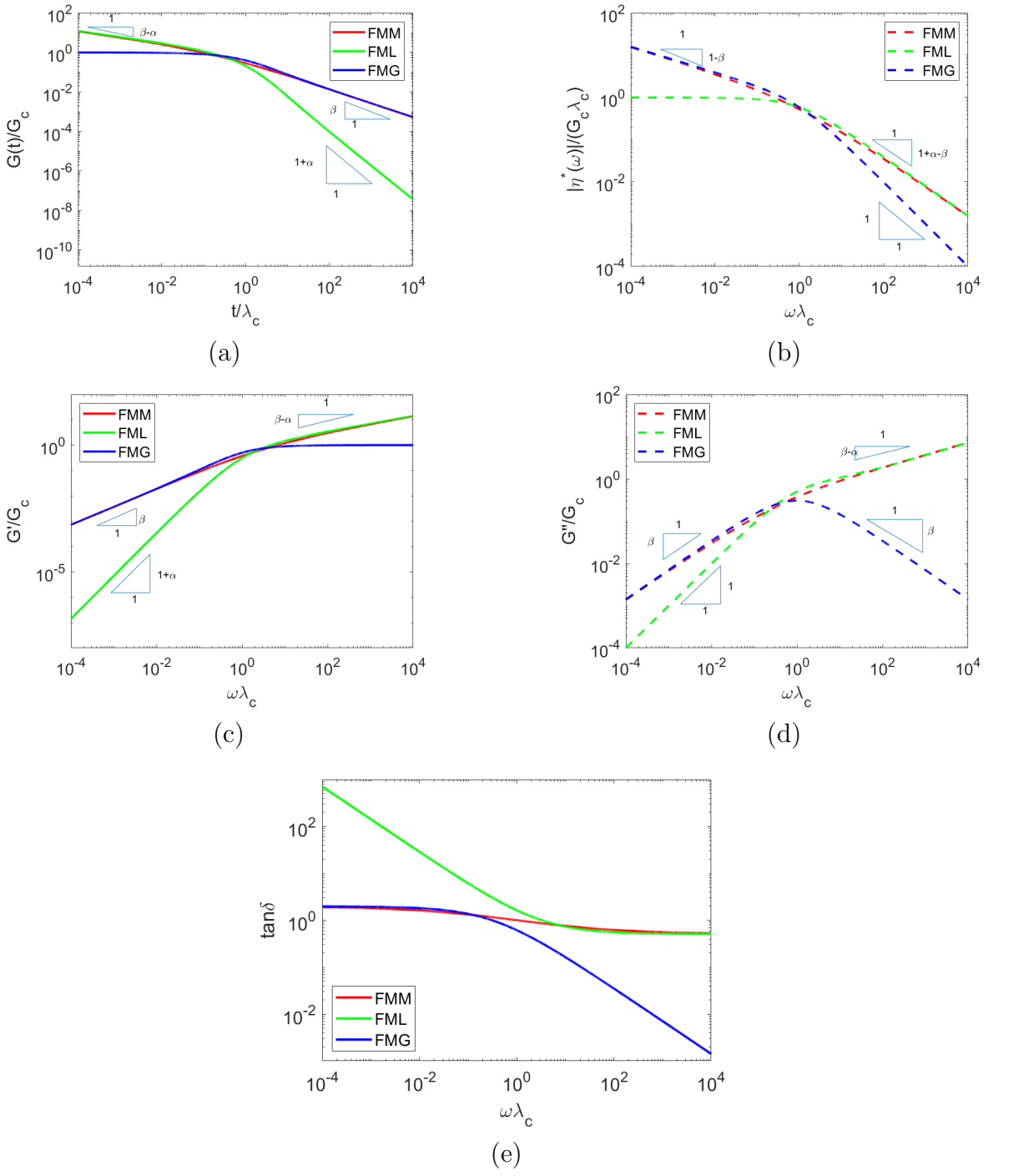

Figure 4.6: The linear viscoelastic characteristics of the FMM ($\alpha = 0.4, \beta = 0.7$), FML ($\alpha = 0.7, \beta = 1$), and FMG ($\alpha = 0.7, \beta = 0.7$). (a) $G(t)$, (b) $\eta^*(\omega)$, (c) G', (d) G'', and (e) $\tan\delta$.

4.3.5 Determination of the Relaxation Spectrum

The relaxation spectrum is an essential tool in the description of viscoelastic polymeric fluids. It is an essential component in the analysis of materials processing like extrusion and can be utilized in predicting the behaviour of a linear viscoelastic fluid. The challenge lies in the fact that the relaxation spectrum is not a quantity that can be measured directly, and trying to extract it from experimental data often results in an ill-posed problem (Owens Phillips, 2002).

Consequently, data from other transient experiments can be simulated once the discrete relaxation spectrum of a material is known. The success of this method is demonstrated by the findings published in H. Winter . (1990). It is important to take into account that the discrete relaxation spectrum is only applicable for the frequency or time frame that corresponds to the input data (HH. Winter Jackson, 1995).

Assume a discrete set of frequencies $\{\omega_j : 1 \leq j \leq M\}$ is used to measure the storage and loss modulus of a sample of polymeric material.

Evaluating the expression in Eq. (4.71) and Eq. (4.72) at $\omega = \omega_j$ gives

$$G'(\omega_j) = G_c \left[\frac{(\omega_j \lambda_c)^\beta \cos(\pi\beta/2) + (\omega_j \lambda_c)^{\alpha+\beta} \cos(\pi(\beta-\alpha)/2)}{1 + 2(\omega_j \lambda_c)^\alpha \cos(\pi\alpha/2) + (\omega_j \lambda_c)^{2\alpha}} \right] \tag{4.76}$$

$$G''(\omega_j) = G_c \left[\frac{(\omega_j \lambda_c)^\beta \sin(\pi\beta/2) + (\omega_j \lambda_c)^{\alpha+\beta} \sin(\pi(\beta-\alpha)/2)}{1 + 2(\omega_j \lambda_c)^\alpha \cos(\pi\alpha/2) + (\omega_j \lambda_c)^{2\alpha}} \right] \tag{4.77}$$

where $\lambda_c = \left(\frac{\mathbb{V}}{\mathbb{G}}\right)^{\frac{1}{\alpha}}$, $G_c = \mathbb{V}\lambda_c^{-\beta} \equiv \left(\frac{\mathbb{G}^\beta}{\mathbb{V}^{\beta-\alpha}}\right)^{\frac{1}{\alpha}}$, α and β are unknown model parameters with $0 < \alpha \leq \beta \leq 1$.

The following objective function is minimised in order to obtain the discrete relaxation times and elastic modulus (Baumgaertel Winter, 1989; Mustapha Phillips, 2000).

$$\begin{aligned} \mathcal{X}^2 &= \sum_{j=1}^{M} \left(\left[\frac{G'(\omega_j)}{G'_j} - 1 \right]^2 + \left[\frac{G''(\omega_j)}{G''_j} - 1 \right]^2 \right) \\ &= \sum_{j=1}^{M} \left(\left[\hat{k}_j G_c - 1 \right]^2 + \left[\bar{k}_j G_c - 1 \right]^2 \right) \end{aligned} \tag{4.78}$$

where

$$\hat{k}_j = \left[\frac{(\omega_j \lambda_c)^\beta \cos(\pi\beta/2) + (\omega_j \lambda_c)^{\alpha+\beta} \cos(\pi(\beta-\alpha)/2)}{(1 + 2(\omega_j \lambda_c)^\alpha \cos(\pi\alpha/2) + (\omega_j \lambda_c)^{2\alpha})\, G'_j} \right] \tag{4.79}$$

and

$$\bar{k}_j = \left[\frac{(\omega_j \lambda_c)^\beta \sin(\pi\beta/2) + (\omega_j \lambda_c)^{\alpha+\beta} \sin(\pi(\beta-\alpha)/2)}{(1 + 2(\omega_j \lambda_c)^\alpha \cos(\pi\alpha/2) + (\omega_j \lambda_c)^{2\alpha})\, G''_j} \right] \tag{4.80}$$

where $G'(\omega_j)$ and $G''(\omega_j)$ are determined by Eq.(4.76) and Eq.(4.77), and the values G'_j and G''_j are the measured data.

4.3.6 Fitting of Single-Mode FMM to data

Curve fitting techniques are employed to determine the optimal values of G_c, λ_c, α and β that best fit the fractional Maxwell model to experimental data. Once these parameters are estimated, the model is validated by comparing its predictions with experimental data to assess its accuracy across the frequency range. Non-linear regression and optimization algorithms are commonly used to minimize the error between experimental observations and model-predicted values.

To fit both the real and imaginary components simultaneously, model functions were designed to return a one-dimensional array containing G' and G''. This was achieved by minimizing the objective function χ^2 that was defined in Eq. (4.78). The fractional Maxwell model (FMM) was fitted using the "minpack.lm" package in R, which provides non-linear least-squares fitting via the Levenberg-Marquardt (LM) algorithm. This approach is particularly effective for curve fitting and parameter estimation in non-linear models.

The fitting procedure was applied to two experimental datasets, the corresponding to

1. Sample B which is Neste HDPE (Grade 3416) at 190 °C from Mustapha Phillips (2000) as shown in Fig. 4.7. Where the initial parameter values were assumed to be $G_c = 10000$, $\lambda_c = 4.7$, $\alpha = 0.4$, and $\beta = 0.7$ and the frequency was $M = 40$ data points. After 100 iterations, the fitted parameters were obtained as follows: $G_c = 146237$, $\lambda_c = 0.0465$, $\alpha = 0.4773$, $\beta = 0.6893$. At these final parameters, the value of $\mathcal{X}^2 = 0.119752$. 0.099020

2. Polyethylene Oxide (PEO) solution, this sample contains a low concentration of polystyrene particles with a diameter of 109 nm. Oscillatory shear experiments were conducted using an MCR 502 WESP temperature-controlled rheometer from Anton Paar (Graz, Austria) in strain-imposed mode. A cone-and-plate measuring system was utilized, featuring a 50 mm diameter and a 1° cone angle, with a fixed gap width of 101 μm. All measurements were performed at a constant temperature of 25 °C. The angular oscillation frequency ranged from 0.1 to 100 rad/s, with a constant strain amplitude of 5%. A total of $M = 25$ frequency data points were recorded (Schmidt ., 2024).

   Figure 4.8 was generated using the same initial parameter values as in Case 1. After 100 iterations, the optimized parameters were obtained as follows:
   $G_c = 215$, $\lambda_c = 1.2175$, $\alpha = 0.5444$, $\beta = 0.6996$. At these final parameters, the value of $\mathcal{X}^2 = 0.099020$.

   The original rheology data used in Fig. 4.8 is publicly available at https://doi.org/10.14279/depositonce-20768.
   The relevant file is named (RS22_230_FS_4000KDa_4wt%_PS109).

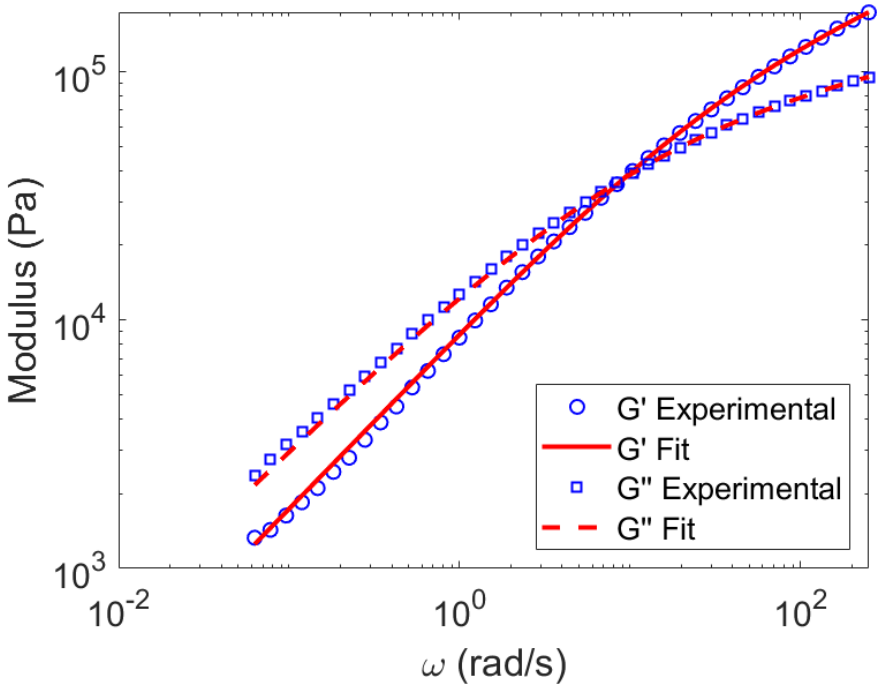

Figure 4.7: Comparison of the data and model predictions for Neste HDPE using the FMM

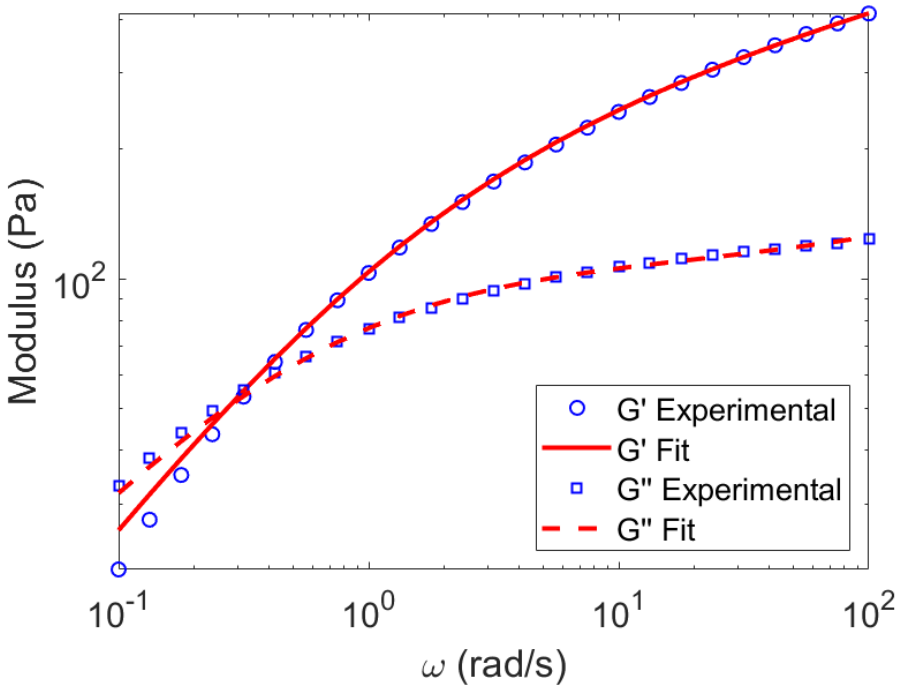

Figure 4.8: Comparison of the data and model predictions for a PEO solution using the FMM

4.4 Multi-mode Fractional Maxwell Model Spectrum of Relaxation Times in Series

In this section we will extend the model given by Eq (2.5) in Yang . (2010) by introducing additional fractional derivatives which generalises the single-mode fractional model. The aim of generalizing the Maxwell model is to allow us to predict different sorts of complex viscoelastic behaviours.

There are 6-parameter linear viscoelastic models that are able to describe a much wider range of complex fluid behaviour when compare to the single-mode fractional Maxwell model with its 4-parameters.

The Multi-mode Fractional Maxwell Model consists of three spring-pots, each characterized by a pair of material parameters (here, denoted by $(\mathbb{G}_1, \alpha_1)$, $(\mathbb{G}_2, \alpha_2)$ and $(\mathbb{V}, \beta)$, respectively), arranged in series as illustrated in Fig. 4.9.

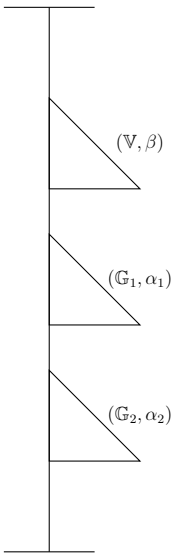

Figure 4.9: Multi-Mode Fractional Maxwell Model

The series combination indicates that the total stress and strain of the system satisfy the following relationships in terms of the stress and strain of the individual components:

$$\tau(t) = \tau_1(t) = \tau_2(t) = \tau_3(t) \tag{4.81}$$

$$\dot{\gamma}(t) = \dot{\gamma}_1(t) + \dot{\gamma}_2(t) + \dot{\gamma}_3(t) \tag{4.82}$$

where $\tau(t)$ is the stress and $\dot{\gamma}(t)$ is the strain rate for the FMM. Also $\tau_i(t)$ and $\dot{\gamma}_i(t)$ are the stress and strain rate in the i-th springpot.

For each springpot we have

$$\tau_1(t) = \mathbb{V}\,\frac{d^{\beta}\gamma_1(t)}{dt^{\beta}} \tag{4.83}$$

$$\tau_2(t) = \mathbb{G}_1\,\frac{d^{\beta-\alpha_1}\gamma_2(t)}{dt^{\beta-\alpha_1}} \tag{4.84}$$

$$\tau_3(t) = \mathbb{G}_2\,\frac{d^{\beta-\alpha_2}\gamma_3(t)}{dt^{\beta-\alpha_2}} \tag{4.85}$$

where $0 < \alpha_2 < \alpha_1 \leq \beta \leq 1$.

For a fixed α_1, α_2 and β, each of the constants $\mathbb{V}$, $\mathbb{G}_1$ and $\mathbb{G}_2$ have physical dimensions Pa.s$^{\beta}$, Pa.s$^{\beta-\alpha_1}$ and Pa.s$^{\beta-\alpha_2}$, respectively. The parameters $\mathbb{V}$, $\mathbb{G}_1$ and $\mathbb{G}_2$ represent a quasi-property and a generalised modulus. These quasi-properties are more clearly recognised as the numerical measurements of a dynamical process, as they are not actual material properties like a modulus or viscosity.

Now

$$\gamma(t) = \gamma_1(t) + \gamma_2(t) + \gamma_3(t) \tag{4.86}$$

so that

$$\frac{d^{\beta}\gamma(t)}{dt^{\beta}} = \frac{d^{\beta}\gamma_1(t)}{dt^{\beta}} + \frac{d^{\beta}\gamma_2(t)}{dt^{\beta}} + \frac{d^{\beta}\gamma_3(t)}{dt^{\beta}} \tag{4.87}$$

Now, from Eq.(4.81) and Eq.(4.83) we obtain

$$\frac{d^{\beta}\gamma_1(t)}{dt^{\beta}} = \frac{1}{\mathbb{V}}\tau_1(t) = \frac{1}{\mathbb{V}}\tau(t) \tag{4.88}$$

and from Eq.(4.81) and Eq.(4.84) we obtain

$$\frac{d^{\alpha_1}\tau_2(t)}{dt^{\alpha_1}} = \frac{d^{\alpha_1}\tau(t)}{dt^{\alpha_1}} = \mathbb{G}_1\frac{d^{\alpha_1}}{dt^{\alpha_1}}\left(\frac{d^{\beta-\alpha_1}\gamma_2(t)}{dt^{\beta-\alpha_1}}\right) = \mathbb{G}_1\frac{d^{\beta}\gamma_2(t)}{dt^{\beta}} \tag{4.89}$$

and from Eq.(4.81) and Eq.(4.85) we obtain

$$\frac{d^{\alpha_2}\tau_3(t)}{dt^{\alpha_2}} = \frac{d^{\alpha_2}\tau(t)}{dt^{\alpha_2}} = \mathbb{G}_2\frac{d^{\alpha_2}}{dt^{\alpha_2}}\left(\frac{d^{\beta-\alpha_2}\gamma_3(t)}{dt^{\beta-\alpha_2}}\right) = \mathbb{G}_2\frac{d^{\beta}\gamma_3(t)}{dt^{\beta}} \tag{4.90}$$

Therefore, the constitutive equation for a multi-mode fractional Maxwell element is

$$\tau(t) + \frac{\mathbb{V}}{\mathbb{G}_1}\frac{d^{\alpha_1}\tau(t)}{dt^{\alpha_1}} + \frac{\mathbb{V}}{\mathbb{G}_2}\frac{d^{\alpha_2}\tau(t)}{dt^{\alpha_2}} = \mathbb{V}\frac{d^{\beta}\gamma(t)}{dt^{\beta}}, \quad 0 < \alpha_2 < \alpha_1 \leq \beta \leq 1 \tag{4.91}$$

where $\frac{\mathbb{V}}{\mathbb{G}_1}$ and $\frac{\mathbb{V}}{\mathbb{G}_2}$ are the relaxation times of the fluid and $\mathbb{V}$ is the viscosity (rate-independent). Eq.(4.91) is a constitutive equation with the ability to describe three different states: a linear elastic solid when $0 < \alpha_2 = \alpha_1 = \beta < 1$, a viscous Newtonian fluid when $0 < \alpha_2 < \alpha_1 < 1$ and $\beta = 1$, and a combination of both states when $0 < \alpha_2 < \alpha_1 < \beta < 1$ (Rathinaraj ., 2021; Yang ., 2010; Ferras ., 2018).

The relationship between $(\mathbb{E}_1, \lambda_1, \mathbb{E}_2, \lambda_2, \mathbb{E}_3, \lambda_3)$, $(\mathbb{E}, \lambda^{\alpha_1}, \lambda^{\alpha_2})$ and $\mathbb{V}, \mathbb{G}_1, \mathbb{G}_2$ is the following:

For each spring-pot we have

$$\tau_1(t) = \mathbb{E}_1\lambda_1^{\beta}\frac{d^{\beta}\gamma_1}{dt^{\beta}} \tag{4.92}$$

$$\tau_2(t) = \mathbb{E}_2\lambda_2^{\beta-\alpha_1}\frac{d^{\beta-\alpha_1}\gamma_2}{dt^{\beta}} \tag{4.93}$$

$$\tau_3(t) = \mathbb{E}_3\lambda_3^{\beta-\alpha_2}\frac{d^{\beta-\alpha_2}\gamma_3}{dt^{\beta}} \tag{4.94}$$

where $0 < \alpha_2 < \alpha_1 \leq \beta \leq 1$.

Then, we have

$$\gamma_1(t) = \frac{1}{\mathbb{E}_1\lambda_1^{\beta}}\frac{d^{-\beta}\tau_1(t)}{dt^{-\beta}} = \frac{1}{\mathbb{E}_1\lambda_1^{\beta}}\frac{d^{-\beta}\tau(t)}{dt^{-\beta}} \tag{4.95}$$

$$\gamma_2(t) = \frac{1}{\mathbb{E}_2\lambda_2^{\beta-\alpha_1}}\frac{d^{-(\beta-\alpha_1)}\tau_2(t)}{dt^{-(\beta-\alpha_1)}} = \frac{1}{\mathbb{E}_2\lambda_2^{\beta-\alpha_1}}\frac{d^{-(\beta-\alpha_1)}\tau(t)}{dt^{-(\beta-\alpha_1)}} \tag{4.96}$$

$$\gamma_3(t) = \frac{1}{\mathbb{E}_3 \lambda_3^{\beta-\alpha_2}} \frac{d^{-(\beta-\alpha_2)}\tau_3(t)}{dt^{-(\beta-\alpha_2)}} = \frac{1}{\mathbb{E}_3 \lambda_3^{\beta-\alpha_2}} \frac{d^{-(\beta-\alpha_2)}\tau(t)}{dt^{-(\beta-\alpha_2)}} \tag{4.97}$$

Substituting Eq.(4.95), Eq.(4.96) and Eq.(4.97) into the following equation

$$\gamma = \gamma_1 + \gamma_2 + \gamma_3 \tag{4.98}$$

yields

$$\frac{1}{\mathbb{E}_1\ \lambda_1^{\beta}} \frac{d^{-\beta}\tau(t)}{d\,t^{-\beta}} + \frac{1}{\mathbb{E}_2\ \lambda_2^{\beta-\alpha_1}} \frac{d^{-(\beta-\alpha_1)}\tau(t)}{dt^{-(\beta-\alpha_1)}} + \frac{1}{\mathbb{E}_3\ \lambda_3^{\beta-\alpha_2}} \frac{d^{-(\beta-\alpha_2)}\tau(t)}{dt^{-(\beta-\alpha_3)}} = \gamma(t) \tag{4.99}$$

Eq.(4.99) can be rearranged to obtain the following equation

$$\tau(t) + \frac{\mathbb{E}_1\ \lambda_1^{\beta}}{\mathbb{E}_2\ \lambda_2^{\beta-\alpha_1}} \frac{d^{\alpha_1}\tau(t)}{d\,t^{\alpha_1}} + \frac{\mathbb{E}_1\ \lambda_1^{\beta}}{\mathbb{E}_3\ \lambda_3^{\beta-\alpha_2}} \frac{d^{\alpha_2}\tau(t)}{d\,t^{\alpha_2}} = \mathbb{E}_1\ \lambda_1^{\beta}\ \frac{d^{\beta}\gamma(t)}{dt^{\beta}} \tag{4.100}$$

where we assume $0 < \alpha_2 \leq \alpha_1 \leq \beta \leq 1$ without loss of generality.

Let $0 < \alpha_2 < \alpha_1 < \beta < 1$, then Eq.(4.100) can be simplified by setting

$$\lambda_1 = \frac{\mathbb{E}_1\ \lambda_1^{\beta}}{\mathbb{E}_2 \lambda_2^{\beta-\alpha_1}}, \quad \lambda_2 = \frac{\mathbb{E}_1\ \lambda_1^{\beta}}{\mathbb{E}_3 \lambda_3^{\beta-\alpha_2}}, \quad E = \mathbb{E}_1 {\lambda_1}^{\beta} \tag{4.101}$$

This leads to

$$\tau(t) + \lambda_1 \frac{d^{\alpha_1}\tau(t)}{d\,t^{\alpha_1}} + \lambda_2 \frac{d^{\alpha_2}\tau(t)}{d\,t^{\alpha_2}} = E\,\frac{d^{\beta}\gamma(t)}{dt^{\beta}} \tag{4.102}$$

where

$$\lambda_1 = \frac{\mathbb{E}_1 \lambda_1^{\beta}}{\mathbb{E}_2 \lambda_2^{\beta-\alpha_1}} \equiv \frac{\mathbb{V}}{\mathbb{G}_1} \tag{4.103}$$

and

$$\lambda^{\alpha_2} = \frac{\mathbb{E}_1 \lambda_1^{\beta}}{\mathbb{E}_3 \lambda_3^{\beta-\alpha_2}} \equiv \frac{\mathbb{V}}{\mathbb{G}_2} \tag{4.104}$$

finally,

$$\mathbb{E}\lambda_1^{\beta} \equiv \mathbb{V} \tag{4.105}$$

then, Eq.(4.102) becomes

$$\tau(t) + \frac{\mathbb{V}}{\mathbb{G}_1} \frac{d^{\alpha_1}\tau(t)}{d\, t^{\alpha_1}} + \frac{\mathbb{V}}{\mathbb{G}_2} \frac{d^{\alpha_2}\tau(t)}{d\, t^{\alpha_2}} = \mathbb{V} \frac{d^{\beta}\gamma(t)}{dt^{\beta}} \tag{4.106}$$

see Yang . (2010)

4.4.1 Derivation of the Exact Solution

Theorem 2

Consider the generalized fractional Maxwell model

$$\tau(t) + \lambda_1 \frac{\partial^{\alpha_1}\tau(t)}{\partial t^{\alpha_1}} + \lambda_2 \frac{\partial^{\alpha_2}\tau(t)}{\partial t^{\alpha_2}} = E \frac{\partial^{\beta}\gamma(t)}{\partial t^{\beta}}, \quad 0 \le \alpha_2 \le \alpha_1 \le \beta \le 1 \tag{4.107}$$

then the Green's function solution is

$$\tau(t) = \int_{-\infty}^{t} G(t-t')\dot{\gamma}(t')dt' \tag{4.108}$$

where

$$G(t) = \sum_{k=0}^{\infty} \frac{(-1)^k}{k!} \frac{C^k}{A^{k+1}}\, t^{\alpha_1(k+1)-\beta}\, E^{(k)}_{\alpha_1-\alpha_2,\, \alpha_1+1-\beta+\alpha_2(k)} \left(-\frac{B}{A}\, t^{\alpha_1-\alpha_2} \right) \tag{4.109}$$

Proof

Let

$$\partial_t^{\beta}\gamma(t) = \partial_t^{\beta-1}\, \partial_t\gamma(t) \tag{4.110}$$

Applying the operator $\partial^{1-\beta}$ to equation (4.107), and using Weyl's rule (see Eq. (3.2)) for each component of τ and γ yields

$$\partial_t^{1-\beta}\, \tau(t) + \lambda_1\, \partial_t^{\alpha_1+1-\beta}\, \tau(t) + \lambda_2\, \partial_t^{\alpha_2+1-\beta}\, \tau(t) = E\, \partial_t\gamma(t), \quad 1 > \beta > \alpha_1 > \alpha_2 > 0 \tag{4.111}$$

We rewrite Eq.(4.111) in the form

$$A\partial_t^{\alpha_1+1-\beta}\ \tau(t) + B\ \partial_t^{\alpha_2+1-\beta}\ \tau(t) + C\ \partial_t^{1-\beta}\tau(t) = D\ \partial_t\gamma(t) = f(t) \tag{4.112}$$

where

$$A = \frac{\lambda_1}{E};\quad B = \frac{\lambda_2}{E};\quad C = \frac{1}{E};\quad D = 1 \tag{4.113}$$

For simplicity, we define

$$\bar{\gamma} = \alpha_1 + 1 - \beta;\ \ \bar{\beta} = \alpha_2 + 1 - \beta;\ \ \bar{\alpha} = 1 - \beta;\ \ 0 < \bar{\alpha} < \bar{\beta} < \bar{\gamma} < 1 \tag{4.114}$$

then we can rewrite Eq.(4.112) in the form

$$A\partial_t^{\bar{\gamma}}\tau(t) + B\ \partial_t^{\bar{\beta}}\tau(t) + C\ \partial_t^{\bar{\alpha}}\tau(t) = D\ \partial_t\gamma(t) \tag{4.115}$$

If $G(t)$ is the fractional Green's function of the equation

$$\mathcal{L}\{\tau(t)\} = f(t) \tag{4.116}$$

with special initial conditions, where

$$\mathcal{L} = A\partial_t^{\bar{\gamma}} + B\ \partial_t^{\bar{\beta}} + C\ \partial_t^{\bar{\alpha}} \tag{4.117}$$

then the Green's function solution is

$$\tau(t) = \int_{-\infty}^{t} G(t-t')f(t')dt' \tag{4.118}$$

Since Eq. (4.115) is the four-term fractional differential equation, then we can find the Green's function by obtaining the inverse Laplace transform of the following expression

$$g(p) = \frac{1}{Ap^{\bar{\gamma}} + Bp^{\bar{\beta}} + Cp^{\bar{\alpha}} + H} \tag{4.119}$$

Here $H = 0$, then the Laplace inversion can be performed in the same way as for the case of the three-term equation and Eq. (4.119) becomes

$$g(p) = \frac{p^{-\bar{\alpha}}}{Ap^{\bar{\gamma}-\bar{\alpha}} + Bp^{\bar{\beta}-\bar{\alpha}} + C}, \quad C \neq 0 \tag{4.120}$$

$$\begin{aligned} g(p) &= \frac{1}{Ap^{\bar{\gamma}-\bar{\alpha}} + Bp^{\bar{\beta}-\bar{\alpha}} + C} \\ &= \frac{1}{C} \frac{Cp^{-(\bar{\beta}-\bar{\alpha})}}{Ap^{\bar{\gamma}-\bar{\beta}} + B} \frac{1}{1 + \frac{Cp^{-(\bar{\beta}-\bar{\alpha})}}{Ap^{\bar{\gamma}-\bar{\beta}}+B}} \\ &= \frac{1}{C} \sum_{k=0}^{\infty} (-1)^k \left(\frac{C}{A}\right)^{k+1} \frac{p^{-\bar{\beta}(k+1)+\bar{\alpha}(k)}}{(p^{\bar{\gamma}-\bar{\beta}} + \frac{B}{A})^{k+1}} \end{aligned} \tag{4.121}$$

To determine the inverse Laplace transform we use Eq. (3.18) for the Laplace transform of the Mittag-Leffler function in two-term

$$\mathcal{L}\{E^{(k)}_{\tilde{\alpha},\tilde{\beta}}(t); p\} = \int_0^\infty e^{-pt}\, t^{\tilde{\alpha}k+\tilde{\beta}-1}\, E^{(k)}_{\tilde{\alpha},\tilde{\beta}}(\pm a\, t^{\tilde{\alpha}})dt = \frac{k!\; p^{\tilde{\alpha}-\tilde{\beta}}}{(p^{\tilde{\alpha}} \mp a)^{k+1}}, \quad k \geq 0 \tag{4.122}$$

we define

$$\begin{aligned} \tilde{\alpha} &= \bar{\gamma} - \bar{\beta} & \tilde{\alpha} - \tilde{\beta} &= -\bar{\beta}(k+1) + \bar{\alpha}(k) & \mp a &= -\frac{B}{A} \\ &= \alpha_1 - \alpha_2 & &= -\alpha_2(k+1) + \beta - 1 & & \end{aligned}$$

and

$$\begin{aligned} \tilde{\beta} &= \tilde{\alpha} + \bar{\beta}(k+1) - \bar{\alpha}(k) & \tilde{\alpha}(k) + \tilde{\beta} - 1 &= \bar{\gamma}(k+1) - \bar{\alpha}(k) - 1 \\ &= (\bar{\gamma} - \bar{\beta}) + \bar{\beta}(k+1) - \bar{\alpha}(k) & &= \alpha_1(k+1) - \beta \\ &= \bar{\gamma} + (\bar{\beta} - \bar{\alpha})(k) & & \\ &= \alpha_1 + 1 - \beta + \alpha_2(k) & & \end{aligned}$$

Thus Eq. (4.122) can be written as

$$\mathcal{L}\{E^{(k)}_{\bar{\gamma}-\bar{\beta},\,\bar{\gamma}+(\bar{\beta}-\bar{\alpha})(k)}\ (t);p\} = \int_0^\infty e^{-pt}\ t^{\bar{\gamma}(k+1)-\bar{\alpha}(k)-1}\ E^{(k)}_{\bar{\gamma}-\bar{\beta},\,\bar{\gamma}+(\bar{\beta}-\bar{\alpha})(k)}\left(-\frac{B}{A}\,t^{\bar{\gamma}-\bar{\beta}}\right)dt$$
$$= \frac{k!\,p^{-\bar{\beta}(k+1)+\bar{\alpha}(k)}}{(p^{\bar{\gamma}-\bar{\beta}}\ -\frac{B}{A})^{k+1}},\quad k\geq 0 \tag{4.123}$$

and then

$$\mathcal{L}\{E^{(k)}_{\alpha_1-\alpha_2,\,\alpha_1+1-\beta+\alpha_2(k)}\ (t);p\} = \int_0^\infty e^{-pt}\ t^{\alpha_1(k+1)-\beta}\ E^{(k)}_{\alpha_1-\alpha_2,\,\alpha_1+1-\beta+\alpha_2(k)}\left(-\frac{B}{A}\,t^{\alpha_1-\alpha_2}\right)dt$$
$$= \frac{k!\ p^{-\alpha_2(k+1)+\beta-1}}{(p^{\alpha_1-\alpha_2}\ -\frac{B}{A})^{k+1}},\quad k\geq 0 \tag{4.124}$$

Also, Eq. (4.121) becomes

$$g(p) = \frac{1}{C}\sum_{k=0}^{\infty}(-1)^k\left(\frac{C}{A}\right)^{k+1}\ \frac{p^{-\alpha_2(k+1)+\beta-1}}{(p^{\alpha_1-\alpha_2}+\frac{B}{A})^{k+1}} \tag{4.125}$$

Since Eq. (4.124) is equivalent to (4.125), then we obtain the form of Green's function as follows

$$G(t) = \sum_{k=0}^{\infty}\frac{(-1)^k}{k!}\frac{C^k}{A^{k+1}}\ t^{\alpha_1(k+1)-\beta}\ E^{(k)}_{\alpha_1-\alpha_2,\,\alpha_1+1-\beta+\alpha_2(k)}\left(-\frac{B}{A}\ t^{\alpha_1-\alpha_2}\right) \tag{4.126}$$

where

$$E^{(k)}_{\alpha,\beta}(y(t)) = \frac{d^k}{dt^k}E_{\alpha,\beta}(y) = \sum_{j=0}^{\infty}\frac{(j+k)\ y^j}{j!\ \Gamma(\alpha j+\alpha k+\beta)} \tag{4.127}$$

Finally, we obtain Green's function solution Eq. (4.118) where $G(t)$ is defined by Eq. (4.126).

If $C=0$, then we have only the case $k=0$, and the Green's function solution is

$$\tau(t) = \int_{-\infty}^{t} G(t-t')\dot{\gamma}(t')dt' \tag{4.128}$$

where

$$G(t) = \frac{1}{A} t^{\alpha_1 - \beta} \; E_{\alpha_1 - \alpha_2,\, \alpha_1 + 1 - \beta} \left(- \frac{B}{A} \; t^{\alpha_1 - \alpha_2} \right) \tag{4.129}$$

Therefore, the Green's function solution Eq. (4.128) is consistent with Eq. (4.60) when $\alpha_1 = \alpha$, $\alpha_2 = 0$, with

$$G(t) = \frac{1}{A} t^{\alpha - \beta} \; E_{\alpha,\, \alpha + 1 - \beta} \left(- \frac{B}{A} \; t^{\alpha} \right) \tag{4.130}$$

4.4.2 Determination of the Dynamic Moduli

The three basic equations of GFMM (Eq. (4.107)) that characterise the viscoelastic properties—the complex, storage, and loss modulus—will now be constructed.

Suppose $\lambda_1 = \frac{\mathbb{V}}{\mathbb{G}_1}$ and $\lambda_2 = \frac{\mathbb{V}}{\mathbb{G}_2}$, where $\lambda_2 < \lambda_1$.

Therefore, Eq. (4.126) can be non-dimensionalized with respect to the largest relaxation time λ_1, and then $\lambda_1 \equiv \lambda_c$.

So, we have

$$\lambda_c = \frac{\mathbb{V}}{\mathbb{G}_1}, \quad G_c = \mathbb{V} \lambda_c^{-\beta} = \frac{\mathbb{G}_1^{\beta}}{\mathbb{V}^{\beta - 1}} \tag{4.131}$$

then,

$$\frac{\mathbb{V}}{\mathbb{G}_2} = \lambda_2 = \lambda_c \left(\frac{\lambda_2}{\lambda_c} \right) = \xi \lambda_c \tag{4.132}$$

where $\xi = \frac{\lambda_2}{\lambda_c}$.

Consequently, the dimensionless form for the relaxation modulus is given by

$$\frac{G(t)}{G_c} = \sum_{k=0}^{m} \frac{(-1)^k}{k!} \left(\frac{t}{\lambda_c} \right)^{\alpha_1 (k+1) - \beta} \; E^{(k)}_{\alpha_1 - \alpha_2,\, 1 + \alpha_1 - \beta + \alpha_2 (k)} \left(- \left(\frac{t}{\lambda_c} \right)^{\alpha_1 - \alpha_2} \right) \tag{4.133}$$

where $m \in \mathbb{Z}$, $m > 0$.

The Fourier integral transform can be used to convert Eq. (4.107) from the time domain into the frequency domain (ω is the frequency of strain oscillation (rad/s)) and obtain the complex modulus.

$$G^*(\omega) = G'(\omega) + i \, G''(\omega) \tag{4.134}$$

The Fourier transform of Eq. (4.107) is given by

$$\tilde{\tau}(\omega) + \lambda_1(i\omega)^{\alpha_1}\tilde{\tau}(\omega) + \lambda_2(i\omega)^{\alpha_2}\tilde{\tau}(\omega) = E(i\omega)^{\beta}\tilde{\gamma}(\omega) \tag{4.135}$$

Consequently, the complex modulus of the Maxwell model, which expresses how it responses to a small-amplitude oscillatory shear (SAOS) deformation, is as follows:

$$G^*(\omega) \equiv \frac{\tilde{\tau}(\omega)}{\tilde{\gamma}(\omega)} = \frac{E\,(i\omega)^{\beta}}{1 + \lambda_1\,(i\omega)^{\alpha_1} + \lambda_2\,(i\omega)^{\alpha_2}} \tag{4.136}$$

Thus, we can use Eq. (4.131) and Eq. (4.132) to rewrite Eq. (4.136) as follows:

$$\begin{aligned}
\frac{G^*(\omega)}{G_c} &= \frac{E\,(i\omega)^{\beta}}{1 + \lambda_c(i\omega)^{\alpha_1} + \xi\lambda_c(i\omega)^{\alpha_2}} \\
&= \frac{E(\omega)^{\beta}\,(e^{i\pi/2})^{\beta}}{1 + \lambda_c(\omega)^{\alpha_1}\,(e^{i\pi/2})^{\alpha_1} + \xi\lambda_c(\omega)^{\alpha_2}\,(e^{i\pi/2})^{\alpha_2}} \\
&= \frac{E(\omega)^{\beta}\,[\cos(\pi\beta/2) + i\,\sin(\pi\beta/2)]}{1 + \lambda_c(\omega)^{\alpha_1}\,[\cos(\pi\alpha_1/2) + i\,\sin(\pi\alpha_1/2)] + \xi\lambda_c(\omega)^{\alpha_2}\,[\cos(\pi\alpha_2/2) + i\,\sin(\pi\alpha_2/2)]} = \frac{N}{D}
\end{aligned} \tag{4.137}$$

Multiply Eq. (4.137) by the complex conjugate of the denominator which is

$$D^* = [1 + \lambda_c(\omega)^{\alpha_1}\cos(\pi\alpha_1/2) + \xi\lambda_c(\omega)^{\alpha_2}\cos(\pi\alpha_2/2)] - i\,[\lambda_c(\omega)^{\alpha_1}\sin(\pi\alpha_1/2) + \xi\lambda_c(\omega)^{\alpha_2}\sin(\pi\alpha_2/2)]$$

then

$$\begin{aligned}
N \times D^* = &\left[E(\omega)^{\beta}\cos(\pi\beta/2) + (\omega\lambda_c)^{\beta+\alpha_1}\cos(\pi(\beta-\alpha_1)/2) + \xi^{\alpha_2}(\omega\lambda_c)^{\beta+\alpha_2}\cos(\pi(\beta-\alpha_2)/2)\right] \\
&+ i\left[(\omega\lambda_c)^{\beta}\sin(\pi\beta/2) + (\omega\lambda_c)^{\beta+\alpha_1}\sin(\pi(\beta-\alpha_1)/2) + \xi^{\alpha_2}(\omega\lambda_c)^{\beta+\alpha_2}\sin(\pi(\beta-\alpha_2)/2)\right]
\end{aligned} \tag{4.138}$$

and

$$\tilde{\mathbb{D}} = D \times D^* = 1 + (\omega\lambda_c)^{2\alpha_1} + \xi^{2\alpha_2}(\omega\lambda_c)^{2\alpha_2} + 2\xi^{\alpha_2}(\omega\lambda_c)^{\alpha_1+\alpha_2}\cos(\pi(\alpha_1-\alpha_2)/2) + 2(\omega\lambda_c)^{\alpha_1}\cos(\pi\alpha_1/2) + 2\xi^{\alpha_2}(\omega\lambda_c)^{\alpha_2}\cos(\pi(\alpha_2)/2) \quad (4.139)$$

Therefore, the complex modulus becomes

$$\frac{G^*(\omega)}{G_c} = \frac{N \times D^*}{\tilde{\mathbb{D}}} \quad (4.140)$$

The real and imaginary parts of the complex modulus provide us with the storage and loss modulus of the complex fluid, respectively.

Therefore, from Eq. (4.140) the storage modulus of the complex fluid is

$$\frac{G'(\omega)}{G_c} = \frac{\left[(\omega\lambda_c)^{\beta}\cos(\pi\beta/2) + (\omega\lambda_c)^{\beta+\alpha_1}\cos(\pi(\beta-\alpha_1)/2) + \xi^{\alpha_2}(\omega\lambda_c)^{\beta+\alpha_2}\cos(\pi(\beta-\alpha_2)/2)\right]}{\tilde{\mathbb{D}}} \quad (4.141)$$

and the loss modulus of the complex fluid is

$$\frac{G''(\omega)}{G_c} = \frac{\left[(\omega\lambda_c)^{\beta}\sin(\pi\beta/2) + (\omega\lambda_c)^{\beta+\alpha_1}\sin(\pi(\beta-\alpha_1)/2) + \xi^{\alpha_2}(\omega\lambda_c)^{\beta+\alpha_2}\sin(\pi(\beta-\alpha_2)/2)\right]}{\tilde{\mathbb{D}}} \quad (4.142)$$

4.4.3 Numerical Results

Figure 4.10 provides insight into how a material might respond to different stresses or deformations, for the following models:

- The Multi-Mode Fractional Maxwell Gel (MM-FMG) where $0 < \alpha_2 < \alpha_1 = \beta < 1$. The mechanical interpretation of the four-parameter MM-FMG model ($\mathbb{G}_1$, $\mathbb{G}_2$, α_2, $\mathbb{V}$, β) is represented in a series as a combination of two spring and spring-pot.

- The Multi-Mode Fractional Maxwell Liquid (MM-FML) corresponds to $\beta = 1$, and it can be described mechanically by a dashpot and two spring-pots in series with

five-parameters ($\mathbb{G}_1$, $\mathbb{G}_2$, α_1, α_2 and $\mathbb{V}$).

- The Multi-Mode Fractional Maxwell Model (MM-FMM) where $0 < \alpha_2 < \alpha_1 < \beta < 1$. The mechanical interpretation of the six-parameter MM-FMM ($\mathbb{G}_1$, α_1, $\mathbb{G}_2$, α_2, $\mathbb{V}$, β) is represented in Fig. 4.9. The first two are specific cases of the MM-FMM.

Table 4.2 tabulates the asymptotic behaviour of the complex moduli in the limits $\omega\,\lambda_c \ll 1$ and $\omega\,\lambda_c \gg 1$ for these three standard models, which may be obtained from Eqs. (4.141) and (4.142).

		$\omega\lambda_c \ll 1$	$\omega\lambda_c \gg 1$
MM-FMM	G'/G_c	$(\omega\lambda_c)^{\beta} \cos(\pi\beta/2)$	$(\omega\,\lambda_c)^{\beta-\alpha_1} \cos(\pi(\beta-\alpha_1)/2)$
	G''/G_c	$(\omega\lambda_c)^{\beta} \sin(\pi\beta/2)$	$(\omega\,\lambda_c)^{\beta-\alpha_1} \sin(\pi(\beta-\alpha_1)/2)$
MM-FML	G'/G_c	$(\omega\,\lambda_c)^{1+\alpha_1} \cos(\pi(1-\alpha_1)/2)$	$(\omega\,\lambda_c)^{1-\alpha_1} \cos(\pi(1-\alpha_1)/2)$
	G''/G_c	$\omega\lambda_c$	$(\omega\,\lambda_c)^{1-\alpha_1} \sin(\pi(1-\alpha_1)/2)$
MM-FMG	G'/G_c	$(\omega\lambda_c)^{\beta} \cos(\pi\beta/2)$	1
	G''/G_c	$(\omega\lambda_c)^{\beta} \sin(\pi\beta/2)$	$(\omega\lambda_c)^{\beta-2\alpha_1+\alpha_2} \sin(\pi(\beta-\alpha_2)/2)$

Table 4.2: The asymptotes of G' and G'' for the MM-FMM ($0 < \alpha_2 < \alpha_1 < \beta < 1$), the MM-FML ($\beta = 1$), and the MM-FMG ($0 < \alpha_2 = \alpha_1 = \beta < 1$)

Using the expressions given above in Equations (4.141) and (4.142), the magnitude of the complex viscosity

$$|\eta^*(\omega)| = \frac{\sqrt{G'(\omega)^2 + G''(\omega)^2}}{\omega} \tag{4.143}$$

can be written in terms of the six MM-FMM parameters as follows:

$$\frac{|\eta^*(\omega)|}{\mathbb{V}\lambda_c^{1-\beta}} = \frac{1}{\sqrt{(\omega\,\lambda_c)^{2-2\beta} + 2(\omega\,\lambda_c)^{2-2\beta+\alpha_1+\alpha_2} \cos(\pi(\alpha_1+\alpha_2)/2) + (\omega\,\lambda_c)^{2(1-\beta+\alpha_1+\alpha_2)}}} \tag{4.144}$$

Fig. 4.10 illustrates the linear viscoelastic properties of three different models: MM-FMM, MM-FML, and MM-FMG. The plots are generated using data from (Rathinaraj ., 2021). Fig. 4.10 (a) represents the time-dependent relaxation modulus, $G(t)/G_c$, for the three models, illustrating how they respond to stress over time. Initially, the modulus is high, indicating that the material behaves more like a solid, resisting deformation. However, as time progresses, the modulus gradually decreases, signifying that the material is losing its ability to maintain stress and transitioning to a more fluid-like state. The rate

at which the modulus declines varies among the models, with some showing a steeper decline than others. These differences in slope highlight the unique relaxation behaviour of each model, reflecting variations in their viscoelastic properties. Fig. 4.10 (b) illustrates the frequency-dependent dynamic viscosity, $\eta^*(\omega)$, for the three models. The plot shows a decreasing trend as frequency increases, indicating shear-thinning behaviour, where the material's resistance to flow decreases at higher deformation rates. Each model exhibits a distinct rate of decline, reflecting differences in their underlying viscoelastic mechanisms. At lower frequencies, the viscosity remains relatively high, suggesting dominant fluid-like behaviour, while at higher frequencies, it drops significantly, indicating a transition toward more elastic or solid-like characteristics. The slopes of the curves reveal variations in the frequency response of each model, emphasizing differences in their ability to dissipate energy under oscillatory stress. Fig. 4.10 (c) presents the storage modulus, $G'(\omega)/G_c$, which characterizes the elastic energy storage capability of the material as a function of frequency. The curves indicate that as the frequency increases, the storage modulus increases, signifying a shift from a more viscous-dominant behaviour at low frequencies to an elastic-dominant response at higher frequencies. The rate of increase differs among the models, suggesting variations in their structural rigidity and ability to store mechanical energy under oscillatory loading. Fig. 4.10 (d) depicts the loss modulus, $G''(\omega)/G_c$, which represents the viscous dissipation of energy. The trends show that at low frequencies, energy dissipation is relatively high, but as the frequency increases, the loss modulus exhibits a crossover behaviour, marking the transition between viscous and elastic dominance. The distinct slopes and crossover points for each model indicate differences in their internal friction and energy dissipation characteristics. Fig. 4.10 (e) illustrates the loss tangent, $\tan\delta$, which represents the ratio of energy dissipated to energy stored during deformation. This parameter provides insight into the dominance of viscous versus elastic behaviour across different frequencies. A higher $\tan\delta$ value indicates greater energy dissipation, meaning the material behaves more like a liquid, while a lower value suggests that elastic properties are more dominant. The curves for the three models exhibit distinct trends, showing variations in damping behaviour. At lower frequencies, $\tan\delta$ is relatively

high, implying a stronger viscous response, whereas at higher frequencies, it decreases, indicating a transition toward more elastic-like behaviour. The differences among the models suggest variations in their ability to balance energy storage and dissipation under oscillatory stress.

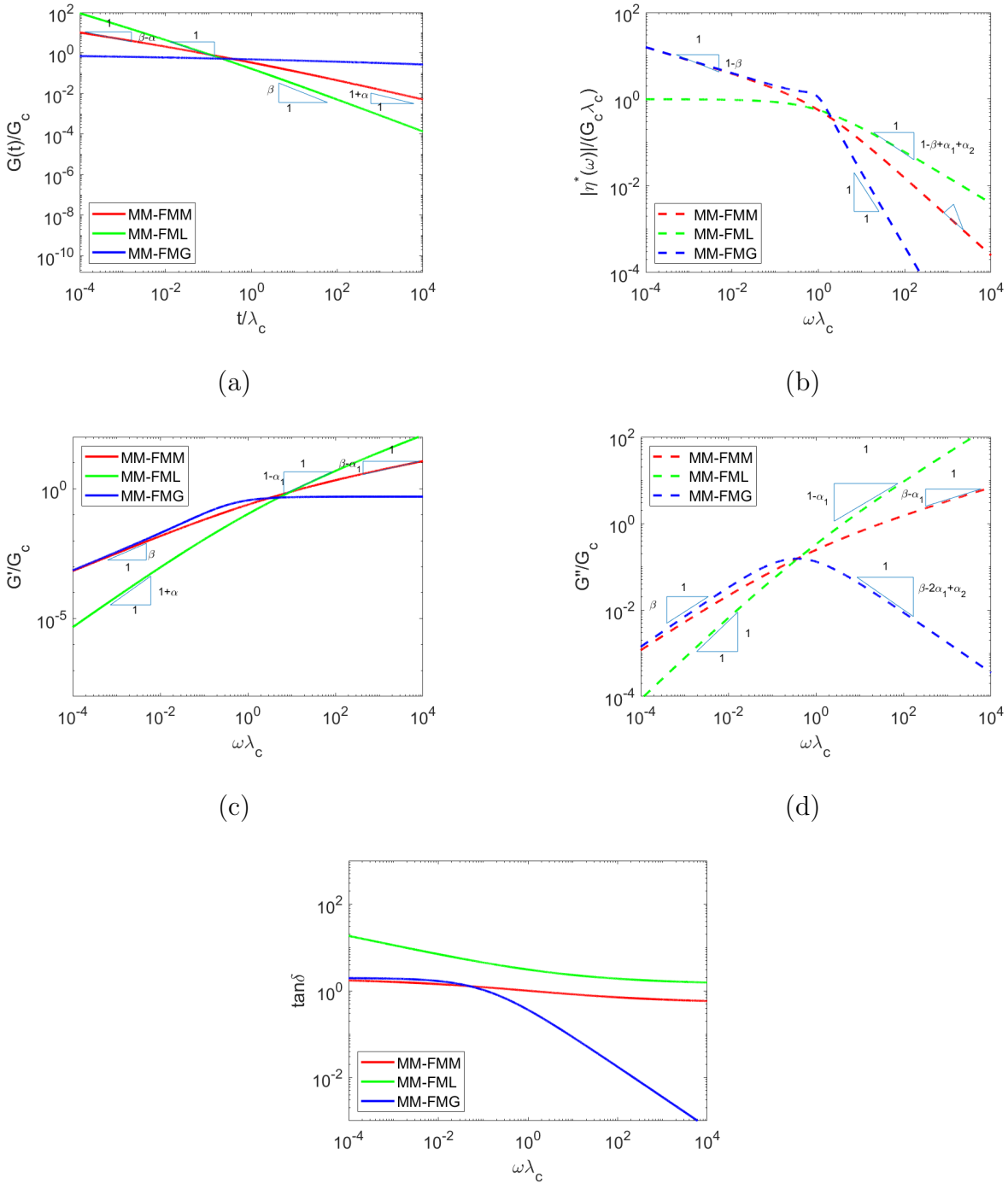

Figure 4.10: Plots illustrating the linear viscoelastic properties of the MM-FMM ($\beta = 0.7, \alpha_1 = 0.4, \alpha_2 = 0.2$), MM-FML ($\beta = 1, \alpha_1 = 0.4, \alpha_2 = 0.2$), and MM-FMG ($\beta = \alpha_1 = \alpha_2 = 0.7$). (a) $G(t)$, (b) $\eta^*(\omega)$, (c) G', (d) G'', and (e) $\tan\delta$.

4.4.4 Determination of the Relaxation Spectrum

Assume a discrete set of frequencies $\{\omega_j : 1 \leq j \leq M\}$ is used to measure the storage and loss modulus of sample of polymeric material.

We rewrite Eq. (4.141) and Eq. (4.142) as follows

$$G'(\omega_j) = \frac{G_c \left[(\omega_j\lambda_c)^\beta \cos(\pi\beta/2) + (\omega_j\lambda_c)^{\beta+\alpha_1} \cos(\pi(\beta-\alpha_1)/2) + \xi^{\alpha_2}(\omega_j\lambda_c)^{\beta+\alpha_2} \cos(\pi(\beta-\alpha_2)/2)\right]}{\tilde{\mathbb{D}}} \tag{4.145}$$

$$G''(\omega_j) = \frac{G_c \left[(\omega_j\lambda_c)^\beta \sin(\pi\beta/2) + (\omega_j\lambda_c)^{\beta+\alpha_1} \sin(\pi(\beta-\alpha_1)/2) + \xi^{\alpha_2}(\omega_j\lambda_c)^{\beta+\alpha_2} \sin(\pi(\beta-\alpha_2)/2)\right]}{\tilde{\mathbb{D}}} \tag{4.146}$$

where α_1, α_2, and β are the unknown parameters, with $0 < \alpha_2 < \alpha_1 \leq \beta \leq 1$.

The discrete relaxation times λ_c and elastic modulus G_c are determined by minimizing the following objective function (Baumgaertel Winter, 1989; Mustapha Phillips, 2000)

$$\begin{aligned} \mathcal{X}^2 &= \sum_{j=1}^{M} \left(\left[\frac{G'(\omega_j)}{G'_j} - 1\right]^2 + \left[\frac{G''(\omega_j)}{G''_j} - 1\right]^2 \right) \\ &= \sum_{j=1}^{M} \left(\left[\hat{k}_j\, G_c - 1\right]^2 + \left[\bar{k}_j\, G_c - 1\right]^2 \right) \end{aligned} \tag{4.147}$$

where

$$\hat{k}_j = \left[\frac{(\omega_j\lambda_c)^\beta \cos(\pi\beta/2) + (\omega_j\lambda_c)^{\beta+\alpha_1} \cos(\pi(\beta-\alpha_1)/2) + \xi^{\alpha_2}(\omega_j\lambda_c)^{\beta+\alpha_2} \cos(\pi(\beta-\alpha_2)/2)}{\tilde{\mathbb{D}}}\right] G'_j \tag{4.148}$$

and

$$\bar{k}_j = \left[\frac{(\omega_j\lambda_c)^\beta \sin(\pi\beta/2) + (\omega_j\lambda_c)^{\beta+\alpha_1} \sin(\pi(\beta-\alpha_1)/2) + \xi^{\alpha_2}(\omega_j\lambda_c)^{\beta+\alpha_2} \sin(\pi(\beta-\alpha_2)/2)}{\tilde{\mathbb{D}}}\right] G''_j \tag{4.149}$$

where $G'(\omega_j)$ and $G''(\omega_j)$ are determined by Eq.(4.145) and Eq.(4.146), and the values G'_j and G''_j are the dynamic data.

4.4.5 Fitting of Multi-Mode FMM to data

To assess the validation and accuracy of the multi-mode fractional Maxwell model (FMM) across the frequency range, we applied the fitting procedure described in Sec. 4.3.6 to two experimental datasets.

The model was fitted to both datasets using the optimal values of the parameters: $G_c, \lambda_c, \alpha_1, \alpha_2, \beta, \zeta$. Here, we define $\lambda_c = \lambda_1$, and $\zeta = \dfrac{\lambda_2}{\lambda_1}$, with the constraints $\lambda_2 < \lambda_1$, and $0 < \alpha_2 < \alpha_1 < \beta < 1$ being satisfied.

For experimental dataset 1 (see Fig. 4.11), the initial parameter estimates were: $(G_c, \lambda_c, \alpha_2, \alpha_1, \beta, \zeta) = [10000, 6, 0.2, 0.4, 0.7, 0.6666]$ corresponding to $\lambda_2 = 4$. After 5000 iterations, the optimized parameters were: $G_c = 104554.5701$, $\lambda_c = 0.2936$, $\alpha_2 = 0.0442$, $\alpha_1 = 0.5083$, $\beta = 0.7140$, $\zeta = 30377.8480$. At these final parameters, the value of $\mathcal{X}^2 = 0.148910$.

Similarly, for experimental dataset 2 (see Fig. 4.12), the initial estimates were: $(G_c, \lambda_c, \alpha_2, \alpha_1, \beta, \zeta) = [100, 22, 0.4, 0.8, 0.999, 0.1818]$ with $\lambda_2 = 4$. After 5000 iterations, the optimized parameters were: $G_c = 63.7892$, $\lambda_c = 1.7109$, $\alpha_2 = 0.7015$, $\alpha_1 = 0.4832$, $\beta = 0.8633$, $\zeta = 0.6676$. At these final parameters, the value of $\mathcal{X}^2 = 0.020844$. This value of χ^2 is an improvement over the value obtained for the single mode approximation given in Section 4.3.6.

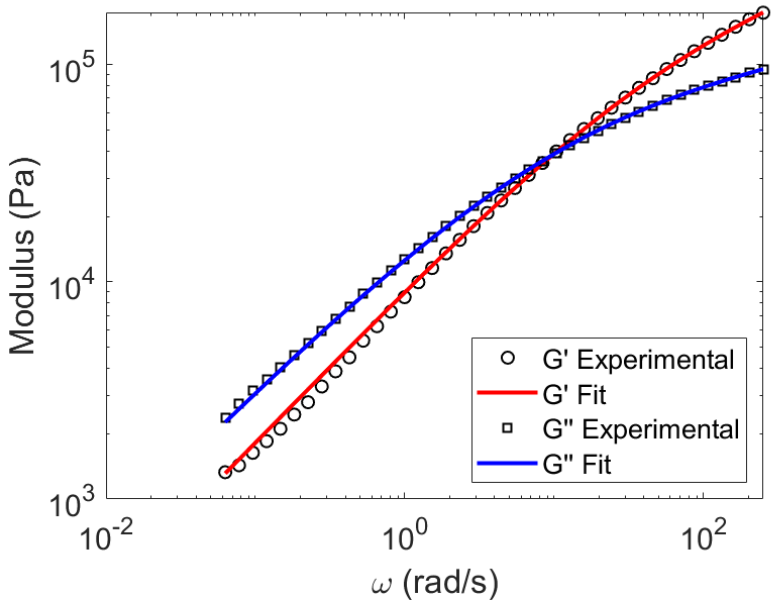

Figure 4.11: Comparison of the data and model predictions for a PEO solution using the MM-FMM. The converged values of the parameters were: $[G_c, \lambda_c, \alpha_2, \alpha_1, \beta, \zeta] = [104554.5701, 0.2936, 0.0442, 0.5083, 0.7140, 30377.8480]$

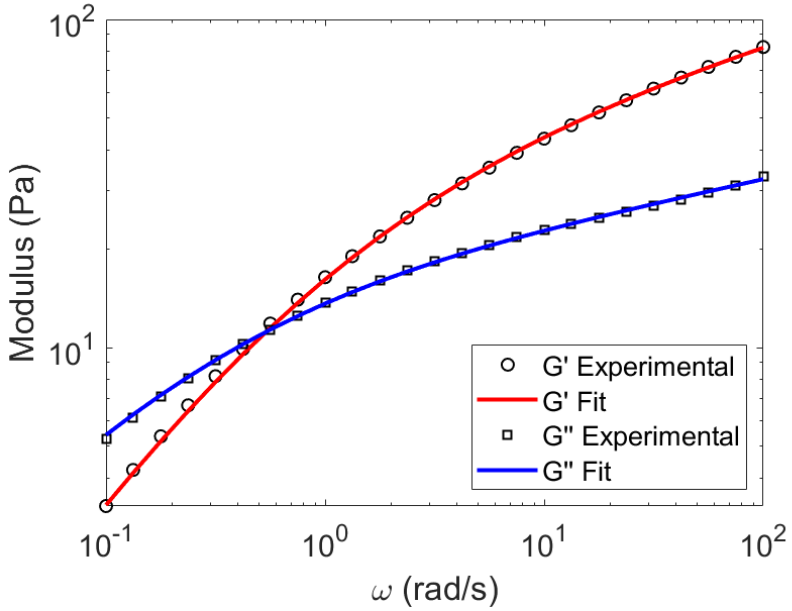

Figure 4.12: Comparison of the data and model predictions for a PEO solution using the MM-FMM. The converged values of the parameters were: $[G_c, \lambda_c, \alpha_2, \alpha_1, \beta, \zeta] = [63.7892, 1.7109, 0.7015, 0.4832, 0.8633, 0.6676]$

4.5 Multi-mode Maxwell model spectrum of relaxation times in parallel

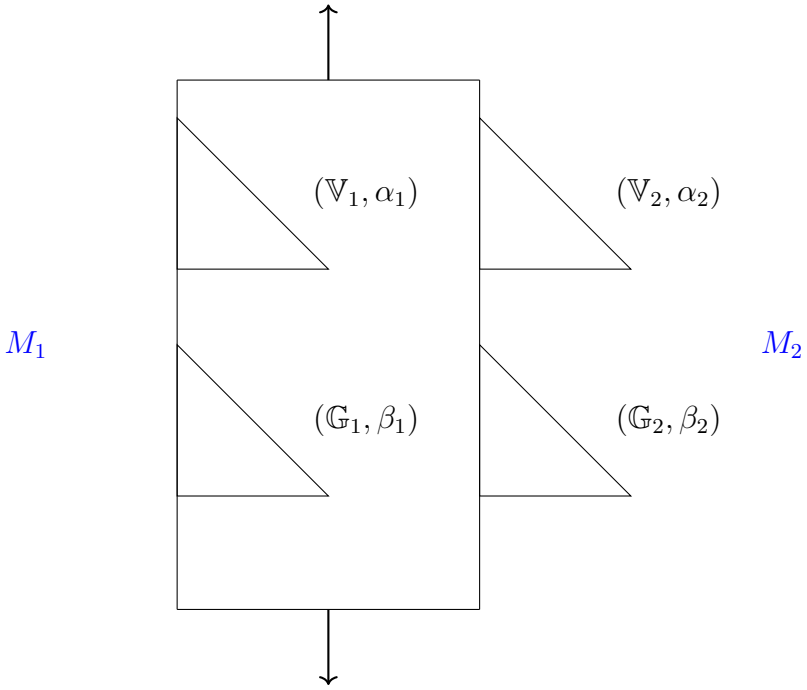

Figure 4.13: Multi-mode fractional Maxwell model

4.5.1 Derivation of the Differential Equation for the Multi-mode Fractional Maxwell Model

Consider the two-mode fractional Maxwell model shown in Fig. 4.13 comprising two fractional Maxwell elements M_1 and M_2 in parallel.

Let τ_i denote the stress in element M_i, $i = 1, 2$. Then in element M_1 we have

$$\tau_1 = \mathbb{V}_1 \, D_t^{\alpha_1} \gamma_{1,1} = \mathbb{G}_1 \, D_t^{\beta_1} \gamma_{1,2} \tag{4.150}$$

where $\gamma_{1,j}$, $j = 1, 2$ is the strain in each of the component of M_1. The total strain in M_1 is given by

$$\gamma_1 = \gamma_{1,1} + \gamma_{1,2} \tag{4.151}$$

Similarly, in element M_2 we have

$$\tau_2 = \mathbb{V}_2\, D_t^{\alpha_2}\gamma_{2,1} = \mathbb{G}_2\, D_t^{\beta_2}\gamma_{2,2} \tag{4.152}$$

and

$$\gamma_2 = \gamma_{2,1} + \gamma_{2,2} \tag{4.153}$$

The overall, stress and strain are given by

$$\tau = \tau_1 + \tau_2, \quad \gamma = \gamma_1 = \gamma_2, \tag{4.154}$$

respectively.

Expressing $\gamma_{1,j}$, $j = 1, 2$, in terms of τ_1:

$$\gamma_{1,1} = \frac{1}{\mathbb{V}_1}\, D_t^{-\alpha_1}\tau_1, \quad \gamma_{1,2} = \frac{1}{\mathbb{G}_1}\, D_t^{-\beta_1}\tau_1 \tag{4.155}$$

allows us to derive the following expression for γ_1,

$$\gamma_1(t) = \frac{1}{\mathbb{V}_1}\, D_t^{-\alpha_1}\tau_1(t) + \frac{1}{\mathbb{G}_1}\, D_t^{-\beta_1}\tau_1(t) \tag{4.156}$$

Similarly, we obtain the following expression for γ_2

$$\gamma_2(t) = \frac{1}{\mathbb{V}_2}\, D_t^{-\alpha_2}\tau_2(t) + \frac{1}{\mathbb{G}_2}\, D_t^{-\beta_2}\tau_2(t) \tag{4.157}$$

Take the Laplace transform of Eq. (4.156)

$$\mathcal{L}\{\gamma_1(t); s\} = \mathcal{L}\left\{\frac{1}{\mathbb{V}_1} D_t^{-\alpha_1}\tau_1(t); s\right\} + \mathcal{L}\left\{\frac{1}{\mathbb{G}_1} D_t^{-\beta_1}\tau_1(t); s\right\} \tag{4.158}$$

Using the Laplace transform of the fractional derivative (Mainardi, 2010)

$$\begin{aligned} \mathcal{L}\{D_t^{-\alpha} f(t); s\} &= s^{-\alpha}\mathcal{L}\{f(t); s\} \\ &= s^{-\alpha}F(s) \end{aligned} \tag{4.159}$$

we obtain

$$\mathcal{L}\{\gamma_1(t);s\} = \frac{1}{\mathbb{V}_1}s^{-\alpha_1}\mathcal{L}\{\tau_1(t);s\} + \frac{1}{\mathbb{G}_1}s^{-\beta_1}\mathcal{L}\{\tau_1(t);s\} \tag{4.160}$$

This expression simplifies to:

$$\mathcal{Q}(s) = \left(\frac{1}{\mathbb{V}_1}s^{-\alpha_1} + \frac{1}{\mathbb{G}_1}s^{-\beta_1}\right)\Sigma_1(s) \tag{4.161}$$

where $\mathcal{Q}(s)$ is the Laplace transform of $\gamma(t)$, and $\Sigma_1(s)$ is the Laplace transform of $\tau_1(t)$. We rearrange Eq.(4.161) to obtain an expression for $\Sigma_1(s)$

$$\begin{aligned}\Sigma_1(s) &= \frac{\mathcal{Q}(s)}{\frac{1}{\mathbb{V}_1 s^{\alpha_1}} + \frac{1}{\mathbb{G}_1 s^{\beta_1}}} \\ &= \left\{\frac{\mathbb{V}_1\mathbb{G}_1 s^{\alpha_1+\beta_1}}{\mathbb{V}_1 s^{\alpha_1} + \mathbb{G}_1 s^{\beta_1}}\right\}\mathcal{Q}(s)\end{aligned} \tag{4.162}$$

The convolution theorem states that the multiplication of two Laplace transforms in the s-domain corresponds to the convolution of their inverse transforms in the time domain. Consider the inverse Laplace transform of

$$\left\{\frac{\mathbb{V}_1\mathbb{G}_1 s^{\alpha_1+\beta_1}}{\mathbb{V}_1 s^{\alpha_1} + \mathbb{G}_1 s^{\beta_1}}\right\}$$

This can be rewritten in the form

$$\frac{\mathbb{G}_1 s^{\beta_1}}{1 + \frac{\mathbb{G}_1}{\mathbb{V}_1}s^{\beta_1-\alpha_1}} \tag{4.163}$$

To find the inverse Laplace transform, recall that

$$\mathcal{L}^{-1}\left\{\frac{s^\gamma}{1+as^\delta}\right\} \tag{4.164}$$

where $\gamma = \beta_1$, $a = \frac{\mathbb{G}_1}{\mathbb{V}_1}$ and $\delta = \beta_1 - \alpha_1$, is known to yields a function involving the Mittag-Leffler function $E_{\delta,\gamma+1}(t)$.

Setting $\gamma = \beta_1$, $a = \frac{\mathbb{G}_1}{\mathbb{V}_1}$ and $\delta = \beta_1 - \alpha_1$ in (4.164) we obtain inverse Laplace transform

of the expression (4.163)

$$\mathcal{L}^{-1}\left\{\frac{\mathbb{V}_1\mathbb{G}_1 s^{\alpha_1+\beta_1}}{\mathbb{V}_1 s^{\alpha_1}+\mathbb{G}_1 s^{\beta_1}}\right\} = \mathbb{G}_1 t^{\alpha_1} E_{\beta_1-\alpha_1,\beta_1+1}\left(-\frac{\mathbb{G}_1}{\mathbb{V}_1}t^{\beta_1-\alpha_1}\right) \tag{4.165}$$

Therefore, the inverse Laplace transform of the entire expression is the convolution of $G(t)$ with the inverse transform of $\left\{\frac{\mathbb{V}_1\mathbb{G}_1 s^{\alpha_1+\beta_1}}{\mathbb{V}_1 s^{\alpha_1}+\mathbb{G}_1 s^{\beta_1}}\right\}$.

We can then write $\tau_1(t)$ using the convolution theorem as follows

$$\tau_1(t) = \int_0^t \mathbb{G}_1(t-t')^{\alpha_1} E_{\beta_1-\alpha_1,\beta_1+1}\left(-\frac{\mathbb{G}_1}{\mathbb{V}_1}(t-t')^{\beta_1-\alpha_1}\right)\dot{\gamma}(t')\,dt' \tag{4.166}$$

Similarly, we can derive the following expression for $\tau_2(t)$:

$$\tau_2(t) = \int_0^t \mathbb{G}_2(t-t')^{\alpha_2} E_{\beta_2-\alpha_2,\beta_2+1}\left(-\frac{\mathbb{G}_2}{\mathbb{V}_2}(t-t')^{\beta_2-\alpha_2}\right)\dot{\gamma}(t')\,dt' \tag{4.167}$$

Substituting Eq.(4.166) and Eq.(4.167) into Eq.(4.154) we obtain the total stress of the two-mode Maxwell model as a function for time

$$\begin{aligned}\tau(t) = \int_0^t \Bigg[&\mathbb{G}_1(t-t')^{\alpha_1} E_{\beta_1-\alpha_1,\beta_1+1}\left(-\frac{\mathbb{G}_1}{\mathbb{V}_1}(t-t')^{\beta_1-\alpha_1}\right)\\ &+ \mathbb{G}_2(t-t')^{\alpha_2} E_{\beta_2-\alpha_2,\beta_2+1}\left(-\frac{\mathbb{G}_2}{\mathbb{V}_2}(t-t')^{\beta_2-\alpha_2}\right)\Bigg]\dot{\gamma}(t')\,dt'\end{aligned} \tag{4.168}$$

This expression represents the combined stress as a function of time, accounting for the contributions from both.

To derive a differential equation corresponding to the integral equation in Eq.(4.168), we first recognize the structure of the fractional integral. The integral expressions involve fractional-order integrals, and the presence of the Mittag-Leffler functions $E_{\beta_1-\alpha_1,\beta_1+1}(\cdot)$ and $E_{\beta_2-\alpha_2,\beta_2+1}(\cdot)$ suggests that the convolution terms are equivalent to a fractional derivative in the time domain. Given that the integrals include terms of the form $(t-t')^{\alpha_1}$ and $(t-t')^{\alpha_2}$, we can convert the integral equation into a differential equation by employing fractional derivatives $D_t^{\alpha_1}$ and $D_t^{\alpha_2}$. Therefore, the differential equation corresponding to

the given integral equation is given by:

$$\mathbb{V}_1 D_t^{\alpha_1}\tau(t) + \mathbb{G}_1 D_t^{\beta_1}\tau(t) + \mathbb{V}_2 D_t^{\alpha_2}\tau(t) + \mathbb{G}_2 D_t^{\beta_2}\tau(t) = \gamma(t) \tag{4.169}$$

This differential equation models the stress-strain relationship in a material described by a two-mode fractional Maxwell model, with orders of differentiation $(\alpha_1, \beta_1, \alpha_2, \beta_2)$ and coefficients $(\mathbb{V}_1, \mathbb{G}_1, \mathbb{V}_2, \mathbb{G}_2)$ governing the material's behaviour.

Then, the equation can be rearranged for simplicity to two grouped terms that represent different modes (M_1, M_2):

$$(\mathbb{V}_1 D_t^{\alpha_1} + \mathbb{G}_1 D_t^{\beta_1})\tau(t) + (\mathbb{V}_2 D_t^{\alpha_2} + \mathbb{G}_2 D_t^{\beta_2})\tau(t) = \gamma(t) \tag{4.170}$$

where $0 < \beta_1 < \alpha_1 < 1$ and $0 < \beta_2 < \alpha_2 < 1$, and $\alpha_2 < \alpha_1, \beta_2 < \beta_1$.

4.5.2 Derivation of the Dynamic Moduli

To derive the loss and storage moduli from the integral equation (4.168), we need to relate the integral form to the frequency domain, where the moduli can be expressed as functions of frequency.

To find the loss and storage moduli, we take the Fourier transform of both sides of the integral equation (4.168). The Fourier transform of $\tau(t)$ is denoted as $\tilde{\tau}(\omega)$ and the Fourier transform of $\mathcal{Q}(t)$ is $\tilde{\mathcal{Q}}(\omega)$.

The Fourier transform of a convolution integral is given by:

$$\mathcal{F}\left\{\int_0^t K(t-t')\mathcal{Q}(t')\,dt'\right\} = \tilde{K}(\omega)\tilde{\mathcal{Q}}(\omega) \tag{4.171}$$

where $\tilde{K}(\omega)$ is the Fourier transform of the kernel $K(t)$.

In Eq.(4.168), the kernel $K(t-t')$ is

$$K(t-t') = \mathbb{G}_1(t-t')^{\alpha_1} E_{\beta_1-\alpha_1,\beta_1+1}\left(-\frac{\mathbb{G}_1}{\mathbb{V}_1}(t-t')^{\beta_1-\alpha_1}\right) + \mathbb{G}_2(t-t')^{\alpha_2} E_{\beta_2-\alpha_2,\beta_2+1}\left(-\frac{\mathbb{G}_2}{\mathbb{V}_2}(t-t')^{\beta_2-\alpha_2}\right) \tag{4.172}$$

To find its Fourier transform, we use the property of the fractional calculus in the frequency domain:

The Fourier transform of the term $(t-t')^{\alpha}$ is:

$$\mathcal{F}\left\{(t-t')^{\alpha}\right\} = \frac{\Gamma(1+\alpha)}{(\mathrm{i}\omega)^{1+\alpha}} \tag{4.173}$$

Then, the Fourier transform of the kernel $K(t)$ is

$$\tilde{K}(\omega) = \mathbb{G}_1 \frac{\Gamma(1+\alpha_1)}{(\mathrm{i}\omega)^{1+\alpha_1}} \tilde{E}_{\beta_1-\alpha_1,\beta_1+1}(\omega) + \mathbb{G}_2 \frac{\Gamma(1+\alpha_2)}{(\mathrm{i}\omega)^{1+\alpha_2}} \tilde{E}_{\beta_2-\alpha_2,\beta_2+1}(\omega) \tag{4.174}$$

where $\tilde{E}$ denotes the frequency-domain representation of the Mittag-Leffler function. The storage modulus $G'(\omega)$ and loss modulus $G''(\omega)$ are derived from the complex modulus $\tilde{K}(\omega)$

$$\tilde{K}(\omega) = G'(\omega) + i\, G''(\omega) \tag{4.175}$$

In this section, we use the notation $\tilde{K}(\omega)$ to represent the complex modulus of the material in the frequency domain. It is important to note that $\tilde{K}(\omega)$ is mathematically equivalent to the commonly used rheological notation $G^*(\omega)$, as defined in Eq. (4.134). This equivalence allows for consistency between the mathematical formulation and standard rheological terminology.

From the differential equation in the frequency domain, we have

$$\tilde{\tau}(\omega) = \tilde{K}(\omega)\tilde{\mathcal{Q}}(\omega) \tag{4.176}$$

Thus

$$\tilde{K}(\omega) = \frac{\tilde{\tau}(\omega)}{\tilde{\mathcal{Q}}(\omega)} \tag{4.177}$$

We express this in terms of real and imaginary parts to find $G'(\omega)$ and $G''(\omega)$

$$\begin{aligned}\tilde{K}(\omega) = &\left[\mathbb{G}_1 \frac{\Gamma(1+\alpha_1)\cos(\theta_1)}{\omega^{1+\alpha_1}} + \mathbb{G}_2 \frac{\Gamma(1+\alpha_2)\cos(\theta_2)}{\omega^{1+\alpha_2}}\right] \\ &+ i\left[\mathbb{G}_1 \frac{\Gamma(1+\alpha_1)\sin(\theta_1)}{\omega^{1+\alpha_1}} + \mathbb{G}_2 \frac{\Gamma(1+\alpha_2)\sin(\theta_2)}{\omega^{1+\alpha_2}}\right]\end{aligned} \tag{4.178}$$

where

$$G'(\omega) = \mathbb{G}_1 \frac{\Gamma(1+\alpha_1)\cos(\theta_1)}{\omega^{1+\alpha_1}} + \mathbb{G}_2 \frac{\Gamma(1+\alpha_2)\cos(\theta_2)}{\omega^{1+\alpha_2}} \tag{4.179}$$

and

$$G''(\omega) = \mathbb{G}_1 \frac{\Gamma(1+\alpha_1)\sin(\theta_1)}{\omega^{1+\alpha_1}} + \mathbb{G}_2 \frac{\Gamma(1+\alpha_2)\sin(\theta_2)}{\omega^{1+\alpha_2}} \tag{4.180}$$

where $\theta_1 = (1+\alpha_1)\frac{\pi}{2}$ and $\theta_2 = (1+\alpha_2)\frac{\pi}{2}$ depend on the phase characteristics of the Mittag-Leffler function.

4.6 Conclusions

To conclude, we derived fractional models using spring-pot elements arranged in series and/or parallel. Also, we derived expression for the relaxation time and the dynamic moduli of Fractional Maxwell models in single-mode and multi-mode settings. In addition to this, we studied the validation and the accuracy of these models. The following summarises our analysis:

1. The exact solution of the Fractional Maxwell Model (FMM) in single-mode and multi-mode settings using the Laplace transform of the Green's function was derived and expanded in terms of the MLF. This is an alternative to the approach of Friedrich (1991) who used Fourier transforms.

2. The Fractional Maxwell Model (FMM) is a general model that was examined for $0 < \alpha < \beta < 1$ (Yang ., 2010). We also looked at two significant limits that were investigated in the literature on fractional viscoelasticity: the Fractional Maxwell Liquid ($0 < \alpha < 1, \beta = 1$), and the Fractional Maxwell Gel ($0 < \alpha = \beta < 1$) (Rathinaraj ., 2021). Table 4.1 provides an overview of the limiting frequency responses of the linear viscoelastic moduli for these models.

3. The single-mode fractional Maxwell model was generalized to a new fractional viscoelastic model, the multi-mode Fractional Maxwell Model (MM-FMM) for $0 < \alpha_2 < \alpha_1 < \beta < 1$. The aim of generalizing the Maxwell model is to allow us to predict different sorts of complex viscoelastic behaviours. We also looked at two

significant limits on fractional viscoelasticity: the multi-mode Fractional Maxwell Liquid $0 < \alpha_2 < \alpha_1 < 1, \beta = 1$, and the multi-mode Fractional Maxwell Gel $0 < \alpha_2 = \alpha_1 = \beta \leq 1$. The details of the limiting frequency responses of the linear viscoelastic moduli for these models can be found in Table 4.2.

4. Following the derivation of new fractional viscoelastic models, an analysis of these models in terms of their rheological behaviour is presented in Fig. 4.6 and Fig. 4.10. The analysis of these plots gives a comprehensive overview of the viscoelastic behaviour of the FMM, FML, and FMG models. The FML exhibits liquid-like behaviour with dominant viscous properties, the FMG behaves more like a solid or gel with high elasticity, and the FMM is intermediate, exhibiting both liquid-like and solid-like properties depending on the time or frequency scale. Finally, the performance of the proposed models was evaluated by fitting them to experimental dynamic data spanning a broad frequency range. Curve fitting techniques were employed to determine the optimal parameter values for each variant of the fractional Maxwell model. The comparison between the experimental data and model predictions is presented in Fig.4.7, Fig.4.8, and Fig. 4.12. The results indicate that the multi-mode model yields a more accurate representation of the data than the single-mode model, highlighting its enhanced capacity to capture the complex viscoelastic behaviour observed in the experiments.

5. The single-mode fractional Maxwell model was also extended to a new fractional viscoelastic model by introducing fractional elements in parallel, resulting in the multi-mode Fractional Maxwell Model (MM-FMM), where $0 < \beta_1 < \alpha_1 < 1$ and $0 < \beta_2 < \alpha_2 < 1$, and $\alpha_2 < \alpha_1, \beta_2 < \beta_1$. This configuration is particularly well-suited for modeling materials with heterogeneous structures.

Chapter 5

Numerical Discretization of Fractional Derivatives

5.1 Introduction

Effective algorithms for the numerical approximation of fractional differential operators are highly desired, given the potential applications of these operators. Fractional derivatives can be discretized to produce a set of quadrature formulas. Various node and coefficient selections result in different orders of accuracy. Three basic paths are used to obtain numerical approximations of fractional derivatives. In general, according to the order of differentiation, numerical schemes can be derived using polynomial interpolation with a derived order of accuracy giving rise to the $L1$, $L2$, and $L2C$ approaches (Cai Li, 2020; Zhang ., 2014).

According to the definition of the Caputo fractional derivative Eq.(5.30), the integral term indicates history dependence and weakly singular behaviour. Therefore, approximating fractional derivatives is much more challenging than approximating classical derivatives. Lubich (1986) describes some basic discretized fractional calculus techniques. For instance, finite differences can be used to discretize the classical derivatives that occur in the definition of a fractional derivative (Pooseh ., 2013).

The main goal of this chapter is to derive highly accurate methods to approximate the Caputo fractional derivative. These will be used in later chapters to solve the Taylor-Couette problem and perform a convergence analysis. Accordingly, this chapter is organised as follows: Some fundamental concepts relevant to the development of numerical methods for treating fractional derivatives are presented in Section 5.2. The first-order

difference scheme for the Caputo fractional derivative for two ranges of fractional order is derived in Section 5.3. Section 5.4 extends these ideas to a second-order difference scheme for the Caputo fractional derivative and also for the two ranges of fractional order. The derivation of the first-order and the second-order time discretization for the Fractional Viscoelastic Fluid model using finite difference method is given in Section 5.5. Finally, some conclusions are made in Section 5.6.

5.2 Numerical Fundamentals

For the discretization of time $t \in [0, T]$, we assume a uniform mesh, with N_T time steps $\Delta t = T/N_T$, and then approximate the fractional derivative at the discrete times $t_n = n\Delta t$, $n = 0, 1, \ldots, N_T$.

At the spatial mesh point r_i, we define $u_i^n = u(r_i, t_n)$. Let U_i^n denote the approximation to $u(r_i, t_n)$ (i.e. $U_i^n \simeq u_i^n$), $i = 0, \ldots, N$, then we can introduce the following notation for the average of u between points (r_i, t_n) and (r_i, t_{n-1})

$$u_i^{n-1/2} = \frac{u_i^n + u_i^{n-1}}{2} \tag{5.1}$$

and the $O(\Delta t^2)$ central difference approximation to $\frac{\partial u}{\partial t}$ at $t = t_{n-1/2}$ is given by

$$\delta_t U_i^{n-1/2} = \frac{U_i^n - U_i^{n-1}}{\Delta t} \tag{5.2}$$

(see Sun Wu (2006), for example).

Now we show how to differentiate an interpolant in order to produce differentiation formulas. The idea behind this technique is simple: the first step is to use the data to create an interpolating polynomial. The interpolant can then be directly differentiated to approximate the derivative at any point (Levy, 2010).

This process is described as follows. If the linear interpolation polynomial of u on $[t_{n-1}, t_n]$,

$n = 1, \ldots, N_T$, is given by the Lagrange formula

$$\Pi_{1,n} u(s) = u(t_{n-1}) \left(\frac{t_n - s}{\Delta t} \right) + u(t_n) \left(\frac{s - t_{n-1}}{\Delta t} \right) \tag{5.3}$$

then the first derivative of $\Pi_{1,n} u(s)$ is

$$\partial_s \left(\Pi_{1,n} u(s) \right) = \frac{u^n - u^{n-1}}{\Delta t} \tag{5.4}$$

Extension to the quadratic interpolation of $u(t)$ on $[t_{n-1}, t_{n+1}]$, $n = 1, \ldots, N_T - 1$, yields

$$\begin{aligned} \Pi_{2,n} u(s) = u(t_{n-1}) \left[\frac{(s - t_n)(s - t_{n+1})}{2(\Delta t)^2} \right] - u(t_n) \left[\frac{(s - t_{n-1})(s - t_{n+1})}{(\Delta t)^2} \right] \\ + u(t_{n+1}) \left[\frac{(s - t_{n-1})(s - t_n)}{2(\Delta t)^2} \right] \end{aligned} \tag{5.5}$$

The first derivative of $\Pi_{2,n} u(s)$ is

$$\partial_s \left(\Pi_{2,n} \; u(s) \right) = u^{n-1} \left[\frac{2s - t_n - t_{n+1}}{2(\Delta t)^2} \right] - u^n \left[\frac{2s - t_{n-1} - t_{n+1}}{(\Delta t)^2} \right] + u^{n+1} \left[\frac{2s - t_n - t_{n-1}}{2(\Delta t)^2} \right] \tag{5.6}$$

and the second derivative of Eq.(5.5) is given by

$$\partial_t^2 \left(\Pi_{2,n} u(s) \right) = \frac{u^{n-1} - 2u^n + u^{n+1}}{(\Delta t)^2} \tag{5.7}$$

5.3 First-order difference scheme for the Caputo fractional derivative

The derivations in this section are based on the methodology of Sun Wu (2006).

5.3.1 Case 1: when $1 < \alpha < 2$

We define the time fractional derivative $D_t^\alpha u(t_n)$ in Caputo sense as

$$D_t^\alpha u(t_n) = \frac{1}{\Gamma(2-\alpha)} \int_0^{t_n} \frac{\partial_s^2 u}{(t_n - s)^{\alpha-1}}\, ds, \quad 1 < \alpha < 2 \tag{5.8}$$

Let

$$y(r, s) = \frac{\partial u(r, s)}{\partial s} \tag{5.9}$$

then

$$\frac{\partial y(r, s)}{\partial s} = \frac{\partial^2 u(r, s)}{\partial s^2} \tag{5.10}$$

Define

$$D_t^\alpha u(t_n) = x(r_i, t_n) \tag{5.11}$$

then equation (5.8) becomes

$$x(r, t_n) = \frac{1}{\Gamma(2-\alpha)} \int_0^{t_n} (t_n - s)^{1-\alpha} \frac{\partial y}{\partial s}\, ds \tag{5.12}$$

Define the grid functions

$$U_i^n \simeq u_i^n, \;\; Y_i^n \simeq y(r_i, t_n), \;\; X_i^n \simeq x(r_i, t_n), \;\; 0 \le i \le N, \;\; n \ge 0. \tag{5.13}$$

Using Taylor expansions, it follows from Eq. (5.9) that a second-order approximation to $y(r_i, t_{n-1/2})$ is

$$Y_i^{n-1/2} = \delta_t U_i^{n-1/2} = \frac{U_i^n - U_i^{n-1}}{\Delta t} \tag{5.14}$$

The local truncation error e_1 of this approximation is defined by

$$(e_1)_i^{n-1/2} = y_i^{n-1/2} - \delta_t u_i^{n-1/2} \tag{5.15}$$

from which we can show, using Taylor series expansions, that

$$|(e_1)_i^{n-1/2}| \leq c_1(\Delta t)^2 \tag{5.16}$$

where c_1 is a constant.

Based on Lemma 2.2 of Sun Wu (2006), and using a Taylor expansion with integral remainder for any function $F(t) \in C^2[0, t_n]$, we have

$$\int_0^{t_n} F'(t)\frac{1}{(t_n - t)^{\alpha-1}}dt \simeq \sum_{k=1}^{n} \frac{F(t_k) - F(t_{k-1})}{\Delta t} \int_{t_{k-1}}^{t_k} \frac{1}{(t_n - t)^{\alpha-1}}dt, \quad \Delta t > 0 \tag{5.17}$$

which is called the L1 method.

Therefore, an approximation to Eq. (5.12) at the point (r_i, t_n) is

$$X_i^n = \frac{1}{\Gamma(2-\alpha)} \left[\sum_{j=1}^{n} \frac{Y_i^j - Y_i^{j-1}}{\Delta t} \int_{t_{j-1}}^{t_j} (t_n - s)^{1-\alpha} ds \right] \tag{5.18}$$

Since

$$\int_{t_{j-1}}^{t_j} (t_n - s)^{1-\alpha} ds = \frac{(\Delta t)^{2-\alpha}}{2-\alpha} \left[(n-j+1)^{2-\alpha} - (n-j)^{2-\alpha} \right], \quad n - j \geq 0. \tag{5.19}$$

and based on Lemma 2.3 of Sun Wu (2006), we can express Eq. (5.18) in the form

$$X_i^n = \frac{\Delta t^{1-\alpha}}{\Gamma(3-\alpha)} \sum_{j=1}^{n} \tilde{a}_{n-j}(\alpha) \ \left(Y_i^j - Y_i^{j-1} \right) \tag{5.20}$$

where

$$\tilde{a}_{n-j}(\alpha) = \left[(n-j+1)^{2-\alpha} - (n-j)^{2-\alpha} \right], \quad n - j \geq 0. \tag{5.21}$$

Let $l = n - j$, then

$$\tilde{a}_l(\alpha) = \left[(l+1)^{2-\alpha} - l^{2-\alpha} \right], \quad l \geq 0. \tag{5.22}$$

then Eq. (5.20) becomes,

$$
\begin{aligned}
X_i^n &= \frac{\Delta t^{1-\alpha}}{\Gamma(3-\alpha)}\Bigg[\tilde{a}_{n-1}(\alpha)\ \left(Y_i^1 - Y_i^0\right) + \tilde{a}_{n-2}(\alpha)\left(Y_i^2 - Y_i^1\right) + \tilde{a}_{n-3}(\alpha)\left(Y_i^3 - Y_i^2\right) \\
&\qquad + \cdots + \tilde{a}_1(\alpha)\left(Y_i^{n-1} - Y_i^{n-2}\right) + \tilde{a}_0(\alpha)\left(Y_i^n - Y_i^{n-1}\right)\Bigg] \\
&= \frac{\Delta t^{1-\alpha}}{\Gamma(3-\alpha)}\Bigg[\tilde{a}_0(\alpha)\ Y_i^n + \left(\tilde{a}_1(\alpha) - \tilde{a}_0(\alpha)\right) Y_i^{n-1} + \cdots + \left(\tilde{a}_{n-2}(\alpha) - \tilde{a}_{n-3}(\alpha)\right) Y_i^2 \\
&\qquad + \left(\tilde{a}_{n-1}(\alpha) - \tilde{a}_{n-2}(\alpha)\right) Y_i^1 - \tilde{a}_{n-1}(\alpha) Y_i^0\Bigg] \\
&= \frac{\Delta t^{1-\alpha}}{\Gamma(3-\alpha)}\Bigg[\tilde{a}_0(\alpha) Y_i^n - \sum_{j=1}^{n-2}\left(\tilde{a}_{n-j-2}(\alpha) - \tilde{a}_{n-j-1}(\alpha)\right)\ Y_i^{j+1} - \left(\tilde{a}_{n-2}(\alpha) - \tilde{a}_{n-1}(\alpha)\right) Y_i^1 \\
&\qquad - \tilde{a}_{n-1}(\alpha) Y_i^0\Bigg]
\end{aligned}
\tag{5.23}
$$

and

$$
X_i^{n-1} = \frac{\Delta t^{1-\alpha}}{\Gamma(3-\alpha)}\left[\tilde{a}_0(\alpha) Y_i^{n-1} - \sum_{j=1}^{n-2}\left(\tilde{a}_{n-j-2}(\alpha) - \tilde{a}_{n-j-1}(\alpha)\right)\ Y_i^j - \tilde{a}_{n-2}(\alpha) Y_i^0\right] \tag{5.24}
$$

Consequently, the temporal discretization of $X_i^{n-1/2}$ is

$$
\begin{aligned}
\frac{X_i^n + X_i^{n-1}}{2} &\simeq X_i^{n-1/2} \\
&= \frac{\Delta t^{1-\alpha}}{\Gamma(3-\alpha)}\Bigg[\tilde{a}_0(\alpha) Y_i^{n-1/2} - \sum_{j=1}^{n-2}\left(\tilde{a}_{n-j-2}(\alpha) - \tilde{a}_{n-j-1}(\alpha)\right)\ Y_i^{j+1/2} \\
&\qquad - \frac{1}{2}\left[\left(\tilde{a}_{n-2}(\alpha) - \tilde{a}_{n-1}(\alpha)\right) Y_i^1 + \tilde{a}_{n-1}(\alpha) Y_i^0 + \tilde{a}_{n-2}(\alpha) Y_i^0\right]\Bigg] \\
&= \frac{\Delta t^{1-\alpha}}{\Gamma(3-\alpha)}\Bigg[\tilde{a}_0(\alpha) Y_i^{n-1/2} - \sum_{j=1}^{n-2}\left(\tilde{a}_{n-j-2}(\alpha) - \tilde{a}_{n-j-1}(\alpha)\right)\ Y_i^{j+1/2} \\
&\qquad - \frac{1}{2}\left(\tilde{a}_{n-2}(\alpha) - \tilde{a}_{n-1}(\alpha)\right)\left(Y_i^1 + Y_i^0\right) - \tilde{a}_{n-1}(\alpha) Y_i^0\Bigg] \\
&= \frac{\Delta t^{1-\alpha}}{\Gamma(3-\alpha)}\left[\tilde{a}_0(\alpha) Y_i^{n-1/2} - \sum_{j=0}^{n-2}\left(\tilde{a}_{n-j-2}(\alpha) - \tilde{a}_{n-j-1}(\alpha)\right)\ Y_i^{j+1/2} - \tilde{a}_{n-1}(\alpha)\, Y_i^0\right]
\end{aligned}
\tag{5.25}
$$

where e_2 is the local truncation error of this approximation $X_i^{n-1/2}$ with

$$|(e_2)_i^{n-1/2}| \leq c_2(\Delta t)^{3-\alpha} \tag{5.26}$$

where c_2 is a constant.

Substituting Eq. (5.14) into Eq. (5.25), we have

$$\begin{aligned} X_i^{n-1/2} = \frac{\Delta t^{1-\alpha}}{\Gamma(3-\alpha)}\left[\tilde{a}_0(\alpha)\ \delta_t U_i^{n-1/2} - \sum_{j=0}^{n-2}\left(\tilde{a}_{n-j-2}(\alpha) - \tilde{a}_{n-j-1}(\alpha)\right)\delta_t U_i^{j+1/2} - \tilde{a}_{n-1}(\alpha)Y_i^0\right] \\ + \frac{\Delta t^{1-\alpha}}{\Gamma(3-\alpha)}\left[\tilde{a}_0(\alpha)\ (e_1)_i^{n-1/2} - \sum_{j=1}^{n-1}\left(\tilde{a}_{n-j-1} - \tilde{a}_{n-j}(\alpha)\right)(e_1)_i^{j-1/2}\right] + (e_2)_i^{n-1/2} \end{aligned} \tag{5.27}$$

Replacing $\delta_t U_i^{n-1/2}$ by Eq. (5.2), and substituting the above results into Eq. (5.8) we obtain the following finite difference approximation to $D_{t_n}^{\alpha} u$:

$$\begin{aligned} D_t^{\alpha} u(t_n) &\simeq \frac{\Delta t^{1-\alpha}}{\Gamma(3-\alpha)}\left[\tilde{a}_0(\alpha)\ \left(\frac{U_i^n - U_i^{n-1}}{\Delta t}\right) - \sum_{j=1}^{n-1}\left(\tilde{a}_{n-j-1}(\alpha) - \tilde{a}_{n-j}(\alpha)\right)\left(\frac{U_i^j - U_i^{j-1}}{\Delta t}\right)\right. \\ &\qquad \left. - \tilde{a}_{n-1}(\alpha)\Phi(r_i)\right] \\ &= \frac{\Delta t^{-\alpha}}{\Gamma(3-\alpha)}\left[\sum_{j=0}^{n}\tilde{A}_j\, U_i^j - \tilde{a}_{n-1}(\alpha)\Phi(r_i)\right] \end{aligned} \tag{5.28}$$

where $\Phi(r_i) = Y_i^0 = y(r_i, 0)$, and

$$\tilde{A}_j = \begin{cases} \tilde{a}_{n-2}(\alpha) - \tilde{a}_{n-1}(\alpha) & \text{if} \quad j = 0 \\ -\tilde{a}_{n-j-1}(\alpha) + 2\tilde{a}_{n-j}(\alpha) - \tilde{a}_{n-j+1}(\alpha), & \text{if} \quad 1 \leq j \leq n-2 \\ -2\tilde{a}_0(\alpha) + \tilde{a}_1(\alpha), & \text{if} \quad j = n-1 \\ \tilde{a}_0(\alpha), & \text{if} \quad j = n \end{cases} \tag{5.29}$$

5.3.2 Case 2: when $0 < \alpha < 1$

The time-fractional derivative $D_t^\alpha u(t_n)$ will be approximated numerically, as described in Sun Wu (2006).

$$D_t^\alpha u(t_n) = \frac{1}{\Gamma(1-\alpha)} \int_0^{t_n} \frac{\partial u_s}{(t_n - s)^\alpha} ds, \quad 0 < \alpha < 1 \tag{5.30}$$

Replacing α by $\alpha + 1$ in Eq. (5.17) gives

$$\int_0^{t_n} F'(t) \frac{dt}{(t_n - t)^\alpha} \simeq \sum_{k=1}^{n} \frac{F(t_k) - F(t_{k-1})}{\Delta t} \int_{t_{k-1}}^{t_k} \frac{dt}{(t_n - t)^\alpha} \tag{5.31}$$

Using Lemma 4.1 of Sun Wu (2006) and following the derivation of the difference scheme Eq. (5.25), the approximation to Eq. (5.30) is,

$$D_t^\alpha u(t_n) \simeq \frac{1}{\Gamma(1-\alpha)} \left[\sum_{j=1}^{n} \frac{U_i^j - U_i^{j-1}}{\Delta t} \int_{t_{j-1}}^{t_j} (t_n - s)^{-\alpha} ds \right] \tag{5.32}$$

Since

$$\int_{t_{j-1}}^{t_j} (t_n - s)^{-\alpha} ds = \frac{(\Delta t)^{1-\alpha}}{1-\alpha} \left[(n-j+1)^{1-\alpha} - (n-j)^{1-\alpha} \right], \quad n - j \geq 0. \tag{5.33}$$

and based on Lemma 2.3 of Sun Wu (2006), we can express Eq. (5.32) in the form

$$D_t^\alpha \; u(t_n) \simeq \frac{\Delta t^{-\alpha}}{\Gamma(2-\alpha)} \sum_{j=1}^{n} \tilde{b}_{n-j}(\alpha) \left(U_i^j - U_i^{j-1} \right) \tag{5.34}$$

where

$$\tilde{b}_{n-j}(\alpha) = (n-j+1)^{1-\alpha} - (n-j)^{1-\alpha}, \quad n - j \geq 0. \tag{5.35}$$

Let $l = n - j$, then define

$$\tilde{b}_l(\alpha) = \tilde{a}_l(\alpha + 1), \quad l \geq 0 \tag{5.36}$$

then Eq. (5.34) becomes

$$
\begin{aligned}
D_t^{\alpha}\ u(t_n) &\simeq \frac{\Delta t^{-\alpha}}{\Gamma(2-\alpha)}\left[\sum_{j=1}^{n}\tilde{b}_{n-j}(\alpha)\ \left(U_i^j-U_i^{j-1}\right)\right] \\
&= \frac{\Delta t^{-\alpha}}{\Gamma(2-\alpha)}\Bigg[\tilde{b}_{n-1}(\alpha)\ \left(U_i^1-U_i^0\right)+\tilde{b}_{n-2}(\alpha)\left(U_i^2-U_i^1\right) \\
&\quad +\tilde{b}_{n-3}(\alpha)\ \left(U_i^3-U_i^2\right)+\cdots+\tilde{b}_1(\alpha)\ \left(U_i^{n-1}-U_i^{n-2}\right)+\tilde{b}_0(\alpha)\ \left(U_i^n-U_i^{n-1}\right)\Bigg] \\
&= \frac{\Delta t^{-\alpha}}{\Gamma(2-\alpha)}\Bigg[\tilde{b}_0(\alpha)\ U_i^n+\left(\tilde{b}_1(\alpha)-\tilde{b}_0(\alpha)\right)U_i^{n-1}+\cdots+\left(\tilde{b}_{n-2}(\alpha)-\tilde{b}_{n-3}(\alpha)\right)U_i^2 \\
&\quad +\left(\tilde{b}_{n-1}(\alpha)-\tilde{b}_{n-2}(\alpha)\right)U_i^1-\tilde{b}_{n-1}U_i^0\Bigg] \\
&= \frac{\Delta t^{-\alpha}}{\Gamma(2-\alpha)}\left[\tilde{b}_0(\alpha)\,U_i^n-\sum_{j=1}^{n-1}\left(\tilde{b}_{n-j-1}(\alpha)-\tilde{b}_{n-j}(\alpha)\right)U_i^j-\tilde{b}_{n-1}(\alpha)U_i^0\right] \\
&= \frac{\Delta t^{-\alpha}}{\Gamma(2-\alpha)}\left[\sum_{j=0}^{n}\tilde{B}_jU_i^j\right]
\end{aligned}
\tag{5.37}
$$

where

$$
\tilde{B}_j=\begin{cases}-\tilde{b}_{n-1}(\alpha) & \text{if} \quad j=0\\ \tilde{b}_{n-j-1}(\alpha)-\tilde{b}_{n-j}(\alpha) & \text{if} \quad 1\le j\le n-1\\ \tilde{b}_0(\alpha) & \text{if} \quad j=n\end{cases}
\tag{5.38}
$$

5.4 A second-order difference scheme for the Caputo fractional derivative

From the truncation error estimate of the $L1$ method on a uniform temporal grid, it is clear that the accuracy is dependent on the fractional order α. It is not so surprising due to the weakly singular kernel $(t_n-s)^{\alpha}$ in Eq. (5.30). To improve the numerical accuracy of the difference approximation of the time-fractional derivative, it is very natural to consider a second-order scheme for discretizing the Caputo fractional derivative.

5.4.1 Case 1: when $1 < \alpha < 2$

The approximation of the Caputo fractional derivative of order α, where $1 < \alpha < 2$, will now be derived. We first use integration-by-parts on the right-hand side of Eq. (5.30) to obtain.

$$\begin{aligned} D_t^\alpha u(t_n) &= \frac{1}{\Gamma(1-\alpha)} \left[\frac{-\frac{\partial u}{\partial s}(t_n - s)^{1-\alpha}}{(1-\alpha)} \Bigg|_0^{t_n} + \frac{1}{(1-\alpha)} \int_0^{t_n} \frac{\partial_s^2 u}{(t_n - s)^{\alpha-1}}\, ds \right] \\ &= \frac{1}{(1-\alpha)\Gamma(1-\alpha)} \left[\frac{\partial u(r,0)}{\partial s} (t_n)^{1-\alpha} + \int_0^{t_n} \frac{\partial_s^2 u}{(t_n - s)^{\alpha-1}}\, ds \right] \\ &= \frac{1}{\Gamma(2-\alpha)} \int_0^{t_n} \frac{\partial_s^2 u}{(t_n - s)^{\alpha-1}}\, ds + \frac{1}{\Gamma(2-\alpha)} \left[\psi(r) \, (t_n)^{1-\alpha} \right] \\ &= \frac{1}{\Gamma(2-\alpha)} \int_0^{t_n} \frac{\partial_s^2 u}{(t_n - s)^{\alpha-1}}\, ds \end{aligned} \tag{5.39}$$

using $\frac{\partial u(r,0)}{\partial t} = \psi(r) = 0$.

Substituting the second derivative of the quadratic interpolation Eq. (5.7) into Eq. (5.39), we obtain

$$\begin{aligned} D_t^\alpha u(t_n) &\simeq \frac{1}{\Gamma(2-\alpha)} \left[\int_{t_{n-1}}^{t_n} \frac{\partial_s^2 \left(\Pi_{2,n-1} u(s) \right)}{(t_n - s)^{\alpha-1}}\, ds + \sum_{j=1}^{n-1} \int_{t_{j-1}}^{t_j} \frac{\partial_s^2 \left(\Pi_{2,j} u(s) \right)}{(t_n - s)^{\alpha-1}}\, ds \right] \\ &= \frac{1}{\Gamma(2-\alpha)} \left[\frac{U^n - 2U^{n-1} + U^{n-2}}{(\Delta t)^2} \int_{t_{n-1}}^{t_n} \frac{ds}{(t_n - s)^{\alpha-1}} \right. \\ &\qquad \left. + \sum_{j=1}^{n-1} \frac{U^{j+1} - 2U^j + U^{j-1}}{(\Delta t)^2} \int_{t_{j-1}}^{t_j} \frac{ds}{(t_n - s)^{\alpha-1}} \right] \end{aligned} \tag{5.40}$$

Substitute Eq. (5.19) and Eq.(5.21) into Eq. (5.40) to obtain

$$
\begin{aligned}
D_t^{\alpha}u(t_n) &\simeq \frac{1}{(\Delta t)^{\alpha}\Gamma(3-\alpha)}\left[\left(U^n-2U^{n-1}+U^{n-2}\right)+\sum_{j=1}^{n-1}\tilde{a}_{n-j}(\alpha)\left(U^{j+1}-2U^j+U^{j-1}\right)\right]\\
&= \frac{1}{(\Delta t)^{\alpha}\Gamma(3-\alpha)}\left[\left(U^n-2U^{n-1}+U^{n-2}\right)+\tilde{a}_{n-1}(\alpha)\left(U^2-2U^1+U^0\right)\right.\\
&\qquad\left.+\tilde{a}_{n-2}(\alpha)\left(U^3-2U^2+U^1\right)+\cdots+\tilde{a}_1(\alpha)\left(U^n-2U^{n-1}+U^{n-2}\right)\right]\\
&= \frac{1}{(\Delta t)^{\alpha}\Gamma(3-\alpha)}\left[\left(\tilde{a}_{n-1}(\alpha)\right)U^0+(\tilde{a}_{n-2}(\alpha)-2\tilde{a}_{n-1}(\alpha))U^1+(\tilde{a}_{n-1}(\alpha)-2\tilde{a}_{n-2}(\alpha))U^2\right.\\
&\qquad\left.+\cdots+(1+\tilde{a}_1(\alpha))U^{n-2}+(-2-2\tilde{a}_1(\alpha))U^{n-1}+(1+\tilde{a}_1(\alpha))U^n\right]\\
&= \frac{1}{(\Delta t)^{\alpha}\Gamma(3-\alpha)}\left[\left(\tilde{a}_{n-1}(\alpha)\right)U^0+(\tilde{a}_{n-2}(\alpha)-2\tilde{a}_{n-1}(\alpha))U^1\right.\\
&\qquad+\sum_{j=2}^{n-3}(\tilde{a}_{n-j-1}(\alpha)-2\tilde{a}_{n-j}(\alpha)+\tilde{a}_{n-j+1}(\alpha))U^j+(1+\tilde{a}_1(\alpha)-2\tilde{a}_2(\alpha)+\tilde{a}_3(\alpha))U^{n-2}\\
&\qquad\left.+(-2-2\tilde{a}_1(\alpha)+\tilde{a}_2(\alpha))U^{n-1}+(1+\tilde{a}_1(\alpha))U^n\right]\\
&= \frac{1}{(\Delta t)^{\alpha}\Gamma(3-\alpha)}\sum_{j=0}^{n}C_jU^j
\end{aligned}
\tag{5.41}
$$

using Eq. (5.21) and Eq. (5.22) to define the following coefficients as,

$$
C_j(\alpha)=\begin{cases}
\tilde{a}_{n-1}(\alpha) & \text{if} \quad j=0\\
\tilde{a}_{n-2}(\alpha)-2\tilde{a}_{n-1}(\alpha) & \text{if} \quad j=1\\
\tilde{a}_{n-j-1}(\alpha)-2\tilde{a}_{n-j}(\alpha)+\tilde{a}_{n-j+1}(\alpha) & \text{if} \quad 2\le j\le n-3\\
1+\tilde{a}_1(\alpha)-2\tilde{a}_2(\alpha)+\tilde{a}_3(\alpha) & \text{if} \quad j=n-2\\
-2\tilde{a}_1(\alpha)+\tilde{a}_2(\alpha)-2 & \text{if} \quad j=n-1\\
1+\tilde{a}_1(\alpha) & \text{if} \quad j=n
\end{cases}
\tag{5.42}
$$

5.4.2 Case 2: when $0 < \alpha < 1$

We consider the Caputo time derivative of order α, where $0 < \alpha < 1$,

$$D_t^\alpha u(t_n) = \frac{1}{\Gamma(1-\alpha)} \int_0^{t_n} \frac{\partial_s u}{(t_n - s)^\alpha}\, ds, \quad t > 0 \tag{5.43}$$

Define the finite difference approximation of $D_t^\alpha u(t)$ at $t = t_1$ as follows:

$$\begin{aligned} D_t^\alpha u(t_1) &\simeq \frac{1}{\Gamma(1-\alpha)} \int_{t_0}^{t_1} \left\{ \frac{u(t_1) - u(t_0)}{\Delta t} \right\} \frac{1}{(t_1 - s)^\alpha}\, ds \\ &= \frac{1}{\Gamma(1-\alpha)} \frac{u(t_1) - u(t_0)}{\Delta t} \int_{t_0}^{t_1} \frac{1}{(t_1 - s)^\alpha}\, ds \\ &= \frac{1}{\Gamma(1-\alpha)} \frac{u(t_1) - u(t_0)}{\Delta t} \left[-\frac{(t_1 - s)^{-\alpha+1}}{(1-\alpha)} \right]_0^{t_1} \\ &= \frac{1}{\Gamma(2-\alpha)} \frac{u(t_1) - u(t_0)}{(\Delta t)^\alpha} \end{aligned} \tag{5.44}$$

Substituting the first derivative of the quadratic interpolant in Eq.(5.6) into Eq.(5.43), we obtain, for $n \geq 2$,

$$\begin{aligned} D_t^\alpha u(t_n) &= \frac{1}{\Gamma(1-\alpha)} \left[\int_{t_{n-1}}^{t_n} \frac{\partial_s \left(\Pi_{2,n-1} u(s) \right)}{(t_n - s)^\alpha}\, ds + \sum_{j=1}^{n-1} \int_{t_{j-1}}^{t_j} \frac{\partial_s \left(\Pi_{2,j} u(s) \right)}{(t_n - s)^\alpha}\, ds \right] \\ &= \frac{1}{\Gamma(1-\alpha)} \left[A_n + \sum_{j=1}^{n-1} B_{n,j} \right] \end{aligned} \tag{5.45}$$

where

$$A_n = \int_{t_{n-1}}^{t_n} \frac{\partial_s \left(\Pi_{2,n-1} u(s) \right)}{(t_n - s)^\alpha}\, ds, \quad B_{n,j} = \int_{t_{j-1}}^{t_j} \frac{\partial_s \left(\Pi_{2,j} u(s) \right)}{(t_n - s)^\alpha}\, ds \tag{5.46}$$

The integrals defining A_n, and $B_{n,j}$ can be evaluated analytically as follows:

$$\begin{aligned}
A_n &= \frac{U^{n-2}}{2(\Delta t)^2}\int_{t_{n-1}}^{t_n}\frac{2s-t_n-t_{n-1}}{(t_n-s)^\alpha}\,ds - \frac{U^{n-1}}{(\Delta t)^2}\int_{t_{n-1}}^{t_n}\frac{2s-t_{n-2}-t_n}{(t_n-s)^\alpha}\,ds \\
&\quad + \frac{U^n}{2(\Delta t)^2}\int_{t_{n-1}}^{t_n}\frac{2s-t_{n-2}-t_{n-1}}{(t_n-s)^\alpha}\,ds \\
&= \frac{1}{(1-\alpha)(2-\alpha)}\left[\left(\frac{\alpha}{2(\Delta t)^\alpha}\right)U^{n-2} - \left(\frac{2}{(\Delta t)^\alpha}\right)U^{n-1} + \left(\frac{4-\alpha}{2(\Delta t)^\alpha}\right)U^n\right] \\
&= \frac{1}{(1-\alpha)(2-\alpha)(\Delta t)^\alpha}\Big[a(\alpha)\,U^{n-2} + b\,U^{n-1} + c(\alpha)\,U^n\Big]
\end{aligned} \tag{5.47}$$

where

$$a(\alpha) = \left[\frac{\alpha}{2}\right] \tag{5.48}$$

$$b = -2 \tag{5.49}$$

$$c(\alpha) = \left[\frac{4-\alpha}{2}\right] \tag{5.50}$$

Similarly,

$$\begin{aligned}
B_{n,j} &= \frac{U^{j-1}}{2(\Delta t)^2}\int_{t_{j-1}}^{t_j}\frac{2s-t_j-t_{j+1}}{(t_n-s)^\alpha}\,ds - \frac{U^j}{(\Delta t)^2}\int_{t_{j-1}}^{t_j}\frac{2s-t_{j+1}-t_{j-1}}{(t_n-s)^\alpha}\,ds \\
&\quad + \frac{U^{j+1}}{2(\Delta t)^2}\int_{t_{j-1}}^{t_j}\frac{2s-t_j-t_{j-1}}{(t_n-s)^\alpha}\,ds \\
&= \frac{U^{j-1}}{2(\Delta t)^\alpha}\left(\frac{[(n-j)^{1-\alpha}-3(n-j+1)^{1-\alpha}]}{(1-\alpha)} - \frac{2\,[(n-j)^{2-\alpha}-(n-j+1)^{2-\alpha}]}{(1-\alpha)(2-\alpha)}\right) \\
&\quad - \frac{U^j}{(\Delta t)^\alpha}\left(\frac{2(n-j+1)^{1-\alpha}}{(1-\alpha)} + \frac{2[(n-j)^{2-\alpha}-(n-j+1)^{2-\alpha}]}{(1-\alpha)(2-\alpha)}\right) \\
&\quad + \frac{U^{j+1}}{2(\Delta t)^\alpha}\left(\frac{[(n-j)^{1-\alpha}+(n-j+1)^{1-\alpha}]}{(1-\alpha)} + \frac{2[(n-j)^{2-\alpha}-(n-j+1)^{2-\alpha}]}{(1-\alpha)(2-\alpha)}\right) \\
&= \frac{U^{j-1}}{2(\Delta t)^\alpha}\left(\frac{(2-\alpha)[(n-j)^{1-\alpha}-3(n-j+1)^{1-\alpha}] - 2\,[(n-j)^{2-\alpha}-(n-j+1)^{2-\alpha}]}{(1-\alpha)(2-\alpha)}\right) \\
&\quad - \frac{U^j}{(\Delta t)^\alpha}\left(\frac{2(2-\alpha)(n-j+1)^{1-\alpha} + 2[(n-j)^{2-\alpha}-(n-j+1)^{2-\alpha}]}{(1-\alpha)(2-\alpha)}\right) \\
&\quad + \frac{U^{j+1}}{2(\Delta t)^\alpha}\left(\frac{-(2-\alpha)\,[(n-j)^{1-\alpha}-(n-j+1)^{1-\alpha}] - 2[(n-j)^{2-\alpha}-(n-j+1)^{2-\alpha}]}{(1-\alpha)(2-\alpha)}\right) \\
&= \frac{1}{(\Delta t)^\alpha\,(1-\alpha)(2-\alpha)}\left(a_{n-j}(\alpha)\,U^{j-1} + b_{n-j}(\alpha)\,U^j + c_{n-j}(\alpha)\,U^{j+1}\right)
\end{aligned} \tag{5.51}$$

where

$$a_{n-j}(\alpha) = \left[\frac{1}{2}(2-\alpha)\,(n-j)^{1-\alpha} - \frac{3}{2}(2-\alpha)(n-j+1)^{1-\alpha} - (n-j)^{2-\alpha} + (n-j+1)^{2-\alpha}\right] \tag{5.52}$$

$$b_{n-j}(\alpha) = \left[(2-\alpha)\,(n-j+1)^{1-\alpha} + (n-j)^{2-\alpha} - (n-j+1)^{2-\alpha}\right] \tag{5.53}$$

$$c_{n-j}(\alpha) = \left[\frac{-(2-\alpha)}{2}\,(n-j)^{1-\alpha} + \frac{(2-\alpha)}{2}(n-j+1)^{1-\alpha} - (n-j)^{2-\alpha} + (n-j+1)^{2-\alpha}\right] \tag{5.54}$$

Let $l = n - j$, then we define

$$a_l(\alpha) = \left[\frac{1}{2}(2-\alpha)\,l^{1-\alpha} - \frac{3}{2}(2-\alpha)(l+1)^{1-\alpha} - l^{2-\alpha} + (l+1)^{2-\alpha}\right] \tag{5.55}$$

$$b_l(\alpha) = \left[2(2-\alpha)\,(l+1)^{1-\alpha} + 2l^{2-\alpha} - 2(l+1)^{2-\alpha}\right] \tag{5.56}$$

$$c_l(\alpha) = \left[\frac{-(2-\alpha)}{2}\,l^{1-\alpha} + \frac{(2-\alpha)}{2}(l+1)^{1-\alpha} - l^{2-\alpha} + (l+1)^{2-\alpha}\right] \tag{5.57}$$

Combining the above results, Eq. (5.45) becomes

$$
\begin{aligned}
D_t^\alpha u(t_n) &= \frac{1}{\Gamma(1-\alpha)}\left[A_n + \sum_{j=1}^{n-1} B_{n,j}\right] \\
&= \frac{1}{\Gamma(1-\alpha)}\left[\frac{1}{(\Delta t)^\alpha(1-\alpha)(2-\alpha)}\left(a(\alpha)\,U^{n-2} + b\,U^{n-1} + c(\alpha)\,U^n\right)\right. \\
&\quad \left. + \frac{1}{(\Delta t)^\alpha\,(1-\alpha)(2-\alpha)}\sum_{j=1}^{n-1}\left(a_{n-j}(\alpha)\,U^{j-1} + b_{n-j}(\alpha)U^j + c_{n-j}(\alpha)U^{j+1}\right)\right] \\
&= \frac{1}{(\Delta t)^\alpha(2-\alpha)(1-\alpha)\Gamma(1-\alpha)}\left[\left(a(\alpha)\,U^{n-2} + b\,U^{n-1} + c(\alpha)\,U^n\right)\right. \\
&\quad \left. + \sum_{j=1}^{n-1}\left(a_{n-j}(\alpha)\,U^{j-1} + b_{n-j}(\alpha)U^j + c_{n-j}(\alpha)U^{j+1}\right)\right] \\
&= \frac{1}{(\Delta t)^\alpha\Gamma(3-\alpha)}\left[\left(a(\alpha)\,U^{n-2} + b\,U^{n-1} + c(\alpha)\,U^n\right)\right. \\
&\quad \left. + \sum_{j=1}^{n-1}\left(a_{n-j}(\alpha)U^{j-1} + b_{n-j}(\alpha)U^j + c_{n-j}(\alpha)U^{j+1}\right)\right] \\
&= \frac{1}{(\Delta t)^\alpha\Gamma(3-\alpha)}\left[\left(c(\alpha)+c_1(\alpha)\right)U^n + \left(b + c_2(\alpha) + b_1(\alpha)\right)U^{n-1} + \left(a(\alpha) + b_2(\alpha) + a_1(\alpha)\right)U^{n-2}\right. \\
&\quad \left. + \sum_{j=2}^{n-3}\left(a_{n-j-1}(\alpha) + b_{n-j}(\alpha) + c_{n-j+1}(\alpha)\right)U^j + \left(a_{n-2}(\alpha) + b_{n-1}(\alpha)\right)U^1 + a_{n-1}(\alpha)\,U^0\right]
\end{aligned}
\tag{5.58}
$$

We rearrange the formula as follows for convenience:

$$
D_t^\alpha u(t_n) = \frac{1}{(\Delta t)^\alpha\Gamma(3-\alpha)}\sum_{j=0}^{n} E_j\,U^j \tag{5.59}
$$

using Eq. (5.48)-Eq. (5.50) and Eq. (5.52)-Eq. (5.57), we can define

$$E_j(\alpha) = \begin{cases} a_{n-1}(\alpha) & \text{if} \quad j = 0 \\ a_{n-2}(\alpha) + b_{n-1}(\alpha) & \text{if} \quad j = 1 \\ a_{n-j-1}(\alpha) + b_{n-j}(\alpha) + c_{n-j+1}(\alpha) & \text{if} \quad 2 \leq j \leq n-3 \\ a_1(\alpha) + b_2(\alpha) + c_3(\alpha) + a(\alpha) & \text{if} \quad j = n-2 \\ c_2(\alpha) + b_1(\alpha) + b & \text{if} \quad j = n-1 \\ c(\alpha) + c_1(\alpha) & \text{if} \quad j = n \end{cases} \tag{5.60}$$

5.5 Time Discretization of FVF Model

In this section, we refer to the Fractional Viscoelastic Fluid (FVF) model as a special case of the Fractional Maxwell Model (FMM), specifically when the order of the fractional derivative is set to $\alpha = 1$. This formulation corresponds to a configuration where a spring-pot (defined by fractional order β) is placed in series with a dashpot, capturing the intermediate behaviour between purely viscous and elastic responses.

It is important to note that in Chapter 4, the same configuration was previously referred to as the Fractional Maxwell–Like (FML) model. For consistency, we now use the term Fractional Viscoelastic Fluid (FVF) throughout this section and in Chapter 6, recognizing that both terms describe the same constitutive model—specifically, the Fractional Maxwell Model (FMM) with $\alpha = 1$. Additionally, to align the notation with Chapters 4 and 7, the parameter α used here and in Chapter 6 corresponds to β in those Chapters, while the parameter β used here and in Chapter 6 corresponds to $\zeta = \beta - \alpha$ in Chapters 4 and 7.

The expression:

$$\tau(t) + \frac{\mathbb{V}}{\mathbb{G}} D_t^{1-\beta} \tau(t) = \mathbb{V}\left(\frac{\partial u}{\partial r} - \frac{u}{r}\right), \quad 0 < \beta < 1 \tag{5.61}$$

is a fractional viscoelastic constitutive law for shear stress in a cylindrical polar coordinate system.

The strain rate term $\frac{\partial u}{\partial r} - \frac{u}{r}$ is the curvilinear form of the shear strain rate (Ferras ., 2018). The approximation of $\tau(r_i, t_n)$ is denoted by τ_i^n.

5.5.1 A first-order difference scheme for the Caputo fractional derivative

Define the fractional derivative in a Caputo sense

$$D_t^{1-\beta}\tau(t_n) = \frac{1}{\Gamma(\beta)} \int_0^{t_n} \frac{\partial_s \tau}{(t_n - s)^{1-\beta}}\, ds, \quad 0 < \beta < 1 \tag{5.62}$$

Substituting Eq.(5.4) in Eq.(5.62), we obtain

$$D_t^{1-\beta}\tau(t_n) \simeq \frac{1}{\Gamma(\beta)} \left[\sum_{j=1}^{n} \frac{\tau^j - \tau^{j-1}}{\Delta t} \int_{t_{j-1}}^{t_j} \frac{ds}{(t_n - s)^{1-\beta}} \right] \tag{5.63}$$

Since

$$\begin{aligned} \int_{t_{j-1}}^{t_j} \frac{ds}{(t_n - s)^{1-\beta}} &= \frac{1}{\beta} \left[(t_n - t_j)^\beta - (t_n - t_{j-1})^\beta \right] \\ &= \frac{(\Delta t)^\beta}{\beta} \left[(n - j + 1)^\beta - (n - j)^\beta \right], \quad n - j \geq 0 \end{aligned} \tag{5.64}$$

we can express Eq. (5.63) in the form

$$D_t^{1-\beta}\tau(t_n) = \frac{1}{\Delta t^{1-\beta}\ \Gamma(1-\beta)} \sum_{j=1}^{n} \ddot{b}_{n-j}(1-\beta) \left[\tau(t_j) - \tau(t_{j-1}) \right] \tag{5.65}$$

where

$$\ddot{b}_{n-j}(1-\beta) = \left[(n - j + 1)^\beta - (n - j)^\beta \right] \tag{5.66}$$

Let $l = n - j$, then

$$\ddot{b}_l(1-\beta) = \left[(l + 1)^\beta - l^\beta \right] \tag{5.67}$$

Based on Lemma 2.3 of Sun Wu (2006), Eq. (5.65) becomes

$$
\begin{aligned}
D_t^{1-\beta}\tau(t_n) = \frac{1}{\Delta t^{1-\beta}\,\Gamma(1-\beta)}\Big[&\ddot{b}_{n-1}(1-\beta)\left[\tau^1-\tau^0\right]+\ddot{b}_{n-2}(1-\beta)\left[\tau^2-\tau^1\right]+\ddot{b}_{n-3}(1-\beta)\left[\tau^3-\tau^2\right]\\
&+\cdots+\ddot{b}_1(\beta)\left[\tau^{n-1}-\tau^{n-2}\right]+\ddot{b}_0(\beta)\left[\tau^n-\tau^{n-1}\right]\Big]\\
=\frac{1}{\Delta t^{1-\beta}\,\Gamma(1-\beta)}\Big[&\ddot{b}_0(\beta)\;\tau^n-\sum_{j=1}^{n-1}[\ddot{b}_{n-j-1}(\beta)-\ddot{b}_{n-j}(\beta)]\;\tau^j-\ddot{b}_{n-1}(\beta)\,\tau^0\Big]
\end{aligned}
\tag{5.68}
$$

5.5.2 A second-order difference scheme for the Caputo fractional derivative

Define the finite difference approximation of $D_t^{1-\beta}\tau(t)$ at $t=t_1$ in $[t_0,t_1]$ as follows:

$$
\begin{aligned}
D_t^{1-\beta}\tau(t_1) &\simeq \frac{1}{\Gamma(\beta)}\int_{t_0}^{t_1}\left(\frac{\tau^1-\tau^0}{\Delta t}\right)\frac{1}{(t_1-s)^{1-\beta}}\;ds\\
&=\frac{1}{\Gamma(\beta)}\frac{\tau^1-\tau^0}{\Delta t}\int_{t_0}^{t_1}\frac{1}{(t_1-s)^{1-\beta}}\;ds\\
&=\frac{1}{\Gamma(\beta)}\frac{\tau^1-\tau^0}{\Delta t}\left[-\frac{(t_1-s)^{\beta}}{(\beta)}\right]_0^{t_1}\\
&=\frac{1}{\Gamma(1+\beta)}\frac{\tau^1-\tau^0}{(\Delta t)^{1-\beta}}
\end{aligned}
\tag{5.69}
$$

Substituting Eq.(5.6) into Eq.(5.62) for $n\geq 2$, we obtain

$$
\begin{aligned}
D_t^{1-\beta}\tau(t_n) &\simeq \frac{1}{\Gamma(\beta)}\left[\int_{t_{n-1}}^{t_n}\frac{\partial_s\left(\Pi_{2,n-1}\tau(s)\right)}{(t_n-s)^{1-\beta}}\;ds+\sum_{j=1}^{n-1}\int_{t_{j-1}}^{t_j}\frac{\partial_s\left(\Pi_{2,j}\tau(s)\right)}{(t_n-s)^{1-\beta}}\;ds\right]\\
&=\frac{1}{\Gamma(\beta)}\left[\overset{*}{A}_n+\sum_{j=1}^{n-1}\overset{*}{B}_{n,j}\right]
\end{aligned}
\tag{5.70}
$$

where

$$
\overset{*}{A}_n=\int_{t_{n-1}}^{t_n}\frac{\partial_s\left(\Pi_{2,n-1}\tau(s)\right)}{(t_n-s)^{1-\beta}}\;ds,\quad \overset{*}{B}_{n,j}=\int_{t_{j-1}}^{t_j}\frac{\partial_s\left(\Pi_{2,j}\tau(s)\right)}{(t_n-s)^{1-\beta}}\;ds
\tag{5.71}
$$

The integrals defining $\overset{*}{A}_n$, and $\overset{*}{B}_{n,j}$ can be evaluated analytically as follows:

$$\begin{aligned}
\overset{*}{A}_n &= \frac{\tau^{n-2}}{2(\Delta t)^2}\int_{t_{n-1}}^{t_n}\frac{2s-t_n-t_{n-1}}{(t_n-s)^{1-\beta}}ds - \frac{\tau^{n-1}}{(\Delta t)^2}\int_{t_{n-1}}^{t_n}\frac{2s-t_{n-2}-t_n}{(t_n-s)^{1-\beta}}ds \\
&\quad + \frac{\tau^{n}}{2(\Delta t)^2}\int_{t_{n-1}}^{t_n}\frac{2s-t_{n-2}-t_{n-1}}{(t_n-s)^{1-\beta}}ds \\
&= \tau^{n-2}\left[\frac{-3-\beta}{2(\Delta t)^{1-\beta}\beta(\beta+1)}\right] - \tau^{n-1}\left[\frac{2}{(\Delta t)^{1-\beta}\beta(\beta+1)}\right] + \tau^{n}\left[\frac{\beta-1}{2(\Delta t)^{1-\beta}\beta(\beta+1)}\right] \\
&= \frac{1}{\beta(\beta+1)(\Delta t)^{1-\beta}}\left[\hat{a}(\beta)\,\tau^{n-2} - \hat{b}(\beta)\,\tau^{n-1} + \hat{c}(\beta)\,\tau^{n}\right]
\end{aligned} \tag{5.72}$$

where

$$\hat{a}(\beta) = \left[\frac{-3-\beta}{2}\right], \quad \hat{b} = 2, \quad \hat{c}(\beta) = \left[\frac{\beta-1}{2}\right] \tag{5.73}$$

and

$$\begin{aligned}
\overset{*}{B}_{n,j} &= \frac{\tau^{j-1}}{2(\Delta t)^2}\int_{t_{j-1}}^{t_j}\frac{2s-t_{j+1}-t_j}{(t_j-s)^{1-\beta}}\,ds - \frac{\tau^{j}}{(\Delta t)^2}\int_{t_{j-1}}^{t_j}\frac{2s-t_{j-1}-t_{j+1}}{(t_j-s)^{1-\beta}}\,ds \\
&\quad + \frac{\tau^{j+1}}{2(\Delta t)^2}\int_{t_{j-1}}^{t_j}\frac{2s-t_j-t_{j-1}}{(t_j-s)^{1-\beta}}\,ds \\
&= \left(\frac{[(n-j)^{\beta}-3(n-j+1)^{\beta}]}{2(\Delta t)^{1-\beta}\beta} - \frac{[(n-j)^{1+\beta}-(n-j+1)^{1+\beta}]}{(\Delta t)^{\beta-1}\beta(\beta+1)}\right)\tau^{j-1} \\
&\quad - 2\left(\frac{[(n-j+1)^{\beta}]}{(\Delta t)^{1-\beta}\beta} + \frac{[(n-j)^{1+\beta}-(n-j+1)^{1+\beta}]}{(\Delta t)^{1-\beta}\beta(\beta+1)}\right)\tau^{j} \\
&\quad + \left(\frac{[-(n-j)^{\beta}-(n-j+1)^{\beta}]}{2\,(\Delta t)^{1-\beta}\beta} - \frac{[(n-j)^{1+\beta}-(n-j+1)^{1+\beta}]}{(\Delta t)^{\beta-1}\beta\,(\beta+1)}\right)\tau^{j+1} \\
&= \frac{1}{(\Delta t)^{1-\beta}\beta(\beta+1)}\left[\acute{a}_{n-j}(\beta)\,\tau^{j-1} - 2\acute{b}_{n-j}(\beta)\,\tau^{j} + \acute{c}_{n-j}(\beta)\,\tau^{j+1}\right]
\end{aligned} \tag{5.74}$$

where

$$\acute{a}_{n-j}(\beta) = \left[\frac{(\beta+1)}{2}\,(n-j)^{\beta} - \frac{3(\beta+1)}{2}(n-j+1)^{\beta} - (n-j)^{1+\beta} + (n-j+1)^{1+\beta}\right] \tag{5.75}$$

$$\acute{b}_{n-j}(\beta) = \left[(\beta+1)\,(n-j+1)^{\beta} + (n-j)^{1+\beta} - (n-j+1)^{1+\beta}\right] \tag{5.76}$$

$$\acute{c}_{n-j}(\beta) = \left[-\frac{(\beta+1)}{2}\,(n-j)^{\beta} - \frac{(\beta+1)}{2}(n-j+1)^{\beta} - (n-j)^{1+\beta} + (n-j+1)^{1+\beta}\right] \tag{5.77}$$

Let $l = n - j$, then

$$\acute{a}_l(\beta) = \left[\frac{(\beta+1)}{2}(l)^{\beta} - \frac{3(\beta+1)}{2}(l+1)^{\beta} - (l)^{1+\beta} + (l+1)^{1+\beta}\right] \tag{5.78}$$

$$\acute{b}_l(\beta) = \left[(\beta+1)(l+1)^{\beta} + (l)^{1+\beta} - (l+1)^{1+\beta}\right] \tag{5.79}$$

$$\acute{c}_l(\beta) = \left[-\frac{(\beta+1)}{2}(l)^{\beta} - \frac{(\beta+1)}{2}(l+1)^{\beta} - (l)^{1+\beta} + (l+1)^{1+\beta}\right] \tag{5.80}$$

Inserting the above approximations into Eq. (5.72) gives

$$\begin{aligned}
D_t^{1-\beta}\tau(t_n) &= \frac{1}{\Gamma(\beta)}\left[\overset{*}{A}_n + \sum_{j=1}^{n-1}\overset{*}{B}_{n,j}\right] \\
&= \frac{1}{\Gamma(\beta)}\left[\frac{1}{(\Delta t)^{1-\beta}\beta(\beta+1)}\left(\hat{a}\,\tau^{n-2} + \hat{b}\,\tau^{n-1} + \hat{c}\,\tau^{n}\right)\right. \\
&\quad \left. + \frac{1}{(\Delta t)^{1-\beta}\beta(\beta+1)}\sum_{j=1}^{n-1}\left(\acute{a}_{n-j}\,\tau^{j-1} - 2\acute{b}_{n-j}\,\tau^{j} + \acute{c}_{n-j}\,\tau^{j+1}\right)\right] \\
&= \frac{1}{(\Delta t)^{1-\beta}\Gamma(\beta+2)}\left[\left(\hat{a}\,\tau^{n-2} + \hat{b}\,\tau^{n-1} + \hat{c}\,\tau^{n}\right)\right. \\
&\quad \left. + \sum_{j=1}^{n-1}\left(\acute{a}_{n-j}\,\tau^{j-1} - 2\acute{b}_{n-j}\,\tau^{j} + \acute{c}_{n-j}\,\tau^{j+1}\right)\right] \\
&= \frac{1}{(\Delta t)^{1-\beta}\Gamma(\beta+2)}\left[(\hat{c}+\acute{c}_1)\tau^{n} + (\hat{b} - 2\acute{b}_1 + \acute{c}_2)\tau^{n-1} + (\hat{a} - 2\acute{b}_2 + \acute{a}_1)\tau^{n-2}\right. \\
&\quad \left. + \sum_{j=2}^{n-3}(\acute{a}_{n-j} - 2\acute{b}_{n-j} + \acute{c}_{n-j})\,\tau^{j} + (\acute{a}_{n-2} - 2\acute{b}_{n-1})\,\tau^{1} + (\acute{a}_{n-1})\,\tau^{0}\right]
\end{aligned} \tag{5.81}$$

For convenience, we rearrange the formula as follows

$$D_t^{1-\beta}\tau(t_n) = \frac{1}{(\Delta t)^{1-\beta}\Gamma(\beta+2)}\sum_{j=0}^{n}\acute{E}_j\tau^{j}, \;\; 0 \le j \le n \tag{5.82}$$

where $\acute{E}_j$ are defined by

$$\acute{E}_j(\beta) = \begin{cases} \acute{a}_{n-1}(\beta) & \text{if} \quad j = 0 \\ \acute{a}_{n-2}(\beta) - 2\acute{b}_{n-1}(\beta) & \text{if} \quad j = 1 \\ \acute{a}_{n-j-1}(\beta) - \acute{b}_{n-j}(\beta) + \acute{c}_{n-j+1}(\beta) & \text{if} \quad 2 \leq j \leq n-3 \\ \acute{a}_1(\beta) - 2\acute{b}_2(\beta) + \acute{c}_3(\beta) + \hat{a}(\beta) & \text{if} \quad j = n-2 \\ \acute{c}_2(\beta) - 2\acute{b}_1(\beta) - \hat{b} & \text{if} \quad j = n-1 \\ \hat{c}(\beta) + \acute{c}_1(\beta) & \text{if} \quad j = n \end{cases} \tag{5.83}$$

5.6 Conclusions

The goal of this thesis is to solve the coupled set of PDEs for Taylor-Couette flow numerically. This requires the development of an accurate and stable numerical discretization in time and space. In this chapter, following the discretization method of Sun Wu (2006) we have derived a numerical discretization of $O(\Delta t)$, for the time-fractional derivative defined in the Caputo sense with the fractional order α, in two cases: $0 < \alpha < 1$ and $1 < \alpha < 2$. Furthermore, to obtain a more precise approximation, we have extended the work of Sun Wu (2006) by constructing a second order approximation of the Caputo fractional derivative using the first and second derivatives of the quadratic interpolation polynomial of u in the two distinct intervals of α: $0 < \alpha < 1$ and $1 < \alpha < 2$. In the final section, we derived a first-order difference scheme for the Caputo fractional derivative for the Fractional Viscoelastic Fluid (FVF) model with special case of fractional order $\alpha = 1$, which we will utilize it in Chapter 6. In addition, the corresponding second-order difference scheme for the same model was also derived; however, this higher-order scheme is not utilized further in this thesis.

Chapter 6

Unsteady Flows in Simple Geometry

6.1 Introduction

Many phenomena in applied mathematics can be modelled using ordinary or partial differential equations. Finding numerical approximations to their solution is often required since some of these problems are complex and do not have closed-form analytical solutions.

In this chapter, we employ spectral methods and develop MATLAB code to solve the steady and unsteady unidirectional flow of fractional viscoelastic fluids inside a real concentric cylinder rheometer (annular flow). Both space and time are discretized in the equations. This procedure will be described in detail in this chapter. Section 6.2 provides a description of the Taylor-Couette flow geometry. The numerical discretization of the problem is described in Section 6.3 which is based on finite differences in time and spectral approximations in space. These methods are applied to the governing equation for velocity and shear stress to form the linear system for the unknowns at each time step. The convergence behaviour of the spectral approximation is studied in Section 6.4. In Section 6.5 some numerical results are presented and compared with the finite difference approach of Ferras . (2018). The advantages and disadvantages of both approaches are described. In Section 6.6 the fully coupled scheme is presented. In Section 6.7, the influence of fractional orders on the velocity and shear stress approximations is investigated and a brief description of the stress relaxation achieved for FMM is provided. The conclusions of this chapter are given in Section 6.8.

6.2 Taylor–Couette flow

Taylor–Couette flow is named after two scientists who made significant contributions to the study of fluid motion between rotating cylinders. The British mathematician and physicist Sir Geoffrey Ingram Taylor is well known for his important contributions to fluid dynamics, especially his examination of the stability of flow between two rotating cylinders. The French physicist Maurice Marie Alfred Couette initially studied viscosity measurement techniques and the viscous flow between concentric cylinders. Their combined contributions laid the groundwork for what is now known as Taylor–Couette flow (see e.g (Taylor, 1923; Donnelly, 1991; Drazin Reid, 2004).

The eccentricity, denoted by e, refers to the distance between the centres of the two cylinders. When the cylinders are concentric, this distance is zero ($e = 0$; see Fig. 6.1). In the Taylor-Couette problem, a fluid occupies the space between two concentric cylinders and flows within the annular gap (see Fig. 6.2). This type of flow plays a crucial role in the rheological analysis of materials. It involves introducing the material into the annular space and rotating one or both cylinders (either at a constant or varying rate) while measuring the torque exerted on the second cylindrical surface (Dontula ., 2005; Owens Phillips, 2002). The characteristics of the flow are affected by factors such as the rotational velocities of the cylinders, the viscosity of the fluid, and the width of the annular gap.

In the case of a purely tangential flow within an annular region, where the velocity field is defined as $(u_r, u_\theta, u_z) = (0, u_\theta(r,t), 0)$, the θ-component of the momentum equation for the Maxwell model—expressed in terms of the tangential velocity u_θ and the shear stress $\tau_{r\theta}$ — can be written as follows:

$$\rho\left(1+\lambda\frac{\partial}{\partial t}\right)\frac{\partial u_\theta}{\partial t} = \eta\left(\frac{\partial^2}{\partial r^2}+\frac{1}{r}\frac{\partial}{\partial r}-\frac{1}{r^2}\right)u_\theta \tag{6.1}$$

$$\left(1+\lambda\frac{\partial}{\partial t}\right)\tau_{r\theta} = \eta\left(\frac{\partial u_\theta}{\partial r}-\frac{u_\theta}{r}\right) \tag{6.2}$$

To extend the model to a fractional viscoelastic fluid (FVF) in the regime where $Wi \ll 1$, the operator $\left(1+\lambda\frac{\partial}{\partial t}\right)$ in Eqs. (6.1) and (6.2) is replaced with the fractional derivative $\left(1+\frac{\mathbb{V}}{\mathbb{G}}D_t^{1-\beta}\right)$. Additionally, Eq. (6.1) is divided by the viscosity $\eta = \mathbb{V}$, considering that $\lambda \equiv \frac{\mathbb{V}}{\mathbb{G}}$. This fractional model introduces three key parameters to be identified through fitting to experimental data: two quasi-material properties, $\mathbb{V}$ and $\mathbb{G}$, and a fractional order exponent β, constrained by $0 < \beta < \alpha = 1$.

$$\frac{\rho}{\mathbb{V}}\frac{\partial u_\theta}{\partial t} + \frac{\rho}{\mathbb{G}}D_t^{(2-\beta)}u_\theta = \left(\frac{\partial^2}{\partial r^2} + \frac{1}{r}\frac{\partial}{\partial r} - \frac{1}{r^2}\right)u_\theta + f(r,t) \tag{6.3}$$

$$\tau_{r\theta} + \frac{\mathbb{V}}{\mathbb{G}}D_t^{(1-\beta)}\tau_{r\theta} = \mathbb{V}\left(\frac{\partial}{\partial r} - \frac{1}{r}\right)u_\theta \tag{6.4}$$

In the next section, we discuss the discretization and the solution of these equations numerically using the spectral method and finite difference method.

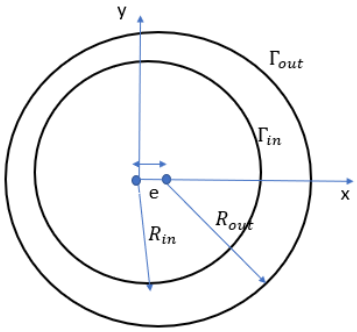

Figure 6.1: The eccentric cylinder geometry with eccentricity e

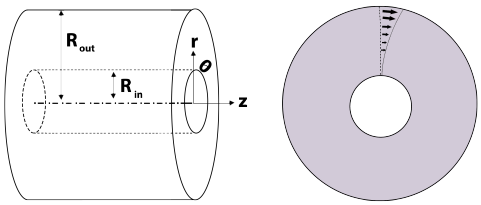

Figure 6.2: An annular geometry and flow

6.3 Numerical Discretization

This section concentrates on discretizing Eqs. (6.3) and (6.4), including both temporal and spatial derivative terms, to develop a numerical scheme for solving the system of fractional partial differential equations, subject to the given boundary and initial conditions.

$$u_\theta(R_{in}, t) = \phi_i(t), \quad u_\theta(R_{out}, t) = \phi_0(t), \quad 0 < t < T, \tag{6.5}$$

$$u_\theta(r, 0) = \frac{\partial u_\theta(r, 0)}{\partial t} = 0, \quad \tau_{r,\theta}(r, 0) = 0, \quad R_{in} < r < R_{out} \tag{6.6}$$

To formulate the discrete version of the problem, the equations (6.3) and (6.4) are discrtized at the Gauss-Legendre-Lobatto (GLL) nodes r_i, $i = 0, \ldots, N$, within the domain $[R_{in}, R_{out}]$. At each spatial point r_i, we define the function value as $u_i^n = u(r_i, t_n)$. The numerical approximation of this value is denoted by U_i^n where $U_i^n \simeq u_i^n$ for $i = 0, \ldots, N$. To proceed, we introduce notation to represent the average value of u between the time levels t_n and t_{n-1} at the spatial location r_i.

$$u_i^{n-1/2} = \frac{u_i^n + u_i^{n-1}}{2} \tag{6.7}$$

and the $O(\Delta t^2)$ central difference approximation to $\frac{\partial u}{\partial t}(t)$ at $t = t_{n-1/2}$ is given by

$$\delta_t U_i^{n-1/2} = \frac{U_i^n - U_i^{n-1}}{\Delta t} \tag{6.8}$$

To discretize the fractional time derivative, a uniform grid in time is employed with a step size of $\Delta t = \frac{T}{S}$, where T denotes the final time. The corresponding time levels are defined as $t_n = n\Delta t$ for $n = 0, 1, \ldots, S$. (see Sun Wu (2006), for example).

Discretization in Time

To derive the numerical approximation of the time-fractional derivative $D_t^{2-\beta} u$, we utilize the numerical approximation for the fractional diffusion-wave equation described by Sun Wu (2006).

Let $u = u_\theta$, then the fractional derivative in Eq. (6.3) is defined in the Caputo sense.

$$D_t^\epsilon u(t_n) = \frac{1}{\Gamma(2-\epsilon)} \int_0^{t_n} (t_n - t')^{1-\epsilon} \frac{\partial^2 u}{\partial t'^2} dt', \quad 1 < \epsilon < 2 \tag{6.9}$$

with $\epsilon = 2 - \beta$.

Let

$$y(r, t') = \frac{\partial u(r, t')}{\partial t'} \tag{6.10}$$

then

$$\frac{\partial y(r, t')}{\partial t'} = \frac{\partial^2 u(r, t')}{\partial t'^2} \tag{6.11}$$

Define

$$D_t^\epsilon u(t_n) = x(r, t_n) \tag{6.12}$$

then Eq. (6.9) becomes

$$x(r, t_n) = \frac{1}{\Gamma(2-\epsilon)} \int_0^{t_n} (t_n - t')^{1-\epsilon} \frac{\partial y}{\partial t'} \, dt' \tag{6.13}$$

Define the grid functions

$$U_i^n \simeq u_i^n, \quad Y_i^n \simeq y(r_i, t_n), \quad X_i^n \simeq x(r_i, t_n), \quad 0 \le i \le N, \ n \ge 0. \tag{6.14}$$

Using Taylor expansions, it follows from Eq. (6.10) that a second-order approximation to $y(r_i, t_{n-1/2})$ is

$$Y_i^{n-1/2} = \delta_t U_i^{n-1/2} \tag{6.15}$$

The local truncation error e_1 of this approximation is defined by

$$(e_1)_i^{n-1/2} = Y_i^{n-1/2} - \delta_t U_i^{n-1/2} \tag{6.16}$$

from which we can show, using Taylor series expansions, that

$$|(e_1)_i^{n-1/2}| \le c_1 (\Delta t)^2 \tag{6.17}$$

where c_1 is a constant.

Based on Lemma 2.2 of Sun Wu (2006), and using a Taylor expansion with integral remainder for any function $F(t) \in C^2[0, t_n]$, we have

$$\int_0^{t_n} F'(t) \frac{1}{(t_n - t)^{\alpha-1}} dt \simeq \sum_{k=1}^{n} \frac{F(t_k) - F(t_{k-1})}{\Delta t} \int_{t_{k-1}}^{t_k} \frac{1}{(t_n - t)^{\alpha-1}} dt, \quad \Delta t > 0 \tag{6.18}$$

which is called the L1 method.

Therefore, the approximation of Eq. (6.13) at the point (r_i, t_n) is

$$X_i^n \simeq \frac{1}{\Gamma(2-\epsilon)} \left[\sum_{j=1}^{n} \frac{Y_i^j - Y_i^{j-1}}{\Delta t} \int_{t_{j-1}}^{t_j} (t_n - t')^{1-\epsilon} dt' \right] \tag{6.19}$$

Since

$$\int_{t_{j-1}}^{t_j} (t_n - t')^{1-\epsilon} dt = \frac{(\Delta t)^{2-\epsilon}}{2-\epsilon} \left[(n-j+1)^{2-\epsilon} - (n-j)^{2-\epsilon} \right], \quad n - j \geq 0. \tag{6.20}$$

and based on Lemma 2.3 of Sun Wu (2006), we can express Eq. (6.19) in the form

$$X_i^n = \frac{(\Delta t)^{1-\epsilon}}{\Gamma(2-\epsilon)} \left[\sum_{j=1}^{n} a_{n-j}(\beta) \left(Y_i^j - Y_i^{j-1} \right) \right] \tag{6.21}$$

where

$$a_{n-j}(\beta) = \left[(n-j+1)^{2-\epsilon} - (n-j)^{2-\epsilon} \right], \quad n - j \geq 0. \tag{6.22}$$

Let $l = s - j$, then

$$a_l(\beta) = \left[(l+1)^{2-\epsilon} - (l)^{2-\epsilon} \right], \quad l \geq 0. \tag{6.23}$$

then Eq. (6.21) becomes,

$$\begin{aligned} X_i^n &\simeq \frac{(\Delta t)^{1-\epsilon}}{\Gamma(2-\epsilon)}\left[\sum_{j=1}^{n} a_{n-j}\ \left(Y_i^j - Y_i^{j-1}\right)\right] \\ &= \frac{(\Delta t)^{1-\epsilon}}{\Gamma(2-\epsilon)}\Bigg[a_{n-1}\ \left(Y_i^1 - Y_i^0\right) + a_{n-2}\ \left(Y_i^2 - Y_i^1\right) + a_{n-3}\ \left(Y_i^3 - Y_i^2\right) + \\ &\quad \cdots + a_1\ \left(Y_i^{n-1} - Y_i^{n-2}\right) + a_0\ \left(Y_i^n - Y_i^{n-1}\right)\Bigg] \\ &= \frac{(\Delta t)^{1-\epsilon}}{\Gamma(2-\epsilon)}\Bigg[a_0 Y_i^n - (a_{n-1} - a_{n-2})\, Y_i^1 - (a_{n-3} - a_{n-2})\, Y_i^2 - \\ &\quad \cdots - (a_0 - a_{-1})\, Y_i^{n-1} - a_{n-1} Y_i^0\Bigg] \\ &= \frac{(\Delta t)^{1-\epsilon}}{\Gamma(2-\epsilon)}\left[a_0 Y_i^n - \sum_{j=1}^{n-1} (a_{n-j-1} - a_{n-j})\, Y_i^j - a_{n-1} Y_i^0\right] \end{aligned} \tag{6.24}$$

and

$$X_i^{n-1} = \frac{\Delta t^{1-\epsilon}}{\Gamma(2-\epsilon)}\left[a_0(\beta) Y_i^{n-1} - \sum_{j=1}^{n-2} \left(a_{n-j-2}(\beta) - a_{n-j-1}(\beta)\right)\ Y_i^j - a_{n-2}(\beta) Y_i^0\right] \tag{6.25}$$

Consequently,

$$\begin{aligned} \frac{X_i^n + X_i^{n-1}}{2} &\simeq X_i^{n-1/2} \\ &= \frac{(\Delta t)^{1-\epsilon}}{\Gamma(2-\epsilon)}\left[a_0 Y_i^{n-1/2} - \sum_{j=1}^{n-1} (a_{n-j-1} - a_{n-j})\ Y_i^{j-1/2} - a_{n-1} Y_i^0\right] \end{aligned} \tag{6.26}$$

where e_2 is the local truncation error of this approximation $X_i^{n-1/2}$ with

$$|(e_2)_i^{n-1/2}| \leq c_2 (\Delta t)^{2-\epsilon} \tag{6.27}$$

where c_2 is a constant.

Substituting Eq. (6.15) into Eq. (6.26), we have

$$X_i^{n-1/2} = \frac{(\Delta t)^{1-\epsilon}}{\Gamma(2-\epsilon)}\left[a_0\delta_t U_i^{n-1/2} - \sum_{j=1}^{n-1}(a_{n-j-1}-a_{n-j})\delta_t U_i^{j-1/2} - a_{n-1}Y_i^0\right] + \frac{(\Delta t)^{1-\epsilon}}{\Gamma(2-\epsilon)}\left[a_0(e_1)_i^{n-1/2} - \sum_{j=1}^{n-1}(a_{n-j-1}-a_{n-j})(e_1)_i^{j-1/2}\right] + (e_2)_i^{n-1/2} \quad (6.28)$$

Replacing $\delta_t U_i^{n-1/2}$ by Eq. (6.15), and substituting the above results into Eq. (6.9) we obtain the following finite difference approximation to $D_{t_n}^{\epsilon}u$:

$$D_t^{\epsilon}u(t_n) \simeq \frac{(\Delta t)^{1-\epsilon}}{\Gamma(2-\epsilon)}\left[a_0\left(\frac{U_i^n - U_i^{n-1}}{\Delta t}\right) - \sum_{j=1}^{n-1}\left(a_{n-j-1}-a_{n-j}\right)\left(\frac{U_i^j - U_i^{j-1}}{\Delta t}\right) - a_{n-1}\Phi(r_i)\right] \quad (6.29)$$

where $\Phi(r_i) = Y_i^0 = y(r_i, 0)$.

Discretization in Space

We employ the spectral method (SM), which requires the problem to be written in its weak formulation. In this section we shall describe the procedures needed both before and after applying the SM to the momentum equations in detail. Before we write down the weak formulation, we must define a suitable function space for the solution u. Define $H^1([a,b])$ to be the Sobolev space comprising square-integrable functions with square-integrable generalized first derivatives. The space $H_0^1([a,b])$ is a subspace of $H^1([a,b])$ containing functions that vanish at a and b i.e $H_0^1([a,b]) = \{v \in H^1([a,b]) : v(a) = v(b) = 0\}$. The test space $W = H_0^1([a,b])$. The solution space is $V = \{v \in H^1([a,b]) : v(a), v(b)$ satisfy prescribed Dirichlet boundary condition$\}$.

6.3.1 Weak Formulation of Velocity Equation

Multiply Eq. (6.3) by a test function $v \in W$ and integrate over the entire radial domain $[R_{in}, R_{out}]$, then the weak form is: Find $u \in V$ such that

$$\frac{\rho}{\mathbb{V}} \int_{R_{in}}^{R_{out}} \frac{\partial u}{\partial t} v dr + \frac{\rho}{\mathbb{G}} \int_{R_{in}}^{R_{out}} (D_t^{2-\beta} u) v dr = \int_{R_{in}}^{R_{out}} \frac{\partial^2 u}{\partial r^2} v dr + \int_{R_{in}}^{R_{out}} \frac{1}{r} \frac{\partial u}{\partial r} v dr - \int_{R_{in}}^{R_{out}} \frac{u}{r^2} v dr + \int_{R_{in}}^{R_{out}} f(r,t) v dr, \quad \forall\, v \in W \tag{6.30}$$

Integrating the first term on the right−hand side by parts we obtain

$$\int_{R_{in}}^{R_{out}} \frac{\partial^2 u}{\partial r^2} v dr = - \int_{R_{in}}^{R_{out}} \frac{\partial u}{\partial r} \frac{\partial v}{\partial r} dr \tag{6.31}$$

(Boundary terms vanish since $v \in W$, i.e. $v(R_{in}) = v(R_{out}) = 0$)

6.3.2 Discrete problem

In Time

The equation (6.30) is discretized at $t = t_{n-1/2}$ and an approximation that is averaged over t_{n-1} and t_n is used. In particular, at each point $r = r_i$ we have

$$\frac{\partial u}{\partial t}(r_i, t_{n-1/2}) \simeq \delta_t U_i^{n-1/2} = \frac{U_i^n - U_i^{n-1}}{\Delta t} \tag{6.32}$$

The numerical approximation to the fractional derivative, $D_t^{(2-\beta)} u$, is given by Sun Wu (2006), and was derived in the previous subsection (see Eq. (6.29)).

In space

We first transform the physical domain $[R_{in}, R_{out}]$ to the computational domain $[-1, 1]$ as follows:

Define points in the physical domain that correspond to the GLL points,

$$r_i = R_{in} + (\tilde{r}_i + 1) \frac{(R_{out} - R_{in})}{2}, \quad r_i \in [R_{in}, R_{out}] \tag{6.33}$$

Then

$$\tilde{r_i} = \frac{2r_i - (R_{in} + R_{out})}{(R_{in} - R_{out})}, \quad \tilde{r_i} \in [-1, 1] \tag{6.34}$$

Let $\Delta = \frac{R_{in} - R_{out}}{2}$, then

$$\frac{d\tilde{r}}{dr} = \Delta^{-1}$$

$$\frac{\partial u}{\partial r} = \frac{\partial u}{\partial \tilde{r}} \frac{\partial \tilde{r}}{\partial r} = \Delta^{-1} \frac{\partial u}{\partial \tilde{r}}, \quad etc.$$

and $u_i^{n-1/2} = \frac{u_i^n + u_i^{n-1}}{2}$ is the average of u at the points (r_i, t_n) and (r_i, t_{n-1}). The spectral approximation of u is given by

$$u_N(r) = \sum_{j=0}^{N} u_j h_j(\tilde{r}) \tag{6.35}$$

and the test functions are chosen to be $v = h_k(\tilde{r})$ for $k = 1, \ldots, N-1$.

Inserting these spectral approximations in the weak formulation (6.30) we obtain,

$$\begin{aligned}
\int_{R_{in}}^{R_{out}} \frac{\partial^2 u}{\partial r^2} v dr &= -\frac{1}{\Delta} \int_{-1}^{1} \frac{\partial u}{\partial \tilde{r}} \frac{\partial v}{\partial \tilde{r}} d\tilde{r} \\
&\simeq -\frac{1}{\Delta} \sum_{l=0}^{N} w_l \left(\sum_{j=0}^{N} U_j h_j'(\tilde{r}_l) \right) h_k'(\tilde{r}_l) \\
&= -\frac{1}{\Delta} \sum_{l=0}^{N} w_l \left(\sum_{j=0}^{N} U_j D_{l,j} \right) D_{l,k} \\
&= -\frac{1}{\Delta} \sum_{j=0}^{N} \left(\sum_{l=0}^{N} w_l D_{l,j} D_{l,k} \right) U_j \\
&\simeq -\frac{1}{\Delta} \sum_{j=0}^{N} B_{k,j} U_j^{n-1/2} \\
&= -\frac{1}{\Delta} \sum_{j=0}^{N} B_{k,j} \left(\frac{U_j^n + U_j^{n-1}}{2} \right)
\end{aligned} \tag{6.36}$$

where $B_{k,j} = \sum_{l=0}^{N} w_l D_{l,j} D_{l,k}$.

$$\begin{aligned}
\int_{R_{in}}^{R_{out}} \frac{1}{r}\frac{\partial u}{\partial r} v dr &= \Delta \int_{-1}^{1} \Delta^{-1} \frac{1}{r}\frac{\partial u}{\partial \tilde{r}} v(\tilde{r}) d\tilde{r} \\
&\simeq \sum_{l=0}^{N} \frac{w_l}{r_l} \left(\sum_{j=0}^{N} U_j h_j'(\tilde{r}_l) \right) h_k(\tilde{r}_l) \\
&= \sum_{l=0}^{N} \frac{w_l}{r_l} \left(\sum_{j=0}^{N} U_j D_{l,j} \right) h_k(\tilde{r}_l) \\
&\simeq \frac{w_k}{r_k} \sum_{j=0}^{N} D_{k,j} U_j^{n-1/2} \\
&= \frac{w_k}{r_k} \sum_{j=0}^{N} D_{k,j} \left(\frac{U_j^n + U_j^{n-1}}{2} \right)
\end{aligned} \tag{6.37}$$

$$\begin{aligned}
\int_{R_{in}}^{R_{out}} \frac{u}{r^2} v dr &= \Delta \int_{-1}^{1} \frac{u}{r^2} v(\tilde{r}) d\tilde{r} \\
&\simeq \Delta \sum_{l=0}^{N} \frac{w_l}{r_l^2} \left(\sum_{j=0}^{N} U_j h_j(\tilde{r}_l) \right) h_k(\tilde{r}_l) \\
&= \Delta \sum_{l=0}^{N} \frac{w_l}{r_l^2} \left(U_l \right) h_k(\tilde{r}_l) \\
&\simeq \frac{\Delta w_k}{r_k^2} \left(U_k^{n-1/2} \right) \\
&= \frac{\Delta w_k}{r_k^2} \left(\frac{U_k^n + U_k^{n-1}}{2} \right) \\
&\simeq \frac{\Delta w_k}{(\Delta \tilde{r}_k + \frac{R_{in}+R_{out}}{2})^2} \left(\frac{U_k^n + U_k^{n-1}}{2} \right)
\end{aligned} \tag{6.38}$$

The source term is given by,

$$\begin{aligned}
\int_{R_{in}}^{R_{out}} f(t,r) v(r) dr &= \Delta \int_{-1}^{1} f(t,\tilde{r}) v(\tilde{r}) d\tilde{r} \\
&\simeq \Delta \sum_{l=0}^{N} w_l f(t_{n-1/2}, \tilde{r}_l) h_k(\tilde{r}_l) \\
&= \Delta w_k \left(\frac{f(t_n, r_k) + f(t_{n-1}, r_k)}{2} \right)
\end{aligned} \tag{6.39}$$

where $r_k \in [R_{in}, R_{out}]$.

The full discretization of Eq.(6.30) is

$$\left[\frac{\rho}{\mathbb{V}}\frac{w_k}{\Delta t}\right](U_k^n - U_k^{n-1}) + \frac{\rho}{\mathbb{G}}\frac{w_k}{\Delta t}\frac{1}{\Gamma(\beta)}\left[a_0\frac{U_k^n - U_k^{n-1}}{\Delta t} - \sum_{j=1}^{n-1}(a_{n-j-1} - a_{n-j})\frac{U_k^j - U_k^{j-1}}{\Delta t}\right]$$
$$= -\frac{1}{2\Delta t}\left[\sum_{j=0}^{n-1} B_{k,j}(U_j^n + U_j^{n-1})\right] - \frac{w_k\Delta}{2r_k^2}(U_k^n + U_k^{n-1}) + \frac{w_k}{2r_k}\left[\sum_{j=0}^{n-1} D_{k,j}(U_j^n + U_j^{n-1})\right]$$
$$+ \frac{\Delta w_k}{2}\left[f(t_n, r_k) + f(t_{n-1}, r_k)\right], \quad k = 1, \ldots, N-1, \quad n = 1, \ldots, S \tag{6.40}$$

**Note as mentioned by Ferras . (2018) this is a time-averaged approximation over the interval $[t_{n-1}, t_n]$. It can be viewed as the approximation at $t = t_{n-1/2}$.

A linear system of the form $\boldsymbol{AU} = \boldsymbol{b}$ is solved at each new time level.

The initial conditions are

$$U_k^0 = 0, \quad 1 \le k \le N-1 \tag{6.41}$$

Rearrange Eq. (6.40) we obtain

$$\left[\frac{\rho}{\mathbb{V}}\frac{w_k}{\Delta t} + \frac{\rho}{\mathbb{G}}\frac{a_0}{\Gamma(\beta)}\frac{w_k}{(\Delta t)^2} + \frac{\Delta w_k}{2r_k^2}\right]U_k^n + \sum_{j=0}^{N}\left[\frac{1}{2\Delta}B_{k,j} - \frac{w_k}{r_k}D_{k,j}\right]U_j^n$$
$$= \left[\frac{\rho}{\mathbb{V}}\frac{w_k}{\Delta t} + \frac{\rho}{\mathbb{G}}\frac{a_0}{\Gamma(\beta)}\frac{w_k}{(\Delta t)^2} - \frac{\Delta w_k}{2r_k^2}\right]U_k^{n-1} - \sum_{j=0}^{N}\left[\frac{1}{2\Delta}B_{k,j} - \frac{w_k}{r_k}D_{k,j}\right]U_j^{n-1}$$
$$+ \frac{\rho}{\mathbb{G}}\frac{w_k}{\Gamma(\beta)}\frac{1}{(\Delta t)^2}\sum_{j=1}^{n-1}(a_{n-j-1} - a_{n-j})(U_k^j - U_k^{j-1}) + \frac{\Delta w_k}{2}\left[f(t_n, r_k) + f(t_{n-1}, r_k)\right] \tag{6.42}$$

The values of u on each of the cylinder boundaries are given by the prescribed boundary conditions

$$U_0^n = \phi_0(n\Delta t) \tag{6.43}$$

$$U_N^n = \phi_N(n\Delta t) \tag{6.44}$$

Then $\boldsymbol{U}$ is the vector of unknown components u_k^n where $1 \le k \le N-1$, at each time level $n = 0, 1, \ldots, S$, and $\boldsymbol{b}$ is the vector of the right-hand side of Eq. (6.42) together with the terms from the left-hand side involving u_0^n and u_N^n. The entries of the $(N-1) \times (N-1)$

matrix $\boldsymbol{A}$ are given by

$$A_{k,j} = \left[\frac{\rho}{\mathbb{V}}\frac{w_k}{\Delta t} + \frac{\rho}{\mathbb{G}}\frac{a_0}{\Gamma(\beta)}\frac{w_k}{(\Delta t)^2} + \frac{\Delta w_k}{2r_k^2}\right]\delta_{k,j} + \left[\frac{1}{2\Delta}B_{k,j} - \frac{w_k}{2r_k}D_{k,j}\right] \tag{6.45}$$

The system of equations is solved using a direct method for $n = 1, \ldots, S$. This gives an approximation to the velocity at the mesh points in time and space.

We solve separately the evolution equation for the shear stress Eq. (6.4) with initial condition $\tau_{r\theta}(r, 0) = 0$, since the right-hand side of Eq. (6.4) is known.

6.3.3 Weak Formulation of the Shear Stress Equation

Let $\tau = \tau_{r\theta}$. Multiply the evolution equation for the shear stress (6.4) by a test function $\eta \in V$ where V is the solution space i.e $V = \{v \in H^1([a, b]) : v(a), v(b)$ satisfy prescribed Dirichlet boundary condition$\}$, and integrate over the domain $[R_{in}, R_{out}]$ to obtain the weak formulation.

$$\int_{R_{in}}^{R_{out}} \tau(t)\ v\ dr + \frac{\mathbb{V}}{\mathbb{G}}\int_{R_{in}}^{R_{out}} \left(D_t^{1-\beta}\tau(t)\right) v\ dr = \int_{R_{in}}^{R_{out}} \mathbb{V}\left(\frac{\partial u}{\partial r} - \frac{u}{r}\right) v\ dr \tag{6.46}$$

6.3.4 Discrete problem

To derive the discrete form of the weak formulation of Eq. (6.46) we consider each term separately.

$$\begin{aligned}
\int_{R_{in}}^{R_{out}} \tau(t)\ v\ dr &= \Delta \int_{-1}^{1} \tau(t)\ v\ d\tilde{r} \\
&\simeq \Delta \sum_{l=0}^{N} w_l \left(\sum_{j=0}^{N} \tau_j h_j(\tilde{r}_l)\right) h_k(\tilde{r}_l) \\
&= \Delta \sum_{l=0}^{N} w_l\,(\tau_l)\, h_k(\tilde{r}_l) \\
&= \Delta w_k \tau_k^n
\end{aligned} \tag{6.47}$$

Here, we will use Eq. (5.68) to substitute the discrtization of $D_t^{1-\beta}\tau(t)$

$$\begin{aligned}
\int_{R_{in}}^{R_{out}} \left(D_t^{1-\beta}\tau(t)\right)\ v\ dr &= \Delta \int_{-1}^{1} \left(D_t^{1-\beta}\tau(t)\right)\ v\ d\tilde{r} \\
&\simeq \Delta \sum_{l=0}^{N} w_l \left(D_t^{1-\beta}\tau_l\right) h_k(\tilde{r}_l) \\
&= \Delta w_k \left(D_t^{1-\beta}\tau_k\right) \\
&= \frac{\Delta w_k}{\Gamma(\beta)} \frac{1}{\Delta t} \left[b_0 \tau_k^n - \sum_{j=1}^{n-1} (b_{n-j-1} - b_{n-j}) \tau_k^j - b_{n-1}\tau_k^0 \right]
\end{aligned} \tag{6.48}$$

where the coefficient defined in Ch.5 by Eq. (5.64)

$$\begin{aligned}
\int_{R_{in}}^{R_{out}} \frac{\partial u}{\partial r}\ v\ dr &= \Delta \int_{-1}^{1} \left(\Delta^{-1} \frac{\partial u}{\partial \tilde{r}}\right)\ v\ d\tilde{r} \\
&\simeq \sum_{l=0}^{N} w_l \left(\sum_{j=0}^{N} U_j h_j'(\tilde{r}_l) \right) h_k(\tilde{r}_l) \\
&= \sum_{l=0}^{N} w_l \left(\sum_{j=0}^{N} D_{l,j} U_j \right) h_k(\tilde{r}_l) \\
&\simeq w_k \sum_{j=0}^{N} D_{k,j} U_j^n
\end{aligned} \tag{6.49}$$

$$\begin{aligned}
\int_{R_{in}}^{R_{out}} \frac{u}{r}\ v\ dr &= \Delta \int_{-1}^{1} \frac{u}{r}\ v\ d\tilde{r} \\
&\simeq \Delta \sum_{l=0}^{N} \frac{w_l}{r_l} \left(\sum_{j=0}^{N} U_j h_j(\tilde{r}_l) \right) h_k(\tilde{r}_l) \\
&= \Delta \sum_{l=0}^{N} \frac{w_l}{r_l} (U_l)\, h_k(\tilde{r}_l) \\
&= \frac{\Delta w_k}{\Delta \tilde{r}_k + 1/2(R_{in} + R_{out})} U_k^n \\
&= \frac{\Delta w_k}{r_k^2} U_k^n
\end{aligned} \tag{6.50}$$

for $k = 1, \ldots, N-1$ and $n = 1, \ldots, S$.

Inserting these approximations into Eq. (6.46) forms the linear system $\boldsymbol{M\tau} = \boldsymbol{b}$ at each time step. Here $\boldsymbol{M}$ is a diagonal matrix so the solution can be obtained simply.

The full discretization of the stress equation is

$$\Delta w_k \tau_k^n + \Delta w_k \frac{\mathbb{V}}{\mathbb{G}\Gamma(\beta)} \frac{1}{\Delta t} \left[b_0 \tau_k^n - \sum_{j=1}^{n-1} (b_{n-j-1} - b_{n-j}) \tau_k^j - b_{n-1} \tau_k^0 \right] = \mathbb{V} w_k \sum_{j=0}^{N} D_{k,j} U_j^n - \mathbb{V} \frac{w_k \Delta}{r_k^2} U_k^n \tag{6.51}$$

Dividing by Δw_k yields

$$\left[1 + \frac{\mathbb{V}}{\mathbb{G}} \frac{1}{\Gamma(\beta)} \frac{b_0}{\Delta t} \right] \tau_k^n = \frac{\mathbb{V}}{\mathbb{G}} \sum_{j=1}^{n-1} (b_{n-j-1} - b_{n-j}) \tau_k^j + b_{n-1} \tau_k^0 + \frac{\mathbb{V}}{\Delta} \sum_{j=0}^{N} D_{k,j} U_j^n - \frac{\mathbb{V}}{r_k^2} U_k^n \tag{6.52}$$

for $k = 1, \ldots, N-1$ and $n = 1, \ldots, S$.

Here $\boldsymbol{\tau}$ is the vector of unknowns components τ_k^n where $1 \leq k \leq N-1$, for $n = 0, 1, \ldots, S$, and $\boldsymbol{b}$ is the vector of the right-hand side of equation (6.52), and finally $\boldsymbol{M} = c\boldsymbol{I}$ is the $(N-1) \times (N-1)$ diagonal matrix where

$$\boldsymbol{c} = \left[1 + \frac{\mathbb{V}}{\mathbb{G}} \frac{1}{\Gamma(\beta)} \frac{b_0}{\Delta t} \right] \tag{6.53}$$

and $\boldsymbol{I}$ is the identity matrix.

6.4 Convergence behaviour of Spectral Approximation

Suppose the error in a spectral approximation decays algebraically i.e

$$E = CN^{-\alpha} \tag{6.54}$$

where C and α are constants. The value of α measures the order of convergence.

Take the log of both sides of equation (6.54):

$$\begin{aligned} \ln(E) &= \ln(CN^{-\alpha}) \\ &= \ln(C) - \alpha \ln(N) \end{aligned} \tag{6.55}$$

If we plot ($\ln E$ vs. $\ln N$) then the (negative) slope of the straight line will give us the value of α.

The idea is to plot ($\ln E$ vs. $\ln N$) for $N = 4, 8, 16, \ldots$ etc and find the slope. If the solution to the PDE is smooth (i.e infinitely differentiable) then the convergence should be exponential rather than algebraic and the ($\ln E$ vs. $\ln N$) plot will look like the plot in Fig. 6.3.

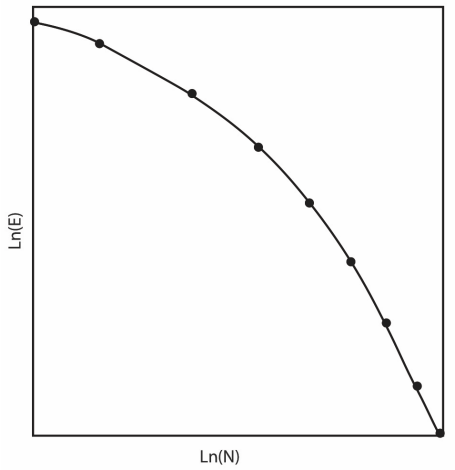

Figure 6.3: Typical $\ln E$ vs. $\ln N$ plot for an exponentially convergent spectral approximation.

6.5 Numerical Results

In this section we will use numerical analysis to examine the convergence of the numerical approach, plot the solutions, and then show the comparison with the results of the Finite Difference Method (FDM).

6.5.1 Study solvability and convergence order

To prove the validation of the proposed numerical method (SM) and the numerical code that was developed using Matlab, we will present some examples that compare the numerical results obtained with the existing analytical solution for the Newtonian case. We also investigate the dependence of the L_2 norm of the error on N and Δt. The convergence of the proposed method and the order of convergence is then determined, and the outcomes are compared with the Finite Difference Method (FDM) of Ferras . (2018).

We analyze the following examples to show numerically the expected spectral precision. Firstly we only verify the discretised velocity equation, that is independent of the stress, secondly we verify the discretised stress equation, which depends on the computed velocity profile and its spatial derivative, and then we establish the steady velocity problem that is independent of time. Finally we solve the system of differential equations (coupled problem) governing the steady or unsteady flow of a fractional viscoelastic fluid in an annular geometry.

Example 1: (Momentum equation for the tangential velocity)

We investigate the same problem that was considered by Ferras . (2018), which is the evolution of the discretized tangential velocity equation independent of the stress, by choosing the following parameters: $\rho = 1$ kg/m^3, $\mathbb{V} = 1$ Pa.s$^\alpha$, $\mathbb{G} = 1$ Pa.s$^\alpha$, so $\beta = 0.5$, $R_{in} = 1$ m, $R_{out} = 2$ m. We also choose a range of discretization parameters:

$\Delta t = 1/8, 1/16, 1/32, 1/64, 1/128, 1/256, 1/512$, and $N = 4, 8, 16, 32, 64, 128$.

The tangential component of the momentum equation is

$$\frac{\partial u}{\partial t} + D_t^{2-\beta} u = \frac{\partial^2 u}{\partial r^2} + \frac{1}{r}\frac{\partial u}{\partial r} - \frac{u}{r^2} + f(t, r) \tag{6.56}$$

where the source term $f(t,r)$ is given by

$$f(r,t) = 3t^2r^3\left(r - \frac{3}{10}\right) + \frac{3r^3(10r-3)}{5\Gamma(\beta+2)}t^{\beta+1} - 7r^2t^3 - 8rt^3\left(r - \frac{3}{10}\right) \tag{6.57}$$

with boundary and initial conditions:

$$u(R_{in},t) = t^3R_{in}^3\left(R_{in} - \frac{3}{10}\right), \quad u(R_{out},t) = t^3R_{out}^3\left(R_{out} - \frac{3}{10}\right), \quad 0 < t < T \tag{6.58}$$

$$u(r,0) = 0, \quad \frac{\partial u(r,0)}{\partial t} = 0, \quad R_{in} < r < R_{out} \tag{6.59}$$

The analytical solution is given by

$$u(r,t) = t^3r^3\left(r - \frac{3}{10}\right). \tag{6.60}$$

Table 6.1 displays the L^2 error norm obtained as a function of N for different time steps Δt. For fixed value of Δt the L^2-norm of the error is independent of N.

Δt	$N = 4$	$N = 8$
0.125	0.0475	0.0475
0.0625	0.0162	0.0162
0.03125	0.0056	0.0056
0.015625	0.0019	0.0019
0.0078125	6.7406×10^{-4}	6.7401×10^{-4}
0.0039062	2.3615×10^{-4}	2.3613×10^{-4}
0.0019531	8.2952×10^{-5}	8.2945×10^{-5}

Table 6.1: Dependence of the L^2 norm of the error on Δt for $N = 4$ and $N = 8$.

Figure 6.4 illustrates the comparison between the approximate and exact solutions at various times $(T = 0, 0.5, 1)$s. The exact and approximate velocity at different spatial points $(r = 1, 1.1, 0.5, 1.8, 2)$ for varying values of N is shown in Figure 6.5. While the surface plots Fig. 6.6 (a) and (b) represent the exact and numerical solution of the velocity profile, respectively, for $N = 32$.

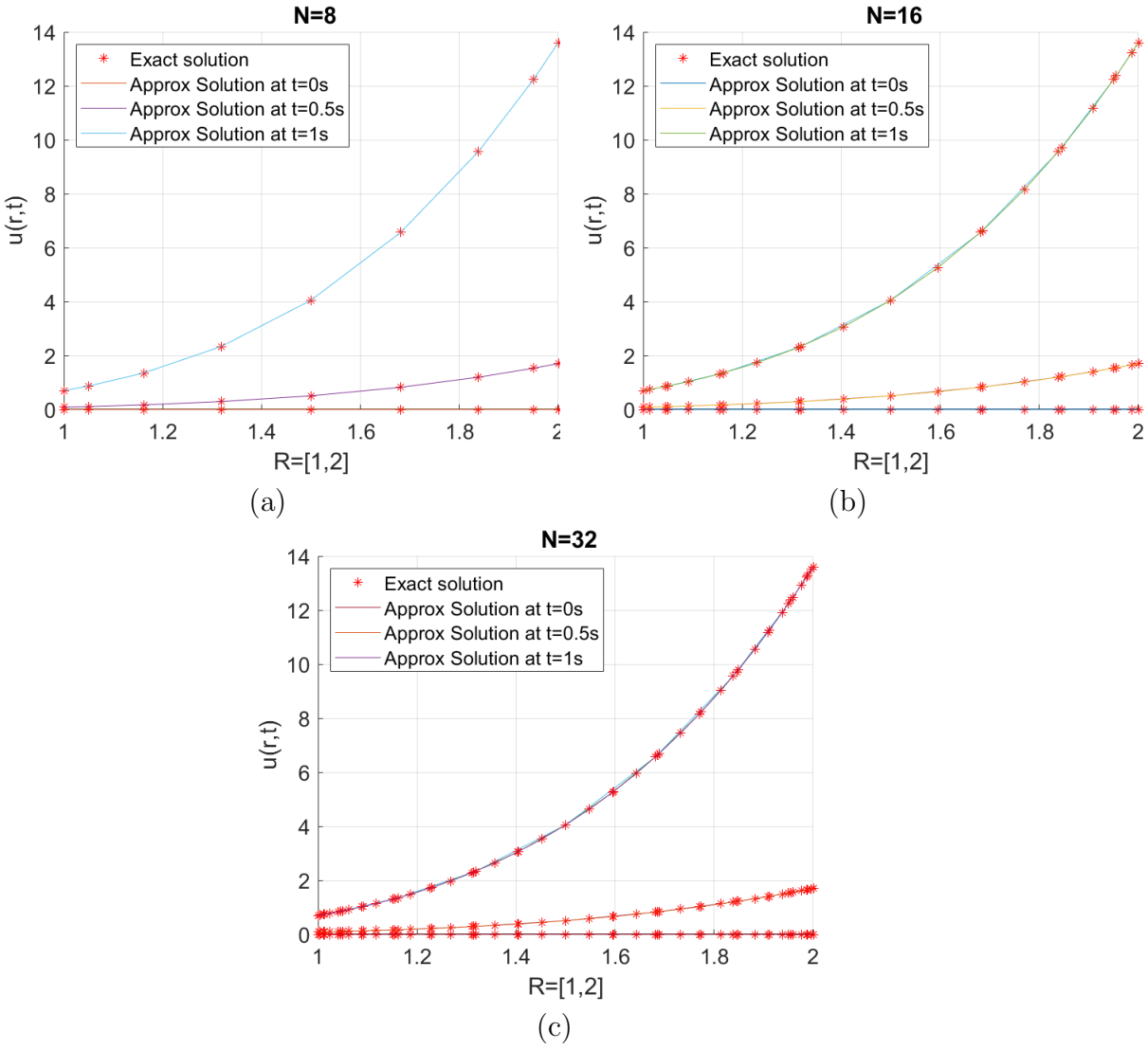

Figure 6.4: Comparison of the exact and approximate velocity profiles at $t = 0, 0.5, 1$ s for (a) $N = 8$, (b) $N = 16$, (c) $N = 32$.

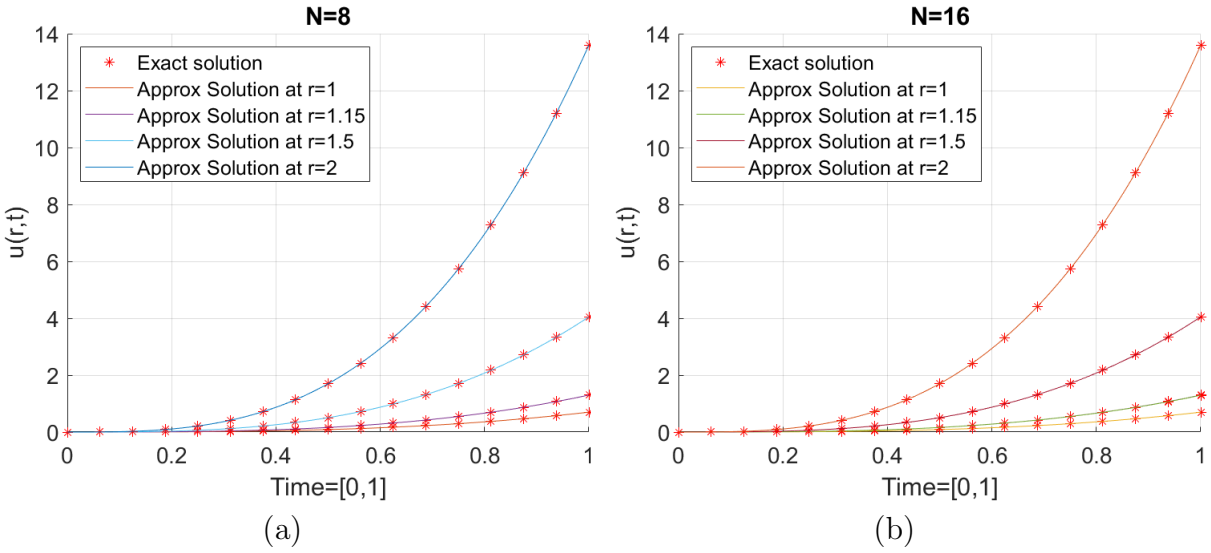

(a)

(b)

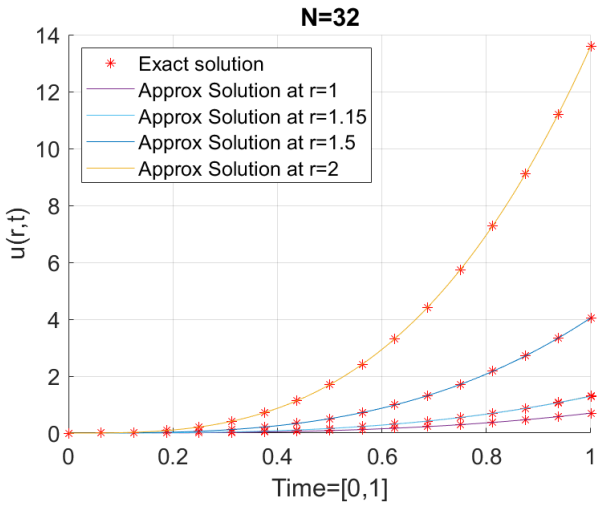

(c)

Figure 6.5: Comparison of the exact and approximate velocity profiles at $r = 1, 1.1, 0.5, 1.8, 2$ for (a) $N = 8$, (b) $N = 16$, (c) $N = 32$.

To determine the order of convergence (q_u) of the numerical approximation we define

$$q_u = \frac{\log\left(\frac{\bar{\epsilon}_{N,\Delta t}}{\bar{\epsilon}_{N,\Delta t/2}}\right)}{\log 2} \tag{6.61}$$

where

$$\epsilon_{N,\Delta t} = \max_{\substack{1\le i\le N-1 \\ 1\le j\le S}} |u_{\text{exact}}(r_i, t_j) - u_{\text{num}}(r_i, t_j)|, \quad j = 1, 2, .., S \tag{6.62}$$

In Table 6.2 we use equation (6.61) and (6.62) to calculate the maximum error with respect to Δt for fixed $N = 128$ and then determine the convergence order for velocity

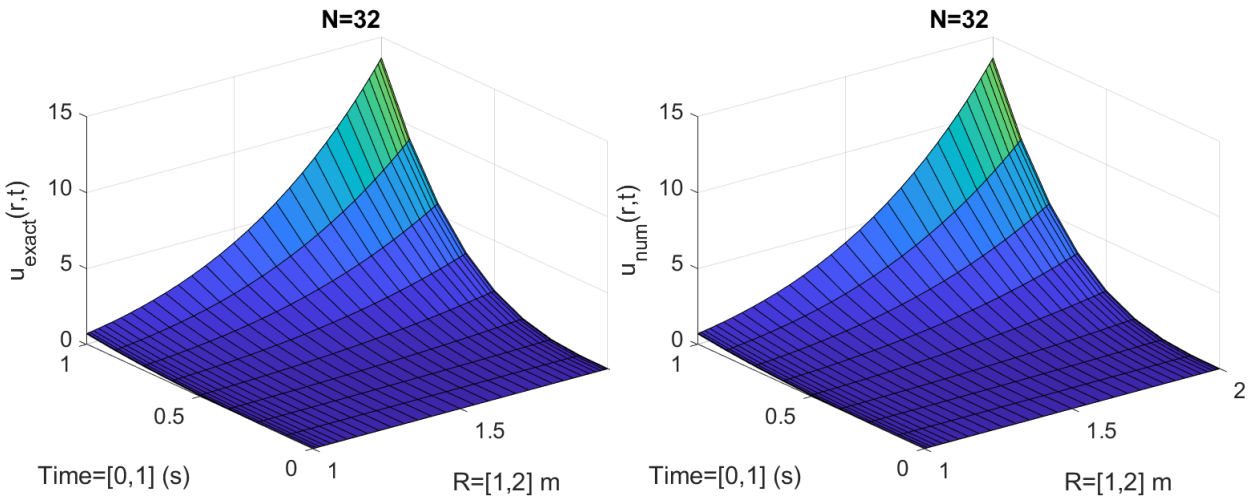

(a) (b)

Figure 6.6: (a) Exact and (b) numerical velocity profiles for $N = 32$.

in time (q_u). Note that the maximum error here is over all discretization points in space and time (r_k, t_i). The final time was $T = 1$, and the number of time steps was $S = 512$ for $\Delta t = 1/8, 1/16, 1/32, 1/64, 1/128, 1/256, 1/512$. The convergence order can be seen to be approximately 1.5 in time. In comparison the convergence order is approximately 1 in time using the finite difference method in Ferras . (2018).

We may estimate the convergence order in space (p_u) by fixing $\Delta t = 1/512$ and determine the spatial error with respect to N at the final time $T = 1$. The total number of time steps $S = 512$, and then using the following formula:

$$p_u = \frac{\log\left(\frac{\epsilon_{N,\Delta t}}{\epsilon_{2N,\Delta t}}\right)}{\log 2} \tag{6.63}$$

where $\epsilon_{N,\Delta t}$ is given by Eq. (6.62).

However, the spatial error can not be measured since it is at the level of machine precision for all values of N. Instead we consider a steady state problem - see example 3 - and perform a convergence study for this.

Example 2: (Constitutive equation for the tangential stress)

As in Ferras . (2018) we verify the discretized stress equation, which depends on the computed velocity profile and its spatial derivative.

We assume the following parameters for the discretised stress equation $\beta = 0.5$, $R_{in} = 1$

Δt	ϵ_N	q_u
$\frac{1}{8}$	0.0461	–
$\frac{1}{16}$	0.0157	1.5549
$\frac{1}{32}$	0.0054	1.5382
$\frac{1}{64}$	0.0019	1.5266
$\frac{1}{128}$	6.5470×10^{-4}	1.5187
$\frac{1}{256}$	2.2936×10^{-4}	1.5132
$\frac{1}{512}$	8.0569×10^{-5}	1.5093

Table 6.2: Error norms and rates of convergence with $N = 128$.

m, $R_{out} = 2$ m. We have also assumed $\rho = 1$ kg/m^3, $\mathbb{V} = 1$ Pa.s$^\alpha$, $\mathbb{G} = 1$ Pa.s$^\alpha$, and $\Delta t \in [1/8, 1/512]$ s and the stress profile given by,

$$\tau(r,t) = r^2 t^3 \tag{6.64}$$

The differential equation below can be solved analytically by substituting this stress profile into equation (6.4),

$$\frac{\partial u(r,t)}{\partial r} - \frac{u(r,t)}{r} = r^2 t^3 \left(\frac{6t^{\beta-1}}{\Gamma(4-(1-\beta))} + 1 \right) \tag{6.65}$$

For the solution of this differential equation, we choose the boundary condition $u(1,t) = 0$ (the boundary condition is not important here), resulting in the following velocity profile,

$$u(r,t) = \frac{r(r^2-1)t^{3-(1-\beta)}(\Gamma(4-(1-\beta))t^{1-\beta} + 6)}{2\Gamma(4-(1-\beta))} \tag{6.66}$$

The L^2-norm of the error with respect to N, is computed in Table 6.3. We note that the L^2-norm of the error is independent of the N for fixed values of Δt.

A representative consistency between the calculated solution produced by the numerical scheme at different times $T = 0, 0.5, 1$ s and the exact solution is shown in Figure 6.7. Again, Figure 6.8 displays how the exact and approximate stress match at various spatial positions $r = 1, 1.1, 0.5, 1.8, 2$ for several values of N. The surface plots Fig. 6.9 (a) and (b) show the exact and numerical solutions to the stress profile, respectively, for $N = 32$.

Δt	$N = 4$	$N = 8$
0.125	0.0747	0.0789
0.0625	0.0281	0.0297
0.03125	0.0104	0.0109
0.015625	0.0038	0.0040
0.0078125	0.0014	0.0014
0.0039062	4.8492×10^{-4}	5.1199×10^{-4}
0.0019531	1.7293×10^{-4}	1.8259×10^{-4}

Table 6.3: Dependence of the L^2 norm of the error on Δt for $N = 4$ and $N = 8$.

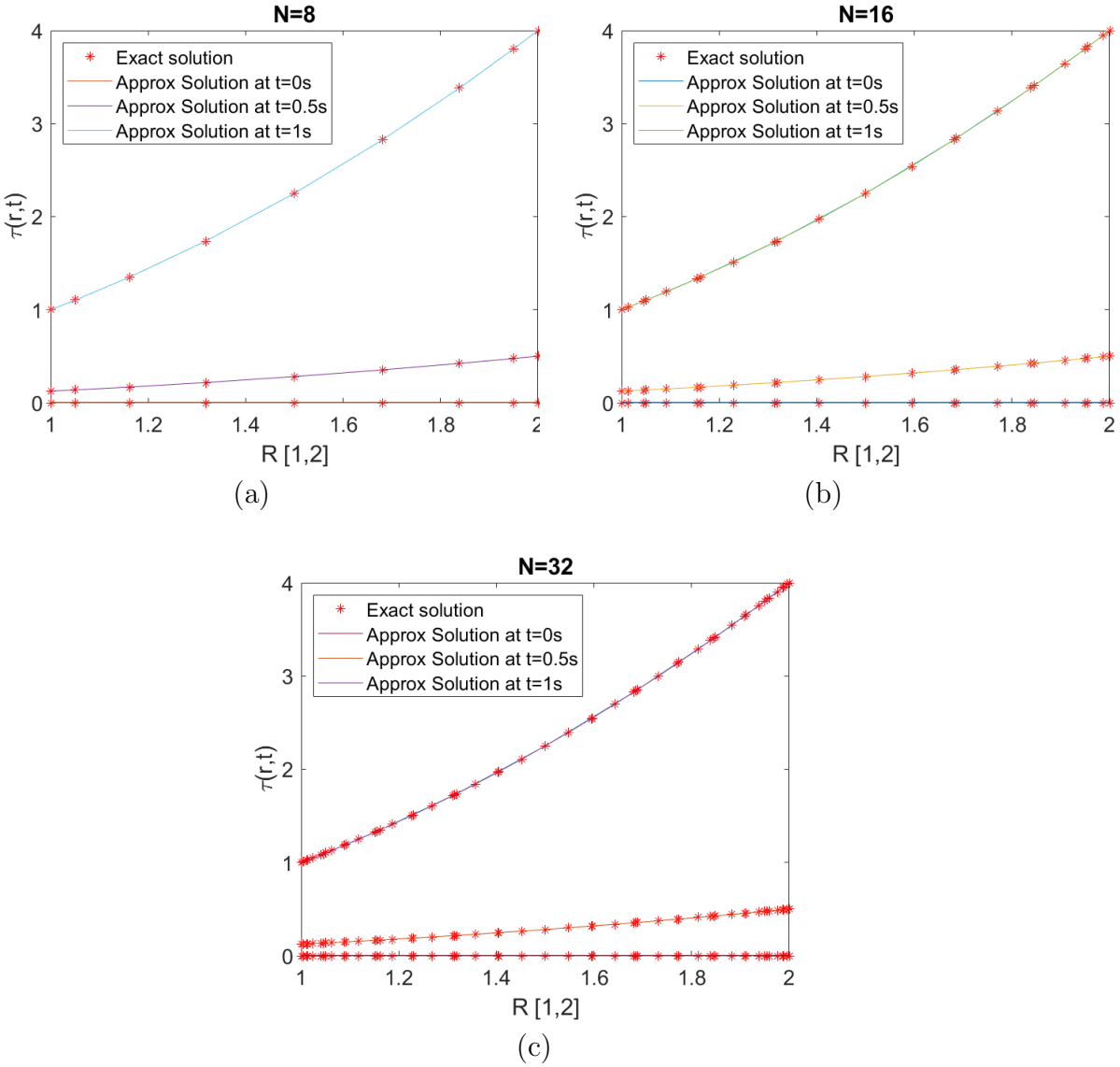

Figure 6.7: Comparison of the exact and approximate stress profiles at $t = 0, 0.5, 1$ s for (a) $N = 8$, (b) $N = 16$, (c) $N = 32$.

The convergence order for time is given by:

$$q_u = \frac{\log\left(\frac{\bar{\epsilon}_{N,\Delta t}}{\bar{\epsilon}_{N,\Delta t/2}}\right)}{\log 2} \tag{6.67}$$

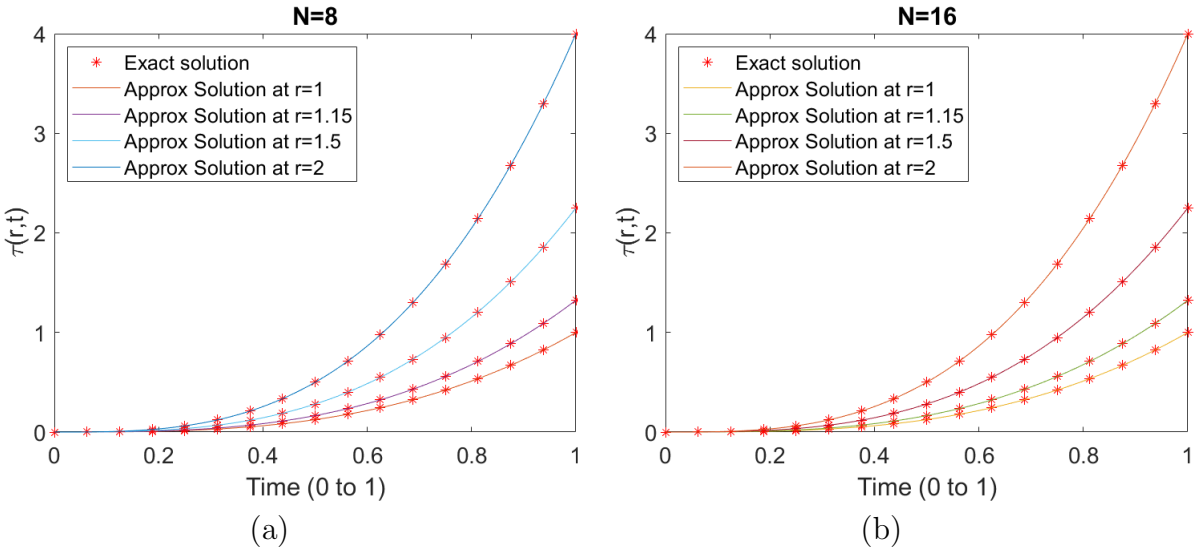

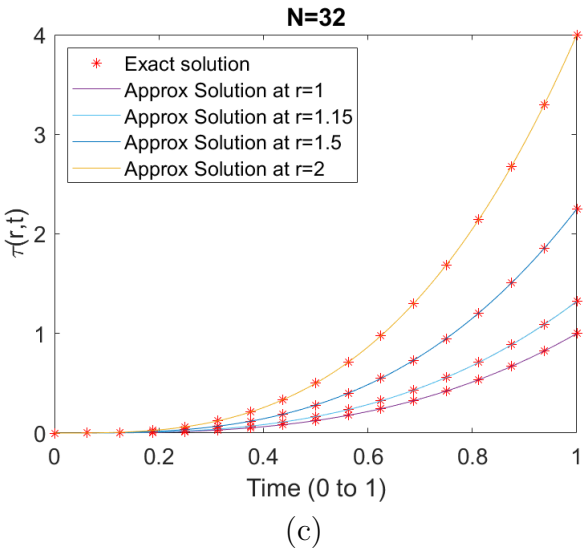

Figure 6.8: Comparison of the exact and approximate stress profiles at $r = 1, 1.15, 1.5, 2$ mm for (a) $N = 8$, (b) $N = 16$, (c) $N = 32$.

where $\bar{\epsilon}_{N,\Delta t}$ = max error with N, Δt i.e

$$\epsilon^{\tau}_{N,\Delta t} = \max_{\substack{1\le i\le N-1\\ 1\le j\le S}} |\tau_{\text{exact}}(r_i, t_j) - \tau_{\text{num}}(r_i, t_j)|, \quad j = 1, 2, .., S \tag{6.68}$$

To establish the convergence order for the stress in time (q_u), we first evaluate the maximum error with N and Δt in Table 6.4 using equation (6.67) and then equation (6.68). With the final time being $T = 1$ and the number of time steps being $S = 512$, we fix the finest mesh $N = 128$ and examine the temporal error. It resulted in an order of convergence ≈ 1.5 in time, which is similar to the convergence order in time calculated

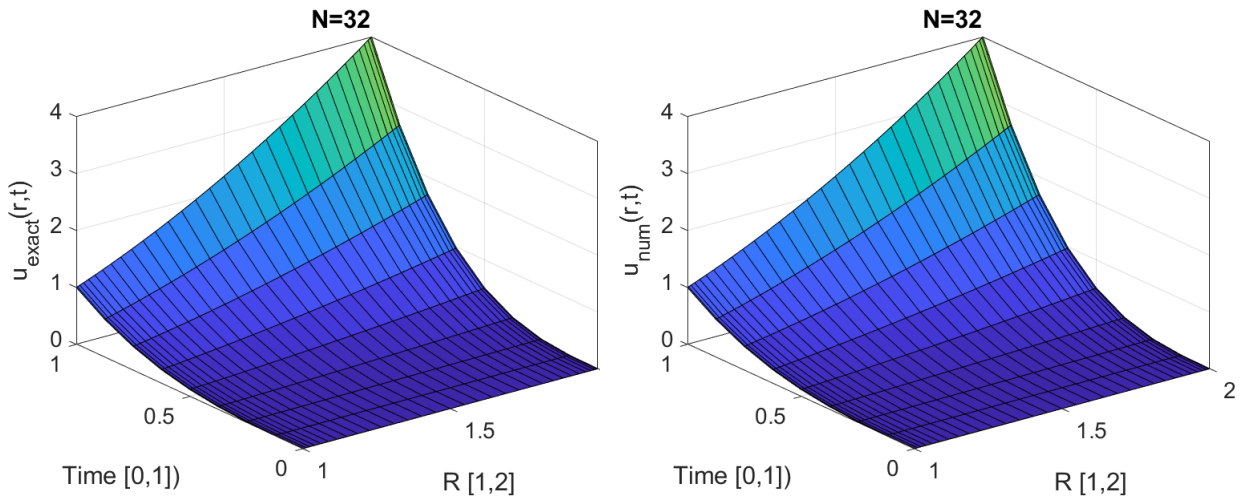

(a) (b)

Figure 6.9: (a) Exact and (b) numerical solutions of stress profiles for $N = 32$.

by the finite difference method in Ferras . (2018).

Δt	ϵ_N	q_u
$\frac{1}{8}$	0.0914	–
$\frac{1}{16}$	0.0344	1.4101
$\frac{1}{32}$	0.0127	1.4413
$\frac{1}{64}$	0.0046	1.4609
$\frac{1}{128}$	0.0017	1.4736
$\frac{1}{256}$	5.9285×10^{-4}	1.4819
$\frac{1}{512}$	2.1142×10^{-4}	1.4875

Table 6.4: Error norms and rates of convergence at $N = 128$

.

Example 3: Steady State Problem

Consider the steady velocity equation

$$\frac{\partial^2 u_\theta}{\partial r^2} + \frac{1}{r}\frac{\partial u_\theta}{\partial r} - \frac{u_\theta}{r^2} + f(r) = 0 \qquad R_{in} \leq r \leq R_{out} \tag{6.69}$$

with source term given by

$$f(r) = \left(\frac{\pi}{2\Delta}\right)^2 \sin\left(\left(\frac{r - R_{in}}{R_{out} - R_{in}}\right)\pi\right) - \left(\frac{\pi}{2\Delta}\right)\frac{1}{r}\cos\left(\left(\frac{r - R_{in}}{R_{out} - R_{in}}\right)\pi\right) + \frac{1}{r^2}\sin\left(\left(\frac{r - R_{in}}{R_{out} - R_{in}}\right)\pi\right) \tag{6.70}$$

and boundary conditions:

$$u_\theta(R_{in}) = 0, \quad u_\theta(R_{out}) = 0 \tag{6.71}$$

The exact solution to this problem is

$$u_\theta(r) = \sin\left(\left(\frac{r - R_{in}}{R_{out} - R_{in}}\right)\pi\right) = \sin\left(\left(\frac{r - R_{in}}{2\Delta}\right)\pi\right) \tag{6.72}$$

The dependence of the L^2 norm of the error on N is shown in Table 6.5. We then display those results using a log-log plot in Fig. 6.10. Additionally, Fig. 6.11 demonstrates the excellent agreement between the exact and approximate steady velocity at each grid point $R = [1, 2]$. Since the end time was $T = 1$ and the total number of time steps was $S = 512$, the maximum error decreased as the spatial error N increased. This caused the convergence order for the velocity to be $p_u \approx 24$ in space, which is calculated using equation (6.63), and the result is shown in Table 6.6.

N	L^2-norm
4	0.0016
6	9.1567×10^{-6}
8	4.2851×10^{-8}
12	4.1878×10^{-13}
16	2.4425×10^{-15}

Table 6.5: The L^2 norm of the error with respect to N.

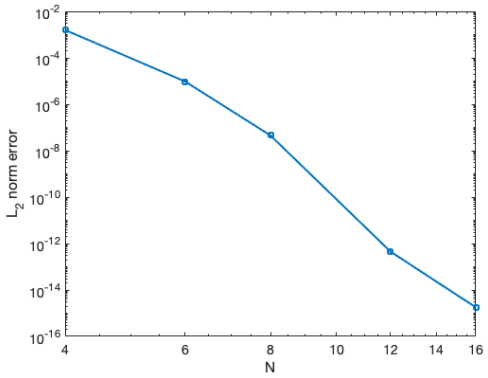

Figure 6.10: log-log plot of the L^2-norm of the error vs. N

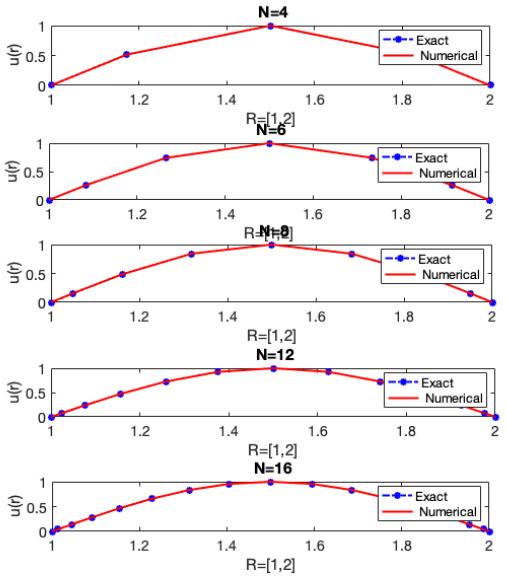

Figure 6.11: The exact and approximate solution of the steady-state problem for different values of N.

N	ϵ_N	p_u
4	0.0016	-
6	9.1567×10^{-6}	-
8	4.2851×10^{-8}	15.224
12	4.1878×10^{-13}	24.382
16	2.4425×10^{-15}	24.064

Table 6.6: Error norms and rates of convergence

.

6.6 Fully Coupled Problem

In order to perform additional experiments, we have developed a spectral code in Matlab to solve the following system of differential equations governing the unsteady unidirectional flow of the FMM in an annular geometry. In this section, we investigate the solution of the annular flow of the FMM model using the proposed numerical method:

$$\rho\left(1+\frac{\mathbb{V}}{\mathbb{G}}D_t^{2-\beta}\right)\frac{\partial u_\theta}{\partial t}=\mathbb{V}\left(\frac{\partial^2 u_\theta}{\partial r^2}+\frac{1}{r}\frac{\partial u_\theta}{\partial r}-\frac{u_\theta}{r^2}\right) \tag{6.73}$$

$$\tau_{r\theta}+\frac{\mathbb{V}}{\mathbb{G}}D_t^{1-\beta}\tau_{r\theta}=\mathbb{V}\left(\frac{\partial u_\theta}{\partial r}-\frac{u_\theta}{r}\right) \tag{6.74}$$

The boundary conditions are

$$u_\theta(R_{in},t)=\phi_i(t),\quad u_\theta(R_{out},t)=\phi_0(t). \tag{6.75}$$

and initial conditions are

$$u_\theta(r,0)=0,\quad \frac{\partial u_\theta}{\partial t}(r,0)=0,\quad \tau_{r\theta}(r,0)=0. \tag{6.76}$$

For each $n=1,2,\ldots,S$, we solve the following $(N-1)\times(N-1)$ discretised system of equations:

$$\begin{aligned}&\Big[\frac{\rho}{\mathbb{V}}\frac{w_k}{\Delta t}+\frac{\rho}{\mathbb{G}}\frac{a_0}{\Gamma(\beta)}\frac{w_k}{(\Delta t)^2}+\frac{\Delta w_k}{2r_k^2}\Big]U_k^n+\sum_{j=0}^{N}\Big[\frac{1}{2\Delta}B_{k,j}-\frac{w_k}{2r_k}D_{k,j}\Big]U_j^n\\&\quad=\left[\frac{\rho}{\mathbb{V}}\frac{w_k}{\Delta t}+\frac{\rho}{\mathbb{G}}\frac{a_0}{\Gamma(\beta)}\frac{w_k}{(\Delta t)^2}-\frac{\Delta w_k}{2r_k^2}\right]U_k^{n-1}-\sum_{j=0}^{n-1}\Big[\frac{1}{2\Delta}B_{k,j}-\frac{w_k}{2r_k}D_{k,j}\Big]U_j^{n-1}\\&\quad+\frac{\rho}{\mathbb{G}}\frac{w_k}{\Gamma(\beta)}\frac{1}{(\Delta t)^2}\sum_{j=0}^{n-1}(a_{n-j-1}-a_{n-j})(U_k^j-U_k^{j-1}),\ \ 1\le k\le N-1\end{aligned} \tag{6.77}$$

with boundary conditions:

$$U_0^n=\phi_i(t_n)=\Omega_i(t)R_{in}=c_i(n\Delta t)R_{in} \tag{6.78}$$

$$U_N^n=\phi_0(t_n)=\Omega_0(t)R_{out}=c_i(n\Delta t)R_{out} \tag{6.79}$$

where $t_n=n\Delta t$, and $c_i=c_0=1$.

Then we solve the stress using

$$\left[1+\frac{\mathbb{V}}{\mathbb{G}}\frac{1}{\Gamma(\beta)}\frac{b_0}{\Delta t}\right]\tau_k^n=\frac{\mathbb{V}}{\mathbb{G}}\sum_{j=0}^{n-1}(b_{n-j-1}-b_{n-j})\tau_k^j+\frac{\mathbb{V}}{\Delta}\sum_{j=0}^{N}D_{k,j}U_j^n-\frac{\mathbb{V}}{r_k^2}U_k^n,\ \ 0\le k\le N-1 \tag{6.80}$$

6.6.1 Newtonian fluid

We compare the numerical results for Newtonian annular Couette flow presented by Ferras . (2018) in Fig. 7 with those obtained using the proposed method (SM) in Fig. 6.12, for $\beta \to 0$, $\frac{\mathbb{V}}{\mathbb{G}} \to 0$. We have chosen the discretisation parameters $\Delta t/t_c = 3.50 \times 10^{-3}$ (with $t_c = \frac{h^2}{\nu}$) and $\Delta r/h = 5 \times 10^{-3}$ with the following fluid parameters $\beta = 1 \times 10^{-3}$, $\mathbb{V} = 5$, $\lambda \equiv \frac{\mathbb{V}}{\mathbb{G}} = 1 \times 10^{-5} [s^{1-\beta} \approx s]$, $\mathbb{G} = \frac{\mathbb{V}}{\lambda}$, $\nu = \frac{\mu}{\rho} = \frac{\mathbb{V}}{\rho} = 2 \times 10^{-3}$ m^2 s^{-1} (ν is the kinematic, η is the dynamic viscosity), and the elasticity number was $El = 0$. The gap is $h = R_{out} - R_{in}$, where $R_{out} = 0.5$ m, and $R_{in} = 0.3$ m, and the finest mesh $N = 128$.

The evolution of the velocity and stress profiles at different radial locations are shown in Fig. 6.12. Here $\frac{t}{t_c} = 3.50 \times 10^{-1}$ and the normalized radius given by $\bar{r} = \frac{r - R_{in}}{(R_{out} - R_{in})}$. We plot the velocity at the wall and at $\bar{r} = [0.25,\ 0.5,\ 0.75]$, while the stress is plotted at $\bar{r} = [0.005,\ 0.25,\ 0.5,\ 0.75,\ 0.995]$. The numerical method proved successful in precisely capturing the evolution of the various variables in this transient flow.

Due to the outer cylinder rotating at a faster linear speed than the inner cylinder, we predictably obtain higher velocities for the fluid there. The same holds true for stresses. Because of the variation in sign of the velocity gradient $\frac{\partial u_\theta}{\partial r}$ seen in Fig. 6.12 (c), note that the shear stress is negative near the inner cylinder and positive near the outer cylinder as shown in Fig. 6.12 (d) when the stress profiles plotted at $\frac{t}{t_c} = 3.50 \times 10^{-1}$.

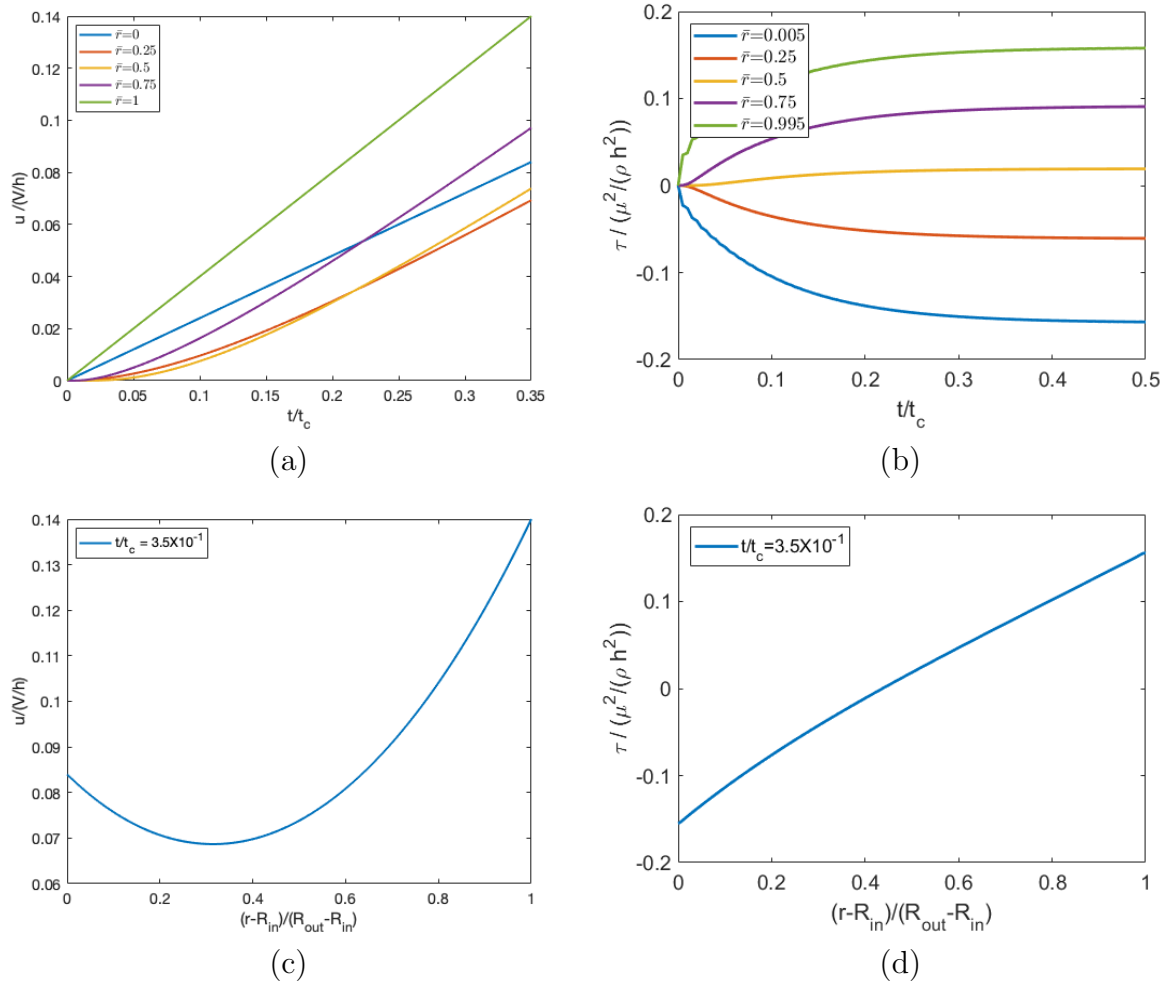

Figure 6.12: (a), (b) Variation of velocity and shear stress with time, at different radial locations; (c), (d) velocity and shear stress profiles for $t/t_c = 3.50 \times 10^{-1}$.

6.6.2 Viscoelastic fluid

As in the Newtonian fluid simulations, the same set of parameters and mesh resolution was utilized to model the Fractional Viscoelastic Fluid (FVF). However, for the viscoelastic case, the elasticity number is set to $El = \frac{\lambda}{t_v} = 6.25 \times 10^{-2}$, where $t_v = \frac{h^2}{v}$ and the fractional order is chosen as $\beta = 1 \times 10^{-6}$.

Figure 6.13 presents the time evolution of shear stress and angular velocity at selected radial locations within the cylinder gap. These results are similar to those generated by (Ferras ., 2018) (see Fig. 8 in that paper). A comparison between Figs. 6.12 (a) and 6.13 (a) highlights the influence of the viscoelastic relaxation time. In contrast to the Newtonian fluid, the viscoelastic model exhibits a noticeable delay in momentum

transmission from the boundaries to the fluid interior.

At the midpoint $\bar{r} = 0.5$, which is the furthest location from both rotating cylinders, the fluid exhibits the slowest dynamic response. Moreover, the temporal variation in shear stress appears more gradual compared to the Newtonian case, especially during the initial motion of the outer cylinder. In the Newtonian example, this behaviour is attributed to the quick, purely diffusive transmission of momentum from the boundary into the fluid domain.

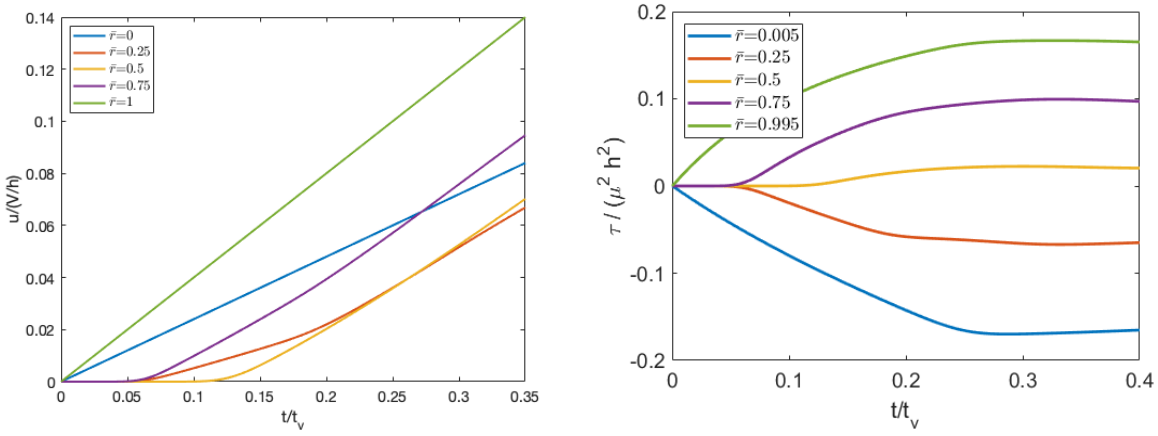

(a) (b)

Figure 6.13: (a) Evolution of velocity at radial locations $\bar{r} = 0.25,\ 0.5,\ 0.75$; (b) shear stress at radial locations $\bar{r} = 0.005,\ 0.25,\ 0.5,\ 0.57,\ 0.995$.

6.7 Influence of fractional order

We explore how using different fractional orders affects the velocity and shear stress in this section, as well as a brief explanation of the stress relaxation achieved for the FMM model.

6.7.1 Stress relaxation

To investigate how the order of the fractional derivative influences the evolution of the stress field, we simulated a classic stress relaxation test within an annular flow configuration. A step strain is applied by initiating a rapid rotation of the outer cylinder, which is

then stop after approximately 50 milliseconds. Following this, we analyze the subsequent relaxation behaviour of the fluid's tangential stress.

The setup involves a viscoelastic fluid confined in the annular space between two coaxial cylinders, where the inner and outer radii are $R_{in} = 22.65$ mm and $R_{out} = 25$ mm, respectively, resulting in a narrow gap of 2.35 mm (Keshavarz ., 2017). It is important to highlight that when this gap is small relative to the inner radius—i.e., $(R_{out} - R_{in}) \ll R_{in}$, as shown in Fig. 6.14—the flow closely resembles idealized Couette flow. This geometric condition should be kept in mind when interpreting the velocity and stress development within the system. In this case, the ratio $\frac{h}{R_{in}} = \frac{R_{out}-R_{in}}{R_{in}} \approx 0.1$ confirms the small-gap approximation. The viscoelastic parameters used for the simulation correspond to a $0.25wt\%$ Xanthan gum solution, with values taken from (Ferras ., 2018): $\beta = 0.31$, $\lambda_c = 55.6\,\mathrm{s}$, $\mathbb{V} = 24.96$ Pa.s, and $\mathbb{G} = 1.56$ Pa.s.

Immediately after $t = 0$, the outer cylinder starts rotating with a tangential velocity described by $u_\theta(R_{out}, t) = \dot{\theta}(t)R_{out}$, where the angular velocity function is defined as:

$$\dot{\theta}(t) = \frac{\Delta\theta}{\psi\sqrt{\pi}} \exp^{-\frac{(t-t_d)^2}{\psi^2}} \tag{6.81}$$

Here, t_d is taken as zero. As $\psi \to 0$, the velocity profile $u_\theta(R_{out}, t)$ approaches a Dirac delta function scaled by the rotation angle $\Delta\theta\sigma(t)$ (Dirac, 1981). Since the initial rate of change in tangential velocity, $\frac{du_\theta}{dt}(R_{out}, 0) = 0$, and the derivative tends toward zero as $t \to \infty$, introducing a delay time t_d becomes essential.

In the numerical simulations, the following parameters were used: $\Delta t/\lambda_c = 1.79856 \times 10^{-5}$, $\Delta r/h = 1 \times 10^{-2}$, and three different strain levels corresponding to $\gamma_0 = \frac{\Delta\theta R_{out}}{h}$, specifically 1%, 5% and 100%

The outer cylinder rotates clockwise from point A to point B and comes to a stop after 50 milliseconds ($t/\lambda_c \sim 0.0009$) as shown in Fig. 6.15(a). It's important to note that the final position B varies depending on the magnitude of the applied strain. Figure 6.15 (b) illustrates the normalized tangential velocity of the outer cylinder—evaluated at its peak value $u_{\theta max} = u_\theta(R_{out}, t_d)$—for the case with $\gamma_0 = 100\%$. The results are presented for three different levels of refinement: $\psi/\lambda_c = 1.0 \times 10^{-4}, 1.8 \times 10^{-4}, 2.7 \times$

10^{-4}, corresponding to normalized delay times $t_d/\lambda_c = 4.5 \times 10^{-4}, 7.4 \times 10^{-4}, 1.1 \times 10^{-3}$, respectively. In addition, the evolution of shear stress is monitored at the radial location $\bar{r} = (r - R_{in})/(R_{out} - R_{in}) = 0.25$ throughout the rapid straining event.

In the case of a step-strain experiment with an applied deformation of $\gamma_0 = 100\%$, a fractional parameter $\beta = 0.31$, and three different temporal resolutions—namely $\psi/\lambda_c = 1.0 \times 10^{-4}$, 1.8×10^{-4}, 2.7×10^{-4} — corresponding to normalized delay times of $t_d/\lambda_c = 4.5 \times 10^{-4}$, 7.4×10^{-4}, 1.1×10^{-3}, the normalized shear stress relaxation results are presented in Fig. 6.16 (a). It is important to highlight that as $\psi \to 0$, the outer cylinder must accelerate more sharply to achieve the same angular displacement within a shorter time span, which increases the computational complexity due to the need for high-resolution gradients. Figure 6.16 (b) displays the temporal evolution of the applied strain $\gamma_0 = \frac{\Delta\theta R_{out}}{h}$ for the three different tangential velocity profiles imposed at the outer cylinder. As expected, progressively faster rotation leads to a closer approximation of an ideal step-strain input. In Fig. 6.16 (c), the normalized stress relaxation curves are shown for three different strain magnitudes: 1%, 5% and 100%, using the parameters $\psi/\lambda_c = 1.0 \times 10^{-4}$ and $t_d/\lambda_c = 4.5 \times 10^{-4}$. A magnified view of the stress relaxation behaviour for the smaller deformations is provided in Fig. 6.16 (d).

The versatility of the fractional model becomes particularly evident when various fractional exponents are introduced, as demonstrated in Fig. 6.17 for a strain level of $\gamma_0 = 100\%$, with parameters $\psi/\lambda_c = 7.4 \times 10^{-5}$, $t_d/\lambda_c = 6.2 \times 10^{-4}$, and fractional orders $\beta = 0.1, 0.25$ and 0.5. To manage the long simulation durations associated with these cases, the numerical algorithm was enhanced to incorporate time-graded meshes. According to earlier computational findings, an effective non-uniform temporal grid can be defined as follows (Ferras ., 2018):

$$t_s = \begin{cases} 2t_d - 2t_d(1 - \frac{s}{N_1})^{r_1}, & s < N_1 \\ 2t_d + (T - 2t_d)(\frac{s-N_1}{N_2})^{r_2}, & s \geq N_1 \end{cases} \tag{6.82}$$

Here, the parameters used are $r_1 = 1$, $r_2 = 1.693$, $N_1 = 50$, $N_2 = 1000$, and the total simulation time is $T = 3$. This approach yielded a 55- fold increase in computational

efficiency, allowing simulations with $\frac{\Delta t_{exp}}{\lambda_c} \approx 2.2$ to be completed within practical time limits.

Figure 6.17 presents the normalized stress relaxation profiles on a logarithmic scale. It is widely recognized that, for the Fractional Maxwell Model, the stress relaxation exhibits a power-law decay given by $G(t) \approx \frac{\mathbb{V}t^{\beta}}{\Gamma(1-\beta)}$ in the early-time regime ($t \ll \lambda_c$) (Podlubny, 1999).

From the figure, we observe that for lower values of β, the spring-pot element behaves more like a pure spring, approximating the classical Maxwell model. This transition is achieved as $\alpha \to 1$ and $\beta \to 0$, leading to a reduced stress peak but slower relaxation, as described by the governing relation $\tau(t) + \frac{\mathbb{V}}{\mathbb{G}}\frac{d\tau(t)}{dt} = \mathbb{V}\dot{\gamma}(t)$. Conversely, as $\beta \to 1$, the spring-pot behaves increasingly like a dashpot. In this limit, with $\alpha \to 1$ and $\beta \to 1$, the fractional viscoelastic fluid model tends toward Newtonian behaviour, increasing the rate of relaxation and following the relation $\tau(t) = \frac{\mathbb{V}\mathbb{G}}{\mathbb{V}+\mathbb{G}}\dot{\gamma}(t)$.

Figure 6.17 exhibits a slight irregularity in the otherwise smooth stress relaxation curve specifically, a noticeable "blip" around $t \approx 10^{-3}$ which deviates from the expected monotonic behaviour. This anomaly arises due to the use of a non-uniform time-stepping scheme, as defined in Eq. (6.82). While the time grid is constructed to be continuous at $s = N_1$, a closer inspection reveals a discontinuity in the derivative of t_s with respect to s. In other words, although both expressions for t_s match at the transition point, their slopes do not, resulting in a jump in the time-step gradient. This discontinuity in the time discretization can lead to small perturbations in the numerical solution, such as the observed artifact in the stress profile.

(a) (b)

Figure 6.14: Influence of the gap on the type of flow (a) $\frac{h}{R_{in}} \sim O(1)$; (b) $\frac{h}{R_{in}} \ll 1$ (Ferras ., 2018).

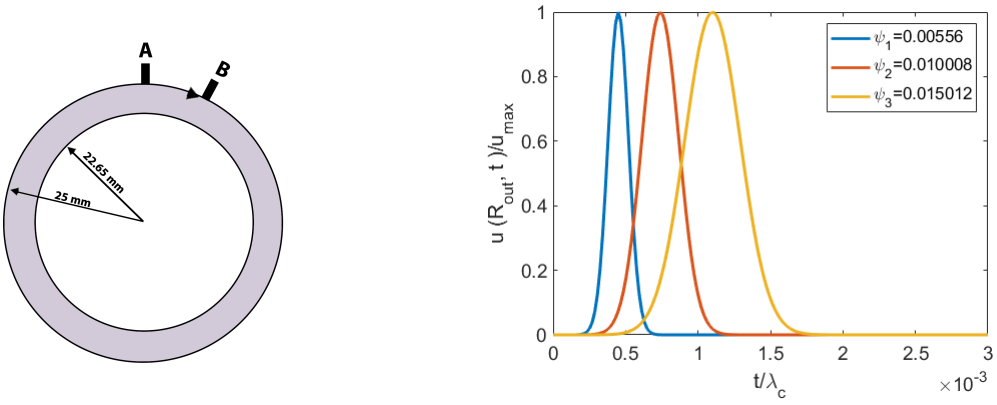

(a) (b)

Figure 6.15: Stress relaxation test in a narrow gap cylindrical Couette cell following a sudden straining deformation (a) annular geometry and dimensions; (b) normalised tangential velocity $[u_{max} = u(R_{out}, t_d)]$ of the outer cylinder (Ferras ., 2018).

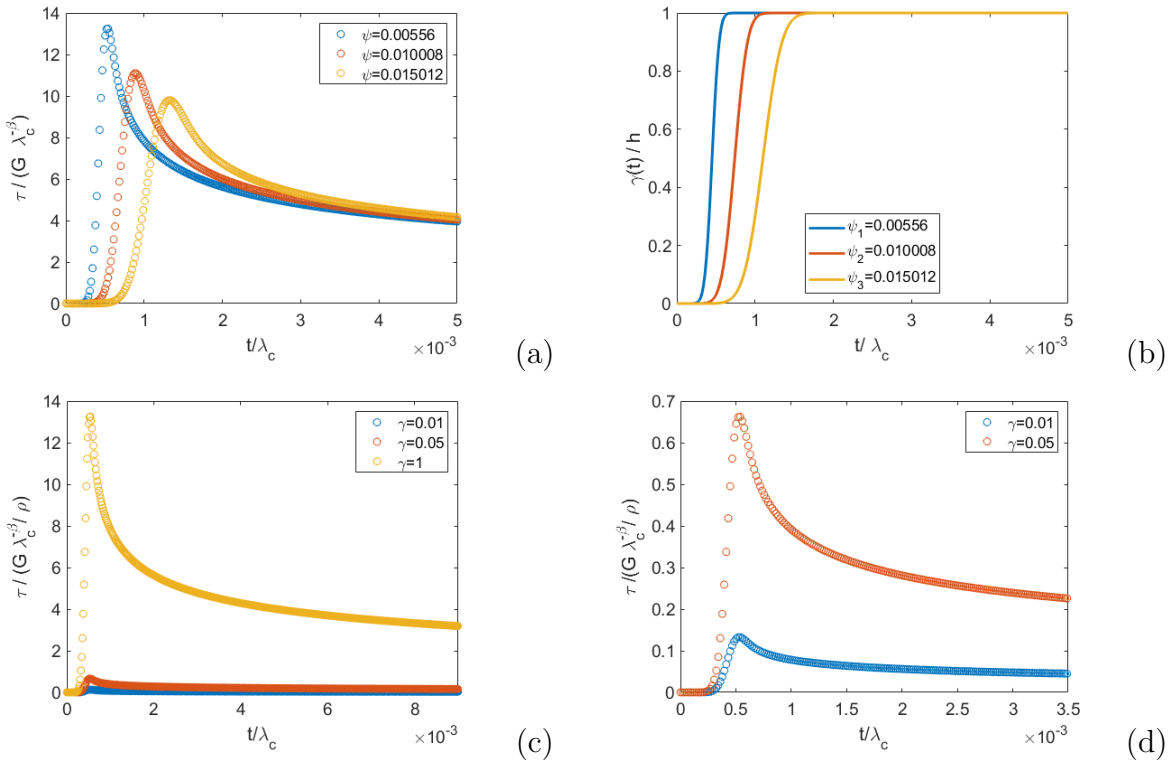

Figure 6.16: (a) Normalised shear stress relaxation obtained for a step-strain test with deformation of $\gamma_0 = 100\%$, $\beta = 0.31$ and three different levels of refinement; (b) evolution of the deformation in time for the three different tangential velocities imposed; (c) stress relaxation for three different deformations; (d) zoomed view of the stress relation obtained for the two smaller deformations (Ferras ., 2018).

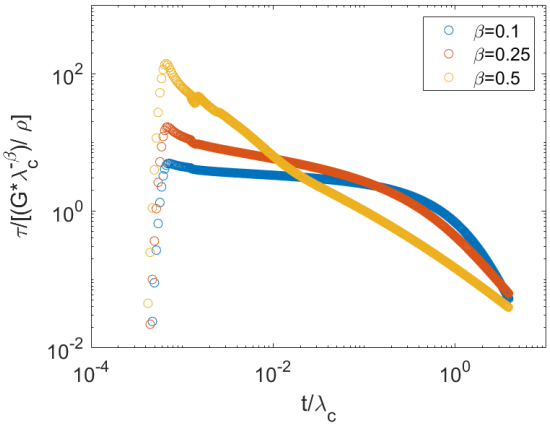

Figure 6.17: Normalised shear stress relaxation obtained for the step-strain test ($\dot{\gamma} = 100\%$) (Ferras ., 2018).

6.8 Conclusions

The coupled system of equations describing the pure tangential annular flow of fractional viscoelastic fluids was solved numerically and analysed. In this chapter, we employed the spectral method instead of the finite difference method that was used in (Ferras ., 2018). We observed that the Spectral Method (SM) demonstrates significantly higher accuracy and computational efficiency compared to the Finite Difference (FD) approach used by (Ferras ., 2018), particularly in the context of unsteady and fractional viscoelastic flows. One of the most compelling advantages of the Spectral Method lies in its exponential convergence for smooth problems, as opposed to the algebraic (typically first- or second-order) convergence achieved by FD methods. This is evidenced in the study's steady-state velocity example, where the spatial convergence rate reaches approximately 24 (as shown in Table 6.6), far exceeding the capabilities of finite difference techniques. Furthermore, for unsteady problems, the spectral approach achieves a temporal convergence order of about 1.5 for both velocity and stress (see Tables 6.2 and 6.4), while the Finite Difference method demonstrates a lower order of approximately 1 in time. This higher accuracy is achieved using significantly fewer spatial grid points, resulting in reduced computational cost. The efficiency of the Spectral Method is further validated by its ability to reach machine-precision error levels for relatively small values of N, a feat not attainable with Finite Difference methods without substantially increasing grid resolution. In addition to its superior convergence characteristics, the spectral method proves robust in handling complex systems involving fractional derivatives and coupled stress-velocity equations, making it particularly suitable for viscoelastic fluid modelling. Numerical experiments show excellent agreement with analytical solutions, and the method successfully replicates benchmark results obtained via finite differences for Newtonian flow. Moreover, the Spectral Method effectively captures fast transients and stress relaxation phenomena with high temporal and spatial resolution, which collectively underscore its advantages over finite difference schemes and reinforce its suitability as a more accurate and efficient alternative for simulating fractional viscoelastic flows. This is further demonstrated

through the implementation of the three-parameter Fractional Viscoelastic Fluid (FVF) model, which closely fits experimental data and captures bounded stress growth following the onset of steady shear. The model's complexity highlights the suitability of Spectral Method for advanced rheological applications, and the use of graded temporal meshes enabled efficient resolution of long-time behaviour without excessive computational cost.

Chapter 7

Taylor-Couette Flow: Enhanced Models and Numerical Schemes

7.1 Introduction

In this chapter we developed enhanced models and numerical schemes to introduce additional flexibility in modelling and increased accuracy in numerical predictions. In particular, we study fractional Maxwell models in the Taylor-Couette geometry for following cases: $\beta = 1$, as studied in Chapter 6, corresponding to α in the same chapter; and $0 < \beta < 1$, which will be explored in this chapter. The aim is to analyse and understand the effects of fractional viscoelasticity on the flow behaviour and stress relaxation properties. The fractional Maxwell model introduces memory effects through the fractional derivatives, allowing for a more accurate description of complex fluids that exhibit both elastic and viscous behaviour over a wide range of timescales.

Furthermore, after validating our numerical scheme for the three-parameter Fractional Viscoelastic Fluid (FVF) model in Chapter 6 for the Taylor-Couette problem, we now focus on the four-parameter Fractional Maxwell Model (FMM) in the context of the Taylor-Couette problem introduced in Section 4.3.1, and develop a numerical scheme to solve it. To enhance numerical accuracy, we employ first-order and second-order finite difference approximations for the time-fractional derivative, as derived in Chapter 5. Additionally, to characterize the behaviour of more complex viscoelastic fluids, we solve the Taylor-Couette problem using the six-parameter Multi-Mode Fractional Maxwell Model (MM-FMM), as introduced in Section 4.4, and solve it numerically by extending the existing numerical scheme for the FMM.

This chapter is structured as follows: Section 7.3 outlines the derivation of the Taylor-Couette problem for the Single-Mode Fractional Maxwell Model. We begin by deriving the weak formulation of the system and discretizing it in time using a first-order difference scheme for the time-fractional derivative, alongside spectral approximations for the spatial discretization. These methods are applied to the governing equation for velocity and shear stress to form the linear system for the unknowns at each time step. Numerical results are provided to validate the proposed method. To enhance the accuracy of the numerical scheme, we switch to a second-order difference scheme for the time-fractional derivative, while maintaining the spectral approximation for spatial discretization. Additional numerical results are presented to further validate the improved method.

Section 7.3 presents the derivation of the Taylor-Couette problem for the Multi-Mode Fractional Maxwell Model. We first derive the weak formulation of the system and discretize it in time using a first-order difference scheme for the time-fractional derivative, while applying spectral approximations for spatial discretization. To validate the proposed method, we provide numerical results. To characterize more complex viscoelastic fluids, we improve the accuracy of the numerical scheme by adopting a second-order difference scheme for the time-fractional derivative, while keeping the spectral approximation for spatial discretization. Further numerical results are presented to validate the enhanced method. The conclusions of this chapter are given in Section 7.4.

7.2 Single-Mode Fractional Maxwell Model

7.2.1 Taylor-Couette Flow

To generate simulations with the FMM, we must make slight modifications to the numerical method presented in Chapter 6 for the FVF model. Following the derivation in Appendix B (Ferras ., 2018), we consider the momentum equation.

$$\rho\left(\frac{\partial u_\theta}{\partial t}\right) = \left(\frac{2}{r} + \frac{\partial}{\partial r}\right)\tau_{r\theta}(t) \tag{7.1}$$

and the fractional Maxwell model (FMM) is given by

$$\left(1+\frac{\mathbb{V}}{\mathbb{G}}\frac{d^{\alpha}}{dt^{\alpha}}\right)\tau_{r\theta}(t)=\mathbb{V}\frac{d^{\beta}}{dt^{\beta}}\gamma(t),\quad 0<\alpha\leq\beta\leq 1 \tag{7.2}$$

Using the Caputo definition, the derivatives $\frac{d^{\alpha}\tau}{dt^{\alpha}}$ and $\frac{d^{\beta}\gamma}{dt^{\beta}}$ can be expressed in their corresponding integral forms as follows:

$$\frac{\partial^{\alpha}\tau_{r\theta}}{\partial t^{\alpha}}=\frac{1}{\Gamma(1-\alpha)}\int_{0}^{t}\frac{1}{(t-s)^{\alpha}}\frac{\partial\tau}{\partial s}ds \tag{7.3}$$

and

$$\frac{\partial^{\beta}\gamma}{\partial t^{\beta}}=\frac{1}{\Gamma(1-\beta)}\int_{0}^{t}\frac{1}{(t-s)^{\beta}}\frac{\partial\gamma}{\partial s}ds \tag{7.4}$$

For this flow, when $\beta=1$, the time derivative of γ is given by

$$\frac{\partial\gamma}{\partial t}=\frac{\partial u_{\theta}}{\partial r}-\frac{u_{\theta}}{r}$$

However, when $\beta\neq 1$, the entire history of deformations is taken into account by calculating the following integral

$$\frac{\partial^{\beta}\gamma}{\partial t^{\beta}}=\frac{1}{\Gamma(1-\beta)}\int_{0}^{t}\frac{1}{(t-s)^{\beta}}\left\{\frac{\partial u_{\theta}(r,s)}{\partial r}-\frac{u_{\theta}(r,s)}{r}\right\}ds \tag{7.5}$$

Applying the operator $\left(\frac{2}{r}+\frac{\partial}{\partial r}\right)$ to both sides of Eq. (7.2), gives

$$\left(\frac{2}{r}+\frac{\partial}{\partial r}\right)\left(1+\frac{\mathbb{V}}{\mathbb{G}}\frac{d^{\alpha}}{dt^{\alpha}}\right)\tau_{r\theta}(t)=\mathbb{V}\left(\frac{2}{r}+\frac{\partial}{\partial r}\right)\frac{d^{\beta}}{dt^{\beta}}\gamma(t) \tag{7.6}$$

Then applying the operator $\left(1+\frac{\mathbb{V}}{\mathbb{G}}\frac{d^\alpha}{dt^\alpha}\right)$ to both sides of Eq. (7.1) yields

$$\begin{aligned}\rho\left(1+\frac{\mathbb{V}}{\mathbb{G}}\frac{d^\alpha}{dt^\alpha}\right)\frac{\partial u}{\partial t} &= \left(\frac{2}{r}+\frac{\partial}{\partial r}\right)\left(1+\frac{\mathbb{V}}{\mathbb{G}}\frac{d^\alpha}{dt^\alpha}\right)\tau_{r\theta}(t)\\ &= \mathbb{V}\left(\frac{2}{r}+\frac{\partial}{\partial r}\right)\frac{d^\beta}{dt^\beta}\gamma(t)\\ &= \mathbb{V}\left(\frac{2}{r}+\frac{\partial}{\partial r}\right)\frac{1}{\Gamma(1-\beta)}\int_0^t\frac{1}{(t-s)^\beta}\left\{\frac{\partial u}{\partial r}-\frac{u}{r}\right\}ds\\ &= \frac{\mathbb{V}}{\Gamma(1-\beta)}\int_0^t\frac{1}{(t-s)^\beta}\left\{\frac{\partial^2 u}{\partial r^2}+\frac{1}{r}\frac{\partial u}{\partial r}-\frac{u}{r^2}\right\}ds\end{aligned} \tag{7.7}$$

Thus, we obtain the following system of equations for u_θ and $\tau_{r,\theta}$ in integral form

$$\rho\left(1+\frac{\mathbb{V}}{\mathbb{G}}\frac{d^\alpha}{dt^\alpha}\right)\frac{\partial u_\theta}{\partial t} = \frac{\mathbb{V}}{\Gamma(1-\beta)}\int_0^t(t-s)^{-\beta}\left(\frac{\partial^2 u_\theta}{\partial r^2}+\frac{1}{r}\frac{\partial u_\theta}{\partial r}-\frac{u_\theta}{r^2}\right)ds \tag{7.8}$$

$$\rho\left(1+\frac{\mathbb{V}}{\mathbb{G}}\frac{d^\alpha}{dt^\alpha}\right)\tau_{r\theta}(t) = \frac{\mathbb{V}}{\Gamma(1-\beta)}\int_0^t(t-s)^{-\beta}\left(\frac{\partial u_\theta}{\partial r}-\frac{u_\theta}{r}\right)ds \tag{7.9}$$

Replacing the ordinary differential operators by fractional differential operators gives

$$\frac{\rho}{\mathbb{V}}\frac{\partial u}{\partial t}+\frac{\rho}{\mathbb{G}}{D_t}^\alpha\left(\frac{\partial u}{\partial t}\right) = \frac{1}{\Gamma(1-\beta)}\int_0^t(t-s)^{-\beta}\left(\frac{\partial^2 u_\theta}{\partial r^2}+\frac{1}{r}\frac{\partial u_\theta}{\partial r}-\frac{u_\theta}{r^2}\right)ds \tag{7.10}$$

$$\tau_{r\theta}+\frac{\mathbb{V}}{\mathbb{G}}D_t^\alpha\tau_{r\theta} = \frac{\mathbb{V}}{\Gamma(1-\beta)}\int_0^t(t-s)^{-\beta}\left(\frac{\partial u_\theta}{\partial r}-\frac{u_\theta}{r}\right)ds \tag{7.11}$$

These equations are solved subjected to the Dirichlet boundary conditions

$$u_\theta(R_{in},t)=\Theta_i(t),\quad u_\theta(R_{out},t)=\Theta_0(t),\quad 0<t<T \tag{7.12}$$

and initial conditions

$$u_\theta(r,0)=\frac{\partial u_\theta(r,0)}{\partial t}=0,\quad \tau_{r,\theta}(r,0)=0,\quad R_{in}<r<R_{out} \tag{7.13}$$

We turn our attention to the numerical discretization of these equations (7.10) and (7.11).

Weak Formulation of The Coupled Problem

To fully discretize the Taylor-Couette problem described by Eqs. (7.10) and (7.11), we first derive their weak formulation. This is done by multiplying both equations by a test function $v \in V$ and integrating over the domain $[R_{in}, R_{out}]$. As a result, the weak formulation is obtained as follows:

$$\frac{\rho}{\mathbb{V}} \int_{R_{in}}^{R_{out}} \left(\frac{\partial u_\theta}{\partial t} \right) v \, dr + \frac{\rho}{\mathbb{V}\,\mathbb{G}} \int_{R_{in}}^{R_{out}} \left({D_t}^{\alpha} \left(\frac{\partial u}{\partial t} \right) \right) v \, dr$$
$$= \frac{1}{\Gamma(1-\beta)} \int_{R_{in}}^{R_{out}} \left\{ \int_0^t (t_n - s)^{-\beta} \left(\frac{\partial^2 u_\theta}{\partial r^2} + \frac{1}{r} \frac{\partial u_\theta}{\partial r} - \frac{u_\theta}{r^2} \right) ds \right\} v \, dr \quad (7.14)$$

$$\int_{R_{in}}^{R_{out}} \tau(t) \; \nu \; dr + \lambda^{\alpha} \int_{R_{in}}^{R_{out}} (D_t^{\alpha} \tau(t)) \, \nu \; dr = E\lambda^{\beta} \int_{R_{in}}^{R_{out}} \left(D_t^{\beta} \gamma(t) \right) \; \nu \; dr \quad (7.15)$$

where $u = u_\theta$ and $\tau = \tau_{r,\theta}$.

Then we transform the physical domain $[R_{in}, R_{out}]$ onto the computational domain $[-1, 1]$ before discretizing the weak formulation using the change of variable

$$\tilde{r} = \frac{2r - (R_{in} + R_{out})}{(R_{in} - R_{out})}, \quad \tilde{r} \in [-1, 1] \quad (7.16)$$

so that

$$\int_{R_{in}}^{R_{out}} w(r) dr = \Delta \int_{-1}^{1} w(\tilde{r}) d\tilde{r} \quad (7.17)$$

where w is some function and Δ is defined by

$$\Delta = \frac{(R_{in} - R_{out})}{2} \quad (7.18)$$

7.2.2 A first-order difference scheme for a time fractional derivative

Numerical Discretization of the Velocity Equation

In Time

We will use the first-order difference scheme for the time-fractional derivative from Section 5.3.1, replacing α with $\alpha+1$, to discretize $\mathcal{D}_t^{1+\alpha}u$, which is defined in the Caputo sense as

$$\mathcal{D}_t^{1+\alpha}\, u = \frac{1}{\Gamma(1-\alpha)} \int_0^t (t-s)^{-\alpha}\, \frac{\partial^2 u}{\partial s^2}\, ds, \quad 1 < 1+\alpha < 2 \tag{7.19}$$

Then the discretization of Eq. (7.10) becomes

$$\frac{\rho}{\mathbb{V}}\, Y_i^{n-1/2} + \frac{\rho}{\mathbb{G}}\, X_i^{n-1/2} = \frac{1}{\Gamma(1-\beta)} \int_0^{t_{n-1/2}} (t_{n-1/2}-s)^{-\beta} \left(\frac{\partial^2}{\partial r^2} + \frac{1}{r}\frac{\partial}{\partial r} - \frac{1}{r^2} \right) u\, ds \tag{7.20}$$

where

$$Y_i^{n-1/2} = \frac{U_i^n - U_i^{n-1}}{\Delta t} \tag{7.21}$$

and

$$\begin{aligned} X_i^{n-1/2} = D_t^{1+\alpha} u(t_n) \simeq \frac{1}{(\Delta t)^{\alpha+1}\Gamma(2-\alpha)} \Bigg[& \tilde{a}_0(\alpha) \left(U_i^n - U_i^{n-1} \right) - \sum_{j=1}^{n-1} \left(\tilde{a}_j - \tilde{a}_{j-1} \right) \left(U_i^{n-j} - U_i^{n-j-1} \right) \\ & - \tilde{a}_{n-1}(\alpha)\Phi(r_i) \Bigg] \\ = \frac{1}{(\Delta t)^{\alpha+1}\Gamma(2-\alpha)} & \left[\sum_{j=0}^{n} \tilde{A}_j\, U_i^j - \tilde{a}_{n-1}(\alpha)\Phi(r_i) \right] \end{aligned} \tag{7.22}$$

where $\Phi(r_i) = Y_i^0 = y(r_i, 0)$, and

$$\tilde{A}_j = \begin{cases} \tilde{a}_{n-2}(\alpha) - \tilde{a}_{n-1}(\alpha) & \text{if} \quad j = 0 \\ -\tilde{a}_{n-j-1}(\alpha) + 2\tilde{a}_{n-j}(\alpha) - \tilde{a}_{n-j+1}(\alpha), & \text{if} \quad 1 \leq j \leq n-2 \\ -2\tilde{a}_0(\alpha) + \tilde{a}_1(\alpha), & \text{if} \quad j = n-1 \\ \tilde{a}_0(\alpha), & \text{if} \quad j = n \end{cases} \tag{7.23}$$

where the coefficients $\tilde{a}_{n-j}$ are given by

$$\tilde{a}_{n-j} = \left[(n-j+1)^{1-\alpha} - (n-j)^{1-\alpha}\right] \tag{7.24}$$

In space

We will derive the numerical approximation of right-hand side of Eq. (7.20) using the first-order discretization of the integral in time derived using linear interpolation on each sub-interval $[t_{j-1}, t_j]$.

Let

$$\Phi(r,t) = \left(\frac{\partial^2}{\partial r^2} + \frac{1}{r}\frac{\partial}{\partial r} - \frac{1}{r^2}\right) u_\theta(r,t) \tag{7.25}$$

and

$$\Pi_{1,j}\Phi(r,s) = \Phi(r,t_{j-1})\frac{(t_j - s)}{\Delta t} + \Phi(r,t_j)\frac{(s - t_{j-1})}{\Delta t}, \quad s \in [t_{j-1}, t_j] \tag{7.26}$$

Therefore, the right-hand side of Eq. (7.20) is approximated by

$$R.H.S \simeq \frac{1}{\Gamma(1-\beta)}\left\{\sum_{j=1}^{n-1}\int_{t_{j-1}}^{t_j}(t_{n-1/2} - s)^{-\beta}\Pi_{1,j}\Phi(r,s)ds + \int_{t_{n-1}}^{t_{n-1/2}}(t_{n-1/2} - s)^{-\beta}\Pi_{1,n}\Phi(r,s)ds\right\} \tag{7.27}$$

To evaluate Eq.(7.27) we need to calculate integrals of the form

$$\begin{aligned} I_1 &= \int_{t_{j-1}}^{t_j}(t_{n-1/2} - s)^{-\beta}(t_j - s)ds \\ &= \frac{(\Delta t)^{2-\beta}}{(1-\beta)(2-\beta)}\left[(2-\beta)(n-j+1/2)^{1-\beta} + (n-j-1/2)^{2-\beta} - (n-j+1/2)^{2-\beta}\right] \end{aligned} \tag{7.28}$$

where

$$f_{n-j} = \left[(2-\beta)(n-j+1/2)^{1-\beta} + (n-j-1/2)^{2-\beta} - (n-j+1/2)^{2-\beta}\right] \tag{7.29}$$

and

$$\begin{aligned} I_2 &= \int_{t_{j-1}}^{t_j} (t_{n-1/2}-s)^{-\beta}(s-t_{j-1})ds \\ &= \frac{(\Delta t)^{2-\beta}}{(1-\beta)(2-\beta)}\left[-(2-\beta)(n-j-1/2)^{1-\beta} - (n-j-1/2)^{2-\beta} + (n-j+1/2)^{2-\beta}\right] \end{aligned} \tag{7.30}$$

where

$$g_{n-j} = \left[-(2-\beta)(n-j-1/2)^{1-\beta} - (n-j-1/2)^{2-\beta} + (n-j+1/2)^{2-\beta}\right] \tag{7.31}$$

$$\begin{aligned} I_3 &= \int_{t_{n-1}}^{t_{n-1/2}} (t_{n-1/2}-s)^{-\beta}(t_n-s)ds \\ &= \left[-\frac{(t_n-s)(t_{n-1/2}-s)^{1-\beta}}{(1-\beta)} + \frac{(t_{n-1/2}-s)^{(2-\beta)}}{(1-\beta)(2-\beta)}\right]_{t_{n-1}}^{t_{n-1/2}} \\ &= \frac{(3/2-\beta)(1/2)^{1-\beta}(\Delta t)^{2-\beta}}{(1-\beta)(2-\beta)} \end{aligned} \tag{7.32}$$

$$\begin{aligned} I_4 &= \int_{t_{n-1}}^{t_{n-1/2}} (t_{n-1/2}-s)^{-\beta}(s-t_{n-1})ds \\ &= \left[-\frac{(s-t_{n-1})(t_{n-1/2}-s)^{1-\beta}}{(1-\beta)} - \frac{(t_{n-1/2}-s)^{(2-\beta)}}{(1-\beta)(2-\beta)}\right]_{t_{n-1}}^{t_{n-1/2}} \\ &= \frac{(1/2)^{2-\beta}\,(\Delta t)^{2-\beta}}{(1-\beta)(2-\beta)} \end{aligned} \tag{7.33}$$

then Eq.(7.27) becomes

$$
\begin{aligned}
R.S.H &= \frac{(\Delta t)^{2-\beta}}{\Gamma(3-\beta)}\left\{\sum_{j=1}^{n-1}\left[f_{n-j}\Phi(r,t_{j-1})+g_{n-j}\Phi(r,t_j)\right]+f_0\Phi(r,t_{n-1})+g_0\Phi(r,t_n)\right\} \\
&= \frac{(\Delta t)^{2-\beta}}{\Gamma(3-\beta)}\Bigg\{f_{n-1}\Phi(r,t_0)+g_{n-1}\Phi(r,t_1)+f_{n-2}\Phi(r,t_1)+g_{n-2}\Phi(r,t_2)+\ldots \\
&\qquad +f_1\Phi(r,t_{n-2})+g_1\Phi(r,t_{n-1})+f_0\Phi(r,t_{n-1})+g_0\Phi(r,t_n)\Bigg\} \\
&= \frac{(\Delta t)^{2-\beta}}{\Gamma(3-\beta)}\left\{f_{n-1}\Phi(r,t_0)+\sum_{j=1}^{n-1}(f_{n-j-1}+g_{n-j})\Phi(r,t_j)+g_0\Phi(r,t_n)\right\} \qquad (7.34)
\end{aligned}
$$

let $l=n-j$, then the coefficients defined as

$$f_l=(2-\beta)(l+1/2)^{1-\beta}+(l-1/2)^{2-\beta}-(l+1/2)^{2-\beta},\ \ l>0 \qquad (7.35)$$

$$g_l=-(2-\beta)(l-1/2)^{1-\beta}-(l-1/2)^{2-\beta}+(l+1/2)^{2-\beta},\ \ l>0 \qquad (7.36)$$

$$f_0=(3/2-\beta)(1/2)^{1-\beta} \qquad (7.37)$$

$$g_0=(1/2)^{2-\beta} \qquad (7.38)$$

Using the above results and the spectral approximation of the dependent variables, we obtain the following contribution to each of the terms in the weak formulation Eq.(7.10)

$$
\begin{aligned}
\frac{\rho}{\mathbb{V}}\int_{R_{in}}^{R_{out}}\left(\frac{\partial u}{\partial t}\right)\,v\,dr &= \Delta\frac{\rho}{\mathbb{V}}\int_{-1}^{1}\left(\frac{\partial u}{\partial t}\right)\,v\,d\tilde{r} \\
&\simeq \Delta\frac{\rho}{\mathbb{V}}\sum_{l=0}^{N}w_l\left(\frac{\partial u(\tilde{r}_l,t_n)}{\partial t}\right)h_k(\tilde{r}_l) \\
&\simeq \Delta\frac{\rho}{\mathbb{V}}w_k\left(\delta_t U_k^{n-1/2}\right) \\
&= \frac{\rho}{\mathbb{V}}\Delta w_k\left(\frac{U_k^n-U_k^{n-1}}{\Delta t}\right)
\end{aligned} \qquad (7.39)
$$

$$
\begin{aligned}
\frac{\rho}{\mathbb{G}}\int_{R_{in}}^{R_{out}}\left(D_t^{\epsilon}u(t)\right)\,nu\;dr &= \Delta\frac{\rho}{\mathbb{G}}\int_{-1}^{1}\left(D_t^{\epsilon}u\right)\,\nu\;d\tilde{r}\\
&\simeq \Delta\frac{\rho}{\mathbb{G}}\sum_{l=0}^{N}w_l\Big(D_t^{\epsilon}U_l\Big)h_k(\tilde{r}_l)\\
&\simeq \Delta\frac{\rho}{\mathbb{G}}w_k\Big(D_t^{\epsilon}\;U_k^{n-1/2}\Big)\\
&= \frac{\rho}{\mathbb{G}}\frac{\Delta w_k}{(\Delta t)^{\alpha}\Gamma(2-\alpha)}\Bigg[\tilde{a}_0\left(\frac{U_k^n-U_k^{n-1}}{\Delta t}\right)\\
&\qquad -\sum_{j=1}^{n-1}\left(\tilde{a}_{n-j-1}-\tilde{a}_{n-j}\right)\left(\frac{U_k^j-U_k^{j-1}}{\Delta t}\right)\Bigg]\\
&= \frac{\rho}{\mathbb{G}}\frac{\Delta w_k}{(\Delta t)^{\alpha+1}\Gamma(2-\alpha)}\Bigg[\tilde{a}_0\left(U_k^n-U_k^{n-1}\right)\\
&\qquad +\sum_{j=1}^{n-1}\left(\tilde{a}_j-\tilde{a}_{j-1}\right)\left(U_k^j-U_k^{j-1}\right)\Bigg]
\end{aligned}
\tag{7.40}
$$

To find the weak form of the right-hand side of Eq.(7.27) we multiply $\Phi(r_k,t_l)$ by by a test function $\nu\in W$ and integrate over $[R_{in},R_{out}]$, then substitute into Eq.(7.34),

$$
\begin{aligned}
&\frac{(\Delta t)^{2-\beta}}{\Gamma(3-\beta)}\int_{R_{in}}^{R_{out}}\left\{f_{n-1}\Phi(r,t_0)+\sum_{j=1}^{n-1}(f_{n-j-1}+g_{n-j})\Phi(r,t_j)+g_0\Phi(r,t_n)\right\}\nu\,dr\\
&\quad=\frac{(\Delta t)^{2-\beta}}{\Gamma(3-\beta)}\Bigg\{f_{n-1}\int_{R_{in}}^{R_{out}}\Phi(r,t_0)\nu\,dr+\sum_{j=1}^{n-1}(f_{n-j-1}+g_{n-j})\int_{R_{in}}^{R_{out}}\Phi(r,t_j)\nu\,dr\\
&\qquad\qquad +g_0\int_{R_{in}}^{R_{out}}\Phi(r,t_n)\nu\,dr\Bigg\}
\end{aligned}
\tag{7.41}
$$

then,

$$
\begin{aligned}
\int_{R_{in}}^{R_{out}}\Phi(r,t)\nu\,dr &= \int_{R_{in}}^{R_{out}}\left(\frac{\partial^2 u_\theta}{\partial r^2}+\frac{1}{r}\frac{\partial u_\theta}{\partial r}-\frac{u_\theta}{r^2}\right)\nu\,dr\\
&= \int_{R_{in}}^{R_{out}}\left(-\frac{\partial u}{\partial r}\frac{\partial \nu}{\partial r}+\frac{1}{r}\frac{\partial u}{\partial r}\nu-\frac{u\nu}{r^2}\right)dr\\
&= \int_{-1}^{1}\left(-\Delta^{-2}\frac{\partial u}{\partial \tilde{r}}\frac{\partial v}{\partial \tilde{r}}+\Delta^{-1}\frac{1}{r}\frac{\partial u}{\partial \tilde{r}}\nu(\tilde{r})-\frac{u}{r^2}\nu(\tilde{r})\right)\Delta d\tilde{r}\\
&= \int_{-1}^{1}\left(-\frac{1}{\Delta}\frac{\partial u}{\partial \tilde{r}}\frac{\partial v}{\partial \tilde{r}}+\frac{1}{r}\frac{\partial u}{\partial \tilde{r}}\nu(\tilde{r})-\Delta\frac{u}{r^2}\nu(\tilde{r})\right)d\tilde{r}
\end{aligned}
\tag{7.42}
$$

Use the spectral approximation $u = \sum_{j=0}^{N} u_j h_j(\tilde{r})$ and $\nu = h_k(\tilde{r})$, then the right hand side of Eq. (7.42) becomes

$$\begin{aligned} R.H.S \simeq \sum_{m=0}^{N} w_m \Bigg[& \frac{-1}{\Delta} \left(\sum_{j=0}^{N} U_j h_j'(\tilde{r}_m) \right) h_k'(\tilde{r}_m) + \frac{1}{r_m} \left(\sum_{j=0}^{N} U_j h_j'(\tilde{r}_m) \right) h_k(\tilde{r}_m) \\ & - \frac{\Delta}{r_m^2} \left(\sum_{j=0}^{N} U_j h_j(\tilde{r}_m) \right) h_k(\tilde{r}_m) \Bigg] \\ = \sum_{m=0}^{N} w_m \Bigg[& \frac{-1}{\Delta} \left(\sum_{j=0}^{N} D_{m,j} U_j \right) D_{m,k} + \frac{1}{r_m} \left(\sum_{j=0}^{N} D_{m,j}\ U_j \right) \delta_{m,k} - \frac{\Delta}{r_m^2} U_m \delta_{m,k} \Bigg] \\ = & \frac{-1}{\Delta} \sum_{j=0}^{N} \left(\sum_{m=0}^{N} w_m D_{m,j} D_{m,k} \right) U_j + \frac{w_k}{r_k} \sum_{j=0}^{N} D_{k,j} U_j - \frac{\Delta w_k}{r_k^2} U_k \\ = & -\frac{1}{\Delta} \sum_{j=0}^{N} B_{k,j} U_j + \frac{w_k}{r_k} \sum_{j=0}^{N} D_{k,j} U_j - \frac{\Delta w_k}{r_k^2} U_k \end{aligned} \tag{7.43}$$

where $B_{j,k} = \sum_{m=0}^{N} w_m D_{m,j} D_{m,k}$.

Substitute Eq.(7.43) into Eq.(7.41), then the full discretisation is

$$\begin{aligned} & \frac{\rho}{\mathbb{V}} \Delta w_k \left(\frac{U_k^n - U_k^{n-1}}{\Delta t} \right) + \frac{\rho}{\mathbb{G}} \frac{\Delta w_k}{(\Delta t)^{\alpha+1} \Gamma(2-\alpha)} \Bigg[\tilde{a}_0 \left(U_k^n - U_k^{n-1} \right) \\ & \qquad - \sum_{j=1}^{n-1} \left(\tilde{a}_j - \tilde{a}_{j-1} \right) \left(U_k^{n-j} - U_k^{n-j-1} \right) \Bigg] \\ = & \frac{(\Delta t)^{2-\beta}}{\Gamma(3-\beta)} \Bigg\{ f_{n-1} \Phi(r_i, t_0) + \sum_{j=1}^{n-1} (f_{n-j-1} + g_{n-j}) \Bigg[\frac{-1}{\Delta} \sum_{l=0}^{N} B_{k,l} U_l^j + \frac{w_k}{r_k} \sum_{l=0}^{N} D_{k,l} U_l^j \\ & \qquad - \frac{\Delta w_k}{r_k^2} U_k^j \Bigg] + g_0 \left[\frac{-1}{\Delta} \sum_{l=0}^{N} B_{k,j} U_l^n + \frac{w_k}{r_k} \sum_{l=0}^{N} D_{k,l} U_l^n - \frac{\Delta w_k}{r_k^2} U_k^n \right] \Bigg\} \end{aligned} \tag{7.44}$$

Rearranging and multiplying by Δt gives

$$\left[\frac{\rho}{\mathbb{V}}\Delta w_k + \frac{\rho}{\mathbb{G}}\frac{\tilde{a}_0}{(\Delta t)^\alpha\Gamma(2-\alpha)}\frac{\Delta w_k}{} + \frac{g_0(\Delta t)^{3-\beta}}{\Gamma(3-\beta)}\frac{\Delta w_k}{r_k^2}\right]U_k^n$$
$$+\frac{g_0\,(\Delta t)^{3-\beta}}{\Gamma(3-\beta)}\left[\frac{1}{\Delta}\sum_{l=0}^{N}B_{k,l}U_l^n - \frac{w_k}{r_k}\sum_{l=0}^{N}D_{k,l}U_l^n\right] = \left[\frac{\rho}{\mathbb{V}}\Delta w_k + \frac{\rho}{\mathbb{G}}\frac{\tilde{a}_0\,\Delta w_k}{(\Delta t)^\alpha\Gamma(2-\alpha)}\right]U_k^{n-1}$$
$$-\frac{\rho}{\mathbb{G}}\frac{\Delta w_k}{(\Delta t)^\alpha\Gamma(2-\alpha)}\left[\sum_{j=1}^{n-1}\left(\tilde{a}_j-\tilde{a}_{j-1}\right)\left(U_k^{n-j}-U_k^{n-j-1}\right)\right]$$
$$+\frac{(\Delta t)^{3-\beta}}{\Gamma(3-\beta)}\left\{\sum_{j=1}^{n-1}(f_{n-j-1}+g_{n-j})\left[\frac{-1}{\Delta}\sum_{l=0}^{N}B_{k,l}U_l^j + \frac{w_k}{r_k}\sum_{l=0}^{N}D_{k,l}U_l^j - \frac{\Delta w_k}{r_k^2}U_k^j\right]\right\} \quad (7.45)$$

where $1 \le k \le N-1$, and the initial condition is

$$U_i^0 = \Phi_i(r_i, t_0) = 0, \qquad 0 \le i \le N, \quad (7.46)$$

and the boundary conditions are

$$U_0^n = 0, \quad U_N^n = 0, \quad n \ge 1 \quad (7.47)$$

Numerical Discretization of Stress Equation

In Time

To discretize Eq. (7.11), we first derive the numerical approximation for the time-fractional derivative $D_t^\beta\gamma(t)$. Additionally, the numerical approximation for the time-fractional derivative $D_t^\alpha\tau(t)$ will be obtained by following the approach outlined in Chapter 5, specifically in Section 5.3.2, using Eq. (5.37), which is given by:

$$D_t^\alpha\ \tau(t_n) = \frac{\Delta t^{-\alpha}}{\Gamma(2-\alpha)}\left[\sum_{j=0}^{n}\tilde{B}_j\tau_i^j\right] \quad (7.48)$$

where the coefficients $\tilde{B}_j$ are defined by Eq. (5.38).

The grid functions τ_i^n are defined as follows $\tau_i^n \simeq \tau(r_i, t_n) = \phi_i(t_n)$, when $0 \le i \le N$, $n \ge 0$, and the initial condition is $\tau_i^0 = \phi_i(t_0),\ 0 \le i \le N$.

Now, we will derive the numerical approximation of the time-fractional derivative $D_t^\beta \gamma(t)$

$$\begin{aligned} D_t^\beta \gamma(t_n) &= \frac{1}{\Gamma(1-\beta)} \int_0^t \frac{1}{(t_n - s)^\beta} \frac{\partial \gamma}{\partial s} ds \\ &= \frac{1}{\Gamma(1-\beta)} \int_0^t \frac{1}{(t_n - s)^\beta} \left\{ \frac{\partial u}{\partial r} - \frac{u}{r} \right\} ds \end{aligned} \tag{7.49}$$

using the first-order discretization of the integral in time derived using linear interpolant for u on each sub-interval $[t_{j-1}, t_j]$ i.e.

$$\Pi_{1,j} u(s) = u(t_{j-1}) \frac{(t_j - s)}{\Delta t} + u(t_j) \frac{(s - t_{j-1})}{\Delta t}, \quad s \in [t_{j-1}, t_j] \tag{7.50}$$

and

$$\Pi_{1,j} \left(\frac{\partial u}{\partial r} \right) = \frac{\partial u}{\partial r}(t_{j-1}) \frac{(t_j - s)}{\Delta t} + \frac{\partial u}{\partial r}(t_j) \frac{(s - t_{j-1})}{\Delta t}, \quad s \in [t_{j-1}, t_j] \tag{7.51}$$

Therefore, Eq. (7.49) is approximated by

$$D_t^\beta \gamma(t_n) \simeq \frac{1}{\Gamma(1-\beta)} \sum_{j=1}^{n} \int_{t_{j-1}}^{t_j} \frac{1}{(t_n - s)^\beta} \left\{ \Pi_{1,j} \left(\frac{\partial u}{\partial r} \right) - \Pi_{1,j} \left(\frac{u}{r} \right) \right\} ds \tag{7.52}$$

To evaluate $D_t^\beta \gamma(t_n)$ we need to calculate integrals of the form

$$\begin{aligned} I_1 &= \int_{t_{j-1}}^{t_j} (t_n - s)^{-\beta} (t_j - s) ds \\ &= \frac{(\Delta t)^{2-\beta}}{(1-\beta)(2-\beta)} \left[(2-\beta)(n-j+1)^{1-\beta} + (n-j)^{2-\beta} - (n-j+1)^{2-\beta} \right] \\ &= \frac{(\Delta t)^{2-\beta}}{(1-\beta)(2-\beta)} \left[\bar{f}_{n-j} \right] \end{aligned} \tag{7.53}$$

where

$$\bar{f}_{n-j} = \left[(2-\beta)(n-j+1)^{1-\beta} + (n-j)^{2-\beta} - (n-j+1)^{2-\beta} \right] \tag{7.54}$$

let $l = n - j$, then

$$\bar{f}_l = (2-\beta)(l+1)^{1-\beta} + l^{2-\beta} - (l+1)^{2-\beta} \tag{7.55}$$

and

$$
\begin{aligned}
I_2 &= \int_{t_{j-1}}^{t_j} (t_n - s)^{-\beta}(s - t_j)ds \\
&= \frac{(\Delta t)^{2-\beta}}{(1-\beta)(2-\beta)} \left[-(2-\beta)(n-j)^{1-\beta} - (n-j)^{2-\beta} + (n-j+1)^{2-\beta}\right] \\
&= \frac{(\Delta t)^{2-\beta}}{(1-\beta)(2-\beta)} \left[\bar{g}_{n-j}\right]
\end{aligned} \tag{7.56}
$$

where

$$
\bar{g}_{n-j} = \left[-(2-\beta)(n-j)^{1-\beta} - (n-j)^{2-\beta} + (n-j+1)^{2-\beta}\right] \tag{7.57}
$$

let $l = n - j$, then

$$
\bar{g}_l = -(2-\beta)l^{1-\beta} - l^{2-\beta} + (l+1)^{2-\beta} \tag{7.58}
$$

then

$$
\begin{aligned}
\frac{1}{\Gamma(1-\beta)} \sum_{j=1}^{n} \int_{t_{j-1}}^{t_j} \frac{1}{(t_n - s)^{\beta}} \left\{\Pi_{1,j} u(s)\right\} ds &\simeq \frac{(\Delta t)^{2-\beta}}{\Gamma(3-\beta)} \sum_{j=1}^{n} \left\{ \frac{\bar{f}_{n-j} U^{j-1} + \bar{g}_{n-j} U^j}{\Delta t} \right\} \\
&= \frac{(\Delta t)^{1-\beta}}{\Gamma(3-\beta)} \left\{ \bar{f}_{n-1} U^0 + \sum_{j=1}^{n-1} (\bar{f}_{n-j-1} + \bar{g}_{n-j}) U^j + \bar{g}_0 U^n \right\} \\
&= \frac{(\Delta t)^{1-\beta}}{\Gamma(3-\beta)} \sum_{j=0}^{n} \bar{A}_j U^j
\end{aligned} \tag{7.59}
$$

Similarly, we have

$$
\frac{1}{\Gamma(1-\beta)} \sum_{j=1}^{n} \int_{t_{j-1}}^{t_j} \frac{1}{(t_n - s)^{\beta}} \left\{\Pi_{1,j} \left(\frac{\partial u}{\partial r}\right)\right\} ds \simeq \frac{(\Delta t)^{1-\beta}}{\Gamma(3-\beta)} \sum_{j=0}^{n} \bar{A}_j \left(\frac{\partial u^j}{\partial r}\right) \tag{7.60}
$$

where,

$$
\bar{A}_j = \begin{cases} \bar{f}_{n-1} & \text{if} \quad j = 0 \\ \bar{f}_{n-j-1} + \bar{g}_{n-j} & \text{if} \quad 1 \le j \le n-1 \\ \bar{g}_0 & \text{if} \quad j = n \end{cases} \tag{7.61}
$$

Inserting the above difference scheme and the spectral approximations to the different terms in the weak formulation Eq. (7.15) gives

$$\begin{aligned}
\int_{R_{in}}^{R_{out}} \tau(t)\ \nu\ dr &= \Delta \int_{-1}^{1} \tau(t)\ \nu\ d\tilde{r} \\
&\simeq \Delta \sum_{l=0}^{N} w_l \left(\sum_{j=0}^{N} \tau_j h_j(\tilde{r}_l) \right) h_k(\tilde{r}_l) \\
&= \Delta \sum_{l=0}^{N} w_l \left(\tau_l\right) h_k(\tilde{r}_l) \\
&= \Delta w_k \tau_k^n
\end{aligned} \tag{7.62}$$

where we have used test function $\nu = h_k(r)$, $k = 0, 1, \ldots, N$

$$\begin{aligned}
\lambda^\alpha \int_{R_{in}}^{R_{out}} (D_t^\alpha \tau(t))\ \nu\ dr &= \Delta\lambda^\alpha \int_{-1}^{1} (D_t^\alpha \tau(t))\ \nu\ d\tilde{r} \\
&\simeq \Delta\lambda^\alpha \sum_{l=0}^{N} w_l \left(D_t^\alpha \tau_l\right) h_k(\tilde{r}_l) \\
&= \Delta w_k \lambda^\alpha \left(D_t^\alpha \tau_k\right) \\
&= \Delta w_k \lambda^\alpha \frac{\Delta t^{-\alpha}}{\Gamma(2-\alpha)} \left[\tilde{b}_0(\alpha)\, \tau_i^n - \sum_{j=1}^{n-1} \left(\tilde{b}_{n-j-1}(\alpha) - \tilde{b}_{n-j}(\alpha) \right) \tau_i^j - \tilde{b}_{n-1}(\alpha) \tau_i^0 \right] \\
&= \frac{\Delta w_k}{\Gamma(2-\alpha)} \frac{\lambda^\alpha}{(\Delta t)^\alpha} \sum_{j=0}^{n} \tilde{B}_j \tau_k^j
\end{aligned} \tag{7.63}$$

$$
\begin{aligned}
E\lambda^\beta \int_{R_{in}}^{R_{out}} \left(D_t^\beta \gamma(t)\right)\ \nu\ dr &= \Delta\ E\ \lambda^\beta \int_{-1}^{1} \left(D_t^\beta \gamma(t)\right)\ \nu\ d\tilde{r} \\
&= \Delta\ E\ \lambda^\beta \int_{-1}^{1} \left(D_t^\beta \left\{\Delta^{-1}\frac{\partial u}{\partial r} - \frac{u}{r}\right\}\right)\ \nu\ d\tilde{r} \\
&\simeq E\ \lambda^\beta \sum_{l=0}^{N} w_l \left(D_t^\beta \left\{\left(\sum_{i=0}^{N} U_i\ h_i'(\tilde{r}_l)\right) - \Delta\left(\frac{U_l}{r_l}\right)\right\}\right) h_k(\tilde{r}_l) \\
&= E\ \lambda^\beta \sum_{l=0}^{N} w_l \left(D_t^\beta \left\{\left(\sum_{i=0}^{N} D_{l,i}\ U_i\right) - \Delta\left(\frac{U_l}{r_l}\right)\right\}\right) h_k(\tilde{r}_l) \\
&= E\ \lambda^\beta\ w_k \left\{\sum_{i=0}^{N} D_t^\beta\ \ (D_{k,i}U_i) - \frac{\Delta}{r_k}\left(D_t^\beta U_k\right)\right\} \\
&= \frac{E\lambda^\beta w_k}{(\Delta t)^{\beta-1}\Gamma(3-\beta)} \left\{\sum_{l=0}^{n} \bar{A}_l \left(\sum_{m=0}^{N} D_{k,m}U_m^l\right)\right\} \\
&\qquad - \frac{E\lambda^\beta \Delta w_k}{r_k(\Delta t)^{\beta-1}\Gamma(3-\beta)} \left\{\sum_{l=0}^{n} \bar{A}_l U_k^l\right\}
\end{aligned}
\tag{7.64}
$$

The full discretization is

$$
\begin{aligned}
&\Delta w_k \left\{\tau_k^n + \frac{1}{\Gamma(2-\alpha)}\frac{\lambda^\alpha}{(\Delta t)^\alpha}\sum_{j=0}^{n} \tilde{B}_j \tau_k^j\right\} \\
&= \frac{E\lambda^\beta w_k}{(\Delta t)^{\beta-1}\Gamma(3-\beta)} \left\{\sum_{l=0}^{n} \bar{A}_l \left(\sum_{m=0}^{N} D_{k,m}U_m^l\right)\right\} - \frac{E\lambda^\beta \Delta w_k}{r_k(\Delta t)^{\beta-1}\Gamma(3-\beta)} \left\{\sum_{l=0}^{n} \bar{A}_l U_k^l\right\}
\end{aligned}
\tag{7.65}
$$

for $k = 1, \ldots, N-1$, $n = 1, \ldots, N_T$ and $U_i^0 = \tau_i^0 = 0$, for $0 \le i \le N$.

Rearranging Eq.(7.65) we obtain

$$
\begin{aligned}
&\Delta w_k \left\{1 + \frac{\tilde{B}_n}{\Gamma(2-\alpha)}\frac{\lambda^\alpha}{(\Delta t)^\alpha}\right\}\tau_k^n = -\frac{\Delta w_k}{\Gamma(2-\alpha)}\frac{\lambda^\alpha}{(\Delta t)^\alpha}\sum_{j=0}^{n-1} \tilde{B}_j \tau_k^j \\
&+ \frac{E\lambda^\beta w_k}{(\Delta t)^{\beta-1}\Gamma(3-\beta)} \left\{\sum_{l=0}^{n} \bar{A}_l \left(\sum_{m=0}^{N} D_{k,m}U_m^l\right)\right\} - \frac{E\lambda^\beta \Delta w_k}{r_k(\Delta t)^{\beta-1}\Gamma(3-\beta)} \left\{\sum_{l=0}^{n} \bar{A}_l U_k^l\right\}
\end{aligned}
\tag{7.66}
$$

where $\lambda^\alpha = \dfrac{\mathbb{V}}{\mathbb{G}}$, $E\lambda^\beta = \mathbb{V}$. The coefficients $\tilde{B}_j$ and $\bar{A}_l$ are defined by Eq.(5.38), and Eq.(7.61), respectively.

7.2.3 Numerical Results

In this section, we perform additional simulations using the same parameter set introduced in Chapter 6, Section 6.6, informed by the experimental and modeling work of Ferras . (2018). The simulations are extended to explore different values of the fractional order parameter, constrained within the interval $0 < \alpha < \beta < 1$, as required by the fractional viscoelastic model. These parameters were originally established to effectively capture the rheological response of Xanthan gum solutions. To solve the system of differential equations governing the unsteady unidirectional flow of the FMM when $0 < \alpha < \beta < 1$ in an annular geometry, we have developed a MATLAB code for the proposed numerical method with the following fluid parameters ($N = 64$, $\beta = 0.999$, $\alpha = 0.8$, the final time is $T = 80$ s, and $S = 1000$) for Newtonian fluid, and ($N = 24$, $\beta = 0.7$, $\alpha = 0.4$, the final time is $T = 90$ s, and $S = 5000$) for Viscoelastic fluid. We study the evolution of the velocity and stress profiles at different radial locations are shown in Figs. 7.1 and 7.2. We plot the velocity at the wall and at $\bar{r} = [0.25,\ 0.5,\ 0.75]$, while the stress is plotted at $\bar{r} = [0.005,\ 0.25,\ 0.5,\ 0.75,\ 0.995]$. The numerical method proved successful in precisely capturing the evolution of the various variables in this transient flow.

Newtonian fluid

Figure. 7.1 illustrates the variation of velocity and shear stress over time in a Newtonian fluid confined between two concentric cylinders, where the outer cylinder rotates at a higher linear speed than the inner one. The velocity profile in Fig. 7.1 (a) shows a rapid and smooth transfer of momentum from the moving walls to the bulk fluid due to the purely viscous nature of Newtonian fluids. Similarly, in Fig. 7.1 (b) the shear stress distribution evolves quickly, reflecting an immediate response to the applied shear. Since Newtonian fluids do not exhibit elasticity, the stress change over time is sudden, governed by simple diffusion without any delay in momentum transfer. Because of the variation in sign of the velocity gradient $\frac{\partial u_\theta}{\partial r}$ seen in Fig. 7.1 (c), note that the shear stress is negative near the inner cylinder and positive near the outer cylinder as shown in Fig. 7.1 (d).

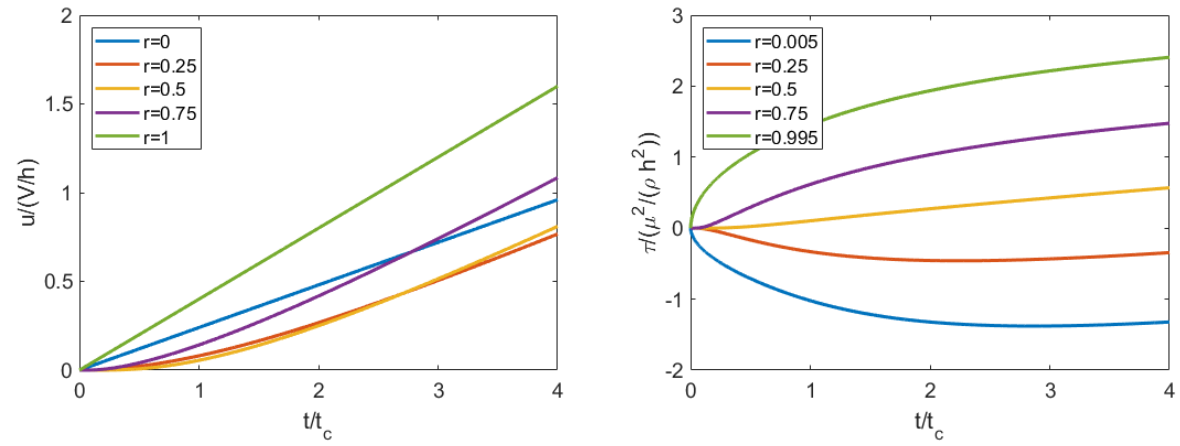

(a)

(b)

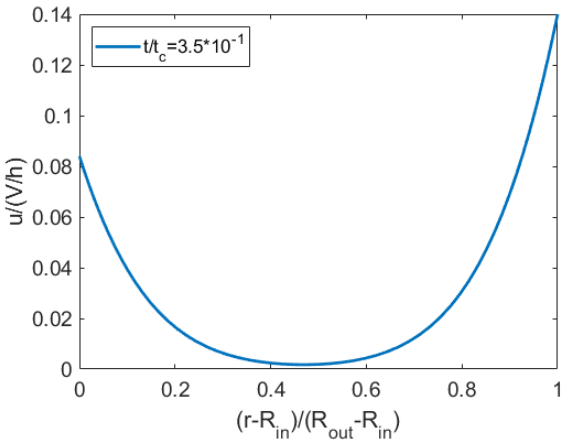

(c)

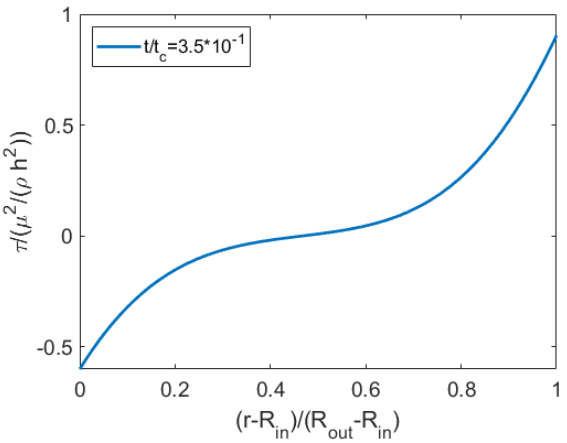

(d)

Figure 7.1: (a), (b) Variation of velocity and shear stress with time, in different regions; (c), (d) Velocity and shear stress profiles for $t/t_c = 3.50 \times 10^{-1}$. The fractional parameters: $\alpha = 0.8$, and $\beta = 0.999$.

Viscoelastic fluid

Figure 7.2 presents the velocity and shear stress evolution in a viscoelastic (non-Newtonian) fluid under the same rotational conditions. Unlike Newtonian fluids, the viscoelastic material exhibits a delayed response in velocity propagation due to elastic effects, leading to a gradual momentum transfer. The shear stress evolution at different radial locations indicates stress relaxation, where the material retains memory of past deformations, causing a smoother and time-dependent transition. This behaviour, described by the Fractional Maxwell Model, highlights the combined influence of viscosity and elasticity, making the response distinct from the instantaneously evolving Newtonian case.

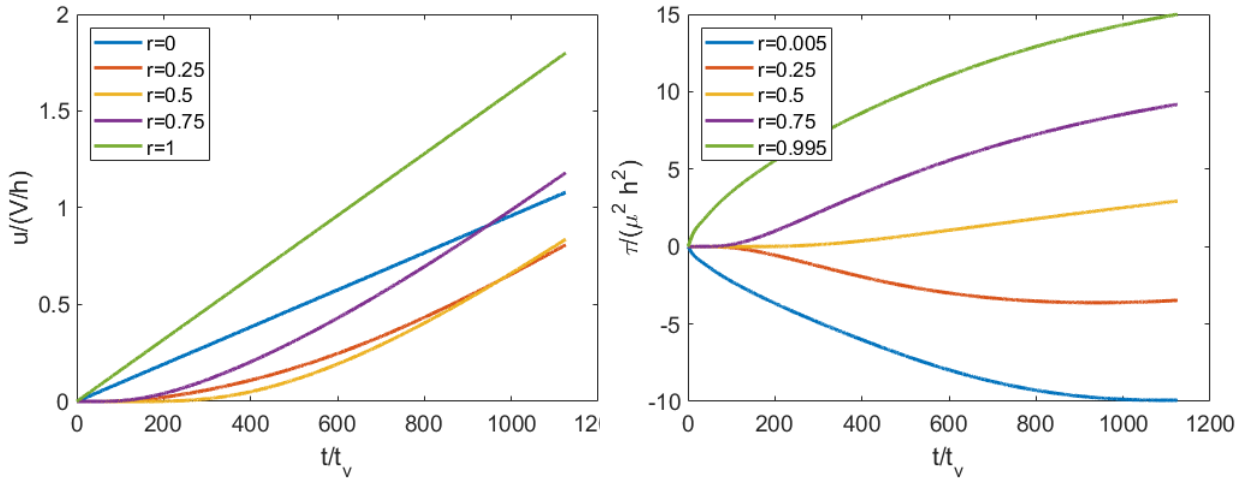

(a) (b)

Figure 7.2: (a) Evolution of velocity at radial location $\bar{r} = 0.25,\ 0.5,\ 0.75$;
(b) Shear stress at radial location $\bar{r} = 0.005,\ 0.25,\ 0.5,\ 0.57,\ 0.995$. The fractional parameters: $\alpha = 0.4$, and $\beta = 0.7$.

Influence of fractional order

This section examines the influence of fractional order on velocity, shear stress, and stress relaxation in the Fractional Maxwell Model (FMM). The results are consistent with previous findings in Chapter 6, demonstrating similar relaxation behaviour.

For the simulation of Xanthan gum at a concentration of $(0.25\,wt\%)$, we adopted the viscoelastic material parameters reported by Ferras . (2018), specifically the characteristic relaxation time $\lambda_c = 55.6\ s$, viscosity-like parameter $\mathbb{V} = 24.96$ Pa.s, and modulus-like

parameter $\mathbb{G} = 1.56$ Pa.s. The fractional orders $\beta = 0.999$, $\alpha = 0.8$, as well as the derived parameter $\zeta = \beta - \alpha$ (corresponding to the fractional parameter (β) defined in Chapter 6), are introduced in this study to generalize the model beyond the original formulation in Ferras . (2018), allowing for enhanced flexibility in capturing the complex rheology of the fluid. Fig. 7.3 (a) measures the normalised tangential velocity ($u_{\theta max} = u_\theta(R_{out}, t_d)$) of the outer cylinder (case of $\gamma_0 = 100\%$). For a step-strain test with a deformation of $\gamma_0 = 100\%$, $\zeta = 0.199$ and three different levels of refinement, $\psi/\lambda_c = 1.0\times10^{-4}$, 1.8×10^{-4}, 2.7×10^{-4} and a normalized delay time of $t_d/\lambda_c = 4.5 \times 10^{-4}$, 7.4×10^{-4}, 1.1×10^{-3}, we display the normalised shear stress relaxation data in Fig. 7.3 (b). Be aware that the outer cylinder must rotate more quickly as $\psi \to 0$ to turn the same constant distance in a decreasingly longer period of time. Since we must precisely capture high gradients, this makes the numerical calculation more difficult.

Figure 7.3 (c) illustrates the progression of the deformation over time ($\gamma_0 = \dfrac{\Delta\theta R_{out}}{h}$) for the three distinct tangential velocities applied to the outer cylinder. As anticipated, a higher approximation of a true step-strain displacement is obtained as the rotational velocity is gradually increased.

Figure 7.3 (d) illustrates the normalized stress relaxation for the three distinct levels of imposed deformations 1%, 5% and 100% ($\psi/\lambda_c = 1.0 \times 10^{-4}$ and $t_d/\lambda_c = 4.5 \times 10^{-4}$). The stress relation derived for the two smaller deformations is shown in Fig. 7.3 (e) in a zoomed-in view.

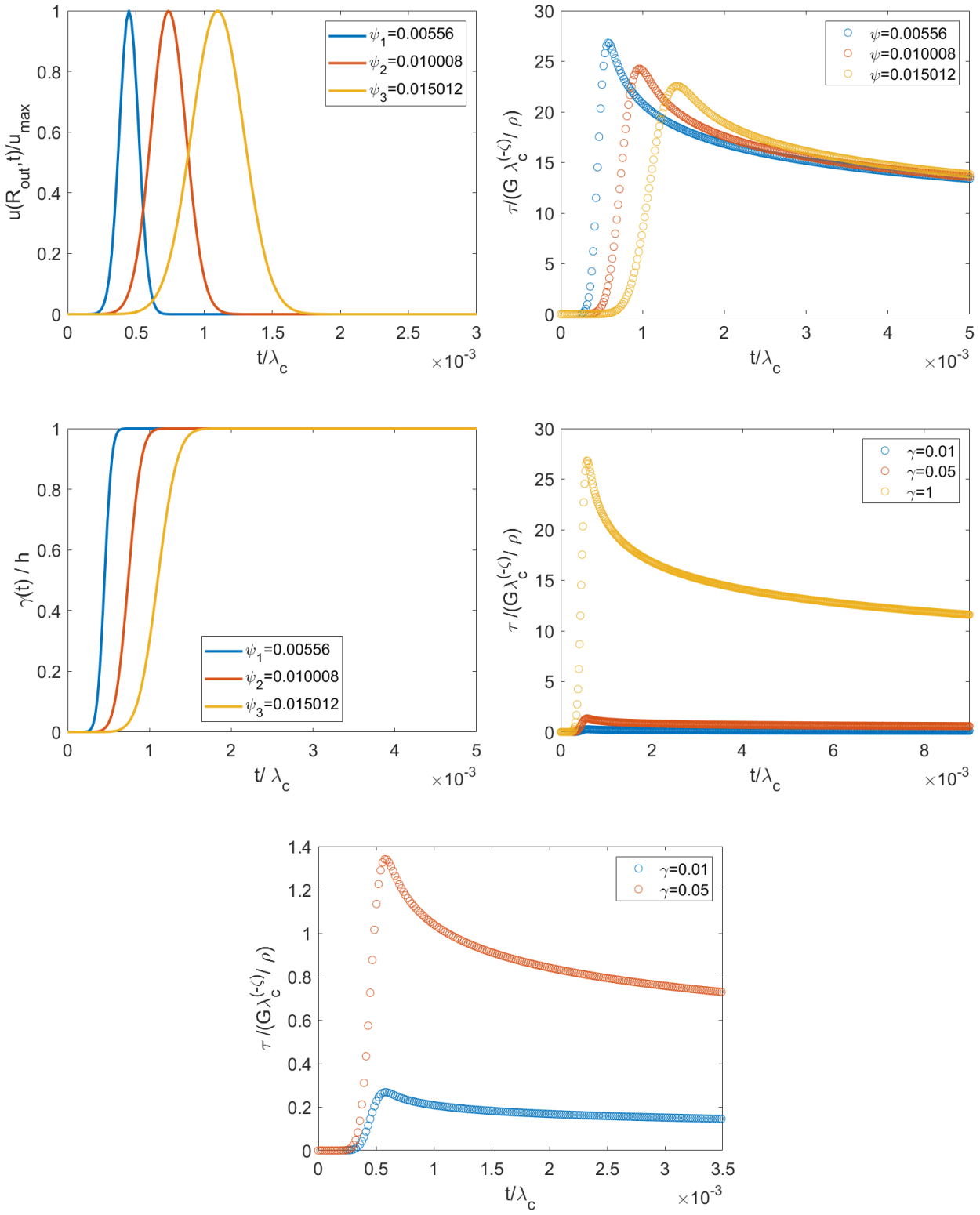

Figure 7.3: (a) Normalized tangential velocity of the outer cylinder; (b) Normalized shear stress relaxation for step-strain test ($\gamma_0 = 100\%$) with parameters $\beta = 0.999$, $\alpha = 0.8$; (c) Evolution of the deformation in time for the three different tangential velocities imposed; (d) Stress relaxation for three different deformations; (e) Zoomed view of the stress relation obtained for the two smaller deformations.

7.2.4 A second-order difference scheme for a time-fractional derivative

In this section, we aim for higher accuracy in the proposed numerical method. Therefore, we will develop difference schemes with a time accuracy order of $O(\Delta t^2)$.

Numerical Discretization of the Velocity Equation

In Time

The second-order approximation for the time derivative $\dfrac{\partial u}{\partial t}$ can be derived using a backward differentiation formula scheme which provides better accuracy and stability compared to a first-order forward or backward scheme.

$$\frac{\partial u}{\partial t} \simeq \frac{3u^n - 4u^{n-1} + u^{n-2}}{2\Delta t} \tag{7.67}$$

inserting this approximation in the first term of the weak formulation (7.10), we obtain

$$\begin{aligned}
\frac{\rho}{\mathbb{V}} \int_{R_{in}}^{R_{out}} \left(\frac{\partial u}{\partial t}\right) v \, dr &= \Delta \frac{\rho}{\mathbb{V}} \int_{-1}^{1} \left(\frac{\partial u}{\partial t}\right) v \, d\tilde{r} \\
&\simeq \Delta \frac{\rho}{\mathbb{V}} \sum_{l=0}^{N} w_l \left(\frac{\partial u(\tilde{r}_l, t_n)}{\partial t}\right) h_k(\tilde{r}_l) \\
&= \frac{\rho}{\mathbb{V}} \Delta w_k \left(\frac{3U_k^n - 4U_k^{n-1} + U_k^{n-2}}{2\Delta t}\right)
\end{aligned} \tag{7.68}$$

where $v = h_k(r)$.

The numerical approximation to the fractional derivative, $D_t^{1+\alpha} u(t)$, is derived in Chapter.5 (Section. 5.4.1, Eq. (5.40)), with α replaced by $1+\alpha$ where $0 < \alpha < 1$.

$$\begin{aligned}
D_t^{1+\alpha} u(t_n) &\simeq \frac{1}{\Gamma(1-\alpha)} \left[\int_{t_{n-1}}^{t_n} \frac{\partial_s^2 \left(\Pi_{2,n-1} u(s)\right)}{(t_n - s)^\alpha} \, ds + \sum_{j=1}^{n-1} \int_{t_{j-1}}^{t_j} \frac{\partial_s^2 \left(\Pi_{2,j} u(s)\right)}{(t_n - s)^\alpha} \, ds \right] \\
&= \frac{1}{\Gamma(1-\alpha)} \left[\frac{(U^n - 2U^{n-1} + U^{n-2})}{(\Delta t)^2} \int_{t_{n-1}}^{t_n} \frac{ds}{(t_n - s)^\alpha} \right. \\
&\qquad \left. + \sum_{j=1}^{n-1} \frac{(U^{j+1} - 2U^j + U^{j-1})}{(\Delta t)^2} \int_{t_{j-1}}^{t_j} \frac{ds}{(t_n - s)^\alpha} \right]
\end{aligned} \tag{7.69}$$

where

$$\begin{aligned}\int_{t_{j-1}}^{t_j}(t_n-s)^{-\alpha}ds &= \frac{(\Delta t)^{1-\alpha}}{1-\alpha}\left[(n-j+1)^{1-\alpha}-(n-j)^{1-\alpha}\right]\\ &= \frac{(\Delta t)^{1-\alpha}}{1-\alpha}\tilde{a}_{n-j},\quad n-j\geq 0\end{aligned} \tag{7.70}$$

where

$$\tilde{a}_l(\alpha)=\left[(l+1)^{1-\alpha}-(l)^{1-\alpha}\right],\quad l\geq 0 \tag{7.71}$$

Therefore, Eq. (7.69) becomes

$$\begin{aligned}D_t^{1+\alpha}u(t_n) &= \frac{1}{(\Delta t)^{1+\alpha}\Gamma(2-\alpha)}\Bigg[\left(\tilde{a}_{n-1}(\alpha)\right)U^0+(\tilde{a}_{n-2}(\alpha)-2\tilde{a}_{n-1}(\alpha))U^1\\ &\quad+\sum_{j=2}^{n-3}(\tilde{a}_{n-j-1}(\alpha)-2\tilde{a}_{n-j}(\alpha)+\tilde{a}_{n-j+1}(\alpha))U^j\\ &\quad+(1+\tilde{a}_3(\alpha)-2\tilde{a}_2(\alpha)+\tilde{a}_1(\alpha))U^{n-2}+(-2+\tilde{a}_2(\alpha)-2\tilde{a}_1(\alpha))U^{n-1}\\ &\quad+(1+\tilde{a}_1(\alpha))U^n\Bigg]\\ &= \frac{1}{(\Delta t)^{1+\alpha}\Gamma(2-\alpha)}\sum_{j=0}^{n}C_jU^j\end{aligned} \tag{7.72}$$

C_j can be defined by substituting Eq. (7.71) into Eq. (5.42).

Inserting this approximation in the second term of the weak formulation (7.10), we obtain.

$$\begin{aligned}\frac{\rho}{\mathbb{G}}\int_{R_{in}}^{R_{out}}\left(D_t^{1+\alpha}u(t)\right)\,v\,dr &= \Delta\frac{\rho}{\mathbb{G}}\int_{-1}^{1}\left(D_{t_n}^{1+\alpha}u\right)\,v\,d\tilde{r}\\ &\simeq \Delta\frac{\rho}{\mathbb{G}}\sum_{l=0}^{N}w_l\left(D_{t_n}^{1+\alpha}U_l\right)h_k(\tilde{r}_l)\\ &\simeq \Delta\frac{\rho}{\mathbb{G}}w_k\left(D_{t_n}^{1+\alpha}\,U_k^{n-1/2}\right)\\ &= \frac{\rho}{\mathbb{G}}\frac{\Delta w_k}{(\Delta t)^{1+\alpha}\Gamma(2-\alpha)}\sum_{j=0}^{n}C_jU_k^j\end{aligned} \tag{7.73}$$

In space

We will derive the numerical approximation of the right-hand side of Eq. (7.10) using a

second-order discretization of the time integral, obtained through quadratic interpolation on each sub-interval $[t_{j-1}, t_j]$, where $1 \leq j \leq n$.

Let

$$\Phi(r,t) = \left(\frac{\partial^2}{\partial r^2} + \frac{1}{r}\frac{\partial}{\partial r} - \frac{1}{r^2}\right) u_\theta(r,t) \tag{7.74}$$

Therefore, the quadratic interpolation of $\Phi(r,t)$ is given by

$$\begin{aligned}\Pi_{2,j}\Phi(r,s) = \Phi(r,t_{j-1})\left[\frac{(s-t_j)(s-t_{j+1})}{2(\Delta t)^2}\right] - \Phi(r,t_j)\left[\frac{(s-t_{j-1})(s-t_{j+1})}{(\Delta t)^2}\right] \\ + \Phi(r,t_{j+1})\left[\frac{(s-t_{j-1})(s-t_j)}{2(\Delta t)^2}\right]\end{aligned} \tag{7.75}$$

and

$$\begin{aligned}\Pi_{2,n-1}\Phi(r,s) = \Phi(r,t_{n-2})\left[\frac{(s-t_n)(s-t_{n-1})}{2(\Delta t)^2}\right] - \Phi(r,t_{n-1})\left[\frac{(s-t_{n-2})(s-t_n)}{(\Delta t)^2}\right] \\ + \Phi(r,t_n)\left[\frac{(s-t_{n-2})(s-t_{n-1})}{2(\Delta t)^2}\right]\end{aligned} \tag{7.76}$$

Therefore, the right-hand side of Eq. (7.20) is approximated by

$$R.H.S \simeq \frac{1}{\Gamma(1-\beta)}\left\{\sum_{j=1}^{n-1}\int_{t_{j-1}}^{t_j}(t_n-s)^{-\beta}\Pi_{2,j}\Phi(r,s)ds + \int_{t_{n-1}}^{t_n}(t_n-s)^{-\beta}\Pi_{2,n-1}\Phi(r,s)ds\right\} \tag{7.77}$$

To evaluate Eq.(7.77) we need to calculate integrals of the following form using integration by parts

$$\begin{aligned}I &= \int (t_n-s)^{-\beta}(s-c)(s-d)ds \\ &= \left[-\frac{(s-c)(s-d)}{(1-\beta)(t_n-s)^{\beta-1}} + \int \frac{(2s-c-d)}{(1-\beta)}(t_n-s)^{1-\beta}ds\right] \\ &= \left[-\frac{(s-c)(s-d)(t_n-s)^{1-\beta}}{(1-\beta)} - \frac{(2s-c-d)(t_n-s)^{2-\beta}}{(1-\beta)(2-\beta)} - \frac{2(t_n-s)^{3-\beta}}{(1-\beta)(2-\beta)(3-\beta)}\right]\end{aligned} \tag{7.78}$$

Applying in Eq.(7.77), we obtain

$$
\begin{aligned}
R.H.S \simeq= \frac{1}{\Gamma(1-\beta)}\Bigg\{ \sum_{j=1}^{n-1} \Bigg(& \frac{\Phi(t_{j-1})}{2(\Delta t)^2}\left[\int_{t_{j-1}}^{t_j} (t_n-s)^{-\beta}(s-t_j)(s-t_{j+1})ds\right] \\
& - \frac{\Phi(t_j)}{(\Delta t)^2}\left[\int_{t_{j-1}}^{t_j} (t_n-s)^{-\beta}(s-t_{j-1})(s-t_{j+1})ds\right] \\
& + \frac{\Phi(t_{j+1})}{2(\Delta t)^2}\left[\int_{t_{j-1}}^{t_j} (t_n-s)^{-\beta}(s-t_{j-1})(s-t_j)ds\right]\Bigg)\Bigg\} \\
+ \frac{1}{\Gamma(1-\beta)}\Bigg\{ \Bigg(& \frac{\Phi(t_{n-2})}{2(\Delta t)^2}\left[\int_{t_{n-1}}^{t_n} (t_n-s)^{-\beta}(s-t_{n-1})(s-t_n)ds\right] \\
& - \frac{\Phi(t_{n-1})}{(\Delta t)^2}\left[\int_{t_{n-1}}^{t_n} (t_n-s)^{-\beta}(s-t_{n-2})(s-t_n)ds\right] \\
& + \frac{\Phi(t_n)}{2(\Delta t)^2}\left[\int_{t_{n-1}}^{t_n} (t_n-s)^{-\beta}(s-t_{n-1})(s-t_{n-2})ds\right]\Bigg)ds\Bigg\} \qquad (7.79)
\end{aligned}
$$

Therefore, Eq. (7.80) yields

$$
\begin{aligned}
R.H.S &= \frac{(\Delta t)^{1-\beta}}{\Gamma(4-\beta)}\Bigg\{ \sum_{j=1}^{n-1} \left(a_{n-j}\Phi(t_{j-1}) + b_{n-j}\Phi(t_j) + c_{n-j}\Phi(t_{j+1})\right) \\
&\quad + \left(\bar{a}\Phi(t_{n-2}) + \bar{b}\Phi(t_{n-1}) + \bar{c}\Phi(t_n)\right)\Bigg\} \\
&= \frac{(\Delta t)^{1-\beta}}{\Gamma(4-\beta)}\Bigg\{ \left(a_{n-1}\Phi(t_0) + b_{n-1}\Phi(t_1) + c_{n-1}\Phi(t_2)\right) + \left(a_{n-2}\Phi(t_1) + b_{n-2}\Phi(t_2) + c_{n-2}\Phi(t_3)\right) \\
&\quad + \cdots + \left(a_2\Phi(t_{n-3}) + b_2\Phi(t_{n-2}) + c_2\Phi(t_{n-1})\right) + \left(a_1\Phi(t_{n-2}) + b_1\Phi(t_{n-1}) + c_1\Phi(t_n)\right) \\
&\quad + \left(\bar{a}\Phi(t_{n-2}) + \bar{b}\Phi(t_{n-1}) + \bar{c}\Phi(t_n)\right)\Bigg\} \\
&= \frac{(\Delta t)^{1-\beta}}{\Gamma(4-\beta)}\Bigg\{ a_{n-1}\Phi(t_0) + (a_{n-2}+b_{n-1})\Phi(t_1) + \sum_{j=2}^{n-3}(a_{n-j-1} + b_{n-j} + c_{n-j+1})\Phi(t_j) \\
&\quad + (a_1 + \bar{a} + b_2 + c_3)\Phi(t_{n-2}) + (c_2 + b_1 + \bar{b})\Phi(t_{n-1}) + (c_1 + \bar{c})\Phi(t_n)\Bigg\}
\end{aligned} \qquad (7.80)
$$

where

$$
\bar{a}(\beta) = \left[\frac{(\beta-1)}{2}\right], \quad \bar{b}(\beta) = \left[(4-\beta)(1-\beta)\right], \quad \bar{c}(\beta) = \left[\frac{(5-\beta)}{2}\right] \qquad (7.81)
$$

and

$$a_{n-j}(\beta) = \frac{1}{2}\Bigg[(3-\beta)(n-j)^{2-\beta} - 2(n-j)^{3-\beta} + 2(2-\beta)(3-\beta)(n-j+1)^{1-\beta} \\ - 3(3-\beta)(n-j+1)^{2-\beta} + 2(n-j+1)^{3-\beta}\Bigg] \quad (7.82)$$

$$b_{n-j}(\beta) = \Big[-(2-\beta)(3-\beta)(n-j)^{1-\beta} + 2(n-j)^{3-\beta} + 2(3-\beta)(n-j+1)^{2-\beta} - 2(n-j+1)^{3-\beta}\Big] \quad (7.83)$$

$$c_{n-j}(\beta) = \frac{1}{2}\Big[-(3-\beta)(n-j)^{2-\beta} - 2(n-j)^{3-\beta} - (3-\beta)(n-j+1)^{2-\beta} + 2(n-j+1)^{3-\beta}\Big] \quad (7.84)$$

Find the weak form of the right-hand side of Eq. (7.77) by multiplying $\Phi(r_k, t_l)$ by by a test function $v \in W$, integrating over $[R_{in}, R_{out}]$, and substituting into Eq. (7.80),

$$\frac{(\Delta t)^{1-\beta}}{\Gamma(4-\beta)} \int_{R_{in}}^{R_{out}} \Bigg\{ a_{n-1}\Phi(t_0) + (a_{n-2} + b_{n-1})\Phi(t_1) + \sum_{j=2}^{n-3}(a_{n-j-1} + b_{n-j} + c_{n-j+1})\Phi(t_j) \\ + (a_1 + \bar{a} + b_2 + c_3)\Phi(t_{n-2}) + (c_2 + b_1 + \bar{b})\Phi(t_{n-1}) + (c_1 + \bar{c})\Phi(t_n) \Bigg\} \nu \, dr \\ = \frac{(\Delta t)^{1-\beta}}{\Gamma(4-\beta)} \sum_{j=0}^{n} \mathcal{A}_j \int_{R_{in}}^{R_{out}} \Phi(r, t_j)\nu \, dr \quad (7.85)$$

where

$$\mathcal{A}_j(\beta) = \begin{cases} a_{n-1}(\beta) & \text{if} \quad j = 0 \\ a_{n-2}(\beta) + b_{n-1}(\beta) & \text{if} \quad j = 1 \\ a_{n-j-1}(\beta) + b_{n-j}(\beta) + c_{n-j+1}(\beta) & \text{if} \quad 2 \leq j \leq n-3 \\ \bar{a}(\beta) + a_1(\beta) + b_2(\beta) + c_3(\beta) & \text{if} \quad j = n-2 \\ \bar{b}(\beta) + b_1(\beta) + c_2(\beta) & \text{if} \quad j = n-1 \\ \bar{c}(\beta) + c_1(\beta) & \text{if} \quad j = n \end{cases} \tag{7.86}$$

Then, Eq. (7.85) becomes

$$\begin{aligned} \frac{(\Delta t)^{1-\beta}}{\Gamma(4-\beta)} \sum_{j=0}^{n} \mathcal{A}_j \int_{R_{in}}^{R_{out}} \Phi(r,t)\nu \, dr &= \frac{(\Delta t)^{1-\beta}}{\Gamma(4-\beta)} \sum_{j=0}^{n} \mathcal{A}_j \int_{R_{in}}^{R_{out}} \left(\frac{\partial^2 u_\theta}{\partial r^2} + \frac{1}{r}\frac{\partial u_\theta}{\partial r} - \frac{u_\theta}{r^2} \right) \nu \, dr \\ &= \frac{(\Delta t)^{1-\beta}}{\Gamma(4-\beta)} \sum_{j=0}^{n} \mathcal{A}_j \int_{R_{in}}^{R_{out}} \left(-\frac{\partial u}{\partial r}\frac{\partial \nu}{\partial r} + \frac{1}{r}\frac{\partial u}{\partial r}\nu - \frac{u\nu}{r^2} \right) dr \\ &= \frac{(\Delta t)^{1-\beta}}{\Gamma(4-\beta)} \sum_{j=0}^{n} \mathcal{A}_j \int_{-1}^{1} \Bigg(-\Delta^{-2}\frac{\partial u}{\partial \tilde{r}}\frac{\partial v}{\partial \tilde{r}} + \Delta^{-1}\frac{1}{r}\frac{\partial u}{\partial \tilde{r}}\nu(\tilde{r}) \\ &\qquad - \frac{u}{r^2}\nu(\tilde{r}) \Bigg) \Delta d\tilde{r} \\ &= \frac{(\Delta t)^{1-\beta}}{\Gamma(4-\beta)} \sum_{j=0}^{n} \mathcal{A}_j \int_{-1}^{1} \Bigg(-\frac{1}{\Delta}\frac{\partial u}{\partial \tilde{r}}\frac{\partial v}{\partial \tilde{r}} + \frac{1}{r}\frac{\partial u}{\partial \tilde{r}}\nu(\tilde{r}) \\ &\qquad - \Delta\frac{u}{r^2}\nu(\tilde{r}) \Bigg) d\tilde{r} \end{aligned} \tag{7.87}$$

Then, the numerical approximation of the right-hand side gives

$$
\begin{aligned}
R.H.S \simeq & \frac{(\Delta t)^{1-\beta}}{\Gamma(4-\beta)} \sum_{j=0}^{n} \mathcal{A}_j \sum_{m=0}^{N} w_m \left[\frac{-1}{\Delta} \left(\sum_{j=0}^{N} U_j h_j'(\tilde{r}_m) \right) h_k'(\tilde{r}_m) \right. \\
& \left. + \frac{1}{r_m} \left(\sum_{j=0}^{N} U_j h_j'(\tilde{r}_m) \right) h_k(\tilde{r}_m) - \frac{\Delta}{r_m^2} \left(\sum_{j=0}^{N} U_j h_j(\tilde{r}_m) \right) h_k(\tilde{r}_m) \right] \\
= & \frac{(\Delta t)^{1-\beta}}{\Gamma(4-\beta)} \sum_{j=0}^{n} \mathcal{A}_j \sum_{m=0}^{N} w_m \left[\frac{-1}{\Delta} \left(\sum_{j=0}^{N} D_{m,j} U_j \right) D_{m,k} \right. \\
& \left. + \frac{1}{r_m} \left(\sum_{j=0}^{N} D_{m,j}\ U_j \right) \delta_{m,k} - \frac{\Delta}{r_m^2} U_m \delta_{m,k} \right] \\
= & \frac{(\Delta t)^{1-\beta}}{\Gamma(4-\beta)} \sum_{j=0}^{n} \mathcal{A}_j \left\{ \frac{-1}{\Delta} \sum_{j=0}^{N} \left(\sum_{m=0}^{N} w_m D_{m,j} D_{m,k} \right) U_j + \frac{w_k}{r_k} \sum_{j=0}^{N} D_{k,j} U_j \right. \\
& \left. - \frac{\Delta w_k}{r_k^2} U_k \right\} \\
= & \frac{(\Delta t)^{1-\beta}}{\Gamma(4-\beta)} \sum_{j=0}^{n} \mathcal{A}_j \left\{ -\frac{1}{\Delta} \sum_{j=0}^{N} B_{k,j} U_j + \frac{w_k}{r_k} \sum_{j=0}^{N} D_{k,j} U_j - \frac{\Delta w_k}{r_k^2} U_k \right\}
\end{aligned}
\tag{7.88}
$$

where $B_{j,k} = \sum_{m=0}^{N} w_m D_{m,j} D_{m,k}$.

Inserting these approximations with the spectral approximations in the weak formulation of the velocity equation (7.14), gives the full discretization

$$
\begin{aligned}
& \frac{\rho}{\mathbb{V}} \Delta w_k \left(\frac{3U_k^n - 4U_k^{n-1} + U_k^{n-2}}{2\Delta t} \right) + \frac{\rho}{\mathbb{G}} \frac{\Delta w_k}{(\Delta t)^{1+\alpha} \Gamma(2-\alpha)} \sum_{j=0}^{n} C_j U_k^j \\
& = \frac{(\Delta t)^{1-\beta}}{\Gamma(4-\beta)} \left\{ \mathcal{A}_0 \Phi(r, t_0) + \mathcal{A}_1 \left[-\frac{1}{\Delta} \sum_{l=0}^{N} B_{k,l} U_l^1 + \frac{w_k}{r_k} \sum_{l=0}^{N} D_{k,l} U_l^1 - \frac{\Delta w_k}{r_k^2} U_k^1 \right] \right. \\
& \quad + \sum_{j=2}^{n-3} \mathcal{A}_j \left[-\frac{1}{\Delta} \sum_{l=0}^{N} B_{k,l} U_l^j + \frac{w_k}{r_k} \sum_{l=0}^{N} D_{k,l} U_l^j - \frac{\Delta w_k}{r_k^2} U_k^j \right] \\
& \quad + \mathcal{A}_{n-2} \left[-\frac{1}{\Delta} \sum_{l=0}^{N} B_{k,l} U_l^{n-2} + \frac{w_k}{r_k} \sum_{l=0}^{N} D_{k,l} U_l^{n-2} - \frac{\Delta w_k}{r_k^2} U_k^{n-2} \right] \\
& \quad + \mathcal{A}_{n-1} \left[-\frac{1}{\Delta} \sum_{l=0}^{N} B_{k,l} U_l^{n-1} + \frac{w_k}{r_k} \sum_{l=0}^{N} D_{k,l} U_l^{n-1} - \frac{\Delta w_k}{r_k^2} U_k^{n-1} \right] \\
& \quad \left. + \mathcal{A}_n \left[-\frac{1}{\Delta} \sum_{l=0}^{N} B_{k,l} U_l^n + \frac{w_k}{r_k} \sum_{l=0}^{N} D_{k,l} U_l^n - \frac{\Delta w_k}{r_k^2} U_k^n \right] \right\}
\end{aligned}
\tag{7.89}
$$

For simplicity, we rewrite Eq.(7.89) as follows

$$\begin{aligned}
&\left[\frac{\rho}{\mathbb{V}}\frac{3\Delta w_k}{2\Delta t}+\frac{\rho}{\mathbb{G}}\frac{C_n\Delta w_k}{(\Delta t)^{1+\alpha}\Gamma(2-\alpha)}+\frac{\mathcal{A}_n}{(\Delta t)^{\beta-1}\Gamma(4-\beta)}\frac{\Delta w_k}{r_k^2}\right]U_k^n\\
&\qquad+\frac{\mathcal{A}_n}{(\Delta t)^{\beta-1}\Gamma(4-\beta)}\sum_{l=0}^{N}\left[\frac{1}{\Delta}B_{k,l}-\frac{w_k}{r_k}D_{k,l}\right]U_l^n\\
&\qquad=\frac{\mathcal{A}_{n-1}}{(\Delta t)^{\beta-1}\Gamma(4-\beta)}\sum_{l=0}^{N}\left[-\frac{1}{\Delta}B_{k,l}+\frac{w_k}{r_k}D_{k,l}\right]U_l^{n-1}\\
&\quad+\left[\frac{\rho}{\mathbb{V}}\frac{4\Delta w_k}{2\Delta t}-\frac{\rho}{\mathbb{G}}\frac{C_{n-1}\Delta w_k}{(\Delta t)^{1+\alpha}\Gamma(2-\alpha)}-\frac{\mathcal{A}_{n-1}}{(\Delta t)^{\beta-1}\Gamma(4-\beta)}\frac{\Delta w_k}{r_k^2}\right]U_k^{n-1}\\
&\quad+\left[\frac{\rho}{\mathbb{V}}\frac{\Delta w_k}{2\Delta t}-\frac{\rho}{\mathbb{G}}\frac{C_{n-2}\Delta w_k}{(\Delta t)^{1+\alpha}\Gamma(2-\alpha)}-\frac{\mathcal{A}_{n-2}}{(\Delta t)^{\beta-1}\Gamma(4-\beta)}\frac{\Delta w_k}{r_k^2}\right]U_k^{n-2}\\
&\qquad+\frac{\mathcal{A}_{n-2}}{(\Delta t)^{\beta-1}\Gamma(4-\beta)}\sum_{l=0}^{N}\left[-\frac{1}{\Delta}B_{k,l}+\frac{w_k}{r_k}D_{k,l}\right]U_l^{n-2}\\
&\qquad+\frac{(\Delta t)^{1-\beta}}{\Gamma(4-\beta)}\sum_{j=2}^{n-3}\left[\mathcal{A}_j\sum_{l=0}^{N}\left(-\frac{1}{\Delta}B_{k,l}+\frac{w_k}{r_k}D_{k,l}\right)\right]U_l^j\\
&\quad-\sum_{j=2}^{n-3}\left[\frac{\mathcal{A}_j}{(\Delta t)^{\beta-1}\Gamma(4-\beta)}\frac{\Delta w_k}{r_k^2}+\frac{\rho}{\mathbb{G}}\frac{C_j\Delta w_k}{(\Delta t)^{1+\alpha}\Gamma(2-\alpha)}\right]U_k^j\\
&\qquad+\frac{\mathcal{A}_1}{(\Delta t)^{\beta-1}\Gamma(4-\beta)}\left[\sum_{l=0}^{N}\left(-\frac{1}{\Delta}B_{k,l}+\frac{w_k}{r_k}D_{k,l}\right)\right]U_l^1\\
&\qquad-\left[\frac{\mathcal{A}_1}{(\Delta t)^{\beta-1}\Gamma(4-\beta)}\frac{\Delta w_k}{r_k^2}+\frac{\rho}{\mathbb{G}}\frac{C_1\Delta w_k}{(\Delta t)^{1+\alpha}\Gamma(2-\alpha)}\right]U_k^1 \qquad (7.90)
\end{aligned}$$

where the coefficients C_j and $\mathcal{A}_j$, $0\le j\le n$, are defined by Eq.(5.42) and Eq. (7.86), respectively.

Numerical Discretazation of Stress Equation

In Time

Now, we consider a second-order scheme to discrete Eq. (7.11), then we will derive the numerical approximation of the time-fractional derivative $D_t^{\beta}\gamma(t)$, and the numerical approximation of the time-fractional derivative $D_t^{\alpha}\tau(t)$ will be obtained by following Ch. 5 (sec.5.4.2) Eq. (5.59).

Define the right-hand side of Eq. (7.11), $D_t^\beta \gamma(t_n)$ in the Caputo sense as

$$D_t^\beta \gamma(t_n) = \frac{1}{\Gamma(1-\beta)} \int_0^t \frac{1}{(t-s)^\beta} \frac{d\gamma}{ds} ds \tag{7.91}$$

where

$$\frac{d\gamma}{ds} = \frac{\partial u}{\partial r}(r,s) - \frac{u(r,s)}{r} \tag{7.92}$$

then Eq.(7.91) becomes

$$D_t^\beta \gamma(t_n) = \frac{1}{\Gamma(1-\beta)} \int_0^t \frac{1}{(t-s)^\beta} \left\{ \frac{\partial u}{\partial r}(r,s) - \frac{u(r,s)}{r} \right\} ds \tag{7.93}$$

Let

$$\Upsilon(r,s) = \left(\frac{\partial u}{\partial r}(r,s) - \frac{u(r,s)}{r} \right) u_\theta \tag{7.94}$$

Now, we use a second-order discretization of the integral in time by using Eq.(5.5).

$$D_t^\beta \gamma(t_n) \simeq \frac{1}{\Gamma(1-\beta)} \left[\int_{t_{n-1}}^{t_n} (t_n - s)^{-\beta} \Pi_{2,n-1} \Upsilon(r,s) ds + \sum_{j=1}^{n-1} \int_{t_{j-1}}^{t_j} (t_n - s)^{-\beta} \Pi_{2,j} \Upsilon(r,s) ds \right] \tag{7.95}$$

To evaluate Eq.(7.95) we will follow the process in Eq.(7.75)- Eq.(7.84) and replacing $\Phi(r,s)$ by $\Upsilon(r,s)$.

Then, Eq. (7.95) becomes

$$\begin{aligned} D_t^\beta \gamma(t_n) &= \frac{(\Delta t)^{1-\beta}}{\Gamma(4-\beta)} \int_{R_{in}}^{R_{out}} \Big\{ a_{n-1}\Upsilon(t_0) + (a_{n-2}+b_{n-1})\Upsilon(t_1) + \sum_{j=2}^{n-3} (a_{n-j-1}+b_{n-j}+c_{n-j+1})\Upsilon(t_j) \\ &\quad + (\bar{a}+a_1+b_2+c_3)\Upsilon(t_{n-2}) + (\bar{b}+b_1+c_2)\Upsilon(t_{n-1}) + (c_1+\bar{c})\Upsilon(t_n) \Big\} \nu \, dr \\ &= \frac{(\Delta t)^{1-\beta}}{\Gamma(4-\beta)} \sum_{j=0}^{n} \mathcal{A}_j \int_{R_{in}}^{R_{out}} \Upsilon(r,t_j) \nu \, dr \end{aligned} \tag{7.96}$$

where $\mathcal{A}_j$, $0 \leq j \leq n$, are defined by Eq. (7.86).

Therefore, the approximation of Eq.(7.95) is given by

$$
\begin{aligned}
\frac{(\Delta t)^{1-\beta}}{\Gamma(4-\beta)} \sum_{j=0}^{n} \mathcal{A}_j \int_{R_{in}}^{R_{out}} \Upsilon(r,t_j)\nu \, dr &= \frac{(\Delta t)^{1-\beta}}{\Gamma(4-\beta)} \sum_{j=0}^{n} \mathcal{A}_j \int_{R_{in}}^{R_{out}} \left(\frac{\partial u_\theta}{\partial r} - \frac{u_\theta}{r} \right) \nu \, dr \\
&= \frac{(\Delta t)^{1-\beta}}{\Gamma(4-\beta)} \sum_{j=0}^{n} \mathcal{A}_j \int_{R_{in}}^{R_{out}} \left(\frac{\partial u}{\partial r}\nu - \frac{u}{r}\nu \right) dr \\
&= \frac{(\Delta t)^{1-\beta}}{\Gamma(4-\beta)} \sum_{j=0}^{n} \mathcal{A}_j \int_{-1}^{1} \left(\Delta^{-1} \frac{\partial u}{\partial \tilde{r}} \nu(\tilde{r}) - \frac{u}{r}\nu(\tilde{r}) \right) \Delta d\tilde{r} \\
&= \frac{(\Delta t)^{1-\beta}}{\Gamma(4-\beta)} \sum_{j=0}^{n} \mathcal{A}_j \int_{-1}^{1} \left(\frac{\partial u}{\partial \tilde{r}} \nu(\tilde{r}) - \Delta \frac{u}{r}\nu(\tilde{r}) \right) d\tilde{r} \\
&\simeq \frac{(\Delta t)^{1-\beta}}{\Gamma(4-\beta)} \sum_{j=0}^{n} \mathcal{A}_j \sum_{m=0}^{N} w_m \left[\left(\sum_{j=0}^{N} U_j h_j'(\tilde{r}_m) \right) h_k(\tilde{r}_m) \right. \\
&\quad \left. - \frac{\Delta}{r_m} \left(\sum_{j=0}^{N} U_j h_j(\tilde{r}_m) \right) h_k(\tilde{r}_m) \right] \\
&= \frac{(\Delta t)^{1-\beta}}{\Gamma(4-\beta)} \sum_{j=0}^{n} \mathcal{A}_j \sum_{m=0}^{N} w_m \left[\left(\sum_{j=0}^{N} D_{m,j} \; U_j \right) \delta_{m,k} - \frac{\Delta}{r_m} U_m \delta_{m,k} \right] \\
&= \frac{(\Delta t)^{1-\beta}}{\Gamma(4-\beta)} \sum_{j=0}^{n} \mathcal{A}_j \left\{ w_k \sum_{j=0}^{N} D_{k,j} U_j - \frac{\Delta w_k}{r_k} U_k \right\} \\
&= \frac{(\Delta t)^{1-\beta}}{\Gamma(4-\beta)} \sum_{j=0}^{n} \mathcal{A}_j \left\{ w_k \sum_{j=0}^{N} D_{k,j} U_j - \frac{\Delta w_k}{r_k} U_k \right\}
\end{aligned}
\tag{7.97}
$$

where the coefficients are defined by Eqs. (7.81) - (7.84).

To derive the discrete form of the weak formulation Eq. (7.15), we analyse each term individually.

$$
\begin{aligned}
\int_{R_{in}}^{R_{out}} \tau(t) \; v \; dr &= \Delta \int_{-1}^{1} \tau(t) \; v \; d\tilde{r} \\
&\simeq \Delta \sum_{l=0}^{N} w_l \left(\sum_{j=0}^{N} \tau_j h_j(\tilde{r}_l) \right) h_k(\tilde{r}_l) \\
&= \Delta \sum_{l=0}^{N} w_l \left(\tau_l \right) h_k(\tilde{r}_l) \\
&= \Delta w_k \tau_k^s
\end{aligned}
\tag{7.98}
$$

Here, we will use Eq. (5.59) to substitute the discretization of $D_t^\alpha \tau(t)$

$$\begin{aligned}\frac{\mathbb{V}}{\mathbb{G}}\int_{R_{in}}^{R_{out}} (D_t^\alpha \tau(t))\ v\ dr &= \Delta\frac{\mathbb{V}}{\mathbb{G}}\int_{-1}^{1} (D_t^\alpha \tau(t))\ v\ d\tilde{r} \\ &\simeq \Delta\frac{\mathbb{V}}{\mathbb{G}}\sum_{l=0}^{N} w_l\,(D_t^\alpha \tau_l)\,h_k(\tilde{r}_l) \\ &= \Delta w_k \frac{\mathbb{V}}{\mathbb{G}}\,(D_t^\alpha \tau_k) \\ &= \frac{\mathbb{V}}{\mathbb{G}}\frac{\Delta w_k}{(\Delta t)^\alpha \Gamma(3-\alpha)}\sum_{j=0}^{n} E_j\,U^j\end{aligned} \tag{7.99}$$

where the coefficients E_j, $0 \le j \le n$, are defined by Eq. (5.60).

$$\begin{aligned}\mathbb{V}\int_{R_{in}}^{R_{out}} \left(D_t^\beta \gamma(t)\right)\ v\ dr &= \Delta\mathbb{V}\int_{-1}^{1} \left(D_t^\beta \gamma(t)\right)\ v\ d\tilde{r} \\ &\simeq \Delta\mathbb{V}\sum_{l=0}^{N} w_l \left(D_t^\beta \gamma_l\right) h_k(\tilde{r}_l) \\ &= \Delta w_k \mathbb{V}\left(D_t^\beta \gamma_k(t_n)\right) \\ &= \frac{\Delta w_k \mathbb{V}}{(\Delta t)^{\beta-1}\Gamma(4-\beta)}\left\{\sum_{l=0}^{N} D_{k,l}\left[\sum_{j=0}^{n}\mathcal{A}_j\,U_l^j\right] - \frac{1}{r_k}\left[\sum_{j=0}^{n}\mathcal{A}_j\,U_k^j\right]\right\}\end{aligned} \tag{7.100}$$

Therefore, the full discretization is

$$\begin{aligned}\left[1+\frac{\mathbb{V}}{\mathbb{G}}\frac{E_n}{(\Delta t)^\alpha\Gamma(3-\alpha)}\right]\tau_k^n = &-\frac{\mathbb{V}}{\mathbb{G}}\frac{1}{(\Delta t)^\alpha\Gamma(3-\alpha)}\left[\sum_{j=0}^{n-1} E_j\,\tau_k^j\right] \\ &+\frac{\mathbb{V}}{(\Delta t)^{\beta-1}\Gamma(4-\beta)}\left\{\sum_{l=0}^{N} D_{k,l}\left[\sum_{j=0}^{n}\mathcal{A}_j\,U_l^j\right] - \frac{1}{r_k}\left[\sum_{j=0}^{n}\mathcal{A}_j\,U_k^j\right]\right\}\end{aligned} \tag{7.101}$$

7.3 Multi-mode Fractional Maxwell model spectrum of relaxation times

To investigate additional applications of fractional viscoelastic models, we will simulate Taylor-Couette flow using the Multi-Mode Fractional Maxwell Model (MM-FMM). This multi-mode approach enables the capture of a wide spectrum of relaxation behaviour,

enhancing the simulation's ability to accurately represent the dynamics of complex fluids. By integrating multiple relaxation modes, the model more effectively reflects the complex relaxation processes observed in real-world non-Newtonian materials, establishing it as a powerful tool for analyzing their behaviour in rotating flow systems.

7.3.1 Taylor-Couette problem

Consider the momentum equation

$$\rho\left(\frac{\partial u}{\partial t}\right) = \left(\frac{2}{r} + \frac{\partial}{\partial r}\right)\tau_{r\theta}(t) \tag{7.102}$$

and the multi-mode fractional Maxwell model is given by

$$\left(1 + \frac{\mathbb{V}}{\mathbb{G}_1}\frac{d^{\alpha_1}}{dt^{\alpha_1}} + \frac{\mathbb{V}}{\mathbb{G}_2}\frac{d^{\alpha_2}}{dt^{\alpha_2}}\right)\tau_{r\theta}(t) = \mathbb{V}\frac{d^{\beta}}{dt^{\beta}}\gamma(t) \tag{7.103}$$

where $\eta = E\,\lambda^{\beta} = \mathbb{V}$, $\lambda^{\alpha_1} = \dfrac{\mathbb{V}}{\mathbb{G}_1}$, $\lambda^{\alpha_2} = \dfrac{\mathbb{V}}{\mathbb{G}_2}$, and $0 < \alpha_2 < \alpha_1 \leq \beta \leq 1$.
Using the Caputo definition, the derivatives $\dfrac{d^{\alpha_1}\tau}{dt^{\alpha_1}}$, $\dfrac{d^{\alpha_2}\tau}{dt^{\alpha_2}}$ and $\dfrac{d^{\beta}\gamma}{dt^{\beta}}$ can be expressed in their corresponding integral forms as follows:

$$\frac{d^{\alpha_1}\tau}{dt^{\alpha_1}} = \frac{1}{\Gamma(1-\alpha_1)}\int_0^t \frac{1}{(t-s)^{\alpha_1}}\frac{\partial\tau}{\partial s}ds \tag{7.104}$$

and

$$\frac{d^{\alpha_2}\tau}{dt^{\alpha_2}} = \frac{1}{\Gamma(1-\alpha_2)}\int_0^t \frac{1}{(t-s)^{\alpha_2}}\frac{\partial\tau}{\partial s}ds \tag{7.105}$$

also, we have

$$\begin{aligned}\frac{d^{\beta}\gamma}{dt^{\beta}} &= \frac{1}{\Gamma(1-\beta)}\int_0^t \frac{1}{(t-s)^{\beta}}\frac{\partial\gamma}{\partial s}ds \\ &= \frac{1}{\Gamma(1-\beta)}\int_0^t \frac{1}{(t-s)^{\beta}}\left\{\frac{\partial u}{\partial r} - \frac{u}{r}\right\}ds\end{aligned} \tag{7.106}$$

For this flow, when $\beta = 1$, the time derivative of γ is given by

$$\frac{\partial\gamma}{\partial t} = \frac{\partial u_\theta}{\partial r} - \frac{u_\theta}{r}$$

However, when $\beta \neq 1$, the entire history of deformations is taken into account. Applying the operator $\left(\frac{2}{r}+\frac{\partial}{\partial r}\right)$ into both sides of Eq. (7.103) to obtain

$$\left(\frac{2}{r}+\frac{\partial}{\partial r}\right)\left(1+\frac{\mathbb{V}}{\mathbb{G}_1}\frac{d^{\alpha_1}}{dt^{\alpha_1}}+\frac{\mathbb{V}}{\mathbb{G}_2}\frac{d^{\alpha_2}}{dt^{\alpha_2}}\right)\tau_{r\theta}(t)=\mathbb{V}\left(\frac{2}{r}+\frac{\partial}{\partial r}\right)\frac{d^{\beta}}{dt^{\beta}}\gamma(t) \tag{7.107}$$

Then applying the operator $\left(1+\frac{\mathbb{V}}{\mathbb{G}_1}\frac{d^{\alpha_1}}{dt^{\alpha_1}}+\frac{\mathbb{V}}{\mathbb{G}_2}\frac{d^{\alpha_2}}{dt^{\alpha_2}}\right)$ to both sides of Eq. (7.102), and using Eq. (7.107) we obtain

$$\begin{aligned}\rho\left(1+\frac{\mathbb{V}}{\mathbb{G}_1}\frac{d^{\alpha_1}}{dt^{\alpha_1}}+\frac{\mathbb{V}}{\mathbb{G}_2}\frac{d^{\alpha_2}}{dt^{\alpha_2}}\right)\frac{\partial u}{\partial t}&=\left(\frac{2}{r}+\frac{\partial}{\partial r}\right)\left(1+\frac{\mathbb{V}}{\mathbb{G}_1}\frac{d^{\alpha_1}}{dt^{\alpha_1}}+\frac{\mathbb{V}}{\mathbb{G}_2}\frac{d^{\alpha_2}}{dt^{\alpha_2}}\right)\tau_{\theta}\\&=\mathbb{V}\left(\frac{2}{r}+\frac{\partial}{\partial r}\right)\frac{d^{\beta}}{dt^{\beta}}\gamma(t)\\&=\mathbb{V}\left(\frac{2}{r}+\frac{\partial}{\partial r}\right)\frac{1}{\Gamma(1-\beta)}\int_0^t\frac{1}{(t_n-s)^{\beta}}\left\{\frac{\partial u}{\partial r}-\frac{u}{r}\right\}ds\\&=\frac{\mathbb{V}}{\Gamma(1-\beta)}\int_0^t\frac{1}{(t_n-s)^{\beta}}\left\{\frac{\partial^2 u}{\partial r^2}+\frac{1}{r}\frac{\partial u}{\partial r}-\frac{u}{r^2}\right\}ds\end{aligned} \tag{7.108}$$

to obtain the following system of equations in integral form

$$\rho\left(1+\frac{\mathbb{V}}{\mathbb{G}_1}\frac{d^{\alpha_1}}{dt^{\alpha_1}}+\frac{\mathbb{V}}{\mathbb{G}_2}\frac{d^{\alpha_2}}{dt^{\alpha_2}}\right)\frac{\partial u_\theta}{\partial t}=\frac{\mathbb{V}}{\Gamma(1-\beta)}\int_0^t(t_n-s)^{-\beta}\left(\frac{\partial^2 u_\theta}{\partial r^2}+\frac{1}{r}\frac{\partial u_\theta}{\partial r}-\frac{u_\theta}{r^2}\right)ds \tag{7.109}$$

$$\rho\left(1+\frac{\mathbb{V}}{\mathbb{G}_1}\frac{d^{\alpha_1}}{dt^{\alpha_1}}+\frac{\mathbb{V}}{\mathbb{G}_2}\frac{d^{\alpha_2}}{dt^{\alpha_2}}\right)\tau_{\theta}=\frac{\mathbb{V}}{\Gamma(1-\beta)}\int_0^t(t_n-s)^{-\beta}\left(\frac{\partial u_\theta}{\partial r}-\frac{u_\theta}{r}\right)ds \tag{7.110}$$

Replacing the ordinary differential operator by the fractional differential operator gives

$$\frac{\rho}{\mathbb{V}}\frac{\partial u}{\partial t}+\frac{\rho}{\mathbb{G}_1}D_t{}^{\alpha_1}\left(\frac{\partial u}{\partial t}\right)+\frac{\rho}{\mathbb{G}_2}D_t{}^{\alpha_2}\left(\frac{\partial u}{\partial t}\right)=\frac{1}{\Gamma(1-\beta)}\int_0^t(t_n-s)^{-\beta}\left(\frac{\partial^2 u_\theta}{\partial r^2}+\frac{1}{r}\frac{\partial u_\theta}{\partial r}-\frac{u_\theta}{r^2}\right)ds \tag{7.111}$$

$$\tau_\theta+\frac{\mathbb{V}}{\mathbb{G}_1}D_t^{\alpha_1}\tau_\theta+\frac{\mathbb{V}}{\mathbb{G}_2}D_t^{\alpha_2}\tau_\theta=\frac{\mathbb{V}}{\Gamma(1-\beta)}\int_0^t(t_n-s)^{-\beta}\left(\frac{\partial u_\theta}{\partial r}-\frac{u_\theta}{r}\right)ds \tag{7.112}$$

with Dirichlet boundary conditions

$$u_\theta(R_{in},t)=\Theta_i(t),\quad u_\theta(R_{out},t)=\Theta_0(t),\quad 0<t<T \tag{7.113}$$

and initial conditions

$$u_\theta(r,0) = \frac{\partial u_\theta(r,0)}{\partial t} = 0, \quad \tau_{r,\theta}(r,0) = 0, \quad R_{in} < r < R_{out} \tag{7.114}$$

The Weak Formulation

To obtain the full discretization of the Taylor-Couette problem Eqs. (7.111) and (7.112), first, we find their weak formulations by multiplying them by a test function $v \in W$ and integrating over the domain $[R_{in}, R_{out}]$. Then the weak formulations become:

$$\frac{\rho}{\mathbb{V}} \int_{R_{in}}^{R_{out}} \left(\frac{\partial u}{\partial t}\right) v\, dr + \frac{\rho}{\mathbb{G}_1} \int_{R_{in}}^{R_{out}} \left(\mathcal{D}_t^{1+\alpha_1}\, u_\theta\right) v\, dr + \frac{\rho}{\mathbb{G}_2} \int_{R_{in}}^{R_{out}} \left(\mathcal{D}_t^{1+\alpha_2}\, u_\theta\right) v\, dr = \mathbb{V} \int_{R_{in}}^{R_{out}} \left(\mathcal{D}_t^{\beta} \gamma(t)\right) \nu\, dr \tag{7.115}$$

$$\int_{R_{in}}^{R_{out}} \tau(t)\, \nu\, dr + \lambda^{\alpha_1} \int_{R_{in}}^{R_{out}} (\mathcal{D}_t^{\alpha_1} \tau(t))\, \nu\, dr + \lambda^{\alpha_2} \int_{R_{in}}^{R_{out}} (\mathcal{D}_t^{\alpha_2} \tau(t))\, \nu\, dr = \mathbb{V} \int_{R_{in}}^{R_{out}} \left(\mathcal{D}_t^{\beta} \gamma(t)\right) \nu\, dr \tag{7.116}$$

7.3.2 A first-order difference scheme for a time-fractional derivative

We extend the numerical discretization approach for the Fractional Maxwell model, outlined in Sec. 7.2.2, by including the first-order numerical approximation of the time derivative to handle α_1 and α_2. Furthermore, we apply spectral approximations to the spatial derivative to complete the discretization of the problem.

Numerical Discretization of the Velocity Equation

The full discretization of the velocity equation is

$$\begin{aligned}
&\frac{\rho}{\mathbb{V}}\Delta w_k\left(\frac{U_k^n-U_k^{n-1}}{\Delta t}\right)+\frac{\rho}{\mathbb{G}_1}\frac{\Delta w_k}{(\Delta t)^{\alpha_1+1}\Gamma(2-\alpha_1)}\Bigg[\tilde{a}_0(\alpha_1)\left(U_k^n-U_k^{n-1}\right)\\
&\qquad-\sum_{j=1}^{n-1}\left(\tilde{a}_j(\alpha_1)-\tilde{a}_{j-1}(\alpha_1)\right)\left(U_k^{n-j}-U_k^{n-j-1}\right)-\tilde{a}_{n-1}(\alpha_1)\Phi_i^0\Bigg]\\
&+\frac{\rho}{\mathbb{G}_2}\frac{\Delta w_k}{(\Delta t)^{\alpha_2+1}\Gamma(2-\alpha_2)}\Bigg[\tilde{a}_0(\alpha_2)\left(U_k^n-U_k^{n-1}\right)-\sum_{j=1}^{n-1}\left(\tilde{a}_j(\alpha_2)-\tilde{a}_{j-1}(\alpha_2)\right)\left(U_k^{n-j}-U_k^{n-j-1}\right)\\
&\qquad-\tilde{a}_{n-1}(\alpha_2)\Phi_i^0\Bigg]\\
&=\frac{(\Delta t)^{2-\beta}}{\Gamma(3-\beta)}\Bigg\{f_{n-1}\Phi(r_i,t_0)+\sum_{j=1}^{n-1}(f_{n-j-1}+g_{n-j})\left[\frac{-1}{\Delta}\sum_{l=0}^{N}B_{k,l}U_l^j+\frac{w_k}{r_k}\sum_{l=0}^{N}D_{k,l}U_l^j-\frac{\Delta w_k}{r_k^2}U_k^j\right]\\
&\qquad+g_0\left[\frac{-1}{\Delta}\sum_{l=0}^{N}B_{k,j}U_l^n+\frac{w_k}{r_k}\sum_{l=0}^{N}D_{k,l}U_l^n-\frac{\Delta w_k}{r_k^2}U_k^n\right]\Bigg\}
\end{aligned}\tag{7.117}$$

where $B_{k,j}=\sum_{l=0}^{N}w_lD_{l,j}D_{l,k}$, $1\le k\le N-1$.

Rearranging and multiplying by Δt:

$$\begin{aligned}
&\left[\frac{\rho}{\mathbb{V}}\Delta w_k+\frac{\rho}{\mathbb{G}_1}\frac{\tilde{a}_0(\alpha_1)}{(\Delta t)^{\alpha_1}}\frac{\Delta w_k}{\Gamma(2-\alpha_1)}+\frac{\rho}{\mathbb{G}_2}\frac{\tilde{a}_0(\alpha_2)}{(\Delta t)^{\alpha_2}}\frac{\Delta w_k}{\Gamma(2-\alpha_2)}+\frac{g_0(\Delta t)^{3-\beta}}{\Gamma(3-\beta)}\frac{\Delta w_k}{r_k^2}\right]U_k^n\\
&\qquad+\frac{g_0\,(\Delta t)^{3-\beta}}{\Gamma(3-\beta)}\left[\frac{1}{\Delta}\sum_{l=0}^{N}B_{k,l}U_l^n-\frac{w_k}{r_k}\sum_{l=0}^{N}D_{k,l}U_l^n\right]\\
&\quad=\left[\frac{\rho}{\mathbb{V}}\Delta w_k+\frac{\rho}{\mathbb{G}_1}\frac{\tilde{a}_0(\alpha_1)\,\Delta w_k}{(\Delta t)^{\alpha_1}\Gamma(2-\alpha_1)}+\frac{\rho}{\mathbb{G}_2}\frac{\tilde{a}_0(\alpha_2)\,\Delta w_k}{(\Delta t)^{\alpha_2}\Gamma(2-\alpha_2)}\right]U_k^{n-1}\\
&\qquad-\frac{\rho}{\mathbb{G}_1}\frac{\Delta w_k}{(\Delta t)^{\alpha_1}\Gamma(2-\alpha)}\left[\sum_{j=1}^{n-1}\left(\tilde{a}_j(\alpha_1)-\tilde{a}_{j-1}(\alpha_1)\right)\left(U_k^{n-j}-U_k^{n-j-1}\right)\right]\\
&\qquad-\frac{\rho}{\mathbb{G}_2}\frac{\Delta w_k}{(\Delta t)^{\alpha_2}\Gamma(2-\alpha)}\left[\sum_{j=1}^{n-1}\left(\tilde{a}_j(\alpha_2)-\tilde{a}_{j-1}(\alpha_2)\right)\left(U_k^{n-j}-U_k^{n-j-1}\right)\right]\\
&+\frac{(\Delta t)^{3-\beta}}{\Gamma(3-\beta)}\left\{\sum_{j=1}^{n-1}(f_{n-j-1}+g_{n-j})\left[\frac{-1}{\Delta}\sum_{l=0}^{N}B_{k,l}U_l^j+\frac{w_k}{r_k}\sum_{l=0}^{N}D_{k,l}U_l^j-\frac{\Delta w_k}{r_k^2}U_k^j\right]\right\},\quad 1\le k\le N-1
\end{aligned}\tag{7.118}$$

where the coefficients $\tilde{a}_{n-j}(\alpha_1)$, $\tilde{a}_{n-j}(\alpha_2)$ are defined by Eq.(7.24) with respect to α_1 and α_2, and the coefficients f_l, g_l, f_0, and g_0 defined by Eq.(7.35)- Eq.(7.38).
In addition, we have the initial condition

$$U_i^0 = \Phi_i(r_i, t_0) = 0, \qquad 0 \leq i \leq N, \tag{7.119}$$

and the boundary conditions are

$$U_0^n = 0, \quad U_N^n = 0, \quad n \geq 1 \tag{7.120}$$

Numerical Discretization of the Stress Equation

The full discretization of the stress equation is

$$\begin{aligned}
&\Delta w_k \left\{ 1 + \frac{\mathbb{V}}{\mathbb{G}_1} \frac{\tilde{B}_n(\alpha_1)}{(\Delta t)^{\alpha_1}\Gamma(2-\alpha_1)} + \frac{\mathbb{V}}{\mathbb{G}_2} \frac{\tilde{B}_n(\alpha_2)}{(\Delta t)^{\alpha_2}\Gamma(2-\alpha_2)} \right\} \tau_k^n \\
&\qquad = -\frac{\mathbb{V}}{\mathbb{G}_1} \frac{\Delta w_k}{(\Delta t)^{\alpha_1}\Gamma(2-\alpha_1)} \left\{ \sum_{j=1}^{n-1} \tilde{B}_j(\alpha_1)\tau_k^j + \tilde{B}_0(\alpha_1)\tau_k^0 \right\} \\
&\qquad\quad - \frac{\mathbb{V}}{\mathbb{G}_2} \frac{\Delta w_k}{(\Delta t)^{\alpha_2}\Gamma(2-\alpha_2)} \left\{ \sum_{j=1}^{n-1} \tilde{B}_j(\alpha_2)\tau_k^j + \tilde{B}_0(\alpha_2)\tau_k^0 \right\} \\
&\quad + \frac{\mathbb{V} w_k}{(\Delta t)^{\beta-1}\Gamma(3-\beta)} \left\{ \sum_{l=0}^{n} \bar{A}_l \left(\sum_{m=0}^{N} D_{k,m} U_m^l \right) \right\} - \frac{\mathbb{V}\Delta w_k}{r_k(\Delta t)^{\beta-1}\Gamma(3-\beta)} \left\{ \sum_{l=0}^{n} \bar{A}_l U_k^l \right\}
\end{aligned} \tag{7.121}$$

where the coefficients $\tilde{B}_j(\alpha_1)$, $\tilde{B}_j(\alpha_2)$ are defined by Eq.(5.38) with respect to α_1 and α_2, and $\bar{A}_l$ is defined by Eq.(7.61).

7.3.3 Numerical Results

In this section, we will carry out additional experiments using the same data from Chapter 6 (Section. 6.6). To solve the system of differential equations governing the unsteady unidirectional flow of the MM-FMM when $0 < \alpha_2 < \alpha_1 < \beta < 1$ in an annular geometry, we have developed a MATLAB code for the proposed numerical method with the following

fluid parameters $\mathbb{V} = 5$, $\lambda_1 \equiv \frac{\mathbb{V}}{\mathbb{G}_1} = 1 \times 10^{-5}[s^{1-\beta} \approx s]$, $\lambda_2 \equiv \frac{\mathbb{V}}{\mathbb{G}_2} = 1 \times 10^{-6}[s^{1-\beta} \approx s]$ (where $\lambda_2 < \lambda_1$), $\mathbb{G}_1 = \frac{\mathbb{V}}{\lambda_1}$, $\mathbb{G}_2 = \frac{\mathbb{V}}{\lambda_2}$, $\nu = \frac{\mu}{\rho} = \frac{\mathbb{V}}{\rho} = 2 \times 10^{-3} m^2.s^{-1}$ (ν is the kinematic, ρ is the dynamic viscosity). We examine the evolution of velocity and stress profiles at various radial locations, presented for a Newtonian fluid in Fig. 7.4 with the final time $T = 80$, the number of time steps $S = 1000$, and $N = 64$, and the final time $T = 120$, the number of time steps $S = 5000$, and $N = 24$ for a non-Newtonian fluid in Fig. 7.5. Figure 7.6 shows the effect of the use of the fractional order on the temporal evolution of the velocity and shear stress, and the stress relaxation obtained for the MM-FMM model. The results are consistent with previous findings of the FMM, demonstrating similar relaxation behaviour.

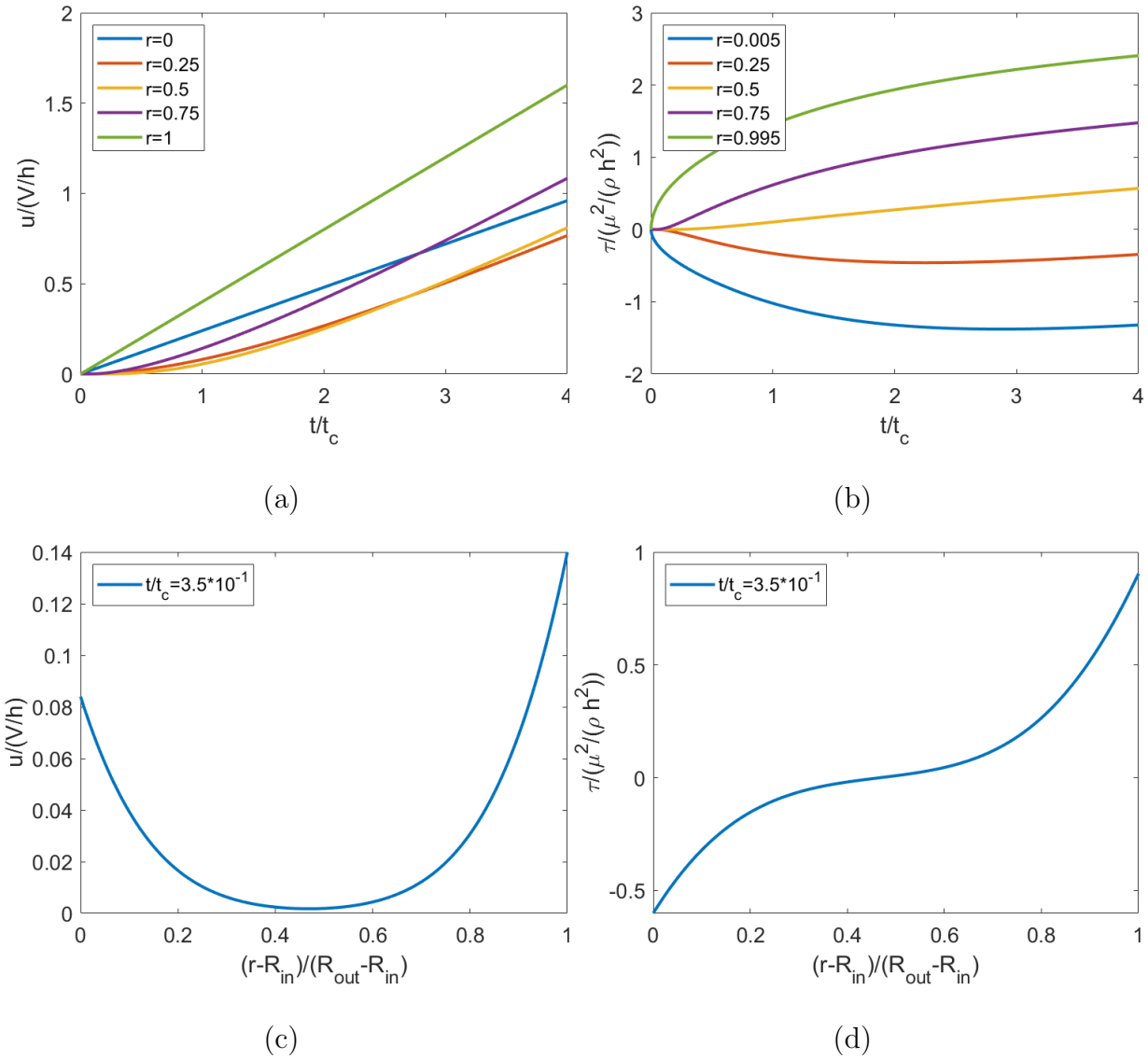

Figure 7.4: (a),(b) Variation of velocity and shear stress with time, in different regions; (c),(d) Velocity and shear stress profiles for $t/t_c = 3.50 \times 10^{-1}$. The fractional parameters: $\alpha_2 = 0.4$, $\alpha_1 = 0.8$, and $\beta = 0.999$.

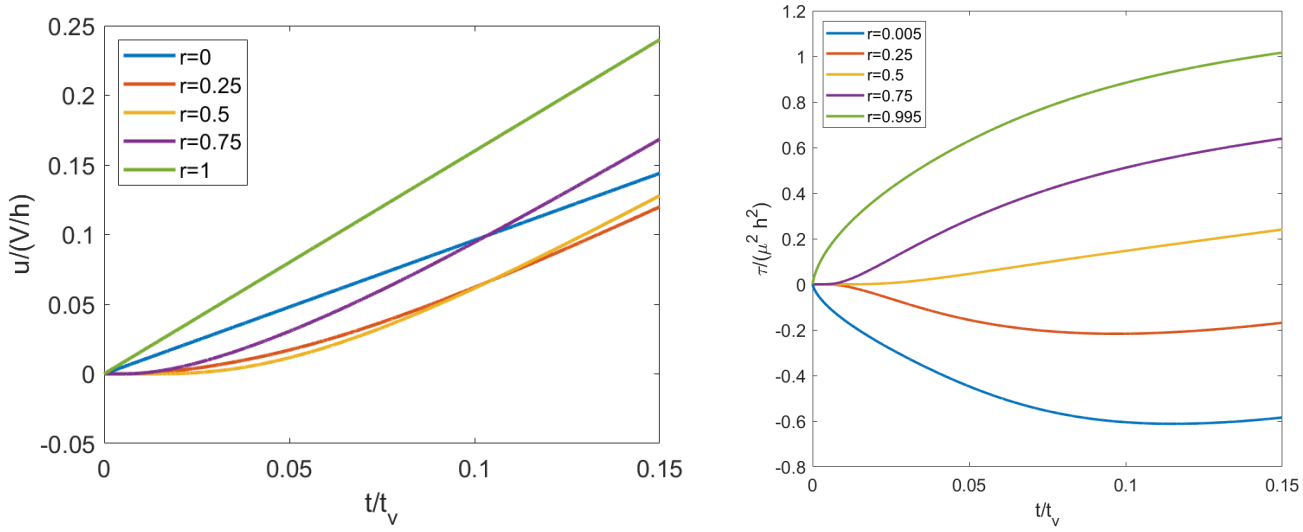

(a) (b)

Figure 7.5: (a) Evolution of velocity at radial location $\bar{r} = 0.25,\ 0.5,\ 0.75$; (b) Shear stress at radial location $\bar{r} = 0.005,\ 0.25,\ 0.5,\ 0.57,\ 0.995$. The fractional parameters: $\alpha_2 = 0.1$, $\alpha_1 = 0.4$, and $\beta = 0.8$.

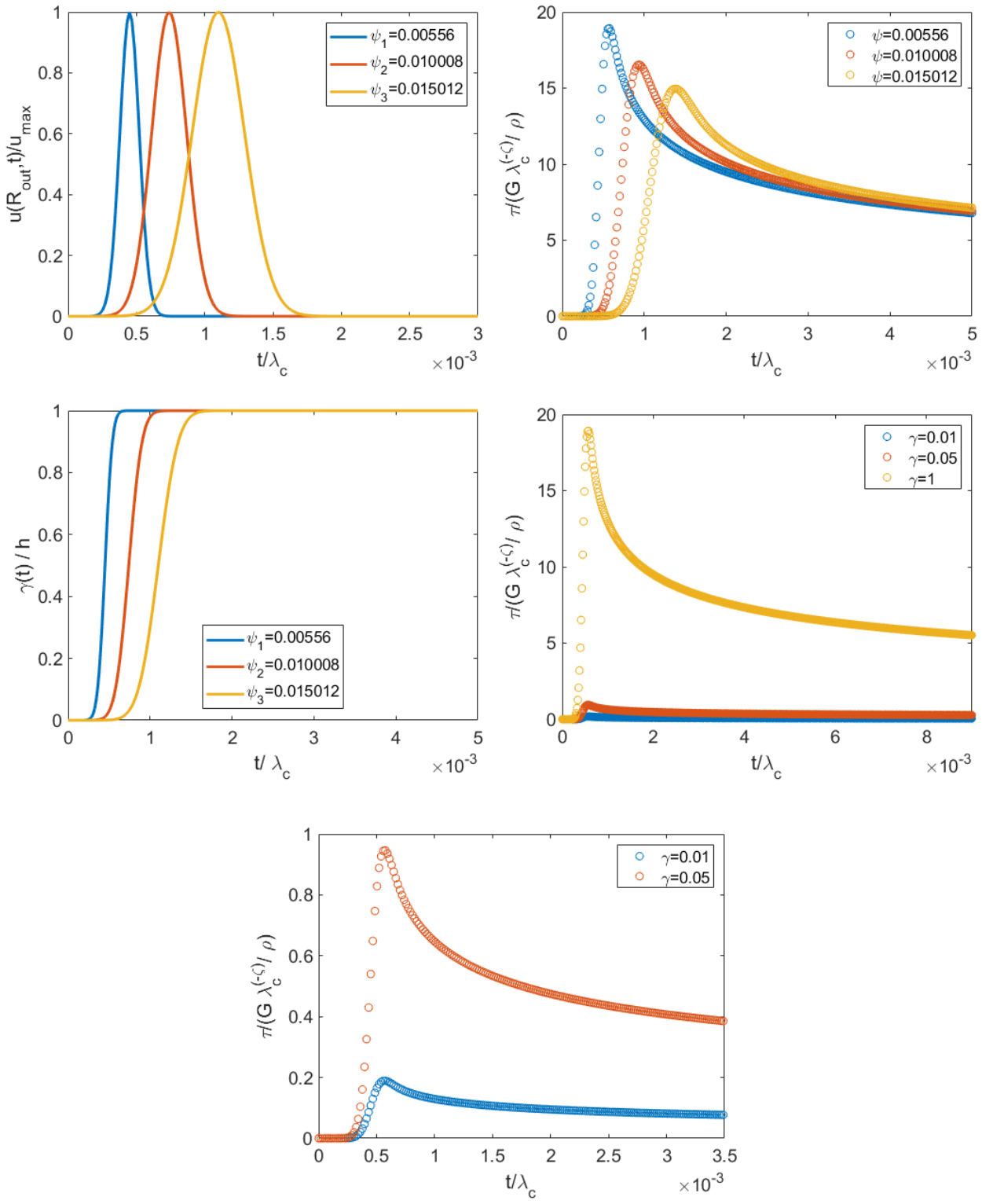

Figure 7.6: (a) Normalized tangential velocity of the outer cylinder; (b) Normalised shear stress relaxation obtained for a step-strain test with deformation of $\gamma_0 = 100\%$, $\beta = 0.999$, $\alpha_1 = 0.8$, $\alpha_2 = 0.6$, $N = 64$ and three different levels of refinement; (b) Evolution of the deformation in time for the three different tangential velocities imposed; (c) Stress relaxation for three different deformations; (d) Zoomed view of the stress relation obtained for the two smaller deformations.

7.3.4 A second-order difference scheme for a time-fractional derivative

In this section, we focus on improving the precision of our numerical method for the multi-mode fractional Maxwell model. To achieve this, we will extend the second-order numerical approximation of the time derivative and spectral approximation of the spatial derivative that we derived in Sec. 7.2.4.

Numerical Discretization of the Velocity Equation

We extend the numerical discretization in Eq. (7.73) to account for α_1 and α_2, thereby discretizing $\mathcal{D}_{t_n}^{1+\alpha_1} u_\theta$ and $\mathcal{D}_{t_n}^{1+\alpha_2} u_\theta$. Then, we apply spectral approximations to Eq. (7.115) to obtain the full discretization as follows:

$$
\begin{aligned}
&\left[\frac{\rho}{\mathbb{V}}\frac{3\Delta w_k}{2\Delta t}+\frac{\rho}{\mathbb{G}_1}\frac{C_n(\alpha_1)\Delta w_k}{(\Delta t)^{1+\alpha_1}\Gamma(2-\alpha_1)}+\frac{\rho}{\mathbb{G}_2}\frac{C_n(\alpha_2)\Delta w_k}{(\Delta t)^{1+\alpha_2}\Gamma(2-\alpha_2)}+\frac{\mathcal{A}_n(\beta)}{(\Delta t)^{\beta-1}\Gamma(4-\beta)}\frac{\Delta w_k}{r_k^2}\right]U_k^n\\
&+\frac{\mathcal{A}_n(\beta)}{(\Delta t)^{\beta-1}\Gamma(4-\beta)}\sum_{l=0}^{N}\left[\frac{1}{\Delta}B_{k,l}-\frac{w_k}{r_k}D_{k,l}\right]U_l^n=\frac{\mathcal{A}_{n-1}(\beta)}{(\Delta t)^{\beta-1}\Gamma(4-\beta)}\sum_{l=0}^{N}\left[-\frac{1}{\Delta}B_{k,l}+\frac{w_k}{r_k}D_{k,l}\right]U_l^{n-1}\\
&+\left[\frac{\rho}{\mathbb{V}}\frac{4\Delta w_k}{2\Delta t}-\frac{\rho}{\mathbb{G}_1}\frac{C_{n-1}(\alpha_1)\Delta w_k}{(\Delta t)^{1+\alpha_1}\Gamma(2-\alpha_1)}-\frac{\rho}{\mathbb{G}_2}\frac{C_{n-1}(\alpha_2)\Delta w_k}{(\Delta t)^{1+\alpha_2}\Gamma(2-\alpha_2)}-\frac{\mathcal{A}_{n-1}(\beta)}{(\Delta t)^{\beta-1}\Gamma(4-\beta)}\frac{\Delta w_k}{r_k^2}\right]U_k^{n-1}\\
&+\left[\frac{\rho}{\mathbb{V}}\frac{\Delta w_k}{2\Delta t}-\frac{\rho}{\mathbb{G}_1}\frac{C_{n-2}(\alpha_1)\Delta w_k}{(\Delta t)^{1+\alpha_1}\Gamma(2-\alpha_1)}-\frac{\rho}{\mathbb{G}_2}\frac{C_{n-2}(\alpha_2)\Delta w_k}{(\Delta t)^{1+\alpha_2}\Gamma(2-\alpha_2)}-\frac{\mathcal{A}_{n-2}(\beta)}{(\Delta t)^{\beta-1}\Gamma(4-\beta)}\frac{\Delta w_k}{r_k^2}\right]U_k^{n-2}\\
&\qquad+\frac{\mathcal{A}_{n-2}(\beta)}{(\Delta t)^{\beta-1}\Gamma(4-\beta)}\sum_{l=0}^{N}\left[-\frac{1}{\Delta}B_{k,l}+\frac{w_k}{r_k}D_{k,l}\right]U_l^{n-2}\\
&\qquad+\frac{(\Delta t)^{1-\beta}}{\Gamma(4-\beta)}\sum_{j=2}^{n-3}\left[\mathcal{A}_j(\beta)\sum_{l=0}^{N}\left(-\frac{1}{\Delta}B_{k,l}+\frac{w_k}{r_k}D_{k,l}\right)\right]U_l^j\\
&-\sum_{j=2}^{n-3}\left[\frac{\mathcal{A}_j(\beta)}{(\Delta t)^{\beta-1}\Gamma(4-\beta)}\frac{\Delta w_k}{r_k^2}+\frac{\rho}{\mathbb{G}_1}\frac{C_j(\alpha_1)\Delta w_k}{(\Delta t)^{1+\alpha_1}\Gamma(2-\alpha_1)}+\frac{\rho}{\mathbb{G}_2}\frac{C_j(\alpha_2)\Delta w_k}{(\Delta t)^{1+\alpha_2}\Gamma(2-\alpha_2)}\right]U_k^j\\
&+\frac{\mathcal{A}_1(\beta)}{(\Delta t)^{\beta-1}\Gamma(4-\beta)}\left[-\frac{1}{\Delta}\sum_{l=0}^{N}B_{k,l}U_l^1+\frac{w_k}{r_k}\sum_{l=0}^{N}D_{k,l}U_l^1-\frac{\Delta w_k}{r_k^2}U_k^1\right]+\frac{\mathcal{A}_0(\beta)}{(\Delta t)^{\beta-1}\Gamma(4-\beta)}\Phi(r,t_0)
\end{aligned}
\tag{7.122}
$$

where the coefficients C_j and $\mathcal{A}_j$, $0 \le j \le n$ are defined by Eq. (5.42) and Eq. (7.86), respectively.

Numerical Discretization of the Stress Equation

To discretize $\mathcal{D}_t^{\alpha_1}\tau(t)$ and $\mathcal{D}_t^{\alpha_2}\tau(t)$, we extend the numerical discretization method from Sec. 5.4.2 (Eq. (5.58)) to handle α_1 and α_2. Additionally, the numerical discretization of $\mathcal{D}_t^{\beta}\gamma(t)$ from Eq. (7.97) is implemented in Eq. (7.116). Finally, spectral approximations are applied to obtain the full discretization as follows:

$$\begin{aligned}
&\left[1+\frac{\mathbb{V}}{\mathbb{G}_1}\frac{E_n(\alpha_1)}{(\Delta t)^{\alpha_1}\Gamma(3-\alpha_1)}+\frac{\mathbb{V}}{\mathbb{G}_2}\frac{E_n(\alpha_2)}{(\Delta t)^{\alpha_2}\Gamma(3-\alpha_2)}\right]\tau_k^n \\
&\quad=-\frac{\mathbb{V}}{\mathbb{G}_1}\frac{1}{(\Delta t)^{\alpha_1}\Gamma(3-\alpha_1)}\left[\sum_{j=0}^{n-1}E_j(\alpha_1)\,\tau_k^j\right]-\frac{\mathbb{V}}{\mathbb{G}_2}\frac{1}{(\Delta t)^{\alpha_2}\Gamma(3-\alpha_2)}\left[\sum_{j=0}^{n-1}E_j(\alpha_2)\,\tau_k^j\right] \\
&\qquad+\frac{\mathbb{V}}{(\Delta t)^{\beta-1}\Gamma(4-\beta)}\left\{\sum_{l=0}^{N}D_{k,l}\left[\sum_{j=0}^{n}\mathcal{A}_j(\beta)\,U_l^j\right]-\frac{1}{r_k}\left[\sum_{j=0}^{n}\mathcal{A}_j(\beta)\,U_k^j\right]\right\} \qquad (7.123)
\end{aligned}$$

where the coefficients E_j and $\mathcal{A}_j$, $0\le j\le n$ are defined by Eq. (5.60) and Eq. (7.86), respectively.

7.4 Conclusions

This chapter presents highly accurate numerical methods for approximating the Caputo fractional derivative, focusing on applications on the Fractional Maxwell models and the Taylor-Couette problem. First-order and second-order temporal difference schemes were developed for two fractional order ranges $0<\alpha<1$ and $1<\alpha<2$. These schemes were constructed using polynomial interpolation techniques and finite difference methods, achieving truncation errors of $O(\Delta t)$ and $O(\Delta t^2)$, respectively. They were employed to discretize time-dependent fractional differential equations, which, when combined with spectral methods for spatial discretization, enabled simulations of Newtonian and viscoelastic fluid behaviours. To solve the Taylor-Couette flow problem, the study combined these time-stepping methods with spectral techniques for the spatial discretization. The simulations successfully modelled both Newtonian and viscoelastic fluids, showing good agreement with previous research. The results captured key features of viscoelastic fluids, such as delayed momentum transfer and smoother stress relaxation. Additionally, the

study introduced the multi-mode Fractional Maxwell Model (MM-FMM), which improves fluid behaviour predictions by considering multiple relaxation times. Experiments showed that adjusting fractional order parameters changes the relaxation speed with smaller values of β slowing it down, while larger values make the fluid behave more like a Newtonian fluid as presented in the previous Chapter. Furthermore, a second-order temporal scheme was derived for both the single-mode and multi-mode Fractional Maxwell models. These higher-order schemes provide improved accuracy but remain to be fully implemented. This will be undertaken in future research. In summary, the proposed methods provide a strong and accurate approach for studying fractional models for applications in fluid dynamics, with applications in engineering and materials science. Future work will refine these models further and improve computational efficiency through better meshing and parallel computing techniques.

Chapter 8

Conclusions and Future Work

This chapter summarizes the key contributions of this thesis and outlines potential directions for future research.

The spectral approximation of the solution to partial differential equation written in their equivalent weak form, was introduced in one and two dimensions in Chapter. 2. The $L2$-error was shown to converge exponentially with respect to the order of the polynomial N, for a few numerical examples.

The fundamental concepts and symbols related to fractional calculus were introduced in Chapter. 3. Specifically, we have listed several definitions of fractional derivatives and their essential characteristics. The theoretical work in this thesis is supported by these ideas. We have described important properties of fractional operators in detail. These are utilised to define the time fractional derivative of Fractional Maxwell Models (FMM) in subsequent chapters. Additionally, we introduced the Laplace transform and Mittag-Leffler function (MLF), which are required to develop the Green's function approach. This method will be used to provide exact solutions to fractional differential equations.

In Chapter.4, we derived fractional viscoelastic models using spring-pot elements arranged in series and/or parallel. Furthermore, we derived expressions for the relaxation time and the dynamic moduli of Fractional Maxwell models in single-mode and multi-mode settings. A novel technique to derive the exact solutions for the Fractional Maxwell Model (FMM) in both single-mode and multi-mode settings was developed using the Laplace transform of the Green's function and expanded in terms of the MLF. This methodology provides an alternative to Fourier-based methods. The analysis explored the FMM for fractional exponents α, β satisfying $0 < \alpha < \beta < 1$ and examined key limiting cases, including the Fractional Maxwell Liquid (FML) and Fractional Maxwell

Gel (FMG). To capture more complex viscoelastic behaviours, the single-mode FMM was extended to a multi-mode version. Rheological analysis of relaxation modulus plots revealed that FML exhibits liquid-like behaviour, FMG behaves as a solid or gel, and FMM transitions between these states based on time or frequency. Finally, the models were validated by fitting them to experimental data using curve-fitting techniques, demonstrating their accuracy across different frequency ranges.

One of the objectives of this thesis was to develop numerical methods that can effectively model the complex behaviour of viscoelastic fluids using fractional viscoelastic models. Specifically, we aimed to numerically solve the system of coupled partial differential equations that describe Taylor-Couette flow. To do this, an accurate and stable discretisation in both time and space is required. In Chapter. 5, we followed the discretisation approach from Sun Wu (2006) to derive a numerical scheme of order $O(\Delta t)$ for the Caputo time-fractional derivative—addressing two cases: $0 < \alpha < 1$ and $1 < \alpha < 2$. Furthermore, we extended the method in Sun Wu (2006) by developing a second-order approximation of the Caputo fractional derivative. This is achieved by utilizing the first and second derivatives from the quadratic interpolation polynomial of the velocity over the two specified intervals of α. Furthermore, we derived first-order and second-order finite difference schemes for the Caputo fractional derivative applied to the Fractional Viscoelastic Fluid (FVF) model for the special case $\alpha = 1$.

The coupled system of equations governing the pure tangential annular flow of fractional viscoelastic fluids was numerically solved and analysed in Chapter. 6. In this chapter, we employed the spectral method instead of the finite difference method used in Ferras . (2018). We found that spectral methods provide excellent efficiency and achieve exponential convergence for smooth problems. This advantage arises because spectral methods utilise global basis functions and require fewer grid points compared to finite difference methods. In contrast, finite difference approaches typically demand more grid points to achieve comparable accuracy while offering lower-order polynomial precision (usually first or second order), which can increase computational costs. The spectral method efficiently resolves fast transients and stress relaxations following step strains.

Through numerical experiments, we examined the convergence order and demonstrated the solvability of the system.

In terms of a specific fractional viscoelastic model, we introduced the three-parameter FVF model, which was shown to accurately fit experimental data and capture bounded stress growth following the onset of steady shear. This model is particularly suitable for complex fluids. Due to the extended simulation time required for the FVF model, graded meshes were employed for time discretization.

In Chapter 7, we developed high-order numerical methods for approximating the Caputo fractional derivative, applied to Fractional Maxwell Models and the Taylor-Couette problem. First-order and second-order temporal difference schemes were derived for different fractional orders, achieving improved accuracy through polynomial interpolation and finite difference methods. These schemes, combined with spectral methods for spatial discretization, enable accurate simulations of Newtonian and viscoelastic fluids to be performed, capturing key viscoelastic effects such as delayed momentum transfer and stress relaxation. The Multi-Mode Fractional Maxwell Model (MM-FMM) is also introduced, which enhances fluid behaviour predictions by incorporating multiple relaxation times. Results showed that adjusting fractional order parameters for stress influences relaxation speed, with lower values slowing it down and higher values making the fluid behave more like a Newtonian fluid. Additionally, a second-order temporal scheme was derived for both single-mode and multi-mode models, improving accuracy but this awaits full implementation. The proposed methods provide a strong framework for studying fractional viscoelastic fluids, with applications in engineering and materials science. Future work will focus on refining these models and enhancing computational efficiency.

There are several possibilities to extend these ideas in the future. These will form the basis of the future research activity. Developing higher-order time discretization methods for fractional viscoelastic models would enhance accuracy and computational efficiency. Additionally, comparing numerical results with further experimental data would help validate and refine the models. Expanding the study to multi-mode fractional models in both series and parallel configurations could provide a more comprehensive understand-

ing of complex fluid behaviour. Another important direction is extending the approach to variable-order fractional linear viscoelasticity to capture time-dependent material properties more effectively. Finally, extending the theoretical and numerical techniques developed in this thesis to more general fractional viscoelastic models could broaden their applicability and improve their robustness.

References

adolfsson2003fractionalAdolfsson, K. Enelund, M. 2003. Fractional derivative viscoelasticity at large deformations Fractional derivative viscoelasticity at large deformations. Nonlinear dynamics33301–321.

afonso2018numericalAfonso, AM. 2018. Numerical simulations of complex fluid-flows at microscale Numerical simulations of complex fluid-flows at microscale. Complex Fluid-Flows in Microfluidics73–94.

apelblat2020differentiationApelblat, A. 2020. Differentiation of the Mittag-Leffler functions with respect to parameters in the Laplace transform approach Differentiation of the Mittag-Leffler functions with respect to parameters in the Laplace transform approach. Mathematics85657.

bagley1991fractionalBagley, RL. Calico, R. 1991. Fractional order state equations for the control of viscoelastically damped structures Fractional order state equations for the control of viscoelastically damped structures. Journal of Guidance, Control, and Dynamics142304–311.

bagley1983theoreticalBagley, RL. Torvik, P. 1983. A theoretical basis for the application of fractional calculus to viscoelasticity A theoretical basis for the application of fractional calculus to viscoelasticity. Journal of Rheology273201–210.

baleanu2012fractionalBaleanu, D., Diethelm, K., Scalas, E. Trujillo, JJ. 2012. Fractional calculus: models and numerical methods Fractional calculus: models and numerical methods (3). World Scientific.

barbati2016complexBarbati, AC., Desroches, J., Robisson, A. McKinley, GH. 2016. Complex fluids and hydraulic fracturing Complex fluids and hydraulic fracturing. Annual Review of Chemical and Biomolecular Engineering71415–453.

barnes2000handbookBarnes, HA. 2000. A Handbook of Elementary Rheology A Handbook of Elementary Rheology (1). University of Wales, Institute of Non-Newtonian Fluid Mechanics Aberystwyth.

baumann1991wgBaumann, G. 1991. WG Gl ockle and TF Nonnenmacher WG Gl ockle and TF Nonnenmacher. Proc. R. Soc. Lond. A434263.

baumgaertel1989determinationBaumgaertel, M. Winter, H. 1989. Determination of discrete relaxation and retardation time spectra from dynamic mechanical data Determination of discrete relaxation and retardation time spectra from dynamic mechanical data. Rheologica Acta28511–519.

bird1987dynamicsBird, RB., Curtiss, CF., Armstrong, RC. Hassager, O. 1987. Dynamics of polymeric liquids, volume 2: Kinetic theory Dynamics of polymeric liquids, volume 2: Kinetic theory. Wiley.

burden1997numericalBurden, RL. Faires, JD. 1997. Numerical Analysis, 9th edition Numerical Analysis, 9th edition. Cole, Thomson Learning Inc14190–192.

cai2020numericalCai, M. Li, C. 2020. Numerical approaches to fractional integrals and derivatives: A review Numerical approaches to fractional integrals and derivatives: A review. Mathematics8143.

canuto2012spectralCanuto, C., Hussaini, MY., Quarteroni, A., Zang, TA. . 2012. Spectral Methods in Fluid Dynamics Spectral Methods in Fluid Dynamics. Springer Science & Business Media.

caputo1969elasticitaCaputo, M. 1969. Elasticita e dissipazione Elasticita e dissipazione. Zanichelli.

caputo1971linearCaputo, M. Mainardi, F. 1971. Linear models of dissipation in anelastic solids Linear models of dissipation in anelastic solids. La Rivista del Nuovo Cimento (1971-1977)12161–198.

childs2020quantumChilds, AM. Liu, JP. 2020. Quantum spectral methods for differential equations Quantum spectral methods for differential equations. Communications in Mathematical Physics37521427–1457.

consiglio2021evolutionConsiglio, A. Mainardi, F. 2021. On the evolution of fractional diffusive waves On the evolution of fractional diffusive waves. Ricerche di Matematica70121–33.

daftardar2004analysisDaftardar-Gejji, V. Babakhani, A. 2004. Analysis of a system of fractional differential equations Analysis of a system of fractional differential equations. Journal of Mathematical Analysis and Applications2932511–522.

deville2012mathematicalDeville, M. Gatski, TB. 2012. Mathematical Modeling for Complex Fluids and Flows Mathematical Modeling for Complex Fluids and Flows. Springer Science & Business Media.

diethelm2010analysisDiethelm, K. 2010. The analysis of fractional differential equations: An application-oriented exposition using differential operators of Caputo type The analysis of fractional differential equations: An application-oriented exposition using differential operators of caputo type. Springer Science & Business Media.

diethelm2004detailedDiethelm, K., Ford, NJ. Freed, AD. 2004. Detailed error analysis for a fractional Adams method Detailed error analysis for a fractional Adams method. Numerical Algorithms3631–52.

dirac1981principlesDirac, PAM. 1981. The Principles of Quantum Mechanics The Principles of Quantum Mechanics (27). Oxford University Press.

doha2011chebyshevDoha, EH., Bhrawy, AH. Ezz-Eldien, SS. 2011. A Chebyshev spectral method based on operational matrix for initial and boundary value problems of fractional order A Chebyshev spectral method based on operational matrix for initial and boundary value problems of fractional order. Computers & Mathematics with Applications6252364–2373.

donnelly1991taylorDonnelly, RJ. 1991. Taylor-Couette flow: The early days Taylor-couette flow: The early days. Physics Today441132–39.

dontula2005originsDontula, P., Macosko, CW. Scriven, L. 2005. Origins of concentric cylinders viscometry Origins of concentric cylinders viscometry. Journal of Rheology494807–818.

drazin2004hydrodynamicDrazin, PG. Reid, WH. 2004. Hydrodynamic Stability Hydrodynamic Stability. Cambridge University Press.

faber2017describingFaber, T., Jaishankar, A. McKinley, GH. 2017. Describing the firmness, springiness and rubberiness of food gels using fractional calculus. Part I: Theoretical framework Describing the firmness, springiness and rubberiness of food gels using fractional calculus. Part I: Theoretical framework. Food Hydrocolloids62311–324.

ferras2018theoreticalFerras, LL., Ford, NJ., Morgado, ML., Rebelo, M., McKinley, GH. Nobrega, JM. 2018. Theoretical and numerical analysis of unsteady fractional viscoelastic flows in simple geometries Theoretical and numerical analysis of unsteady fractional viscoelastic flows in simple geometries. Computers & Fluids17414–33.

fox1961Fox, C. 1961. The G and H functions as symmetrical Fourier kernels The G and H functions as symmetrical Fourier kernels. Transactions of the American Mathematical Society983395–429.

friedrich1991relaxationFriedrich, C. 1991. Relaxation and retardation functions of the Maxwell model with fractional derivatives Relaxation and retardation functions of the Maxwell model with fractional derivatives. Rheologica Acta302151–158.

galindo2018complexGalindo-Rosales, FJ. 2018. Complex Fluids and Rheometry in Microfluidics Complex Fluids and Rheometry in Microfluidics. Springer.

garra2018prabhakarGarra, R. Garrappa, R. 2018. The Prabhakar or three parameter Mittag–Leffler function: Theory and application The Prabhakar or three parameter Mittag–Leffler function: Theory and application. Communications in Nonlinear Science and Numerical Simulation56314–329.

garrappa2018numericalGarrappa, R. 2018. Numerical solution of fractional differential equations: A survey and a software tutorial Numerical solution of fractional differential equations: A survey and a software tutorial. Mathematics6216.

giga2017variationalGiga, MH., Kirshtein, A. Liu, C. 2017. Variational modeling and complex fluids Variational modeling and complex fluids. Handbook of Mathematical Analysis in Mechanics of Viscous Fluids1–41.

gorenflo1997fractionalGorenflo, R. Mainardi, F. 1997. Fractional calculus: integral and differential equations of fractional order Fractional calculus: integral and differential equations of fractional order. Springer.

gottlieb1977numericalGottlieb, D. Orszag, SA. 1977. Numerical Analysis of Spectral Methods: Theory and Applications Numerical Analysis of Spectral Methods: Theory and Applications. Philadelphia, USASIAM.

hajikarimi2021applicationsHajikarimi, P. Nejad, FM. 2021. Applications of viscoelasticity: Bituminous materials characterization and modeling Applications of viscoelasticity: Bituminous materials characterization and modeling. Elsevier.

halliday2010physicsHalliday, D., Resnick, R. Krane, KS. 2010. Physics, Volume 2 Physics, volume 2. John Wiley & Sons.

haubold2011mittagHaubold, HJ., Mathai, AM. Saxena, RK. 2011. Mittag-Leffler functions and their applications Mittag-Leffler functions and their applications. Journal of Applied Mathematics2011.

he2007variationalHe, JH. 2007. Variational iteration method—some recent results and new interpretations Variational iteration method—some recent results and new interpretations. Journal of Computational and Applied Mathematics20713–17.

hohenegger2018reconstructingHohenegger, C. McKinley, SA. 2018. Reconstructing complex fluid properties from the behavior of fluctuating immersed particles Reconstructing complex fluid properties from the behavior of fluctuating immersed particles. SIAM Journal on Applied Mathematics7842200–2226.

hristov2018linearHristov, JY. 2018. Linear viscoelastic responses: The Prony decomposition naturally leads into the Caputo-Fabrizio fractional operator Linear viscoelastic responses: The Prony decomposition naturally leads into the Caputo-Fabrizio fractional operator. Frontiers in Physics6135.

jaishankar2014fractionalJaishankar, A. McKinley, GH. 2014. A fractional K-BKZ constitutive formulation for describing the nonlinear rheology of multiscale complex fluids A fractional K-BKZ constitutive formulation for describing the nonlinear rheology of multiscale complex fluids. Journal of Rheology5861751–1788.

Kang2008Kang, S. Suh, YK. 2008. Spectral Methods Spectral methods (D. Li,). Boston, MA, USSpringer.

keshavarz2017nonlinearKeshavarz, B., Divoux, T., Manneville, S. McKinley, GH. 2017. Nonlinear viscoelasticity and generalized failure criterion for polymer gels Nonlinear viscoelasticity and generalized failure criterion for polymer gels. ACS Macro Letters67663–667.

keshavarz2021timeKeshavarz, B., Rodrigues, DG., Champenois, JB., Frith, MG., Ilavsky, J., Geri, M.Poulesquen, A. 2021. Time–connectivity superposition and the gel/glass duality of weak colloidal gels Time–connectivity superposition and the gel/glass duality of weak colloidal gels. Proceedings of the National Academy of Sciences11815e2022339118.

kexue2011laplaceKexue, L. Jigen, P. 2011. Laplace transform and fractional differential equations Laplace transform and fractional differential equations. Applied Mathematics Letters24122019–2023.

koeller1984applicationsKoeller, R. 1984. Applications of fractional calculus to the theory of viscoelasticity Applications of fractional calculus to the theory of viscoelasticity. Journal of Applied Mechanics.

kumar2020analysisKumar, S., Ghosh, S., Samet, B. Goufo, EFD. 2020. An analysis for heat equations arises in diffusion process using new Yang-Abdel-Aty-Cattani fractional operator An analysis for heat equations arises in diffusion process using new Yang-Abdel-Aty-Cattani fractional operator. Mathematical Methods in the Applied Sciences4396062–6080.

kumar2020chaoticKumar, S., Kumar, R., Cattani, C. Samet, B. 2020. Chaotic behaviour of fractional predator-prey dynamical system Chaotic behaviour of fractional predator-prey dynamical system. Chaos, Solitons & Fractals135109811.

kumar2024numericalKumar, S., Shaw, PK., Abdel-Aty, AH. Mahmoud, EE. 2024. A numerical study on fractional differential equation with population growth model A numerical study on fractional differential equation with population growth model. Numerical Methods for Partial Differential Equations401e22684.

larson1999structureLarson, RG. 1999. The structure and rheology of complex fluids The structure and rheology of complex fluids.

levy2010numericalLevy, D. 2010. Numerical Differentiation Numerical differentiation. University of Maryland.

lubich1986discretizedLubich, C. 1986. Discretized fractional calculus Discretized fractional calculus. SIAM Journal on Mathematical Analysis173704–719.

machado2011recentMachado, JT., Kiryakova, V. Mainardi, F. 2011. Recent history of fractional calculus Recent history of fractional calculus. Communications in nonlinear science and numerical simulation1631140–1153.

mainardi2010fractionalMainardi, F. 2010. Fractional Calculus and Waves in Linear Viscoelasticity: An Introduction to Mathematical Models Fractional Calculus and Waves in Linear Viscoelasticity: An Introduction to Mathematical Models. World Scientific.

mainardi2013someMainardi, F. 2013. On some properties of the Mittag-Leffler function $E_\alpha(-t^\alpha)$, completely monotone for $t > 0$ with $0 < \alpha < 1$ On some properties of the Mittag-Leffler function $E_\alpha(-t^\alpha)$, completely monotone for $t > 0$ with $0 < \alpha < 1$. arXiv preprint arXiv:1305.0161.

maxwell1867ivMaxwell, JC. 1867. IV. On the dynamical theory of gases Iv. on the dynamical theory of gases. Philosophical Transactions of the Royal Society of London15749–88.

meerschaert2019stochasticMeerschaert, MM. Sikorskii, A. 2019. Stochastic models for fractional calculus Stochastic models for fractional calculus. de Gruyter.

miller1993introductionMiller, KS. Ross, B. 1993. An Introduction to the Fractional Calculus and Fractional Differential Equations An Introduction to the Fractional Calculus and Fractional Differential Equations. Wiley.

momani2005numericalMomani, S. Al-Khaled, K. 2005. Numerical solutions for systems of fractional differential equations by the decomposition method Numerical solutions for systems of fractional differential equations by the decomposition method. Applied Mathematics and Computation16231351–1365.

mustapha2000dynamicMustapha, SS. Phillips, T. 2000. A dynamic nonlinear regression method for the determination of the discrete relaxation spectrum A dynamic nonlinear regression method for the determination of the discrete relaxation spectrum. Journal of Physics D: Applied Physics33101219.

ng2006linearNg, TS., McKinley, GH. Padmanabhan, M. 2006. Linear to non-linear rheology of wheat flour dough Linear to non-linear rheology of wheat flour dough. Applied Rheology165265–274.

nigmatullin1984theoreticalNigmatullin, R. 1984. To the theoretical explanation of the "universal response" To the theoretical explanation of the "universal response". Physica Status Solidi (b)1232739–745.

oldham1974fractionalOldham, K. Spanier, J. 1974. The fractional calculus theory and applications of differentiation and integration to arbitrary order The fractional calculus theory and applications of differentiation and integration to arbitrary order. New York, NY, USAElsevier.

owens2002computationalOwens, RG. Phillips, TN. 2002. Computational rheology Computational rheology. London, UKImperial College Press.

palade1996modifiedPalade, LI., Verney, V. Attané, P. 1996. A modified fractional model to describe the entire viscoelastic behavior of polybutadienes from flow to glassy regime A modified fractional model to describe the entire viscoelastic behavior of polybutadienes from flow to glassy regime. Rheologica Acta35265–273.

parada2018idealParada, GA. Zhao, X. 2018. Ideal reversible polymer networks Ideal reversible polymer networks. Soft Matter14255186–5196.

pipe2010wormlikePipe, C., Kim, N., Vasquez, P., Cook, L. McKinley, G. 2010. Wormlike micellar solutions: II. Comparison between experimental data and scission model predictions Wormlike micellar solutions: Ii. comparison between experimental data and scission model predictions. Journal of Rheology544881–913.

podlubny1997laplacePodlubny, I. 1997. The Laplace transform method for linear differential equations of the fractional order The Laplace transform method for linear differential equations of the fractional order. arXiv preprint funct-an/9710005.

podlubny1999fractionalPodlubny, I. 1999. Fractional Differential Equations, Mathematics in Science and Engineering. Fractional Differential Equations, Mathematics in Science and Engineering. Academic press New York.

pooseh2013discretePooseh, S., Almeida, R. Torres, DF. 2013. Discrete direct methods in the fractional calculus of variations Discrete direct methods in the fractional calculus of variations. Computers & Mathematics with Applications665668–676.

rathinaraj2021incorporatingRathinaraj, JDJ., McKinley, GH. Keshavarz, B. 2021. Incorporating rheological nonlinearity into fractional calculus descriptions of fractal matter and multi-scale complex fluids Incorporating rheological nonlinearity into fractional calculus descriptions of fractal matter and multi-scale complex fluids. Fractal and Fractional54174.

rehage1991viscoelasticRehage, H. Hoffmann, H. 1991. Viscoelastic surfactant solutions: model systems for rheological research Viscoelastic surfactant solutions: model systems for rheological research. Molecular Physics745933–973.

sadman2017influenceSadman, K., Wang, Q., Chen, Y., Keshavarz, B., Jiang, Z. Shull, KR. 2017. Influence of hydrophobicity on polyelectrolyte complexation Influence of hydrophobicity on polyelectrolyte complexation. Macromolecules50239417–9426.

samko1987integralsSamko, SG., Kilbas, AA. Marichev, OI. 1987. Integrals and derivatives of fractional order and some of their applications. Integrals and derivatives of fractional order and some of their applications. Nauka i tekhnika, Minsk.

samko1993fractionalSamko, SG., Kilbas, AA., Marichev, OI. . 1993. Fractional integrals and derivatives Fractional integrals and derivatives (1). Gordon and Breach Science Publishers, Yverdon-les-Bains, Switzerland.

saramito2016complexSaramito, P. 2016. Complex Fluids Complex Fluids. Switzerland-Springer International Publishing.

schiessel1993hierarchicalSchiessel, H. Blumen, A. 1993. Hierarchical analogues to fractional relaxation equations Hierarchical analogues to fractional relaxation equations. Journal of Physics A: Mathematical and General26195057.

schiessel1995generalizedSchiessel, H., Metzler, R., Blumen, A. Nonnenmacher, T. 1995. Generalized viscoelastic models: their fractional equations with solutions Generalized viscoelastic models: their fractional equations with solutions. Journal of Physics A: Mathematical and General28236567.

schmidt2024generalizedSchmidt, RF., Winter, HH. Gradzielski, M. 2024. Generalized vs. fractional: a comparative analysis of Maxwell models applied to entangled polymer solutions Generalized vs. fractional: a comparative analysis of Maxwell models applied to entangled polymer solutions. Soft Matter20397914–7925.

schneider1989fractionalSchneider, WR. Wyss, W. 1989. Fractional diffusion and wave equations Fractional diffusion and wave equations. Journal of Mathematical Physics301134–144.

shah2024dropShah, P. Driscoll, MM. 2024. Drop impact dynamics of complex fluids: A review Drop impact dynamics of complex fluids: A review. Soft Matter.

simon2014comparingSimon, T. 2014. Comparing Fréchet and positive stable laws Comparing fréchet and positive stable laws.

stankiewicz2018fractionalStankiewicz, A. 2018. Fractional Maxwell model of viscoelastic biological materials Fractional Maxwell model of viscoelastic biological materials. BIO Web of Conferences Bio web of conferences (10, 02032).

sun2006fullySun, Zz. Wu, X. 2006. A fully discrete difference scheme for a diffusion-wave system A fully discrete difference scheme for a diffusion-wave system. Applied Numerical Mathematics562193–209.

szego1955erdelyiSzegö, G. 1955. A. Erdélyi, Higher Transcendental Functions, Vol. 1 A. Erdélyi, Higher Transcendental Functions, vol. 1. New York, USAMcGraw-Hill.

tattersall1983rheologyTattersall, GH. Banfill, PF. 1983. The Rheology of Fresh Concrete (No. Monograph) The Rheology of Fresh Concrete (no. monograph).

taylor1923viiiTaylor, GI. 1923. VIII. Stability of a viscous liquid contained between two rotating cylinders Viii. stability of a viscous liquid contained between two rotating cylinders. Philosophical Transactions of the Royal Society of London. Series A, Containing Papers of a Mathematical or Physical Character223605-615289–343.

torvik1984appearanceTorvik, PJ. Bagley, RL. 1984. On the appearance of the fractional derivative in the behavior of real materials On the appearance of the fractional derivative in the behavior of real materials.

toschi2019flowingToschi, F. Sega, M. 2019. Flowing Matter Flowing Matter. Cham, GermanySpringer Nature.

troparevsky2019reviewTroparevsky, MI., Seminara, SA. Fabio, MA. 2019. A review on fractional differential equations and a numerical method to solve some boundary value problems A review on fractional differential equations and a numerical method to solve some boundary value problems. Nonlinear systems-theoretical aspects and recent applications3–22.

tschoegl2012phenomenologicalTschoegl, NW. 2012. The Phenomenological Theory of Linear Viscoelastic Behavior: An Introduction The Phenomenological Theory of Linear Viscoelastic Behavior: An Introduction. Springer Science & Business Media.

winter1990computerWinter, H., Baumgaertel, M., Soskey, P. Venkataraman, S. 1990. Computer Aided Rheometry Computer aided rheometry. Third European Rheology Conference and Golden Jubilee Meeting of the British Society of Rheology Third european rheology conference and golden jubilee meeting of the british society of rheology (504–506).

winter1995linearWinter, HH. Jackson, J. 1995. Linear Viscoelasticity: The Search for Patterns in the Relaxation of Polymer Melts and Gels Linear viscoelasticity: The search for patterns in the relaxation of polymer melts and gels. Rheological Fundamentals of Polymer Processing Rheological fundamentals of polymer processing (61–92). Springer.

yahia2016concreteYahia, A., Mantellato, S. Flatt, RJ. 2016. Concrete rheology: A basis for understanding chemical admixtures Concrete rheology: A basis for understanding chemical admixtures. Science and Technology of Concrete Admixtures Science and technology of concrete admixtures (97–127). Elsevier.

yang2010constitutiveYang, P., Lam, YC. Zhu, KQ. 2010. Constitutive equation with fractional derivatives for the generalized UCM model Constitutive equation with fractional derivatives for the generalized UCM model. Journal of Non-Newtonian Fluid Mechanics1653-488–97.

zhang2014finiteZhang, Yn., Sun, Zz. Liao, Hl. 2014. Finite difference methods for the time fractional diffusion equation on non-uniform meshes Finite difference methods for the time fractional diffusion equation on non-uniform meshes. Journal of Computational Physics265195–210.